SANDIA REPORT
SAND2010-6684
Unlimited Release
Printed October 2010

High Fidelity Nuclear Energy System Optimization Towards an Environmentally Benign, Sustainable, and Secure Energy Source

David E. Ames II, Pavel V. Tsvetkov, Gary E. Rochau, Salvador Rodriguez

Prepared by
Sandia National Laboratories
Albuquerque, New Mexico 87185 and Livermore, California 94550

Sandia National Laboratoires is a multiprogram laboratory managed and operated by Sandia Corporation, a wholly owned subsidiary of Lockheed Martin Corporation, for the United States Department of Energy's National Nuclear Security Administration under the Contract DE-AC04-94AL85000.

Sandia National Laboratories

Issued by Sandia National Laboratories, operated for the United States Department of Energy by Sandia Corporation.

Available to DOE and DOE contractors from
U.S. Department of Energy
Office of Scientific and Technical Information
P.O. Box 62
Oak Ridge, TN 37831

Telephone: (865) 576-8401
Facsimile: (865) 576-5728
E-Mail: reports@adonis.osti.gov
Online ordering: http://www.osti.gov/bridge

Available to the public from
U.S. Department of Commerce
National Technical Information Service
5285 Port Royal Rd.
Springfield, VA 22161

Telephone: (800) 553-6847
Facsimile: (703) 605-6900
E-Mail: orders@ntis.fedworld.gov
Online order: http://www.ntis.gov/help/ordermethods.asp?loc=7-4-0#online

SAND2010-6684
Unlimited Release
Printed October 2010

High Fidelity Nuclear Energy System Optimization Towards an Environmentally Benign, Sustainable, and Secure Energy Source

D. E. Ames[1], P. V. Tsvetkov[1], G.E. Rochau[2], S. Rodriguez[2]
[1]Texas A&M University, 129 Zachry Engineering Center, College Station, TX 77843-3133
[2]Sandia National Laboratories, P.O. Box 5800, Albuquerque, NM 87185-0748

Abstract

A new high-fidelity integrated system method and analysis approach was developed and implemented for consistent and comprehensive evaluations of advanced fuel cycles leading to minimized Transuranic (TRU) inventories. The method has been implemented in a developed code system integrating capabilities of Monte Carlo N – Particle Extended (MCNPX) for high-fidelity fuel cycle component simulations.

In this report, a Nuclear Energy System (NES) configuration was developed to take advantage of used fuel recycling and transmutation capabilities in waste management scenarios leading to minimized TRU waste inventories, long-term activities, and radiotoxicities. The reactor systems and fuel cycle components that make up the NES were selected for their ability to perform in tandem to produce clean, safe, and dependable energy in an environmentally conscious manner. The diversity in performance and spectral characteristics were used to enhance TRU waste elimination while efficiently utilizing uranium resources and providing an abundant energy source.

A computational modeling approach was developed for integrating the individual models of the NES. A general approach was utilized allowing for the Integrated System Model (ISM) to be modified in order to provide simulation for other systems with similar attributes. By utilizing this approach, the ISM is capable of performing system evaluations under many different design parameter options. Additionally, the predictive capabilities of the ISM and its computational time efficiency allow for system sensitivity/uncertainty analysis and the implementation of optimization techniques.

ACKNOWLEDGEMENTS

This paper is based upon work supported through the Excellence in Engineering Research Program by the Sandia Research Graduate Program at Texas A&M University and the College of Engineering, Texas A&M University.

CONTENTS

FIGURES

TABLES

NOMENCLATURE

ADS	Accelerator Driven System
AFCI	Advanced Fuel Cycle Initiative
AP1000	Westinghouse Electric Company Reactor
BOC	Beginning of Cycle
CAIN	CAlculation of INventory of Spent Fuel
CPU	Central Processing Unit
D	Deuterium
DOE	U.S. Department of Energy
DU	Depleted Uranium
EFPD	Effective Full Power Days
ENDF/B	Evaluated Nuclear Data Files – Basic
EOC	End of Cycle
FP	Fission Products
GCC	Gulf Cooperation Council
GDP	Gross Domestic Product
Gen-IV	Generation IV Nuclear Fuel Systems
GIF	Generation IV International Forum
HDI	Human Development Index
HEST	High-energy External Source Transmuter
HLW	High Level Waste
HTGR	High Temperature Gas Reactor
HTR	High Temperature Reactor
HTTR	High Temperature Test Reactor
IAEA	International Atomic Energy Agency
IEC	Inertial Electrostatic Confinement
IFBA	Integral Fuel Burnable Absorber
ISM	Integrated System Model
JAERI	Japan Atomic Energy Research Institute
LEU	Low Enriched Uranium
LLW	Low Level Waste
LWR	Light Water Reactor
MCNP	Monte Carlo N – Particle
MCNPX	Monte Carlo N – Particle Extended
MT	Metric Tons
MTU	Metric Tons of Uranium
NES	Nuclear Energy System
NFCSS	Nuclear Fuel Cycle Simulation System
NGNP	Next Generation Nuclear Plant
NRC	Nuclear Regulatory Commission
ORNL	Oak Ridge National Laboratory
OTTO	Once-Through-Then-Out
PWR	Pressurized Water Reactor
PYREX	Discrete Burnable Absorber Rods
SCALE	Standardized Computer Analysis for Licensing Evaluation

SWU	Separative Work Unit
T	Tritium
tIHM	Ton Initial Heavy Metal
TRISO	Tri-structural Isotropic
TRU	Transuranic Isotopes (Np, Pu, Am, Cm)
UNDP	United Nations Development Program
UQ	Uncertainty Quantification
UREX	URanium EXtraction
VHTR	Very High Temperature Reactor

1 INTRODUCTION

It is difficult to describe how important energy has become in the world today. Industrialized nations are totally dependent on an abundantly reliable supply of energy for living and working. Energy is a key ingredient in all sectors of modern economies. Even so, it is often taken for granted because it plays such a large role in our everyday existence. Meanwhile, in developing countries there is almost an unquenchable thirst for substantial increases in energy generation and usage. In any case, energy is one of the single most important factors in regards to living standards of individuals throughout the world. Studies have continually shown an indisputable link between energy consumption and individuals overall wellbeing [1-3].

Extensive data have been collected comparing average energy consumption per capita to measurements that represent the standard of living, or quality of life, achieved in any community. One such measure is the Human Development Index (HDI), which incorporates factors such as life expectancy, education, income inequality, poverty rates, Gross Domestic Product (GDP) per capita, and the environment [2].

The HDI is widely considered the best and most comprehensive measure for quality of life. The index is normalized to give a value between zero and one, with one representing the highest possible standard of living or most developed country, and zero being the least. Countries that score an HDI greater than 0.90 are considered to have a "very high quality of life," while those with values between 0.60 and 0.90 are rated as having an "average quality of life," and those below 0.60 are classified as having a "very low quality of life."

A very compelling relationship exists between HDI and energy usage. The United Nations Development Program (UNDP) released the data presented in Figure 1.1 on December 20, 2008. It includes the HDI and electricity generation per capita (as determined in 2006) for 180 different countries, with some of countries labeled for general reference. As indicated, the results overwhelmingly show that the greater the energy consumption per capita for a community, the greater the standard of living (HDI) for those individuals. Consequently, energy consumption can be used as a litmus test for the overall wellbeing of a society and for a comparison between different societies around the globe.

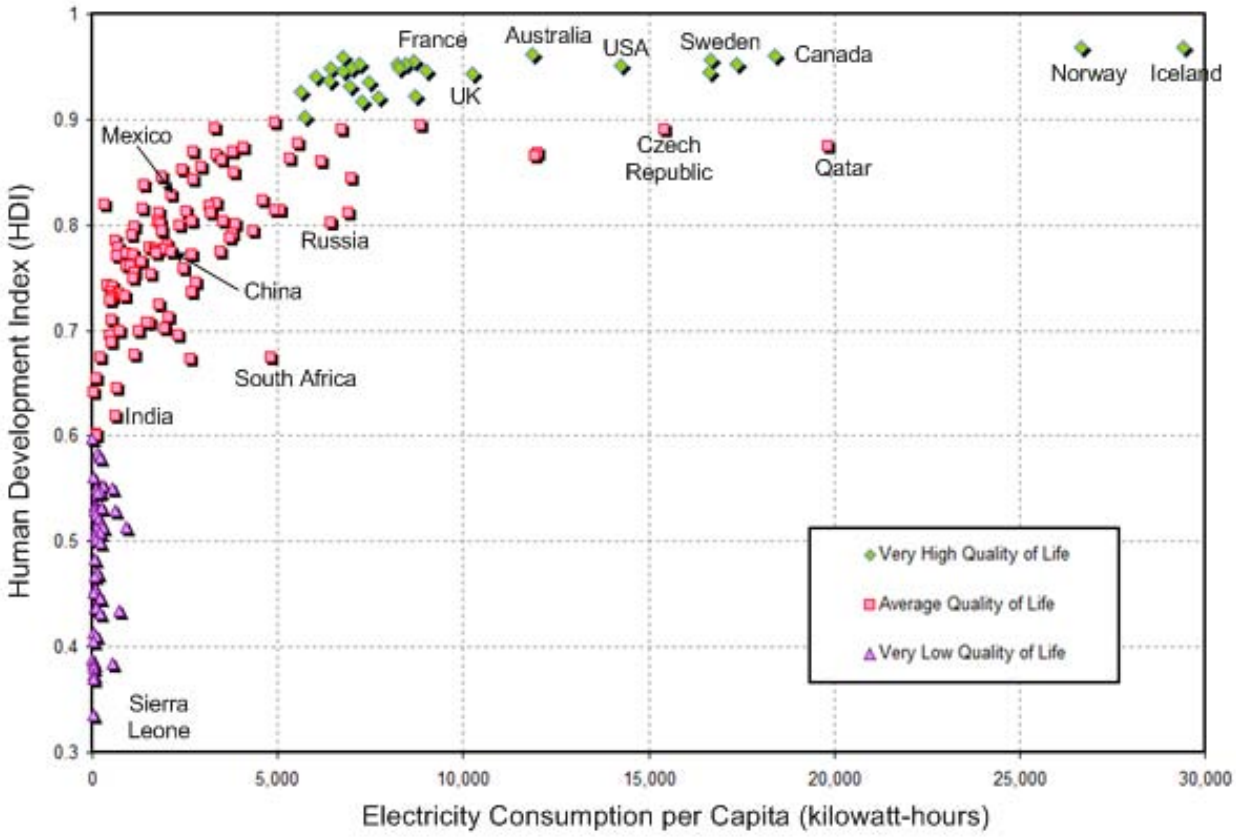

Figure 1.1. Relationship of HDI and Electricity Consumption per Capita.

Iceland and Norway have the highest HDI at 0.968, while Sierra Leone ranks lowest at 0.329, which is shown in the upper right and lower left of Figure 1.1, respectively. The USA has an HDI of 0.950 and is ranked number 15 overall. As expected, all nations strive to increase their HDI standing. The most effective and straightforward way to accomplish this is by adding energy generation capacity. Of particular notice is China and India, the two most populated countries in world, which have HDI values that place them in the lower portion of the "average quality of life" group of nations. India and China are striving to rapidly increase their HDI. Their improved HDI will greatly affect the rest of the world. With over 35% of world's population between these two countries, just a slight increase in either's electricity consumption per capita will have a huge impact on overall energy needs worldwide.

The coupled effect of energy use and living standards leads to an interesting dilemma. Just like energy's link to quality of life, energy is also intricately entwined with the environment. Much of the global-scale environmental degradation seen today is attributed to the adverse effects of energy production and use. Thus, nations are faced with the struggle to increase energy generation in order to provide a higher standard of living for their citizens, but must also do so in an environmentally responsible way.

Figure 1.2 displays HDI data and Carbon Dioxide (CO_2) emissions for 180 countries. The six countries (Bahrain, Kuwait, Oman, Qatar, Saudi Arabia, and the United Arab Emirates) that make up the Gulf Cooperation Council (GCC) are at the top or near the top of the list for CO_2

emitters. Their ranking is mainly due to their high emitting gas production sector, small populations, and exportation of energy. Qatar is the number one emitter, generating 79.3 tones/capita - such a high value that it is off the scale of the provided plot. Most of the GCC countries have taken aggressive measures to reduce their CO_2 emissions. Measures taken including tightening controls on gas flaring, researching carbon capture and sequestration, and investigating the use of non-CO_2 emitting energy forms such as nuclear energy and wind power.

It is interesting to note that counties such as France and Iceland have extremely high HDI values while at the same time generating very low levels of CO_2 emission per capita. Further investigation reveals that France gets about 80% of its electricity generation from nuclear power. Much of Iceland's energy needs are met by renewable sources (particularly geothermal power). Both countries are fulfilling a large portion of their energy needs by using non-CO_2 emitting sources. France and Iceland have something else in common - they both have very few fossil fuel energy resources within their borders. Even so, they have adopted energy plans that have made them much more energy-independent compared to other industrialized nations.

The United States is ninth on the list for CO_2 emissions per capita and second, just behind China, for overall CO_2 emissions. The rest of the world shares the belief that the USA needs to take a more proactive role in CO_2 reduction and set an example for the others around world to follow. Again, as mentioned previously, India and China are of major concern due to their increased energy demands and the impact they will have in the near future.

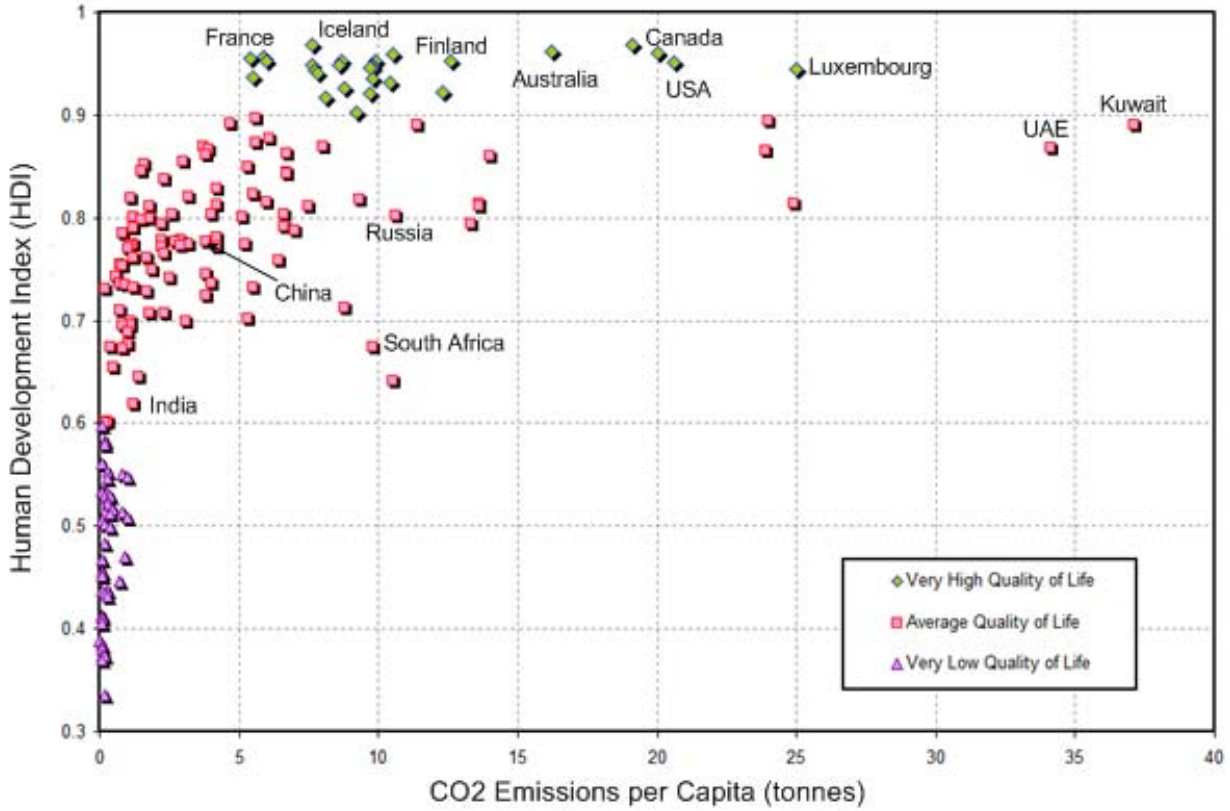

Figure 1.2. HDI vs. CO_2 Emissions per Capita for 180 Countries.

In recent years the world has become much more sensitive to the relationship between energy and the environment, to the point that it has become nearly impossible to discuss one without the other. In response, nations and groups of nations have proposed and/or implemented policies to mitigate the harmful environmental effects associated with energy generation [4, 5]. These energy policies are developed to aid the environment through tactics such as carbon emission caps, emissions trade plans, carbon taxes, efficiency and conservation incentives, clean renewable energy incentives, etc. In addition to the very important environmental issues that have come to the forefront, there are some other important requirements for future energy systems. Important goals and basic principles of future energy sources include:

1) Reducing greenhouse gas emissions,
2) Minimizing the overall environmental footprint,
3) Safety and reliability,
4) Sustainability,
5) Economically viable,
6) Efficiency, and
7) Energy independence.

From the onset nuclear power has shown great promise in meeting all of the above principles. As the technology has matured so has its effectiveness in accomplishing these goals. Today nuclear energy is arguably one of the best sources for electricity generation that can meet future needs and requirements. Even so, advances and improvements must be made for nuclear energy to be competitive in the future. The research work presented within addresses the above principals with emphasis on environmental aspects by means of developing a modeling approach for advanced nuclear energy systems that minimize high level waste inventories while at the same time maximizing fuel utilization.

1.1 The Nuclear Fuel Cycle

The nuclear fuel cycle can be described as the comprehensive collection of components that are linked together for the main purpose of generating electricity by means of nuclear power. It includes everything from the exploration for uranium deposits, to harnessing the energy released during fission, to the disposal of radioactive waste. The nuclear fuel cycle can be thought of as the progression of nuclear fuel through a series of differing stages which involve the production of electricity in nuclear reactors. There are three major parts to the cycle: 1) Front-end, 2) In-core, and 3) Back-end.

The front-end of the fuel cycle begins with the exploration of uranium deposits. Estimates for uranium reserves at different stated costs are developed and reported [6]. Once the uranium deposits have been identified, the uranium ore is extracted by various mining methods. Conventional techniques such as open pit and underground mining are most commonly used. Next the mined uranium ore is processed and treated to extract the uranium through the milling process. The milled uranium is then converted to a form that can be used by commercial facilities to enrich the fissile component by either gaseous diffusion or gas centrifuge enrichment technologies. The last step for the front-end is fuel fabrication, where enriched fuel is converted to a final usable fuel form and incased in a protective cladding for service in nuclear reactors.

The in-core or service period of the fuel cycle makes up the second major category of the fuel cycle. As the name implies, this part of the fuel cycle is concerned with fuel performance while in the reactor core. Much emphasis is placed on fuel management strategies, irradiation effects on the fuel, fuel cladding interactions, and radioactivity release during normal use and accidents. The reactor type, neutron spectrum, and fuel type are important parameters for the service period.

The back-end of the fuel cycle begins when the fuel is discharged from the reactor. Upon removal, the fuel is stored onsite temporarily and then prepared for either permanent storage or for reprocessing. The decision of whether to recycle the used reactor fuel or to place it directly into storage greatly affects the makeup of the back-end of the fuel cycle. Waste management is the key issue with this part of the fuel cycle.

The United States employs what is referred to as the once-through fuel cycle. The fuel makes one pass through a thermal neutron spectrum reactor core and after removal it is prepared for permanent disposal. The cycle is quite wasteful of nuclear energy resources, being that the valuable remaining energy in the used fuel is not reclaimed. For this reason, the once-through cycle is sometimes called a "throw-away" fuel cycle [7]. Due to its wide use the once-through cycle is often used as the standard reference when comparing differing fuel cycles.

1.1.1 Advanced Fuel Cycle Initiative

Making improvements to and/or replacing the once-through fuel cycle with a superior method that recycles used nuclear fuel is a goal that many developed countries are serious about achieving. For instance, the United States Department of Energy (DOE) established the Advanced Fuel Cycle Initiative (AFCI) program to focus on the research and development needed to support a transition from the current once-through fuel cycle to an advanced nuclear fuel cycle. The AFCI program is envisioned to support the growth of nuclear power and enable energy independence in the U.S. by developing and demonstrating technologies that facilitate the transition to a stable, long-term, environmentally, economically, and politically acceptable advanced fuel cycle. The main goals of the AFCI are to reduce high-level waste volume, greatly reduce long-lived and highly radiotoxic elements, and reclaim valuable energy content of spent nuclear fuel. In part, the AFCI program seeks to:

- Reduce the long-term environmental burden of nuclear energy through more efficient disposal of waste materials.
- Enhance overall nuclear fuel cycle proliferation resistance via improved technologies for spent fuel management.
- Reduce the inventories of civilian plutonium
- Enhance energy security by extracting energy recoverable in spent fuel and depleted uranium, ensuring that uranium resources do not become a limiting resource for nuclear power.
- Improve fuel cycle management, while continuing competitive fuel cycle economics and excellent safety performance of the entire nuclear fuel cycle system.

- Develop fuels and fuel cycles for current reactor systems and future Generation IV nuclear fuel systems

The Generation IV International Forum (GIF) focuses on future nuclear energy system concepts to meet the growing energy needs of the world. It is an international program consisting of 13 member nations (United States of America, Argentina, Brazil, Canada, France, Japan, South Korea, South Africa, Switzerland, United Kingdom, the European Union, China, and Russia) coordinating research and working together to develop promising new nuclear energy systems. Attention is given to improving safety features, addressing nuclear nonproliferation and physical protection issues, optimizing natural resource utilization, minimizing waste, and being economically competitive with other energy generating systems. The GIF has selected six systems for further development. The systems are:

1) Gas-Cooled Fast Reactor,
2) Very High Temperature Reactor,
3) Supercritical Water Cooled Reactor,
4) Sodium Cooled Fast Reactor,
5) Lead Cooled Fast Reactor, and
6) Molten Salt Reactor.

As part of the Generation IV program the U.S. DOE has focused efforts on the Next Generation Nuclear Plant (NGNP). The NGNP program promotes research and development specific to the Very High Temperature Reactor (VHTR).

The VHTR is designed to be a high-efficiency energy system, which can supply electricity and process heat to a wide-range of high temperature and energy intensive applications. The VHTR is a passively safe design. The refractory core, low power density, and low excess reactivity enable this design feature. It is a graphite moderated gas-cooled reactor that supplies heat with core outlet temperatures equal to or greater than 850° Celsius, which enables applications such as hydrogen production, process heat for the petrochemical industry, or seawater desalination.

To realize the full potential of advanced fuel cycles, fast neutron spectrum systems must be implemented. Fast systems offer a higher degree of flexibility when it comes to the transmutation process. They not only provide the ability to better control the isotopic makeup of the waste stream through nuclide destruction, but also the capability to fully utilize the available fuel resources with high conversion/breeding ratios. The GIF recognizes this and has included fast neutron spectrum systems for further development.

In addition to the fast reactors within the GIF framework, subcritical systems with external sources, also called hybrid systems, demonstrate significant promise for energy generation as well as an eutron excess which could be used for nuclear waste transmutation [8-12]. Hybrid systems are generally separated into two general concepts that are relevant to the approach used to generate the external source of neutrons. These concepts are: 1) The accelerator driven systems, which combines a particle accelerator with a sub-critical core, and 2) Fusion-fission systems, which take advantage of an intense high-energy fusion neutron source.

Subcritical systems driven by an external neutron source have the ability to achieve extremely high transmutation efficiencies in a single core loading without multiple recycles [13], thus minimizing the handling and storage of nuclear waste, making hybrids highly efficient relative to other waste reduction schemes. In addition, recent developments and advances in the arena of combining neutron-rich fusion with energy-rich fission has made fusion-fission hybrid systems a waste destruction strategy that is considerably less costly than known alternatives [14].

1.2 Objectives

The overall objective of the proposed research is the development of high fidelity nuclear energy system optimization towards an environmentally benign design that is sustainable and provides a secure energy source. System needs and performance requirements that lead to an actinide-free high-level waste assuming partitioning and transmutation will be targeted. The research objectives can be cataloged as follows:

1) Development of Realistic Reactor Core Models:

An integral part of the research is the development of high fidelity whole-core 3D exact geometry models accounting for core physics in the fuel cycle analysis. The modeling approach will be limited to technologically feasible configurations and use hybrid Monte Carlo methods. A major constraint on the computational models will be the computational run time.

2) Code System Integration:

Develop an approach to seamlessly couple the various models that compose the environmentally benign system. The goal being to devise a computational shell that effectively controls the entire set of reactor and component models with control over key user input parameters and the ability to effectively consolidating vital output results into readily usable form for uncertainty/sensitivity analysis and optimization procedures.

3) Uncertainty Quantification (UQ):

Quantify the uncertainties for specific core characteristics that greatly affect performance with respect to nuclear waste minimization and determine which data contribute the most to uncertainty.

4) Optimization Analysis:

High fidelity nuclear energy system multi-objective optimization for minimizing the problematic actinide isotopes as related to long-term repository storage, minimizing used fuel handling issues throughout the process, and at the same time maximizing the efficient use of the fuel component for prolonged usage and sustainability of fuel resources.

5) Environmental Impact Analysis:

Demonstrate the effectiveness of the optimized nuclear energy system as related to environmental impact by drawing comparisons to other proposed advanced fuel cycle schemes and the current once-through fuel cycle.

1.3 Procedures

1.3.1 Nuclear Energy System Setup

In the context of this paper a Nuclear Energy System (NES) is defined as a configuration of nuclear reactors and corresponding fuel cycle components. There are numerous possibilities for nuclear energy systems, many of which have been studied in great detail. The proposed NES has some unique characteristics that set it apart from other systems. It is arranged for minimization or elimination of high-level waste inventories, which is an essential component of publicly acceptable sustainable nuclear energy strategies [15].

The arrangement of the NES is depicted in Figure 1.3. The front-end (mining, milling, enrichment, and fuel fabrication) of the fuel cycle is shown in the top center and follows current practices incorporated and used in the once-through fuel cycle. The only difference is the availability of Depleted Uranium (DU) arising from the reprocessing step, allowing for the recycling of the uranium.

Following the front-end procedures the fuel elements enter the Pressurized Water Reactor (PWR) for reactor operation and power production. When the fuel is exhausted it is removed from the reactor and temporarily stored to allow the used fuel to cool down to the specified limits required before reprocessing can be performed. During reprocessing the fuel is partitioned into three separate streams: 1. Fission Products (FP), 2. Depleted Uranium (DU) and 3. Transuranics (TRU). The FP are conditioned and prepared for long-term High Level Waste (HLW) storage. The DU is stored as Low-Level Waste (LLW) and is also available for recycle. The TRU are fabricated into fuel elements to be recycled in the VHTR, which operates in the Once-Through-Then-Out (OTTO) mode. The fuel is removed from the VHTR once it no longer can sustain criticality. After a decay/cool-down period, the used VHTR fuel is sent to the external source driven subcritical reactor, or High-Energy External Source Transmuter (HEST), where it is transmuted via single pass. After removal, the used HEST fuel is considered HLW and sent to the designated facility for permanent HLW storage.

The material is tracked throughout the NES with emphasis on composition changes within the reactor systems, material streams during reprocessing, and the final affect on HLW waste management strategies. The representative models for the reactor systems and fuel cycle components are stand-alone units that also offer the ability to link each for the purpose of NES uncertainty quantification and optimization procedures.

The proposed advanced NES is anticipated to have a high national and international impact, potentially changing nuclear waste management and reactor deployment paradigms by offering an environmentally benign, sustainable, and secure energy source.

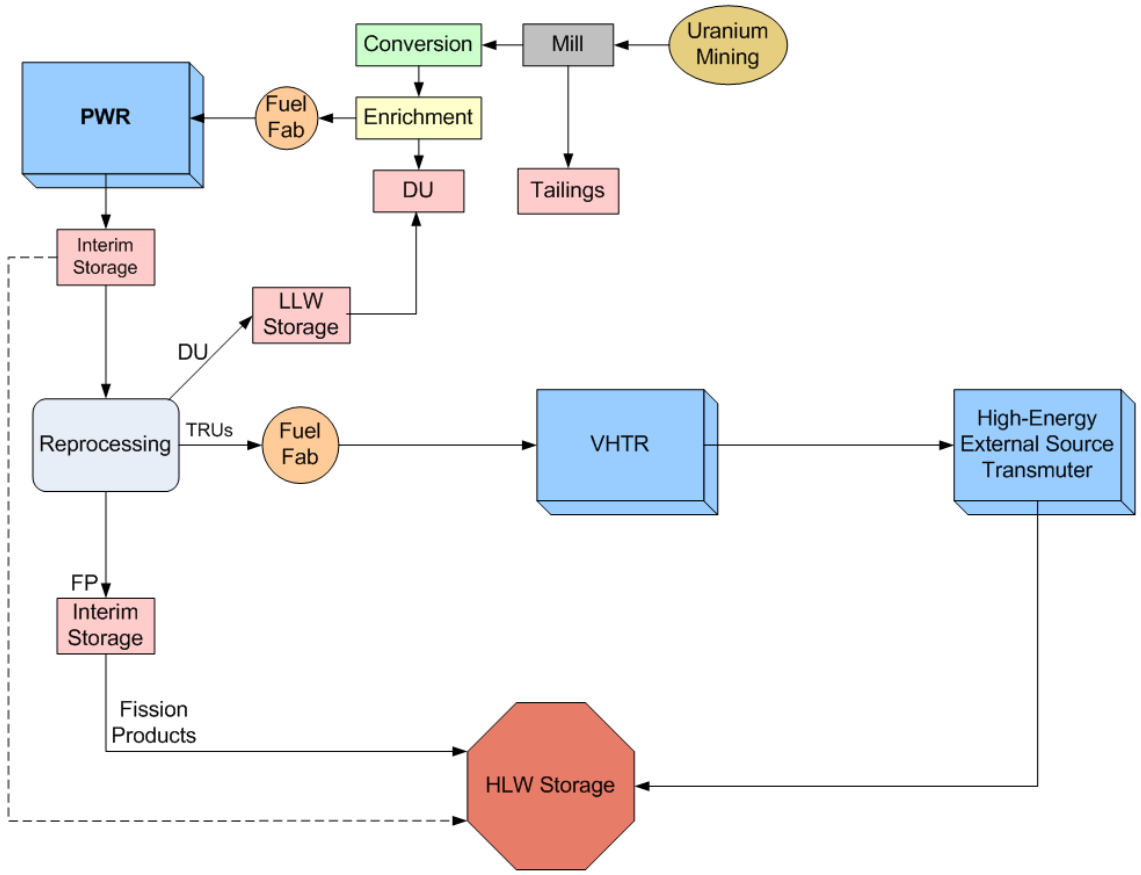

Figure 1.3. Nuclear Energy System Flow Chart.

2 APPLIED CODE SYSTEMS

Modeling and simulation play a critical role in modern scientific and technical endeavors. To the extent that scientific advances are dependent on their effective use. Modeling, theory, and simulation can enhance our understanding of known systems, provide qualitative and quantitative insights into experimental work, guide the choice of the experimental system to study, enable the design of new systems, provide quantitative results to replace experiments, and extend limited experimental data into new domains of parameter space [16]. Due to the difficulties of dealing with radioactive materials, modeling and simulation will play a critical role in advancing nuclear research programs.

Most of the available, well-established, and validated computer code systems are oriented for evaluating light water reactor systems. To apply them for advanced reactor systems a specialized approach of application is required. For instance, previous work has identified insufficiencies in the ability of code systems to accurately account for the multi-heterogeneity effects associated with VHTR systems [17]. Additionally, the modeling of subcritical systems with external sources present challenges involved with accounting for the introduction of a neutron source inside a multiplying media. The neutron kinetic characteristics of subcritical, source-driven cores, as well as the mathematical methods to treat their temporal behavior, are markedly different from those of critical cores [18]. Also, a reliable and consistent procedure for coupling the reactors and other fuel cycle components, while preserving and producing key component parameters, must be approached with great care.

Uncertainty quantification (UQ) is a key component for successfully meeting the overall objectives of the proposed research work. UQ is the science of combining imperfect information from multiple sources to reach conclusions and to evaluate the validity of the conclusions. UQ is thus concerned with the transformation from data to knowledge to decisions. It defines the link between science and the decision process. UQ starts with the identification and characterization of error or uncertainties from all steps in the sequence of approximation that leads to a computational model prediction. UQ uses techniques from fields such as statistics and optimization to determine the sensitivity of models to inputs with errors, and to design models in order to minimize the effect of the errors. Integrating uncertainty quantification approaches into simulation allows potentially more efficient interrogation of parameter dependencies and model certainties [19].

2.1 Code Systems

State-of-the-art computer code systems were utilized to create realistic high fidelity 3D whole-core models representing the reactors and fuel cycle components that compose the NES. A collection of diverse code systems were selected based on their ability to meet the outlined research objectives and the capabilities and limitations accompanying each.

The Monte Carlo based code (MCNP) was heavily utilized for creating the 3D whole-core models representing the reactor units in the NES. Functional modules within the Standardized

Computer Analysis for Licensing Evaluation (SCALE) code system were used to model the HLW facility and for 3D whole-core modeling. The front-end components were modeled using the Nuclear Fuel Cycle Simulation System (NFCSS). The MATrix LABoratory MATLAB/Simulink computational environment was utilized to model the reprocessing facility and provided the means for developing an integrated system model representing the NES.

2.1.1 MCNP

Monte Carlo N-Particle (MCNP) is a general purpose code that can be used for neutron, photon, electron, or coupled neutron/photon/electron transport. MCNP is the internationally recognized code for analyzing the transport of neutrons and gamma rays, and is developed and maintained by Los Alamos National Laboratory.

MCNP5

MCNP is a code that is continuously undergoing development at Los Alamos national Laboratory and has periodic releases. The distinction of the number 5 in MCNP5 is for identifying the version of MCNP. The current release (2010) is version MCNP5 (1.51). MCNP5 is very versatile due to important standard features such as: multiple source description options, flexible tally structure, an extensive collection of cross section data, large collection of variance reduction techniques, and geometry and output tally plotters. Neutron energy ranges in MCNP5 are limited to that of 10^{-11} to 20 MeV [20, 21].

MCNPX

The code system MCNPX (Monte Carlo N-Particle eXtended) extends the capabilities of MCNP4C3 to nearly all particles, nearly all energies, and to nearly all applications without an additional computational time penalty. It is fully 3D and time dependent, and uses up to date nuclear cross section libraries and physics models for particle types and energies where tabular data are not available. MCNPX version 2.6.0 includes depletion/burnup/transmutation capability that is limited to criticality calculations [22].

MAKXSF

The MAKXSF code is part of the MCNP5/MCNPX distribution, but is run external to MCNP. MAKXSF is a utility program for manipulating cross section library files for use in MNCP5. The basic functions performed by MAKXSF include: changing the format of cross section libraries, copying entire libraries to new files or to copy selected nuclide data sets to new libraries, and to create nuclide datasets at new temperatures, resulting in a temperature dependent library for specific application [23].

Capabilities of MAKXSF for creating nuclide datasets at a new temperature involves three operations: 1) Doppler broadening of resolved data to any higher temperature, 2) Interpolation of unresolved resonance data between datasets at two different temperatures, and 3) Interpolation of thermal scattering kernels ($S(\alpha,\beta)$ data) between datasets at two different temperatures.

2.1.2 SCALE

The Standardized Computer Analysis for Licensing Evaluation (SCALE) code system serves in conjunction with MCNP to provide code-to-code benchmarking when applicable and for additional analysis beyond that of MNCP. SCALE is developed and maintained by Oak Ridge National Laboratory (ORNL) and is widely accepted around the world for criticality safety analysis, radiation source term and shielding, problem dependent resonance self-shielding of cross section data, sensitivity and uncertainty, and reactor physics analysis [24].

KENO-VI

KENO-VI is a functional module in the SCALE system. It is a mutigroup Monte Carlo code applied to determine the effective multiplication factor (k_{eff}) for three-dimensional systems. The geometry package in KENO-VI is capable of modeling any volume that can be constructed using quadratic equations [25].

ORIGEN-S

ORIGEN-S is a depletion and decay module in the SCALE code system, and it can be called from a control module or run as a stand-alone program. ORIGEN-S computes time-dependent concentrations and radiation source terms which are simultaneously generated or depleted through neutronic transmutation, fission, and radioactive decay [26]. In relation to this report, ORIGEN-S was used in stand-alone mode for calculating spent fuel radiotoxicities and decay heat terms as a function of time for the TRU nuclides and fission products.

2.1.3 NFCSS

The International Atomic Energy Agency's (IAEA) simulation system, Nuclear Fuel Cycle Simulation System (NFCSS) was used to model fuel cycle components of the NES. NFCSS is a scenario based computer model for the estimation of nuclear fuel cycle material and service requirements. It has been designed to quickly estimate long-term fuel cycle requirements and actinide production. Natural uranium, conversion, enrichment, and fuel fabrication quantities are predicted. Additionally, the quantities and qualities (isotopic composition) of unloaded fuels are evaluated.

The IAEA developed CAIN (CAlculation of Inventory of spent fuel) specifically for the needs of NFCSS. CAIN solves the Bateman's Equations for a point assembly using one group neutron cross sections. In order to meet the accuracy, simplicity, and speed requirements a set of assumptions were built into the code. CAIN currently has 28 reaction and decay chains during irradiation and 14 decay chains during cooling [27].

2.1.4 MATLAB/Simulink

MATrix LABoratory (MATLAB) first appeared in the late 1970s and was originally designed to simplify the implementation of numerical linear algebra routines [28]. MATLAB has since grown into something much bigger, and it is continually developed by the MathWorks Corporation. It is both a powerful computational environment and a programming language that easily handles matrix and complex arithmetic. Typical uses include math/computation, algorithm development, modeling, simulation/prototyping, data analysis, exploration, visualization, scientific graphics, and application development.

Simulink works with MATLAB to offer modeling, simulation, and analysis of multidomain dynamic systems under a graphical user interface environment. Simulink includes a comprehensive set of customizable block libraries for both linear and nonlinear analyses. As Simulink is an integral part of MATLAB, it is easy to switch back and forth during analysis making it possible to take advantage of the features offered in each environment. The available options and flexibility of MATLAB/Simulink make it an ideal candidate for developing an integrated system model representing the NES.

The numerical computing environment and programming language MATLAB serves as the shell, or driver, for the simulated nuclear energy system by interfacing the configuration of nuclear reactors and corresponding fuel cycle components. Simulink, an extension of MATLAB, is utilized for storing system output results and parameters, tracking material streams, data processing, and predicting system performance throughout the NES. The sensitivity/uncertainty analysis and optimization techniques are developed and implemented within the MALAP/Simulink environment.

3 TRU CHARACTERIZATION

The tracking and analysis of the transuranic elements (TRU: *Np*, *Pu*, *Am*, *Cm*) are a key aspect of the project. The TRU inventory is responsible for the long-term heat generation and radiotoxicity that accompanies used nuclear fuel. High-level nuclear waste repository performance parameters are dependent on the TRU composition, which presents challenges for effectively isolating nuclear waste in order to ensure the safety of the public and to protect the surrounding environment. Therefore, focus is placed on the destruction of the TRU stream as a means to alleviate problematic aspects of waste management and to strengthen support for nuclear fission as a future source for clean, sustainable, and environmentally friendly energy production.

Through reprocessing and partitioning techniques the TRU stream can be separated from the other elements present in used nuclear fuel [29]. As a group, the TRU elements exhibit neutronic properties that make them an ideal fuel component that can be taken advantage of by thermal neutron and fast neutron spectrum reactor systems by way of high burnup cores [30,31]. Consequently, the TRU inventory can be considered a valuable fuel resource and if utilized to its potential, nuclear energy can greatly strengthen its position as a sustainable and secure energy source.

3.1 High-Level Waste Management

The top priority in managing radioactive waste is to protect human health and the environment, now and in the future, without imposing undue burdens on future generations. There are a number of different strategies to achieve this end goal, but no matter what the approach, they all have one thing in common, and that is the need to contain and isolate the waste from interacting with the biosphere until it has decayed to harmless levels. Currently the most studied and accepted long-term isolation technique is deep geological disposal.

3.1.1 Geological Disposal

Repositories are normally sited in stable geological environments that offer favorable conditions in which the waste and engineered barriers are protected over a long time period [32]. Key characteristics such as mechanical stability, low groundwater flux, and favorable geochemical conditions that are unlikely to change significantly over relevant timescales at targeted. Currently four types of geological formations are considered as possible candidates for deep disposal of long-lived radioactive waste:

- Hard rock formations, mainly granite;
- Argillaceous formations, clays and mudstones;
- Salt formations, salt domes and salt layers;
- Volcanic formations, tuff and basalt (Yucca Mountain).

Generally, the HLW isotopic compositions resulting from the typical LWR operating on the once through fuel cycle are used to assess repository performance. The compositions along with the type of geological formation and the design details of the repository will set the limits on the amount of HLW that can be stored at any one site. Although there are countless design and locational possibilities, in each case, the maximum HLW allowance will be constrained by just a few common limiting factors. The two major constraints are temperature limits and peak dose rate for repository releases to satisfy regulatory limits.

Results from previous studies have shown that maximum allowable disposal density for a repository is determined mainly by thermal limitations [33]. The removal of TRU elements from the waste stream has a large impact on the long-term (>300 years) heat generation and can significantly increase the amount of allowable waste within a geological repository [33]. As for the maximum dose rate, removal of the TRU inventory does not have much impact on the allowable disposal density, but it does drastically affect the timescale for which the repository must function. Elimination of the long-lived radioactive TRU nuclides reduces the storage timescale from the 100,000 year timeframe to hundreds of years.

By targeting the transmutation of the TRU nuclides that are intense long-lived sources of decay heat and dose rates accomplishes two main goals: 1) more efficient use of the available space within the repository allowing for greater quantities of HLW to be safely stored, and 2) decreasing the amount of time the HLW must be isolated from the biosphere.

3.2 TRU Origins and Constituents

During the operation of a nuclear reactor the composition of the fuel is constantly changing as various fuel nuclei are transmuted by neutron capture and subsequent decay. It is this process through which the TRU inventory is created and subsequently utilized as a fuel component and ultimately destroyed by fission. Within the front-end procedures of the NES uranium ore is mined, milled, converted, enriched, and then fabricated into fresh UO_2 fuel elements for use in the PWR. Once the PWR begins operation, the creation of the TRU nuclides begins. The fresh UO_2 contains uranium that is slightly enriched in ^{235}U (3-6%) and the remaining uranium is made up of ^{238}U (94-97%). It is ^{238}U that is almost entirely responsible for TRU production, which starts with the neutron capture of ^{238}U producing ^{239}U, which is very unstable and quickly beta-decays to ^{239}Np which likewise quickly beta-decays to the more stable ^{239}PU isotope, as shown below.

$$^{238}U + n \rightarrow {}^{239}U \xrightarrow{\beta^-} {}^{239}Np \xrightarrow{\beta^-} {}^{239}Pu$$

The remaining TRU vector is populated by subsequent neutron captures and isotopic decay. The composition of the TRU inventory is changing constantly and at any particular time is dependent on many factors, such as: initial enrichment, neutron flux, fuel burnup, and LWR operational parameters. Upon removal from a typical LWR the fuel contains roughly 95% uranium, 4% fission products, and 1% TRU. The TRU elements have the approximate composition of 90% *Pu*, 5% *Np*, 4% *Am*, and 1% *Cm*. Figure 3.1 shows the important actinide nuclides and their relations as related to neutron absorption events, beta-decay, and alpha-decay. The nuclide half-

life values and thermal energy neutron cross-sections for radiative capture (σ_c) and fission (σ_f) are displayed. The figure is also color coded to emphasize important nuclide characteristics as related to thermal neutron spectrum reactor systems.

Initially ^{235}U is the fissile component of the fuel that allows the reactor to achieve and maintain criticality. As time progresses the ^{235}U is depleted, but simultaneously the fissile isotopes ^{239}Pu and ^{241}Pu are created in the core. In some reactors, although not today's LWR, the core will eventually reach a point where criticality becomes more heavily dependent on the fissile *Pu* isotopes than ^{235}U, and eventually the accumulation of neutron absorbers and the depletion of fissile inventory will cause the reactor to no longer be able to maintain criticality. At this point reactor fuel will have to be replaced with fresh fuel to continue operating.

By referring to Figure 3.1 a few general conclusion can be made about the TRU composition resulting from the irradiation of fresh UO_2 in PWR reactors. To begin with, *Pu* will always have the highest composition percentage, as it is a direct product from neutron capture in ^{238}U, which makes up well over 90% of the fuel. Similarly, *Cm* having the greatest number of protons (Z) in the nucleus will take the most interactions to be formed, thus *Cm* will always have the lowest composition percentage. Also, for thermal neutron fluxes, most of the TRU nuclides have much greater probability to undergo the radiative capture reaction (n,γ) than the fission reaction (n,f). This indicates that, for thermal flux reactors, the longer the fuel is under irradiation, more higher actinides (esp., *Am* and *Cm*) will accumulate in the core.

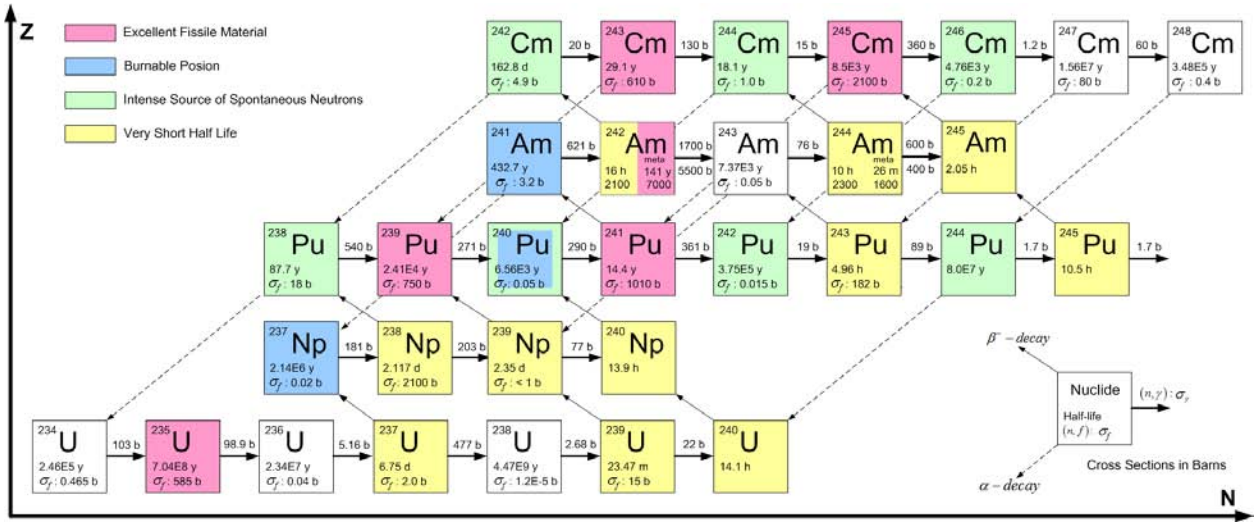

Figure 3.1. Transmutation and Decay Schemes for Important Nuclides.

Table 3.1 is provided as an example of the TRU compositions upon removal from the core. The compositions are representative of a single pass fuel scheme for the AP1000, operating on 4% Low Enriched Uranium (LEU) fuel and irradiated to a burnup level of 40 GWd/tIHM.

Table 3.1. TRU Composition after Irradiation in PWR.

Nuclide	TRU (%)	Nuclide	TRU (%)
^{237}Np	4.68	^{241}Am	0.32
^{238}Np	0.014	^{242m}Am	1.29×10^{-3}
^{239}Np	0.93	^{243}Am	0.83
^{238}Pu	1.37	^{244}Am	7.43×10^{-4}
^{239}Pu	49.69	^{242}Cm	0.14
^{240}Pu	24.37	^{243}Cm	2.57×10^{-3}
^{241}Pu	12.10	^{244}Cm	0.31
^{242}Pu	5.23	^{245}Cm	0.015
^{243}Pu	1.29×10^{-3}	^{246}Cm	1.53×10^{-3}
^{244}Pu	1.56×10^{-4}	^{247}Cm	1.27×10^{-5}

3.3 TRU Isotopic Assessment

The TRU nuclides are evaluated considering the objective of utilizing the TRU inventory as a fuel resource while at the same time seeking to eliminate TRU isotopes that present dangers to the environment and challenges for long-term HLW storage. To accomplish this, individual nuclides are assessed accordingly. Important parameters such as decay heat generation, radioactivity, dose measurements, nuclide lifetimes, and TRU composition are all taken into consideration.

Table 3.2 list parameters, with respect to waste management, that are essential for identifying and ranking the TRU nuclides. One important parameter is radiotoxicity, which is the measure of how nocuous a radionuclide is to human health. The type and energy of rays, absorption in the organism, residence time in the body, etc. influence the degree of radiotoxicity of a radionuclide. The measure of radiotoxicity is very useful for comparing the radiological hazard of different nuclides. Radiotoxicity of the TRU nuclides are determined by using the effective dose coefficients, $e(\tau)$, provided by the International Commission on Radiological Protection (ICRP) [34] and the activity of the isotope of interest. The dose coefficients are applicable for intake by ingestion for adult humans, $e_{ing}(50)$.

Each of the parameters in Table 3.2 are useful in determining what affect each of the TRU nuclides might have on long-term HLW management issues and dangers posed to the environment. The half-life gives a measure of the stability of the isotope and an idea of the timeframe involved with isolating it from the biosphere. The isotopic power relates the amount of decay heat that will be generated and which nuclides present the greatest challenge for meeting repository thermal limits. The radiotoxicity measures how dangerous each radionuclide potentially is to the environment. Related to radiotoxicity, but not included in the calculation, is

the neutron emission originating from (α,n) reactions and spontaneous fission, which is particularly high for a few of the nuclides and can present additional challenges for dealing with HLW. The provided TRU fraction is representative of the used fuel for a PWR, 4% enriched LEU fuel, and 5 years decay time.

Table 3.2. TRU Isotopic Parameters Related to Waste Management.

Nuclide	Half-life (yr)	Iso. Power (w/gm)	Sp. Act. (Ci/gm)	Radiotoxicity (Sv/gm)	Neutron yield (n/g s)	TRU Fraction (%)
^{237}Np	2.14×10^{6}	2.20×10^{-5}	7.05×10^{-4}	2.87	5.11×10^{-5}	4.28
^{238}Pu	87.7	0.568	17.1	1.46×10^{5}	2.60×10^{3}	1.21
^{239}Pu	2.41×10^{4}	1.91×10^{-3}	0.062	574	0.017	52.26
^{240}Pu	6.54×10^{3}	7.10×10^{-3}	0.227	2.10×10^{3}	1.03×10^{3}	24.47
^{241}Pu	14.4	4.06×10^{-3}	103	1.80×10^{4}	9.19×10^{-4}	9.27
^{242}Pu	3.76×10^{5}	1.13×10^{-4}	3.95×10^{-3}	35.1	1.72×10^{3}	4.79
^{244}Pu	8.26×10^{7}	5.30×10^{-7}	1.83×10^{-5}	0.163	1.94×10^{3}	1.30×10^{-4}
^{241}Am	432	0.115	3.43	2.54×10^{4}	1.36	2.80
^{242m}Am	152	4.65×10^{-3}	10.5	7.37×10^{4}	159	1.46×10^{-3}
^{243}Am	7.38×10^{3}	6.42×10^{-3}	0.20	1.48×10^{3}	0.714	0.71
^{242}Cm	0.446	122	3.31×10^{3}	1.47×10^{6}	1.89×10^{7}	5.44×10^{-5}
^{243}Cm	28.5	1.90	51.6	2.87×10^{5}	0.017	1.79×10^{-3}
^{244}Cm	18.1	2.83	80.9	3.60×10^{5}	1.12×10^{7}	0.19
^{245}Cm	8.50×10^{3}	5.89×10^{-3}	0.17	1.33×10^{3}	38.7	0.01
^{246}Cm	4.73×10^{3}	0.010	0.31	2.39×10^{3}	8.80×10^{6}	9.53×10^{-4}

Although the above-mentioned parameters assist in assessing the TRU nuclides, it is difficult to perform a fair comparison because many of the parameters are interrelated. As example, ^{242}Cm has extremely high radiotoxicity and thermal heat output; therefore, one would assume it would dominate long-term HLW storage issues. But ^{242}Cm also has a relatively short half-life and makes up only a small fraction of the TRU inventory, and when this is taken into consideration, other radionuclides will be much more important.

In order to better compare the TRU nuclides a method was developed to combine certain parameters by weighting factors and then normalize the final result. As established previously, the two major concerns are thermal heat sources and dose rates so a factor was determined for each case. For the dose rate a Normalized Radiotoxicity Factor (NRF) for each nuclide is calculated by:

$$RF_i = \left[e_{ing}(50)\right]_i \cdot SA_i \cdot w_{Comp,i} \cdot w_{T_{1/2},i} \quad (1)$$

$$NRF_i = \frac{RF_i}{RF_{\max}} \quad (2)$$

where RF_i is the radiotoxicity factor for nuclide i, $[e_{ing}(50)]_i$ is the effective dose coefficient, SA_i is the specific activity, $\omega_{comp,i}$ is the weighting factor for composition, $\omega_{T1/2,i}$ is the weighting

factor indicating nucleus stability, and RF_{max} is the maximum radiotoxicity factor among the TRU isotopes. Similarly, for the thermal heat source a Normalized Heat Factor (NHF) for each nuclide is calculated by:

$$HF_i = P_i \cdot w_{Comp,i} \cdot w_{T_{1/2},i} \quad (3)$$

$$NHF_i = \frac{HF_i}{HF_{\max}} \quad (4)$$

where HF_i is the heat factor for nuclide i, P_i is the isotopic power, and HF_{max} is the maximum heat factor for the evaluated TRU nuclides.

Table 3.3 is a collection of the normalized heat and radiotoxicity factors as determined first without weighting, then with composition weighting only, and finally with combined composition and half-life weighting. A factor of 1 indicates the nuclide that most strongly affects that particular measure. As the factor approaches zero it becomes more and more benign as related to the determining parameters. The factor for isotopic power and radiotoxicity only takes into account the individual isotope without regard to timescale. The composition weighting factor takes it a step further by incorporating the quantity of the nuclide relative to the rest of TRU stream. The remaining factor is weighted by half-life and the composition; therefore, taking into account not only the makeup of the TRU inventory but also how long the radionuclide needs to be isolated from the biosphere.

Table 3.3. Normalized Heat and Radiotoxicity Factors.

Nuclide	Normalized Heat Factor			Normalized Radiotoxicity Factor		
	Isotopic Power	Comp. Weighted	Comp./ $T_{1/2}$ Weighted	Isotopic Radiotoxicity	Comp. Weighted	Comp./ $T_{1/2}$ Weighted
^{237}Np	1.80×10^{-7}	1.38×10^{-4}	0.084	1.95×10^{-6}	7.00×10^{-5}	0.036
^{238}Pu	4.66×10^{-3}	1.00	0.025	0.099	1.00	0.021
^{239}Pu	1.57×10^{-5}	0.15	1.00	3.90×10^{-4}	0.17	1.00
^{240}Pu	5.82×10^{-5}	0.25	0.47	1.43×10^{-3}	0.29	0.46
^{241}Pu	3.33×10^{-5}	0.055	2.25×10^{-4}	0.012	0.95	3.32×10^{-3}
^{242}Pu	9.26×10^{-7}	7.91×10^{-4}	0.084	2.34×10^{-5}	9.58×10^{-4}	0.087
^{244}Pu	4.34×10^{-9}	1.01×10^{-10}	2.37×10^{-6}	1.11×10^{-7}	1.21×10^{-10}	2.42×10^{-6}
^{241}Am	9.39×10^{-4}	0.47	0.057	0.017	0.40	0.042
^{242m}Am	3.81×10^{-5}	9.93×10^{-6}	4.29×10^{-7}	0.050	6.13×10^{-4}	2.26×10^{-5}
^{243}Am	5.26×10^{-5}	6.67×10^{-3}	0.014	1.00×10^{-3}	5.98×10^{-3}	0.011
^{242}Cm	1.00	9.70×10^{-3}	1.23×10^{-6}	1.00	4.56×10^{-4}	4.94×10^{-8}
^{243}Cm	0.016	4.98×10^{-3}	4.03×10^{-5}	0.19	2.92×10^{-3}	2.02×10^{-5}
^{244}Cm	0.023	0.80	4.10×10^{-3}	0.24	0.39	1.73×10^{-3}
^{245}Cm	4.83×10^{-5}	8.61×10^{-5}	2.08×10^{-4}	9.07×10^{-4}	7.60×10^{-5}	1.57×10^{-4}
^{246}Cm	8.20×10^{-5}	1.39×10^{-5}	1.87×10^{-5}	1.62×10^{-3}	1.30×10^{-5}	1.49×10^{-5}

The normalized radiotoxicity factors are represented graphically in Figure 3.2, giving a side-by-side comparison of each of the TRU nuclides. The radiotoxicity scale on the vertical axis is logarithmic, indicating that differences can be very large and even extent to many orders of magnitude in some cases. The radiotoxicity measure (yellow bar) shows that ^{242}Cm, ^{243}Cm, and ^{244}Cm are ranked the most toxic, with ^{238}Pu and ^{242m}Am the highest among the other TRU nuclides. Also of note are the very small radiotoxicity factors for ^{237}Np and ^{244}Pu, which are each over 6 orders of magnitude lower than the most toxic isotope.

When the relative quantity of each nuclide is taken into consideration, in most cases, the radiotoxicity factor (blue bar) changes quite drastically. Due to their small quantities, the radiotoxic factors for the *Cm* isotopes drop considerably with the exception of ^{244}Cm, which is still one of the highest radiotoxicity contributors. The *Pu* isotopes, with exception of ^{242}Pu and ^{244}Pu, now reach the highest levels. ^{244}Cm and ^{241}Am are also marked as major contributors with high radiotoxicity factors.

Considering the length of time that which the nuclides will remain highly radiotoxic (red bar), the factors again change, and is most noticeable by the decrease in the *Cm* factors due to their relatively short half-lives. The dominant nuclides are now ^{239}Pu, ^{240}Pu, ^{242}Pu, and ^{241}Am, as they will remain at high radiotoxicity levels for many years into the future.

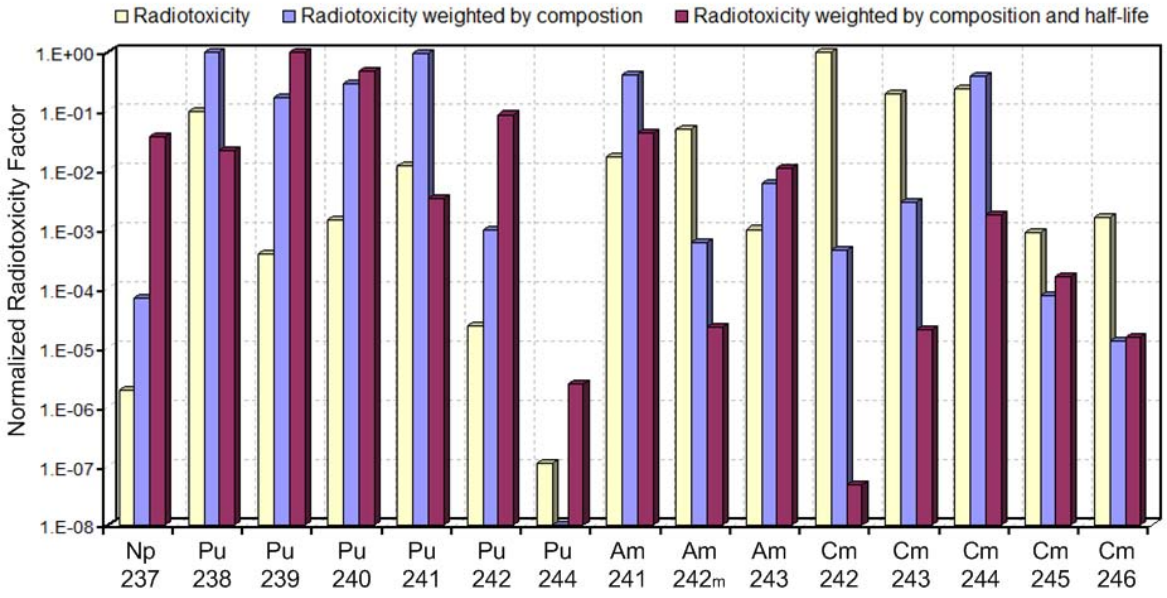

Figure 3.2. Normalized Radiotoxicity Factors.

The normalized heat factors are represented graphically in Figure 3.3, giving a side-by-side comparison of each of the TRU nuclides. Many of the same trends identified with the radiotoxicity factors are seen with the heat factors. The thermal heat scale on the vertical axis is logarithmic, indicating that differences can be very large and even extent to many orders of magnitude in some cases. The heat load measure (yellow bar) shows that ^{242}Cm, ^{243}Cm, and

^{244}Cm produce the most decay heat, with ^{238}Pu and ^{242m}Am close behind. Comparatively, ^{237}Np and ^{244}Pu produce minimal amounts of decay heat.

Once the composition of the TRU stream is taken into account the heat factors (blue bar) for the *Pu* isotopes increase drastically. Now the largest decay heat contributors in descending order are ^{238}Pu, ^{244}Cm, ^{241}Am, ^{240}Pu, ^{239}Pu, and ^{241}Pu. With respect to decay heat, the major concern is repository thermal limits, which deals with maximum heat levels. Therefore, the timescale on which the TRU inventory produces heat is not as important as they were in the case of radiotoxicity factors. Still the half-life weighted heat factors (red bar) are included because they offer additional insight that could prove to be useful once more details concerning the design of the repository are available. Such would be the case for natural or forced ventilation designs that would be operated for a specified number of years, or for permanent closure dates that would affect heat removal capabilities within the repository.

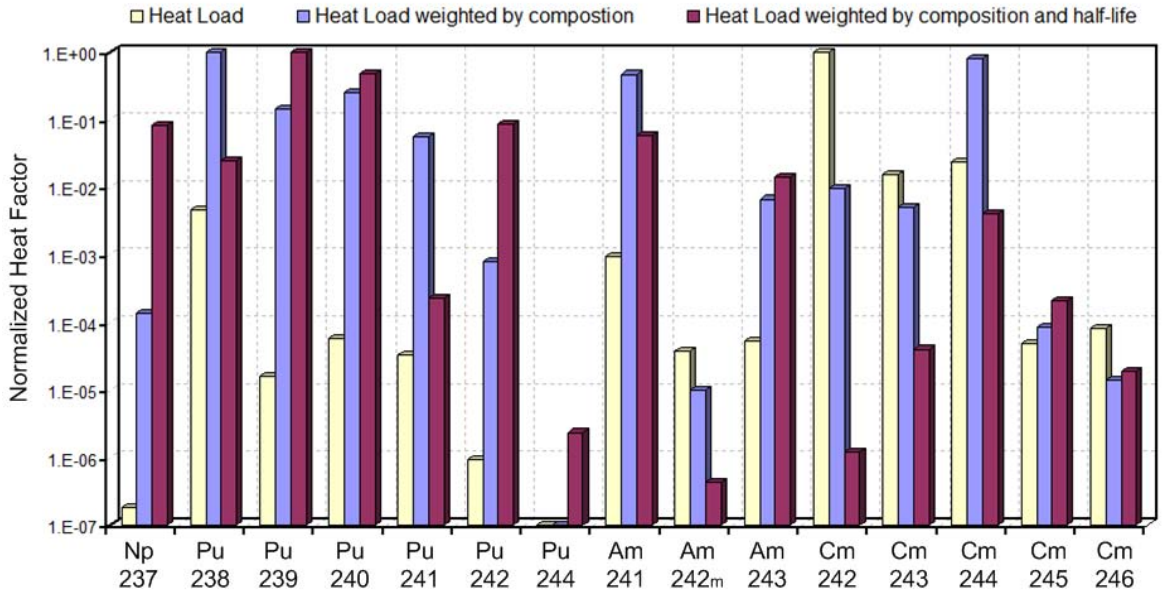

Figure 3.3. Normalized Heat Factors.

A few primary conclusions can be made from Figures 3.1, 3.2, and 3.3. First, the *Pu* isotopes as a whole are the most significant radiotoxicity and decay heat contributors, which can be explained by the high composition percentage of *Pu* in the TRU stream. In any case the *Pu* isotopes should be targeted for destruction by fission. The *Cm* group are very strong heat sources and extremely radiotoxic, but their small fraction of the TRU inventory and shorter half-lives rank them behind a number of the *Pu* and *Am* nuclides. Even so, *Cm* and, in particular, the longer-lived isotopes and ^{244}Cm, need to be monitored closely because irradiating TRU fuels in a thermal neutron spectrum (as is the case with the VHTR component of the NES) will result in a buildup of the *Cm* inventory. In addition, ^{242}Cm, ^{244}Cm, and ^{246}Cm have very high neutron emission rates that cause additional burdensome radiation issues separate from those included in the radiotoxicity calculation.

A phenomenon that does not manifest itself in the heat factor or the radiotoxicity factor calculations is the production of ^{241}Am ($T_{1/2}$ = 432.7 years) from the beta-decay of ^{241}Pu ($T_{1/2}$ = 14.4 years). For a substantial time into the future the radiotoxicity levels and decay heat generated by ^{241}Am will increase and needs to be considered when evaluating ^{241}Am. Similarly, but not as crucial, ^{237}Np ($T_{1/2}$ = 2.14 + 10^6 years) is produced by the alpha-decay of ^{241}Am ($T_{1/2}$ = 432.7 years).

3.3.1 Neptunium

Neptunium, named for the planet Neptune, was the first synthetic transuranic element of the actinide series discovered (1940) [35]. *Np* metal has a silvery appearance, is chemically reactive, and very dense at 20.25 g/cm^3. Nineteen *Np* radioisotopes have been characterized ranging from ^{226}Np to ^{244}Np. The most stable of the isotopes is ^{237}Np with a half-life of 2.14 million years, followed by ^{236}Np with a half-life of 154,000 years, and then ^{235}Np with a half-life of 396.1 days. The remaining isotopes are very short-lived with half-lives less than 4.5 days with a majority of them being less than 50 minutes.

As indicated by the transmutation-decay scheme in Figure 3.1, ^{237}Np and ^{239}Np are mainly produced by the beta-decay of ^{237}U and ^{239}U, and subsequently ^{238}Np and ^{240}Np are produced by neutron capture in ^{237}Np and ^{239}Np. Even so, ^{237}Np is the only neptunium isotope stable enough to accumulate to any meaningful amount within the core or shortly after removal. Also of interest is the alpha-decay of ^{241}Am to ^{237}Np, which can affect long-term waste management issues as it builds on the ^{237}Np inventory. Compared to the other TRU isotopes, ^{237}Np has one of the longest half-lives, indicating it will be around after many of the other isotopes have decayed away. Both the radiotoxicity and decay heat of ^{237}Np is much less than that of the other TRU nuclides.

Neptunium-237

The incore transmutation of ^{237}Np will greatly depend on the neutron energy spectrum. In a thermal neutron spectrum system, like the VHTR, the predominant reaction will be neutron capture and ^{237}Np will mainly contribute to the buildup of higher actinides. In the HEST, or fast neutron spectrum system, there is a much higher probability for fission and the contribution to production of higher actinides will be reduced.

Figure 3.5 shows the radiative capture and fission cross-sections along with the capture-to-fission ratio (α) for ^{237}Np. In TRU-fueled reactors there is minimal production of ^{237}Np. Therefore, in any neutron spectrum ^{237}Np will be depleted under irradiation conditions, and can be represented by the following relation:

$$\frac{dN_{Np237}}{dt} = -\left[N \cdot \sigma_a\right]_{Np237} \phi \qquad (5)$$

where N is the nuclide concentration, σ_a is the absorption cross section ($\sigma_c + \sigma_f$) and Φ is the neutron flux.

The difference between thermal neutron and fast neutron spectrums is the mode of transmutation, whether it is by neutron capture or by fission. As indicated by Figure 3.4, a thermal neutron spectrum system will transmute predominately by capture, while a fast neutron spectrum will increase the amount of fissions in relation to capture. The capture-to-fission ratio does not drop below unity until about 5.5×10^5 *eV*, which means in order to preferentially destroy ^{237}Np by fission, a very high neutron energy spectrum would be needed.

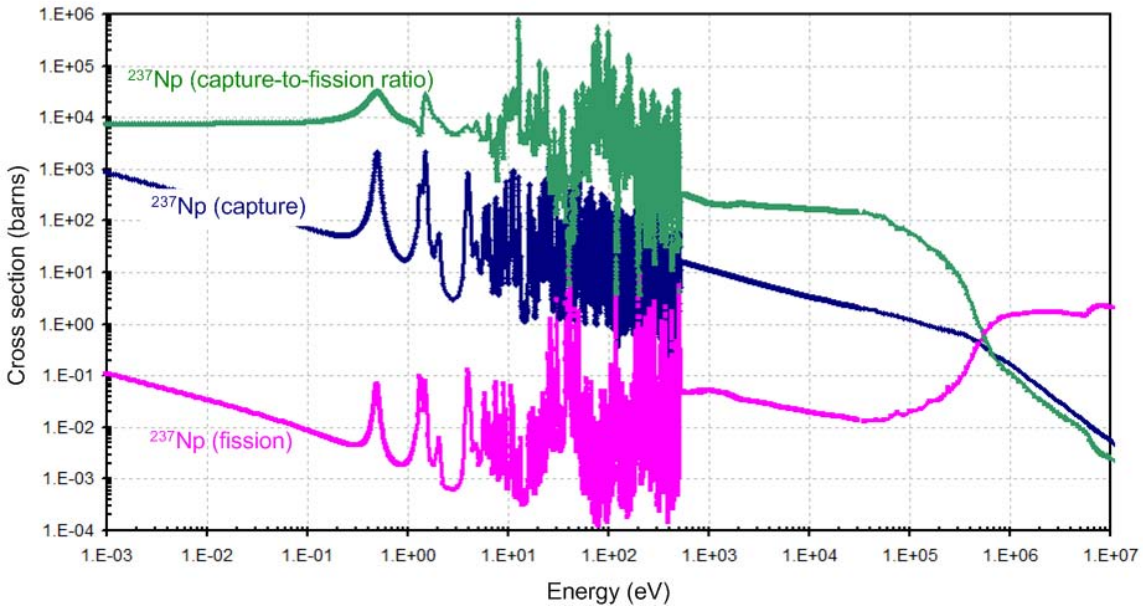

Figure 3.4. Cross-sections and Capture-to-fission Ratio for ^{237}Np.

3.3.2 Plutonium

Plutonium, named for the planet Pluto, was the second synthetic transuranic element of the actinide series discovered (1940) [35]. *Pu* metal has a silvery-white appearance that tarnishes when exposed to air, forming a dull coating when oxidized. It has a density of 19.816 g/cm^3. Twenty *Pu* radioisotopes have been characterized ranging from ^{228}Pu to ^{247}Pu. The most stable of the isotopes is ^{244}Pu with a half-life of 80 million years; long enough to be found in trace quantities in nature. Most important of the isotopes is ^{239}Pu because today it exists in much higher quantities than the other isotopes and it is a key component in nuclear weapon development and nuclear energy. *Pu* is the most prominent of the TRU elements, mainly because of its link to atomic bombs, but also because it has a number of other applications, such as radioisotope thermoelectric generators, radioisotope heater units, and as a power source for artificial heart pacemakers.

There are five *Pu* isotopes (^{238}Pu – ^{242}Pu) that pose environmental dangers and are of main concern for long-term HLW waste management and incore behavior. When UO_2 fuel is irradiated in PWRs the resulting TRU composition at the end of irradiation is mostly composed of *Pu* (~90%). Due to the large quantities of *Pu* relative to the other TRU nuclides, the *Pu* isotopes are exceedingly important for reactor core performance and afterward for long-term

waste management. The NES incorporates the VHTR for the first recycle of the TRU fuel produced by the LWR. Being a thermal neutron spectrum reactor the VHTR relies on the fissile components of the fuel to achieve and maintain criticality, ^{239}Pu and ^{241}Pu fill that role. In particular, ^{239}Pu, alone accounts for about 40-50% of the total composition of the TRU nuclides. A good indicator for the achievable burnup level of the VHTR core is the combined ^{239}Pu and ^{241}Pu composition. With this in mind, the relatively short half-life of ^{241}Pu (14.4 years) will have a noticeable affect on the *Pu* composition during the stage when the TRU is out of core. The transit time can be four or more years as cooling is required before entering the reprocessing stage and time needed to fabricate the fuel. During this time period significant amounts of ^{241}Pu will decay by beta particle emission to ^{241}Am, which translates to a decrease in the fissile inventory and an increase in the fertile inventory; having a considerable effect on reactor performance.

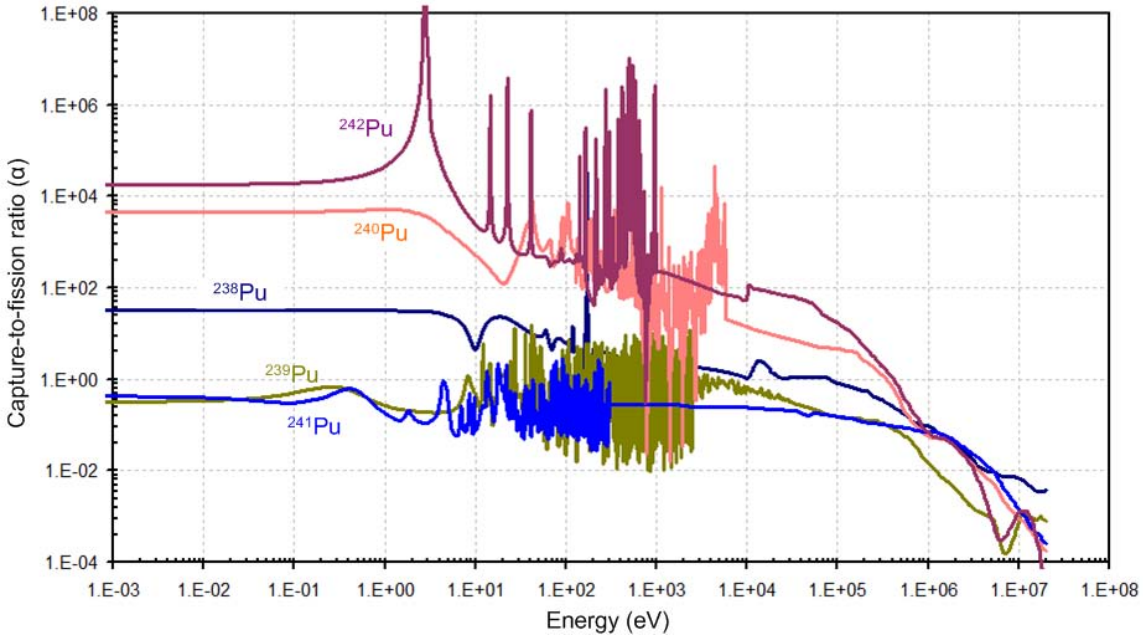

Figure 3.5. Capture-to-fission Ratio for *Pu* Isotopes.

Figure 3.5 shows the capture-to-fission ratio for the *Pu* isotopes. As indicated the two isotopes with higher fission than capture cross-sections throughout the entire spectrum are ^{239}Pu and ^{241}Pu. Whereas, ^{238}Pu, ^{240}Pu, and ^{242}Pu all have much greater probability of radiative capture in the thermal and resonance energy regions. Capture-to-fission ratios greater than unity are of high importance because of the buildup of higher actinides that accompany them. This is especially true for *Pu* as it dominates the TRU vector and can lead to the buildup of problematic *Am* and *Cm* isotopes.

Estimations for the isotopic production and destruction/transmutation rates for the *Pu* nuclides under irradiation in thermal neutron and fast neutron spectrums can be made by referring to isotopic concentrations, the transmutation and decay scheme in Figure 3.2, the capture-to-fission

ratios in Figure 3.5, and the fission and radiative capture cross sections provided in the next five figures.

Plutonium-238

In the TRU-fueled VHTR, at beginning of cycle, ^{237}Np exist at about five times the amount of ^{238}Pu. As evident by the very high capture-to-fission ratio for ^{237}Np in the thermal energy range, it is expected that nearly all of the neutron interactions that take place in ^{237}Np will produce ^{238}Np, which quickly decays to ^{238}Pu. Since the half-life of ^{238}Np is so short the assumption is made that all neutron captures in ^{237}Np immediately produce ^{238}Pu. The destruction of ^{238}Pu is dependent on its absorption cross-section ($\sigma_c + \sigma_f$), its concentration, irradiation time, and the neutron flux. Thus, the overall composition change of ^{238}Pu can be represented by:

$$\frac{dN_{Pu238}}{dt} = \left[N \cdot \lambda\right]_{Np238} - \left[N \cdot \sigma_a\right]_{Pu238} \phi \qquad (6)$$

where N is the nuclide concentration, σ_γ is the radiative capture cross section, σ_a is the absorption cross section ($\sigma_c + \sigma_f$), λ is the decay constant, and Φ is the neutron flux. As indicated, the decay of ^{238}Np can be replaced with the reaction rate for radiative capture in ^{237}Np to give:

$$\frac{dN_{Pu238}}{dt} = \left(\left[N \cdot \sigma_\gamma\right]_{Np237} - \left[N \cdot \sigma_t\right]_{Pu238}\right)\phi \,. \qquad (7)$$

Shown in Figure 3.6, the capture cross-sections for ^{238}Pu below $0.3\,eV$ are higher, but then the capture cross-sections for ^{237}Np dominate for the remainder of the thermal energy region and throughout the resonance energy region. The above observations lead to the assumption that ^{238}Pu will buildup as the VHTR operates. Under continual irradiation a time will eventually come where the production of ^{238}Pu will level off and begin to decrease as result of ^{237}Np being completely depleted, but this is not expected to happen within the lifetime of the core. The same trend is expected for a fast neutron spectrum system such as the HEST, but being that the ratio of ^{237}Np to ^{238}Pu has decreased and the absorption cross-sections for ^{238}Pu are greater than the capture cross-sections for ^{237}Np for neutron energies greater than $1.0 \times 10^5\,eV$, the concentration of ^{238}Pu will increase at a slower rate and reach a turnover point quicker.

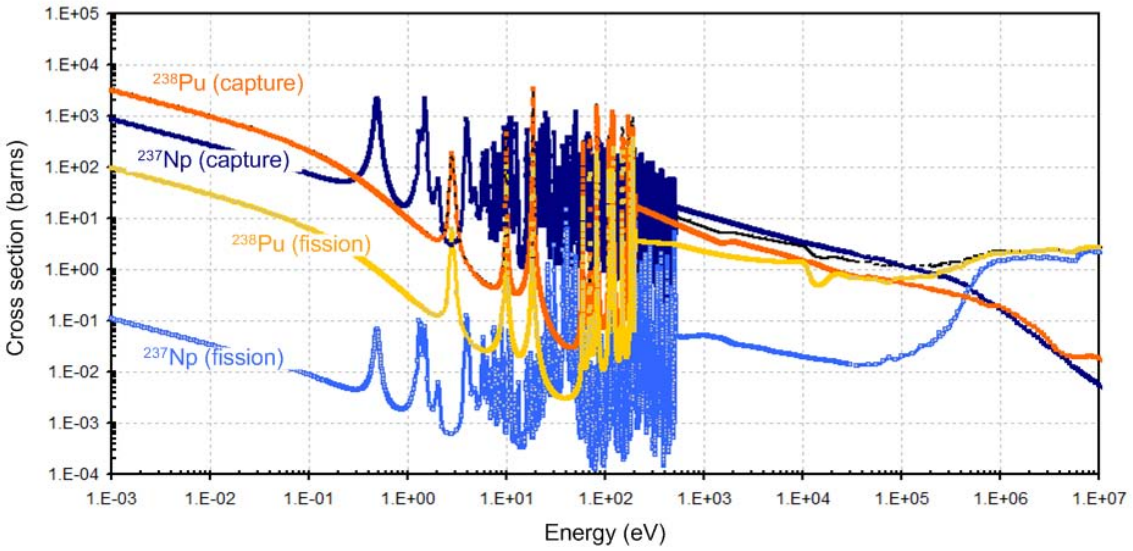

Figure 3.6. Capture and Fission Cross-sections for ^{237}Np and ^{238}Pu.

As shown in Figure 3.5, ^{238}Pu has a relatively low capture-to-fission ratio throughout the energy spectrum. Therefore, neutron capture will dominate below the threshold energy of $3.0 \times 10^5 eV$, but the probability for fission to occur is much greater for ^{238}Pu than for ^{240}Pu and ^{242}Pu. To effectively destroy ^{238}Pu by fission a fast spectrum system would be necessary.

Plutonium-239

As discussed earlier, ^{239}Pu is a fissile isotope and comprises the largest percentage of the TRU inventory. Considering the TRU under irradiation, the production of ^{239}Pu comes almost entirely from neutron capture in ^{238}Pu, which is minimal considering ^{238}Pu exist in such a small amount compared to ^{239}Pu. The destruction of ^{239}Pu is from the combination of capture and fission. The time evolution of ^{239}Pu under irradiation is represented by:

$$\frac{dN_{Pu239}}{dt} = \left(\left[N \cdot \sigma_\gamma \right]_{Pu238} - \left[N \cdot \sigma_a \right]_{Pu239} \right) \phi . \qquad (8)$$

As shown in Figure 3.7, the capture-cross sections for ^{238}Pu in the thermal energy region are much lower than the combined fission and capture cross-sections for ^{239}Pu, especially considering the large resonance peak in ^{239}Pu at $0.32 eV$. Additionally, the cross-sections for ^{239}Pu in the resonance region are larger. This indicates that ^{239}Pu will be depleted at a rapid rate in the VHTR core. Likewise, in a fast neutron spectrum system ^{239}Pu would be fissioned and can reach very high fission efficiencies above $4.5 \times 10^5 eV$, as indicated by Figure 3.5.

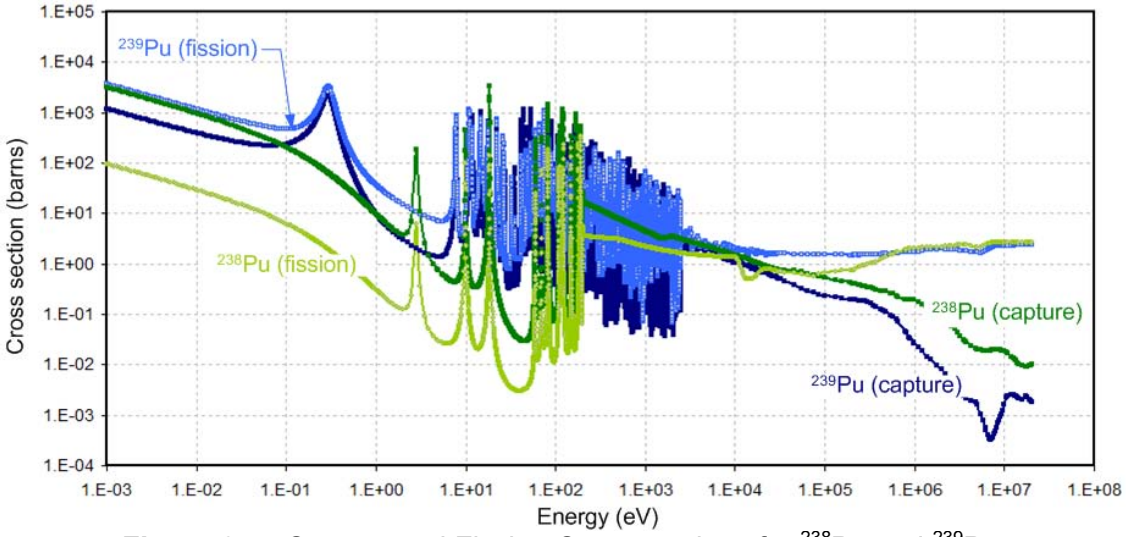

Figure 3.7. Capture and Fission Cross-sections for ^{238}Pu and ^{239}Pu.

Plutonium-240

Upon removal from a typical PWR the isotopic composition of ^{240}Pu will be the second greatest at about 25% of the TRU inventory. The production of ^{240}Pu comes from neutron capture by ^{239}Pu. The absorption of a neutron by ^{240}Pu is the mechanism by which it is destroyed by the transmutation process. The concentration of ^{240}Pu at anytime in the core is signified by the following relation:

$$\frac{dN_{Pu240}}{dt} = \left(\left[N \cdot \sigma_{\gamma} \right]_{Pu239} - \left[N \cdot \sigma_{a} \right]_{Pu240} \right) \phi \,. \qquad (9)$$

As the TRU fuel is irradiated in the VHTR, the ^{240}Pu quantity will slightly increase at the beginning of the cycle, eventually level off, and then start to decrease, and finally end the cycle slightly depleted from its original state. Of course this is just an identified trend and variations are possible. The reasoning behind the described behavior of ^{240}Pu under irradiation in a thermal neutron spectrum system can be explained by the equation above and Figure 3.8, which plots the capture and fission cross-sections for ^{239}Pu and ^{240}Pu across a broad energy spectrum. The capture cross-sections for ^{239}Pu are close to the same as the capture cross-section for ^{240}Pu in the thermal energy region, with the exception being the very large resonance in ^{240}Pu at $1.0\,eV$. The cross-sections in the resonance region are comparable for both isotopes. Taking all this into consideration and also accounting for the greater amount of ^{239}Pu present, the production rate of ^{240}Pu will outpace its transmutation rate, thus a slow increase in ^{240}Pu. Not forgetting though, that fission is the predominant event in ^{239}Pu and when fission and capture are accounted for, ^{239}Pu is being depleted at a much faster rate than ^{240}Pu is being produced and eventually the production/ destruction rate will even out and then turnover. Depending of the burnup of the VHTR core, at the end of cycle ^{240}Pu will likely be depleted from its original composition, but its destruction will contribute to the buildup of higher actinides, through radiative capture.

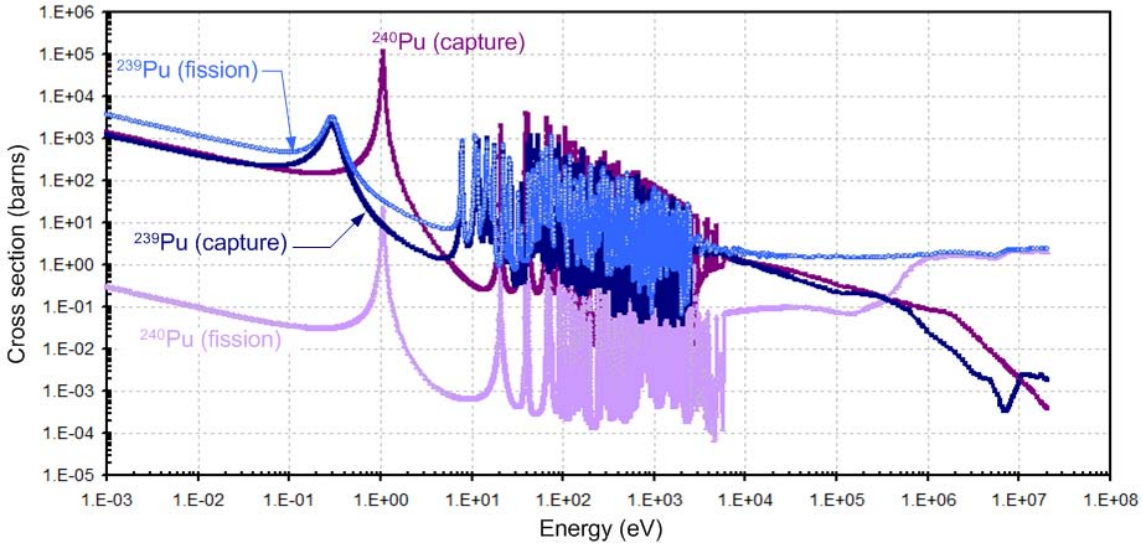

Figure 3.8. Capture and Fission Cross-sections for ^{239}Pu and ^{240}Pu.

In the HEST the ^{239}Pu to ^{240}Pu ratio will be reduced significantly and the capture cross-sections for ^{239}Pu will be lower than the absorption cross-section values for ^{240}Pu, so ^{240}Pu will be depleted throughout the irradiation time in the HEST.

As shown in Figure 3.5, ^{240}Pu has a very large capture-to-fission ratio calculated to be approximately 4,500 in the thermal energy region. For a thermal neutron spectrum system operating on TRU fuel, such as the VHTR, this means ^{240}Pu is removing neutrons from the system and acting as a neutron poison. As this happens the ^{240}Pu is transmuted to ^{241}Pu, and ^{241}Pu is fissile. The end affect is that ^{240}Pu serves as a burnable poison in the VHTR and allows for longer life cores while minimizing reactivity swings. Other TRU isotopes act as burnable poisons (^{237}Np and ^{241}Am), but the higher concentration of ^{240}Pu makes it more effective in this sense.

In order to efficiently destroy ^{240}Pu by fission, a fast neutron spectrum system is required. Neutron energies of $4.5 \times 10^5 eV$ and greater are needed for fission reactions to outweigh capture. In a high-energy system, such as the HEST, elevated ^{240}Pu incineration rates are achievable.

Plutonium-241

The ^{241}Pu composition can be expected to increase with VHTR core lifetime as it is produced at a greater rate than it is destroyed, which is mainly attributed to neutron capture in the more abundant ^{240}Pu. The rate of change in ^{241}Pu is described by:

$$\frac{dN_{Pu241}}{dt} = \left[N \cdot \sigma_\gamma\right]_{Pu240} - \left(\left[N \cdot \lambda\right]_{Pu241} + \left[N \cdot \sigma_a\right]_{Pu241}\right)\phi. \qquad (10)$$

As displayed in Figure 3.9 the neutron capture in ^{240}Pu at thermal energies is comparable to the transmutation of ^{241}Pu ($\sigma_c + \sigma_f$), but that does not include the very large resonance peak at $1.0 eV$

for ^{240}Pu. Once the resonance peak is included, it pushes the production rate of ^{241}Pu to be greater than its transmutation rate. This along with the ^{240}Pu concentration continually increasing under irradiation translates into a buildup in the ^{241}Pu inventory.

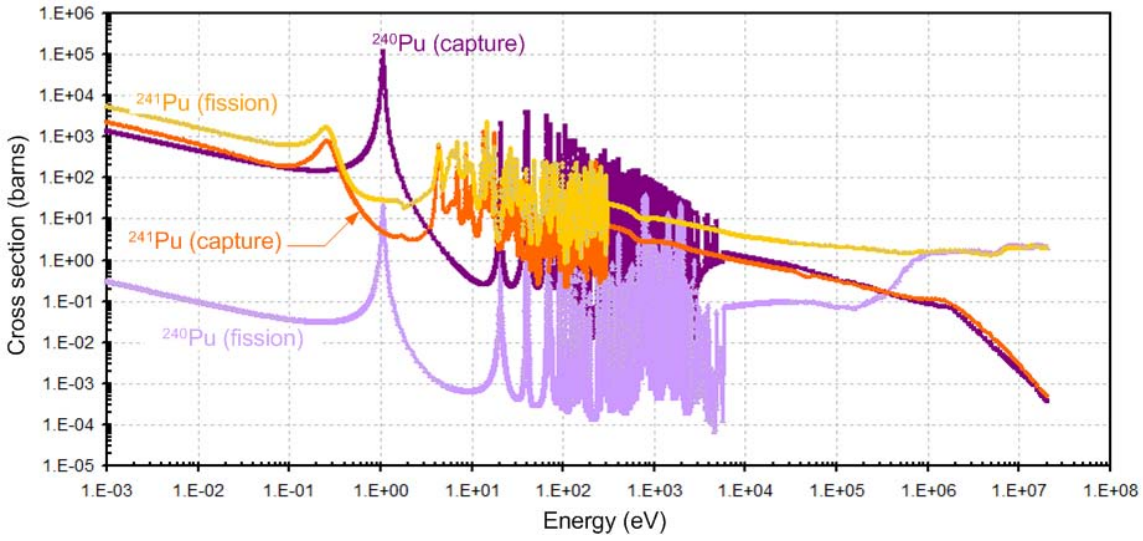

Figure 3.9. Capture and Fission Cross-sections for ^{240}Pu and ^{241}Pu.

As detailed in Figure 3.2, ^{241}Pu has a relatively short half-life of 14.4 years and decays by emitting a beta particle to generate ^{241}Am, thus providing a pathway to the production of the higher actinides *Am* and *Cm*. The destruction rate of ^{241}Pu by decay is minimal in comparison to neutron absorption.

In a fast neutron spectrum ^{241}Pu will experience an even greater divide in the cross-section values for capture and fission that continues to grow with increased neutron energy. The production rate from ^{240}Pu will decrease, but as long as ^{240}Pu makes up more of the fuel composition than ^{241}Pu, the inventory of ^{241}Pu can be expected to also increase.

Plutonium-242

Under irradiation, ^{242}Pu will be produced by neutron capture in ^{241}Pu and transmuted via capture and fission events, represented by:

$$\frac{dN_{Pu242}}{dt} = \left(\left[N \cdot \sigma_{\gamma} \right]_{Pu241} - \left[N \cdot \sigma_{a} \right]_{Pu242} \right) \phi . \qquad (11)$$

Taking a look at Figure 3.10 and the capture cross-sections for ^{241}Pu compared to the capture cross-sections for ^{242}Pu, it is easy to conclude that the ^{241}Pu production outpaces its transmutation rate. As determined previously, ^{241}Pu is also generated throughout the lifetime of the core. Following the same trend ^{242}Pu is also continually generated. This is true for thermal neutron and fast neutron spectrum systems, considering that ^{241}Pu is at comparable or greater quantities than ^{242}Pu, but the fast system's rate of production will be considerably lower, and the

transmutation process will favor fission and limit higher actinide production. Prolonged periods of irradiation in the HEST will eventually deplete the ^{242}Pu inventory.

The transmutation of ^{242}Pu by neutron capture will generate ^{243}Pu. The isotope ^{243}Pu is extremely unstable with a half-life of 4.96 hours, and it promptly beta-decays to ^{243}Am. In this sense ^{242}Pu is very similar to ^{241}Pu, because it provides a pathway for higher actinide production.

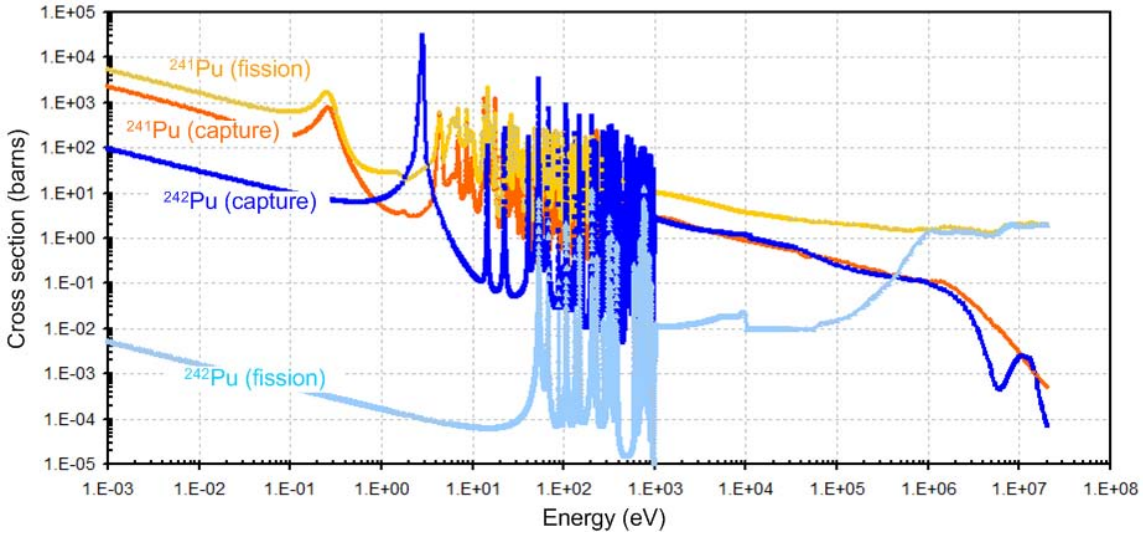

Figure 3.10. Capture and Fission Cross-sections for ^{241}Pu and ^{242}Pu.

3.3.3 Americium

Americium, named after the Americas, was the fourth synthetic transuranic element of the actinide series discovered (1944) [35]. *Am* metal has a silvery-white luster that tarnishes slowly in dry air at room temperature. It has a density of 12 g/cm^3. Sixteen *Am* radioisotopes have been characterized ranging from ^{232}Am to ^{247}Am. The most stable of the isotopes is ^{243}Am with a half-life of 7,370 years, followed by ^{241}Am with a half-life of 432.7 years, and ^{242m}Am with a half-life of 141 years. The remaining isotopes all have half-lives that are less the 51 hours, and a majority have half-lives that are less than 100 minutes. The most famous *Am* isotope is ^{241}Am because it is the only TRU isotope to find its way into the household, by way of americium-based smoke detectors. *Am* is used as a source for gamma rays and alpha particles for a number of medical and industrial uses. *Am* can also be combined with lighter elements to become a neutron emitter with many possible medical and industrial applications.

There are three *Am* isotopes that are of main concern for HLW waste management and incore behavior; they are: ^{241}Am, ^{242m}Am, and ^{243}Am. When UO_2 fuel is irradiated in PWRs the resulting TRU composition at the end of irradiation has a small fraction of *Am* present, typically a few percent by weight. Of the *Am* isotopes ^{243}Am is present in the highest quantities, followed by ^{241}Am, and then by ^{242m}Am. The decay time after removal from the core is important for *Am* because the amount of ^{241}Am will increase considerably with time due to the beta-decay of ^{241}Pu,

which has a half-life of 14.4 years. It will only take a few years of decay for ^{241}Am to become the dominant *Am* nuclide in terms of composition.

Figure 3.11 shows the capture-to-fission ratio for the *Am* isotopes. As indicated ^{242m}Am has a ratio that is less than 1 for the entire energy spectrum and, therefore, is considered a fissile isotope. Both ^{241}Am and ^{243}Am have ratios much greater than one with the threshold energy being at about $7.8 \times 10^5 eV$.

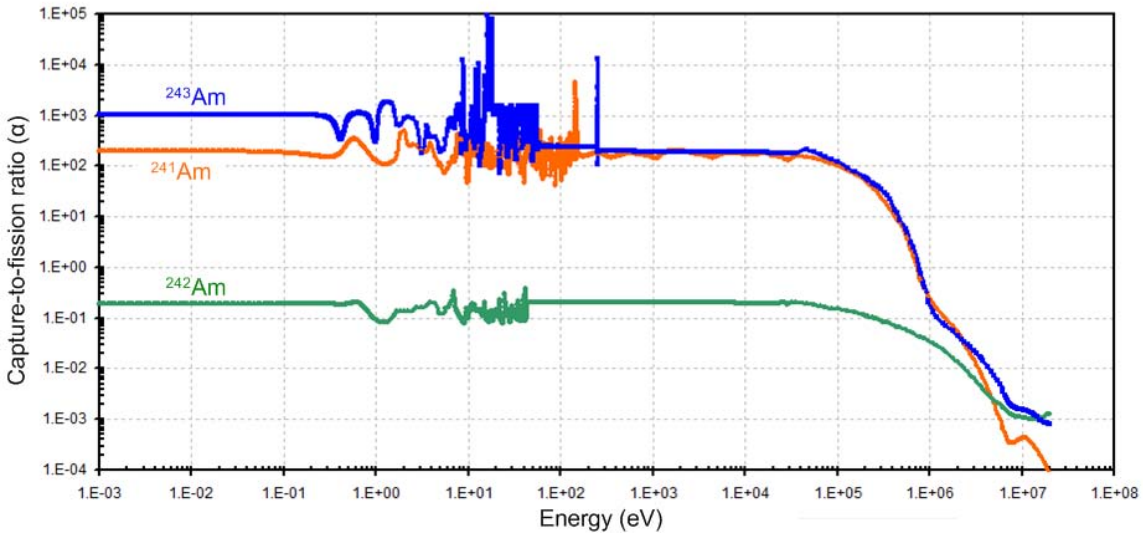

Figure 3.11. Capture-to-fission Ratio for *Am* Isotopes.

Americium-241

Under irradiation the production mechanism for ^{241}Am is the beta-decay of ^{241}Pu and its competing destruction mechanism is radiative capture. Whether the ^{241}Am inventory is depleted or increased has to do with the amount of ^{241}Pu in relation to ^{241}Am and the capture reaction rates throughout the irradiation time, such that:

$$\frac{dN_{Am241}}{dt} = \left[N \cdot \lambda\right]_{Pu241} - \left[N \cdot \sigma_a\right]_{Am241} \phi \,. \qquad (12)$$

Considering the typical TRU composition recycled from a PWR, irradiation in a thermal neutron spectrum system, such as the VHTR, will result in the depletion of ^{241}Am throughout the core lifetime. As for a fast neutron spectrum system, such as the HEST, the ^{241}Pu to ^{241}Am ratio will be greater initially and the absorption cross-section for ^{241}Am will be considerably lower. Therefore, the ^{241}Am concentration will buildup initially, but as time progresses it becomes more difficult to predict exactly what the trend will be without performing detailed depletion calculations.

Americium-242m

Americium has eight meta states, with ^{242m}Am being the most stable. In fact ^{242m}Am is one of the few isotopes that has a much more stable meta state, with a half-life of 142 years compared

to ^{242}Am which has a half life of 16 hours. The production of ^{242m}Am comes from radiative capture in ^{241}Am and is transmuted by neutron absorption, and can be described by the following relationship:

$$\frac{dN_{Am242m}}{dt} = \left(\omega_e \left[N \cdot \sigma\right]_{Am241} - \left[N \cdot \sigma_a\right]_{Am242m}\right)\phi \qquad (13)$$

where ω_e represents the fraction of capture events that lead to ^{242m}Am as opposed to ^{242}Am, and is an energy dependent value that increases with the increase in incident neutron energy.

As shown in Figure 3.12 the absorption cross-sections for ^{242m}Am is much greater than the radiative capture cross-sections for ^{241}Am in the thermal and resonance energy regions, but very similar in the fast region. Even so, the quantity of ^{241}Am present at the start of irradiation in the VHTR greatly outweighs that of ^{242m}Am, and due to this, there will be an increase in the ^{242m}Am inventory upon removal from the VHTR. Likewise, the relative composition at the beginning of cycle for the HEST heavily favors ^{241}Am, but to a lesser amount. Still it is such that a buildup of ^{242m}Am is expected, but at a reduced rate as compared to the VHTR. Protracted irradiation in the HEST will effectively reduce the ^{242m}Am inventory. ^{242m}Am is a fissile isotope so the preferred transmutation mechanism is fission for all neutron energy regions.

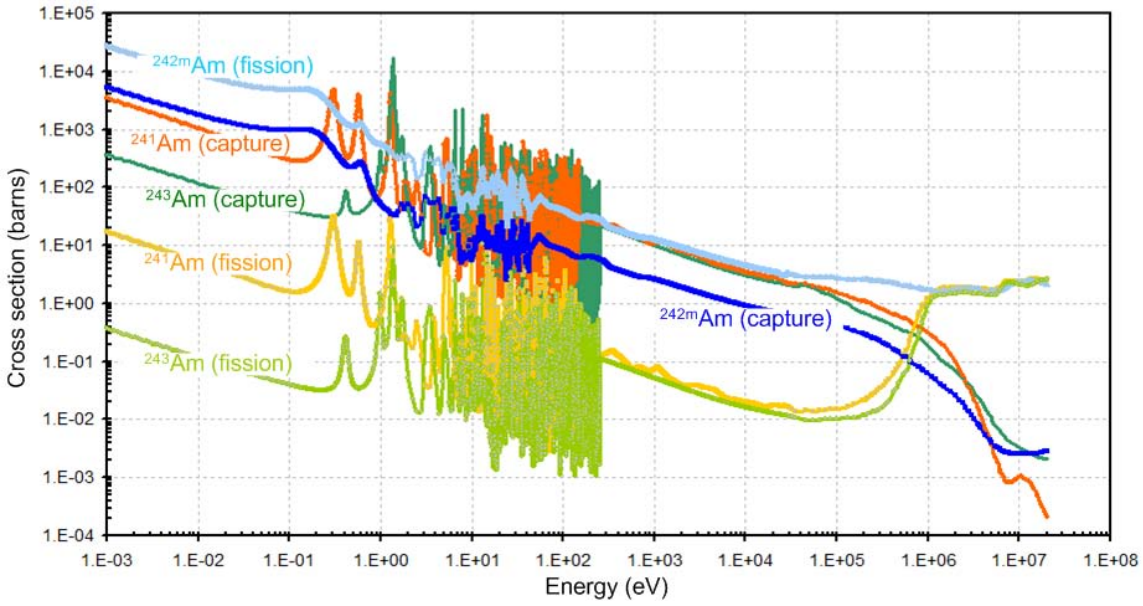

Figure 3.12. Capture and Fission Cross-sections for *Am* Isotopes.

Americium-243

The production of ^{243}Am can be attributed to two sources, one being radiative capture in ^{242m}Am and the other being the beta-decay of ^{243}Pu. The destruction of ^{243}Am is by neutron absorption resulting in either radiative capture or fission. The time dependent representation for the concentration change of ^{243}Am follows:

$$\frac{dN_{Am243}}{dt} = \left[N \cdot \lambda\right]_{Pu243} + \left(\left[N \cdot \sigma_{\gamma}\right]_{Am242m} - \left[N \cdot \sigma_{a}\right]_{Am243}\right)\phi . \quad (14)$$

Since the half-life of ^{243}Pu is so short (4.96 hours) the assumption is made that all radiative neutron captures in ^{242}Pu immediately produce ^{243}Am. The relation above is adjusted to reflect this observation and is now presented as:

$$\frac{dN_{Am243}}{dt} = \left(\left[N \cdot \sigma_{\gamma}\right]_{Pu242} + \left[N \cdot \sigma_{\gamma}\right]_{Am242m} - \left[N \cdot \sigma_{a}\right]_{Am243}\right)\phi . \quad (15)$$

The amount of ^{242m}Am present at any time is very small compared to that of ^{242}Pu and due to this, the production term is dominated by ^{242}Pu. The absorption cross-section values for ^{243}Am are noticeably greater than the radiative capture cross-sections for ^{242}Pu in all energy regions, but ^{242}Pu concentrations heavily outweigh ^{243}Am concentrations. In addition, the concentration rate change for ^{242}Pu increases with time. Using the above information, the inventory of ^{243}Am is expected to increase under irradiation in the VHTR. In the HEST it is expected to initially increase but at a slower rate and then eventually begin to decrease as the ^{242}Pu is depleted.

3.3.4 Curium

Curium, named after Marie Curie and her husband Pierre, was the third synthetic transuranic element of the actinide series discovered (1944) [35], even though it follows americium in the periodic table. *Cm* metal has a silvery color that is chemically reactive and tarnishes slowly in dry air at room temperature. It has a density of 13.51 g/cm^3. Seventeen *Cm* radioisotopes have been characterized ranging from ^{235}Cm to ^{251}Cm. The most stable of the isotopes is ^{247}Cm with a half-life of 1.56×10^7 years. *Cm* has been studied significantly as a potential fuel for radioisotope thermoelectric generators, but radiation issues and cost have prevented extensive use. Applications have included using a ^{244}Cm source for the Alpha particle X-ray spectrometer on board several American and European space missions, and as an alpha particle source.

The *Cm* nuclides are among the most radiotoxic and largest decay heat producers among the TRU. This is particularly the case for ^{242}Cm, ^{243}Cm, and ^{244}Cm. However, their low concentrations and short half-lives greatly reduce the concern they pose for long-term HLW management. ^{242}Cm is the most radiotoxic and biggest contributor of decay heat out of all the TRU isotopes surveyed, but it's very short half-life makes it a non-issue for long-term waste management, but it does pose other problems discussed later. Even though ^{243}Cm and ^{244}Cm have relatively short half-lives and are a small fraction of the TRU inventory, they still need to be closely tracked and assessed. In any case, the *Cm* isotopes need monitored for inventory increases as the TRU fuel is irradiated, particularly in thermal neutron spectrum systems, as their heat load and radiotoxicity levels can be very sensitive to composition changes.

Curium-242

The beta-decay of ^{242}Am generates ^{242}Cm, but considering that ^{242}Am has a very short half-life it can be assumed that the production of ^{242}Cm is a product of neutron capture in ^{241}Am. The

competing factor for the production of ^{242m}Am also has to be accounted for in ^{241}Am capture. The destruction term includes capture and fission events and the alpha-decay of ^{242}Cm. The process can be described by:

$$\frac{dN_{Cm242}}{dt} = \left((1-\omega_e)\left[N\cdot\sigma_\gamma\right]_{Am242} - \left[N\cdot\sigma_a\right]_{Cm242}\right)\phi - \left[N\cdot\lambda\right]_{Cm242}. \quad (16)$$

Considering that ^{242}Cm composition before irradiation in the VHTR is essentially zero, it is only produced during its residency time under irradiation. The goal is to limit its production rate as much as possible and to transmute it by fission in the HEST.

Due to its short half-life ^{242}Cm does not present long-term problems, but it is important because it generates the longer-lived ^{243}Cm. In addition, it causes difficulties in the short-term for radiological protection from neutron emissions and other high-energy radiation fields, along with high heat generation that can make reprocessing procedures complicated.

Curium-243

The production of ^{243}Cm can be attributed to radiative capture in ^{242}Cm. In contrast it is transmuted to another nuclide by radiative capture or by fission. The time dependent representation for the concentration change of ^{243}Cm follows:

$$\frac{dN_{Cm243}}{dt} = \left(\left[N\cdot\sigma_\gamma\right]_{Cm242} - \left[N\cdot\sigma_a\right]_{Cm243}\right)\phi. \quad (17)$$

The rate of increase in ^{243}Cm is linked to production of ^{242}Cm and since ^{242}Cm will continually increase in the VHTR, the same can be expected for ^{243}Cm. However, as indicated in Figure 3.13, the capture cross-sections for ^{242}Cm are considerably smaller than the cross-sections for ^{243}Cm throughout the entire spectrum, so the concentration of ^{243}Cm will be much lower than that of ^{242}Cm. As shown in the plot, ^{243}Cm is a fissile isotope and very high fission efficiencies are achieved in the HEST.

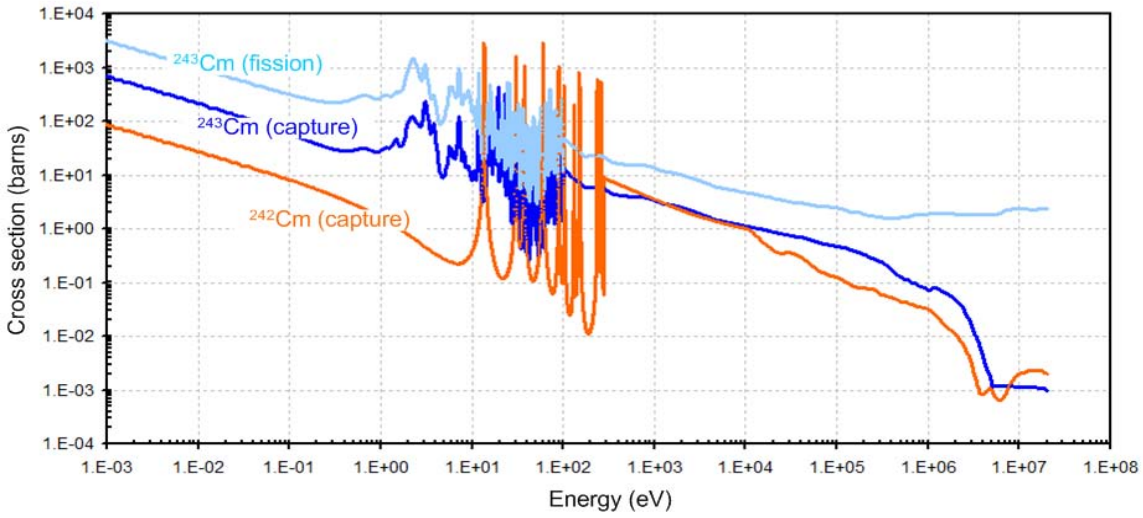

Figure 3.13. Capture and Fission Cross-sections for ^{242}Cm and ^{243}Cm.

Curium-244

The production of ^{244}Cm can be attributed to three sources, one being radiative capture in ^{243}Cm, another being the beta-decay of ^{244}Am, and the last being beta-decay of ^{244m}Am. The destruction of ^{244}Cm is by neutron absorption resulting in either radiative capture or fission. The time dependent representation for the concentration change of ^{244}Cm follows:

$$\frac{dN_{Cm244}}{dt} = \left[N \cdot \lambda\right]_{Am244} + \left[N \cdot \lambda\right]_{Am244m} + \left(\left[N \cdot \sigma_{\gamma}\right]_{Cm243} - \left[N \cdot \sigma_{a}\right]_{Cm244}\right)\phi . \qquad (18)$$

Since the half-life of ^{244}Am is very short (10 hours) the assumption is made that the radiative capture event in ^{243}Am immediately produces ^{244}Am. The meta state ^{244m}Am has even a shorter half-life and it also beta-decays to ^{244}Cm. Therefore, it can be included in the radiative capture term with ^{244}Am. The relation above is adjusted to reflect these observations and presented as:

$$\frac{dN_{Cm244}}{dt} = \left(\left[N \cdot \sigma_{\gamma}\right]_{Am243} + \left[N \cdot \sigma_{\gamma}\right]_{Cm243} - \left[N \cdot \sigma_{a}\right]_{Cm244}\right)\phi . \qquad (19)$$

At the beginning of cycle for the VHTR, the TRU fuel contains essentially no ^{243}Cm, therefore, production will come from ^{243}Am alone. As time proceeds, ^{243}Cm will also contribute. By referring to Figure 3.14 it can be seen that the capture cross-sections for ^{243}Am are greater than the cross-sections for ^{244}Cm. In addition, the initial concentration of ^{243}Am is larger and it increases with irradiation time. All indicate a significant production rate of ^{244}Cm during its time in the VHTR. In the HEST, the production rates will definitely be slowed considerably, and with high burnup, can be reduced and eventually eliminated.

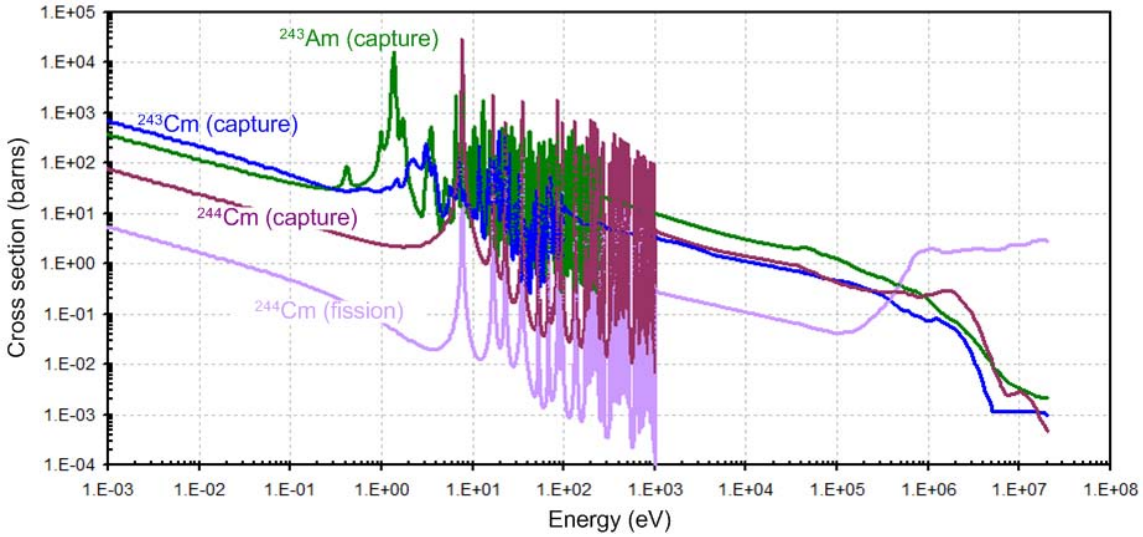

Figure 3.14. Capture and Fission Cross-sections for ^{243}Am, ^{243}Cm, and ^{244}Cm.

3.4 Conclusions

The fuel in an operating nuclear reactor is constantly changing as fuel nuclei are transmuted by neutron capture and subsequent decay. The fresh LEU fuel that enters the reactor and later removed after an irradiation cycle now contains TRU elements that will be highly radioactive for 100's of thousands of years. Currently, the favored plan is to contain and isolate the used fuel from interacting with the biosphere until it has decayed to safe levels, assuring the protection of human health and the environment. Countless challenges exist because of the timeframe involved with such an endeavor, plus it is predicted that it will take a large number of storage facilities to house all of the current and future HLW. Presently, different sites around the world have been characterized to serve as possible deep geological repositories for safe long-term waste storage facilities.

The TRU inventory is responsible for the long-term heat generation and radiotoxicity that accompanies used nuclear fuel. High-level nuclear waste repository performance parameters are dependent on the TRU composition. Therefore, focus is on the destruction of the TRU stream by transmutation as a means to alleviate problematic aspects of waste management.

Highest importance is placed on the TRU nuclides that are intense sources of decay heat and that are highly radiotoxic for many years into the future. Focusing on the elimination of these TRU nuclides accomplishes two main goals: 1) more efficient use of the available space within the repository allowing for greater quantities of HLW to be stored safely, and 2) decreasing the amount of time the HLW must be isolated from the biosphere.

A systematic method was developed and utilized to assess and rank the TRU nuclides according to radiotoxicity, thermal heat generation, relative concentration, timescale, and neutron emissions. Figure 3.15 presents the relevant TRU nuclides with dominant transmutation and decay schemes. The isotopes are color coded to show their ranking, from highest to lowest priority. As indicated, the highest priority isotopes are: ^{239}Pu, ^{240}Pu, ^{241}Pu, and ^{241}Am. The medium high priority isotopes include: ^{238}Pu, ^{242}Pu, ^{243}Am, and ^{244}Cm. The medium low priority isotopes are: ^{242m}Am, ^{242}Cm, ^{243}Cm, and ^{245}Cm. The low priority isotopes are: ^{237}Np, ^{244}Pu, and ^{246}Cm.

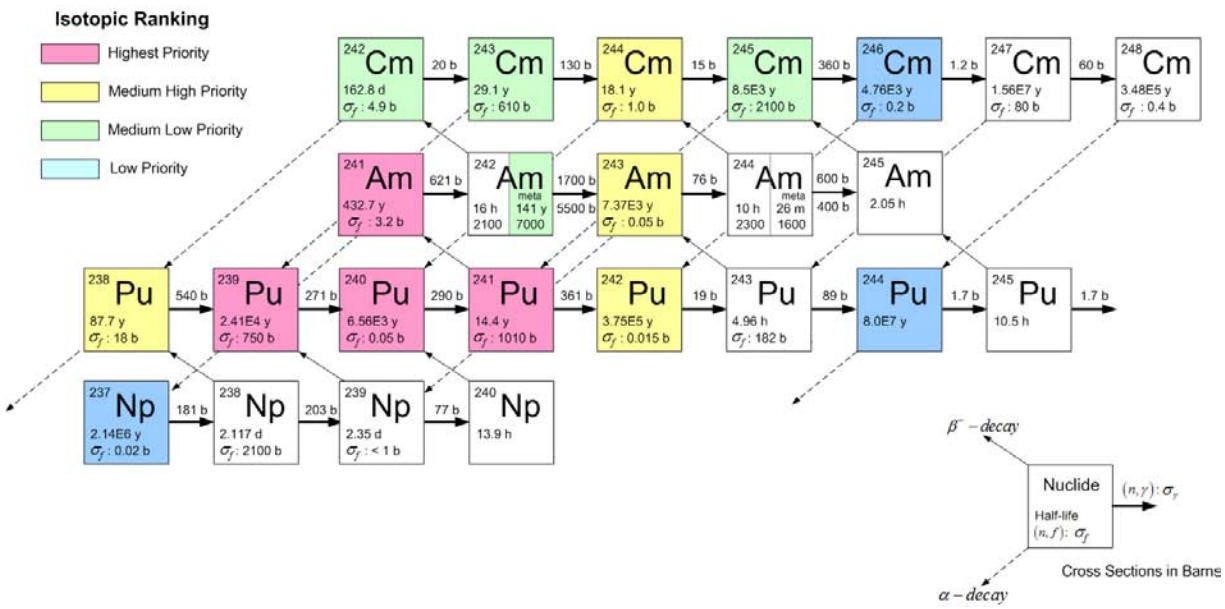

Figure 3.15. TRU Priority Ranking.

The ranking system is based on the TRU composition generated by a typical PWR with five years of decay time. The highest priority ranking identifies isotopes that have the greatest effect on HLW storage and need to be targeted foremost for inventory reduction.

According to the characteristics associated with the TRU nuclides, irradiation in thermal neutron spectrum systems, such as the VHTR, can significantly reduce TRU inventories. Attention to the buildup of higher actinides is a concern for the VHTR, but by linking it to a fast neutron spectrum system, such as the HEST, the inventory increase can be efficiently diminished or eventually eliminated. The beneficial results are twofold, on the one hand reducing the burden on the management of HLW, and while on the other hand, utilizing the valuable fuel resource remaining in PWR used fuel.

4 SYSTEM PARAMETERIZATION AND REPRESENTATIVE MODELS

The NES is composed of different reactors and components that work in coordination with each other to produce the desired output. Each has its own function and each is considered in a standalone fashion. The first section of the chapter (4.1) describes each of the reactor units, followed by chapter section (4.2) which details the fuel cycle components along with the models created to represent each, with the final section (4.3) dedicated to describing the integration of the individual models into a single system model. When possible experiment-to-code and code-to-code benchmarking procedures were applied with results presented within.

4.1 Reactor Units

The performance of the NES is heavily based on the reactor units. The three reactors selected for the system are the AP1000, VHTR, and HEST. The AP1000 is a Gen-III+ PWR design by Westinghouse. The VHTR is a Gen-IV design and currently the candidate for the Next Generation Nuclear Plant (NGNP). It is the prismatic core design and utilizes the Tri-structural isotropic (TRISO) fuel type. The HEST is a subcritical system that takes advantage of the high-energy 14.1 MeV neutrons produced by the DT fusion reaction to drive the system and to eliminate waste.

4.1.1 AP1000

The AP1000 is a Westinghouse Electric Company reactor design and is the first Generation III+ reactor to receive final design approval from the NRC. The AP1000 is a two-loop PWR planned to produce 1154 MW_e. The design is built on proven technology from over 35 years of PWR operating experience. Major improvements over Gen-III reactors include the utilization of passive safety technology, overall system simplification, and modular construction. These improvements make the AP1000 safer, easier and less expensive to build, operate, and maintain.

In the near future the AP1000 is expected to play a large role in nuclear energy generation worldwide. As indication, the Sanmen Nuclear Power Plant in Zhejiang China began construction of two AP1000s in February 2008, which are scheduled to go operational during 2013-15. Construction began in July 2008 of two other units at the Haiyang Nuclear Power Plant in Shandong. China has officially adopted the AP1000 as a standard for inland nuclear projects. Additionally, in the USA, twelve Combined Construction and Operating Licenses have been submitted as of 2009. The AP1000 is seen as the new standard for nuclear energy generation and will bridge the gap from yesterday's Gen-III technology to tomorrow's advanced Gen-IV reactor systems.

The major design parameters for the AP1000 are similar to that of other PWRs. The thermal power is rated at 3400 MW_{th} and with a thermodynamic efficiency of 32.7%, it can produce a

usable electrical power of 1115 MW_e. The fuel type is enriched UO_2 and the coolant/moderator is light water. A listing of the AP1000 design parameters are provided in Table 4.1.

Table 4.1. AP1000 Design Parameters.

Parameter	Value
Thermal power (MW_{th})	3400
Electrical power (MW_e)	1115
Thermodynamic efficiency (%)	32.8
Fuel	UO_2
Average fuel enrichment (wt %)	3.8
Type of fuel assembly	17x17
Number of fuel assemblies	157
Active fuel length (m)	4.3
Equivalent core diameter (m)	3.04
Operating cycle length (months)	18
Linear heat rating (kW/m)	18.7
Operating pressure (Mpa)	15.5
Coolant	light water
Coolant inlet temperature (°C)	280.7
Coolant outlet temperature (°C)	321.1

Model Description

The model is based on the AP1000 Design Control Documentation [36] provided by the US Nuclear Regulatory Commission (NRC). The reactor core consists of 157 fuel assemblies that are arranged in a pattern, which approximates a right circular cylinder. Each fuel assembly contains 264 fuel rods, 24 guide tubes for control rod clusters, and one centrally located guide tube for in-core instrumentation, all of which are arranged in a 17 x 17 square lattice array. Figure 4.1 shows a cross-sectional view of the fuel assembly and related fuel rod and guide tube placements.

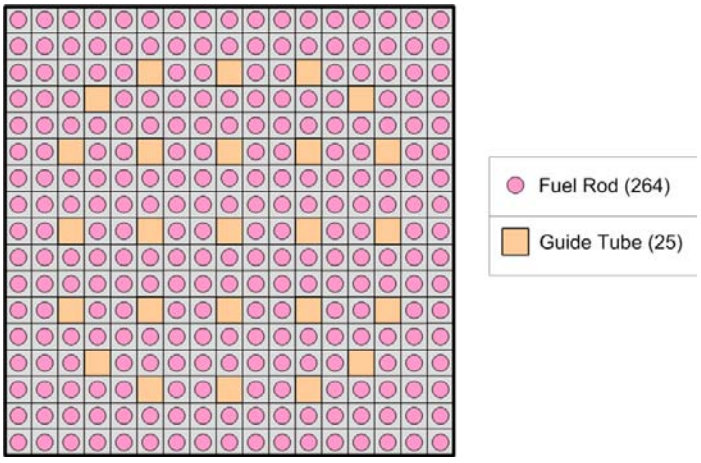

Figure 4.1. AP1000 Fuel Assembly.

The model design is based on the initial core loading, in which the fuel rods within any given assembly have the same uranium enrichment in both the radial and axial planes. Fuel assemblies of three different enrichments are used to establish a favorable radial power distribution.

Figure 4.2 shows the fuel assembly loading pattern used for the AP1000 model. It also shows the placement of the assemblies containing the Discrete Burnable Absorber (PYREX) rods and Integral Fuel Burnable Absorber (IFBA) rods within the core.

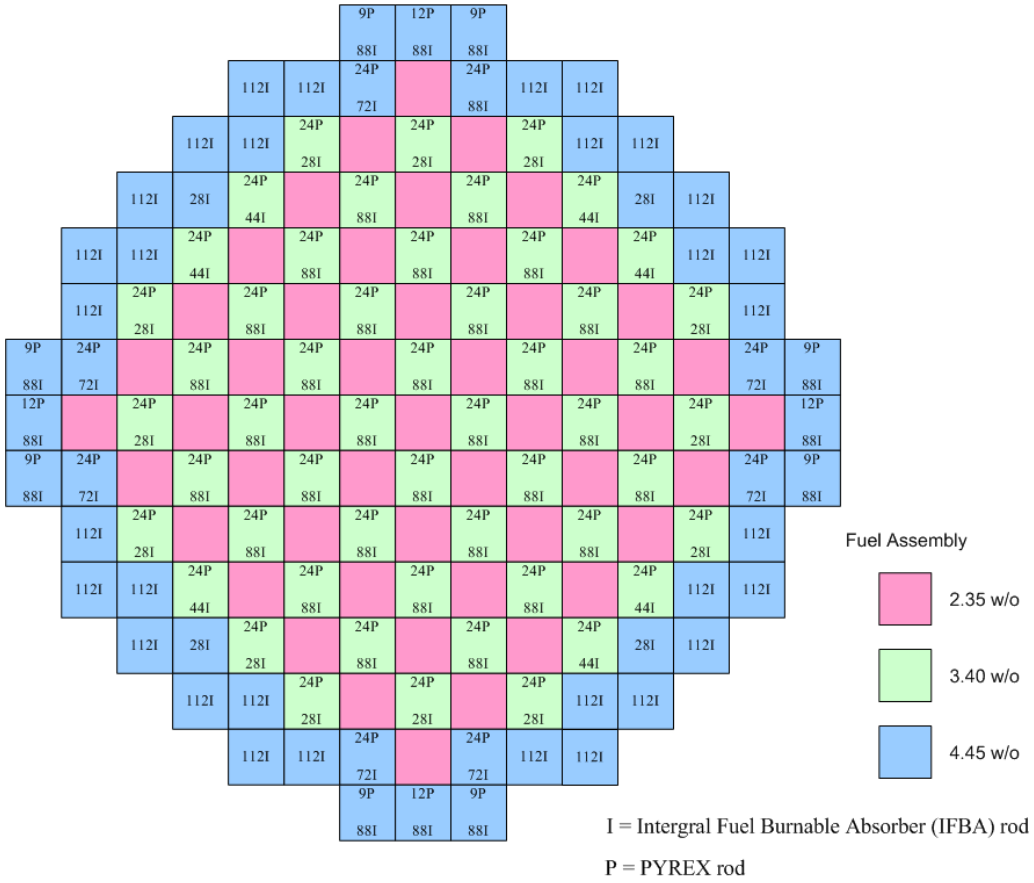

Figure 4.2. AP1000 Reactor Core Map.

Burnable absorbers in the form of PYREX and IFBA rods are used to provide partial control of the excess reactivity present during the fuel cycle. Their main function is to limit peaking factors and prevent the moderator temperature coefficient from being positive at normal operating conditions. Within a chosen fuel assembly, the PYREX rods can be arranged in one of three different configurations, as shown in Figure 4.3. Similarly, the IFBA rods can be arranged in five different configurations as shown in Figure 4.4. The placement of the assemblies containing the burnable absorber within the core is displayed in Figure 4.2. A description of the reactor core, including dimensions and core materials, is provided in Table 4.2.

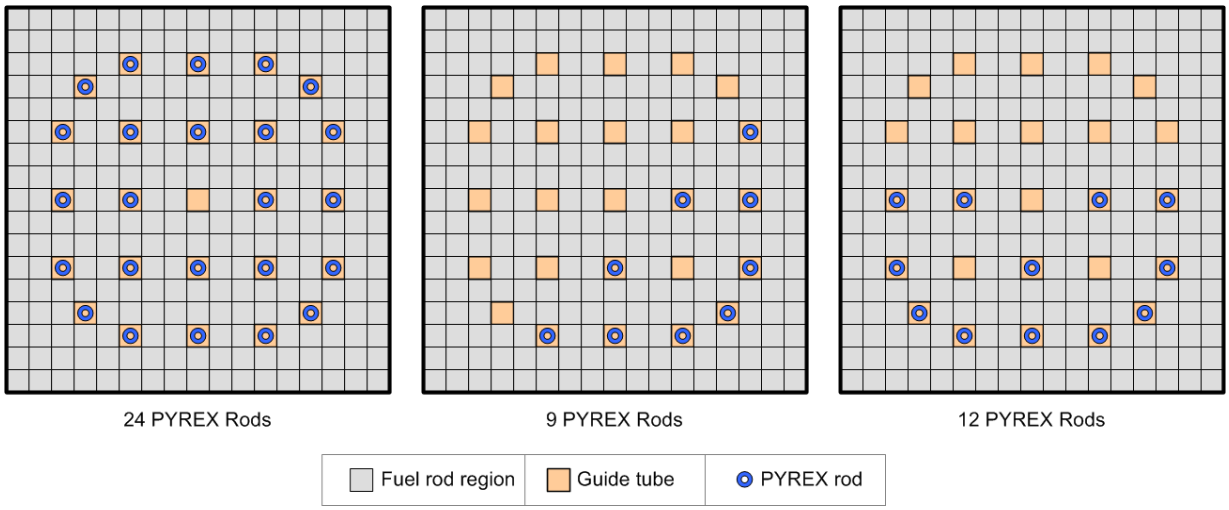

Figure 4.3. PYREX Rod Arrangement within the AP1000 Fuel Assembly.

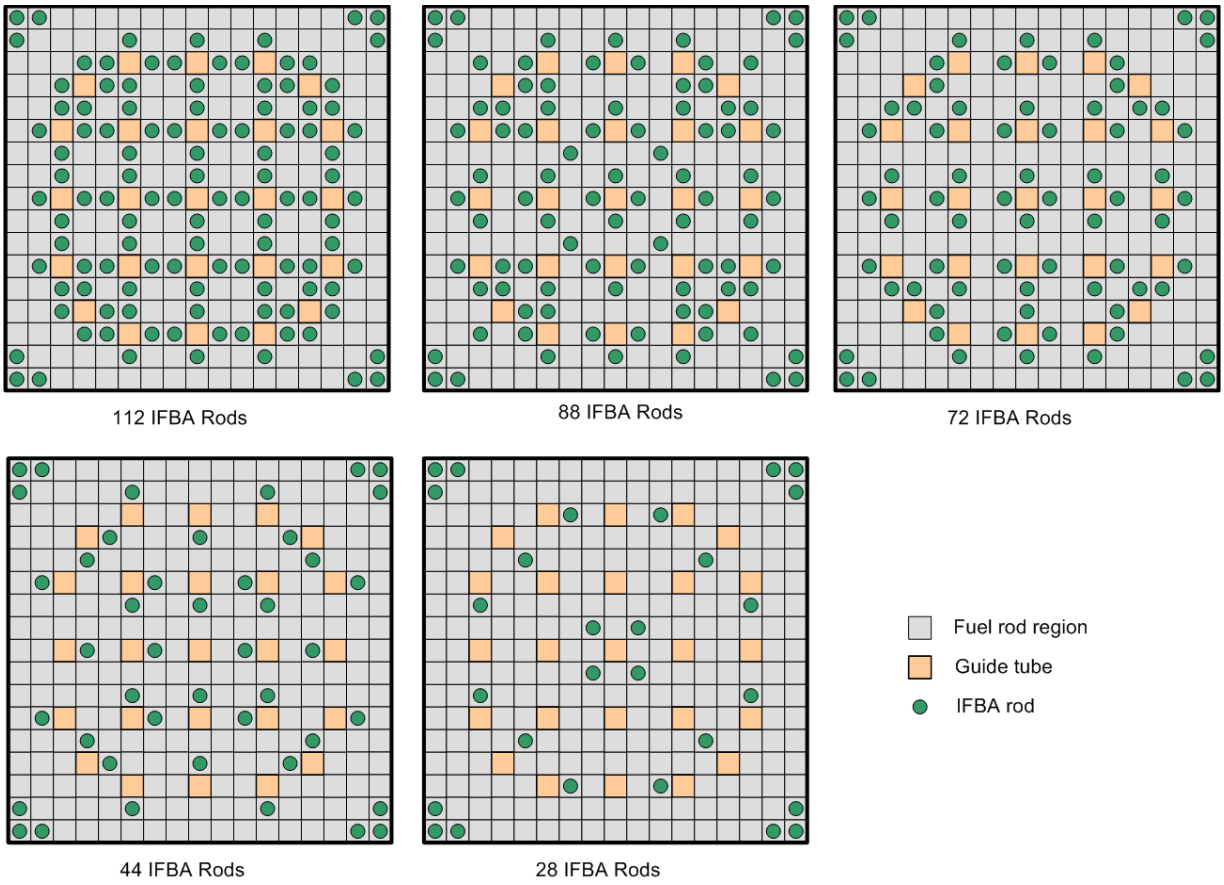

Figure 4.4. IFBA Rod Arrangement within the AP1000 Fuel Assembly.

Table 4.2. Reactor Core Description.

Active Core	
Equivalent diameter (cm)	304.04
Active fuel height (cm)	426.72
Height-to-diameter ration	78.14
Total cross section area (m²)	7.26
Fuel weight, as UO_2 (g)	9.76×10^7
Fuel Assembly	
Number	157
Rod array	17x17
Rods per assembly	264
Rod pitch (cm)	1.26
Overall transverse dimensions (cm)	21.40
Fuel Rods	
Number	41448
Outside diameter (cm)	0.9500
Gap diameter (cm)	0.0165
Clad thickness (cm)	0.0572
Clad material	ZIRLO
Fuel Pellets	
Material	UO2 sintered
Density (% theoretical)	95.5
Fuel Enrichments (weight percent)	
Region 1	2.35
Region 2	3.40
Region 3	4.45
Diameter (cm)	0.819
Length (cm)	0.983
Discrete Burnable Absorber Rods (PYREX)	
Number	1558
Material	Borosilicate Glass
Outside diameter (cm)	0.968
Inner diameter (cm)	0.461
Clad material	Stainless Steel
B_{10} content (Mg/cm)	6.24
Absorber length (cm)	368.30
Integral Fuel Burnable Absorbers (IFBA)	
Number	8832
Type	IFBA
Material	Boride Coating
B_{10} content (Mg/cm)	0.772
Absorber length (cm)	386.08
Absorber coating thickness (cm)	0.00256

Benchmark Analysis

To test the validity of the AP1000 whole-core 3D model, a benchmark test was developed. The AP1000 Design Control Documentation [36] provided by the US NRC for the licensing process was used for the procedure. The report provided the multiplication factor (k_{eff}) for cold, zero power, beginning of cycle, and zero soluble boron core conditions. The code systems, MCNP5 and SCALE (KENO-VI), were used to model the reactor at the specified core conditions in order to benchmark the k_{eff} value against published results and for a code-to-code benchmark procedure.

For both the MCNP and SCALE calculations, the solution was obtained using one million neutron histories, 5,000 histories per cycle for 260 cycles with the first 60 cycles ignored. The results are listed in Table 4.3. As indicated, the MCNP calculation was very accurate when compared to the published results, giving a difference of only 0.0498% between k_{eff} values. The result calculated by SCALE had a slightly higher difference at 0.1942%. Comparing the two codes systems (MCNP vs. SCALE) the difference was measured at 0.1445%.

Table 4.3. AP1000 Multiplication Factor Results.

Multiplication Factor Origin	k_{eff}	% difference (published-to-code)	% difference (code-to-code)
AP1000 Design Control Documentation	1.205	na	na
MCNP Code System (version 5 1.51)	1.2044	0.0498	0.1445
SCALE Code System (KENO-VI)	1.2026	0.1942	

The average energy-dependent neutron flux in the fuel elements, as produced by MCNP and SCALE, are provided in Figure 4.5. As shown, the profile is as expected for a PWR, but what is of more interest is the direct comparison of the two code systems. It is easily determined that the spectrum produced by MCNP and SCALE are nearly identical, as they appear to be directly on top of each other.

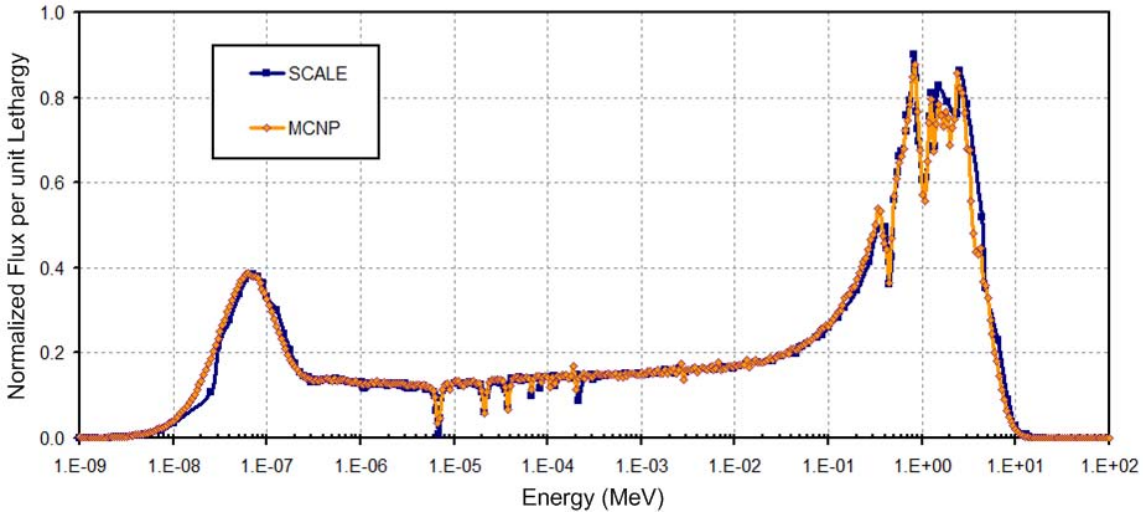

Figure 4.5. Neutron Flux Profiles in the AP1000 Fuel Rods (MCNP vs. SCALE).

4.1.2 VHTR

The United States Department of Energy has given priority to the VHTR concept making it the focus of intensive research programs. The VHTR is designed to be a high-efficiency system, which can supply electricity and process heat to a wide-range of high temperature and energy intensive applications. The VHTR is a passively safe design. The refractory core, low power density, and low excess reactivity enable this design feature.

The VHTR is a graphite moderated gas-cooled reactor that supplies heat with core outlet temperatures in the range of 850 - 1000° C. This enables applications such as hydrogen production, process heat for the petrochemical industry, or seawater desalination. Its basic technology has been well established in former High Temperature Gas Reactors (HTGR), such as the German AVR and THTR prototypes, and the US Fort Saint Vrain and Peach Bottom prototypes. The VHTR extends the capabilities of HTGR to achieve further improvements in thermal efficiency and future additional high-temperature applications.

The reactor core can be a prismatic block core or a pebble bed core design. Both the prismatic and pebble bed cores have the same key design characteristics and use the same ceramic or TRIstructual ISOtropic (TRISO) coated fuel particles. The TRISO coating provides a miniature containment vessel for each fuel particle, allowing complete retention of fission fragments at high temperatures [37].

The core type utilized in the nuclear energy system is the prismatic block design. The prototypical prismatic VHTR produces a thermal power of 600 MW_{th} with a low power density of approximately 7 W/cm^3 and a annular fuel configuration. In basic terms, the core is composed of fuel blocks, control rod guide blocks, and reflectors blocks. The fuel blocks consist of a hexagonal graphite block with borings for the placement of fuel compacts and helium coolant channels. The control rod guide blocks are hexagonal graphite blocks with borings for the control rods to pass through. The reflector blocks are simply solid graphite hexagonal blocks used to limit neutron leakage. The fuel blocks, control rod guide blocks, and reflector blocks are stacked on top of one another and then arranged side-to-side in a hexagonal lattice to create a cylindrically shaped core.

Model Description

The VHTR model is based on the High Temperature Test Reactor (HTTR) of the Japan Atomic Energy Research Institute (JAERI) [38]. The HTTR was selected because of the documented experimental test results and the opportunity it presented for performing an experiment-to-code benchmark analysis, as described later in this section. The basic design features of the smaller HTTR were used to create the scaled-up VHTR power reactor. The VHTR design parameters are listed in Table 4.4.

Table 4.4. VHTR Design Parameters.

Fuel	UO_2		Power (MW_{th})	*600*
Enrichment(%)	*8*		Power Density (W/cm^3)	*6.9*
Coolant	*He*		Pressure (MPa)	*7.0*
			Inlet/Outlet Temperature (°C)	*490/950*
# of Columns	*102*		# of Fuel Columns	*66*
			# of Control Columns	*36*
			# of Blocks/Column	*13*
Block Pitch (cm)	*36*		# of Fuel Pins/Fuel Block	*32*
Block Height (cm)	*58*		# of Burnable Poison Rods/Fuel Block	*2*
			Control Rods/Control Block	*2*
			Emergency Rods/Control Block	*1*
			Compact Pitch (cm)	*5.15*
			Fuel Hole Radius (cm)	*4.1*
			Compact Inner Radius (cm)	*0.5*
			Compact Outer Radius (cm)	*1.3*
Packing (%)	*30*		10.41 g/cm^3 Kernel Radius (cm)	*0.0300*
			1.14 g/cm^3 Buffer Radius (cm)	*0.0359*
			1.89 g/cm^3 PyC1 Radius (cm)	*0.0390*
			3.20 g/cm^3 SiC Radius (cm)	*0.0419*
			1.87 g/cm^3 PyC2 Radius (cm)	*0.0465*
			Matrix (g/cm^3)	*1.77*
			Block (g/cm^3)	*1.69*

The general procedure for creating the model was to build the three types of prismatic hexagonal blocks that compose the VHTR, and then arrange these blocks in an array of rows and columns to construct the core. The three prismatic blocks include: fuel assembly blocks, replaceable reflector blocks, and control rod guide blocks. To complete the core the configuration of prismatic blocks was then surrounded by a permanent graphite reflector.

The fuel assemble block consists of 33 fuel elements with helium coolant channels and two burnable poison rods, which are arranged in a hexagonal graphite block to create a pin-in-block type assembly. The fuel block is 36 cm in width across the flats and 58 cm in height. The block has 33 vertical borings with a diameter of 4.1 cm for placement of the annular fuel rods. In addition, each fuel graphite block has three burnable poison insertion holes measuring 50 cm in height and 1.5 cm in diameter. Two are loaded with burnable poison rods, while the third is left empty. In the center of each block is a fuel-handling hole.

Figure 4.6 shows the arrangement and dimensions of the prismatic fuel block. The measurements and material properties of the block are given in Table 4.5, with all measurements provided in units of cm.

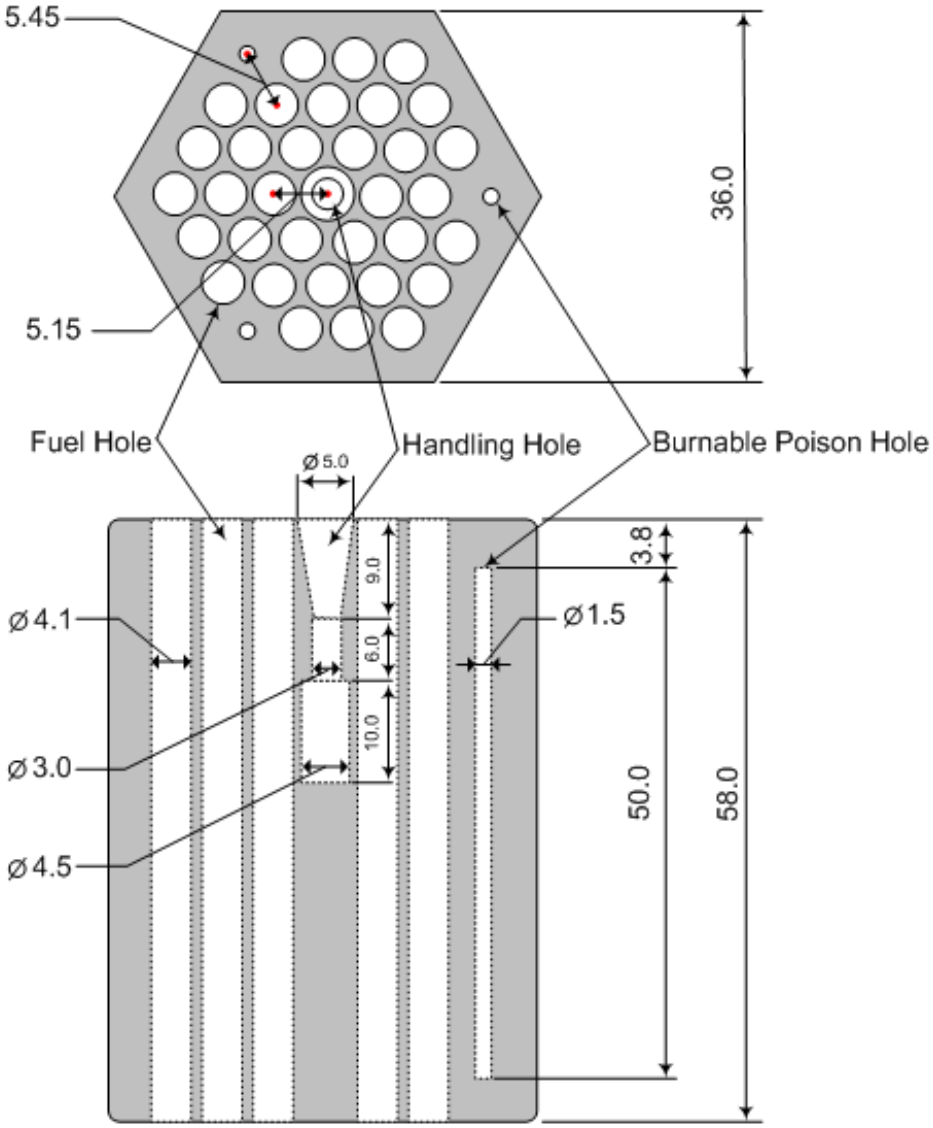

Figure 4.6. VHTR Prismatic Fuel Block (measurements in cm).

Table 4.5. VHTR Prismatic Fuel Block Properties.

Type	Pin-in-block
Configuration	Hexagonal
Material	IG-110 Graphite
Density (g/cm³)	1.77
Height (cm)	58
Width Across the Flats (cm)	36
# of Fuel Holes/Block	33
Fuel Hole Diameter (cm)	4.1
Fuel Hole Height (cm)	58
# of Burnable Poison Holes/Block	3
Burnable Poison Hole Diameter (cm)	1.5
Burnable Poison Hole Height (cm)	50

The fuel element consists of TRISO fuel particles imbedded within a graphite matrix in the form of an annular rod (fuel compact), that is encapsulated by a graphite sleeve. Figure 4.7 illustrates how the TRISO particles, fuel compact, and protective sleeve are arranged to create the fuel element. Each fuel element contains 176,515 TRISO particles within the fuel compact with a packing fraction of 30 %. Table 4.6 contains the fuel element dimensions and material properties. The MCNP model uses a square lattice array for the TRISO particles contained in the graphite matrix of the fuel compact.

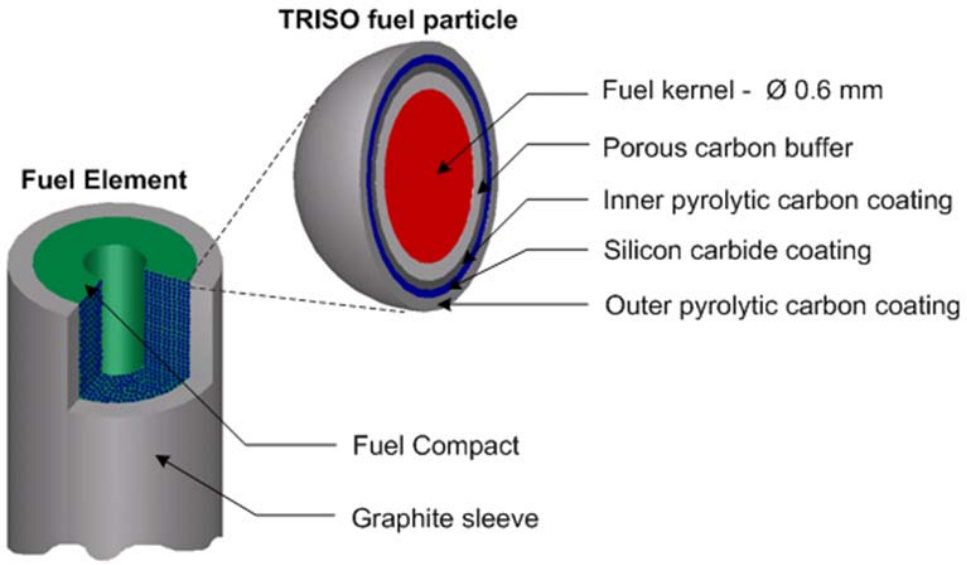

Figure 4.7. VHTR Fuel Element.

Table 4.6. VHTR Fuel Element Properties.

a) TRISO particle	Material	Density (g/cm³)	Radius (cm)
Fuel kernel	UO_2	10.41	0.0300
1st coating	PyC	1.14	0.0359
2nd coating	PyC	1.89	0.0390
3rd coating	SiC	3.2	0.0419
4th coating	PyC	1.87	0.0465

b) Fuel Compact		c) Graphite Sleeve	
Number of fuel particles	176,515	Material	Graphite
Graphite matrix density	1.690 g/cm³	Density	1.770 g/cm³
Diameter-inner	1.0 cm	Diameter-inner	2.6 cm
Diameter-outer	2.6 cm	Diameter-outer	3.4 cm
Height	54.6 cm	Height	57.7 cm

The burnable poison rod is 1.4 cm in diameter and 50 cm in height. It is made up of two neutron absorber sections (20 cm in height) separated by a graphite section (10 cm in height). Table 4.7 lists the properties of the burnable poison rods.

Figure 4.8 shows a three-dimensional representation of the prismatic fuel block and the relative locations of the annular fuel rods, coolant channels, burnable poison rods, and fuel-handling hole. Within the core there are 858 fuel blocks.

Table 4.7. VHTR Burnable Poison Rod Properties.

Absorber Section Material	B_4C-C
Density (g/cm³)	*1.82*
Natural Boron Concentration (wt. %)	*2.74*
Diameter (cm)	*1.39*
Height (cm)	*2.5*
B-10 Abundance Ratio (wt. %)	*18.7*
Graphite Section Density (g/cm³)	*1.77*
Diameter (cm)	*1.4*
Height (cm)	*10*

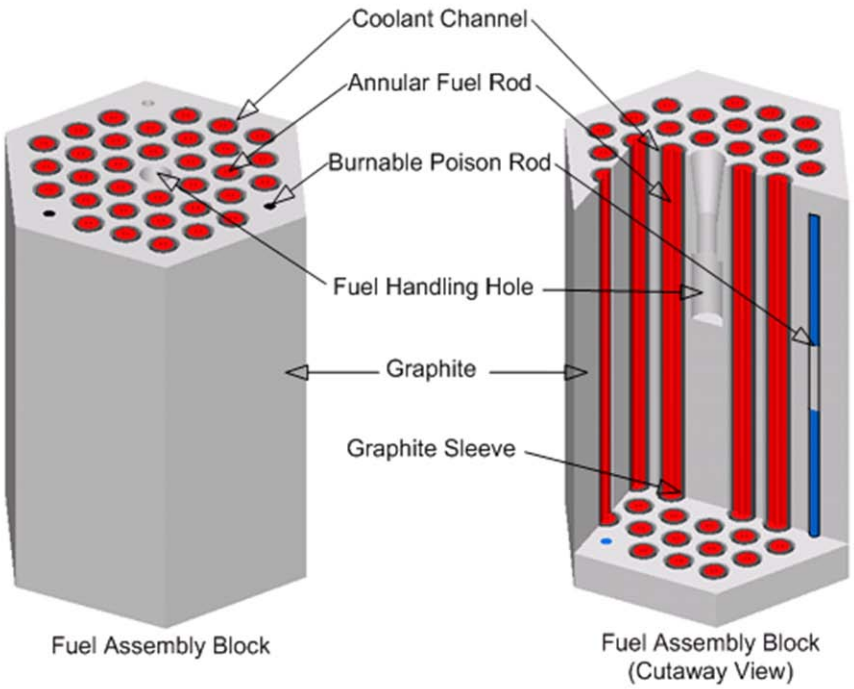

Figure 4.8. VHTR Prismatic Fuel Block.

The replaceable reflector block has the same external form as the fuel assembly block, 36 cm in width across the flats and 58 cm in height with a handling hole in the center of the block. There are two types of reflector blocks: one being a solid graphite block and the other having helium coolant channels in it. Examples of the replaceable reflector blocks are provided in Figure 4.9, with the properties listed in Table 4.8.

Table 4.8. VHTR Replaceable Reflector Block Properties.

Configuration	*Hexagonal*
Material	*IG-110 Graphite*
Density (g/cm³)	*1.76*
Height (cm)	*58*
Width across the flats (cm)	*36*
Coolant hole diameter (cm)	*4.1*
Coolant hole height (cm)	*58*

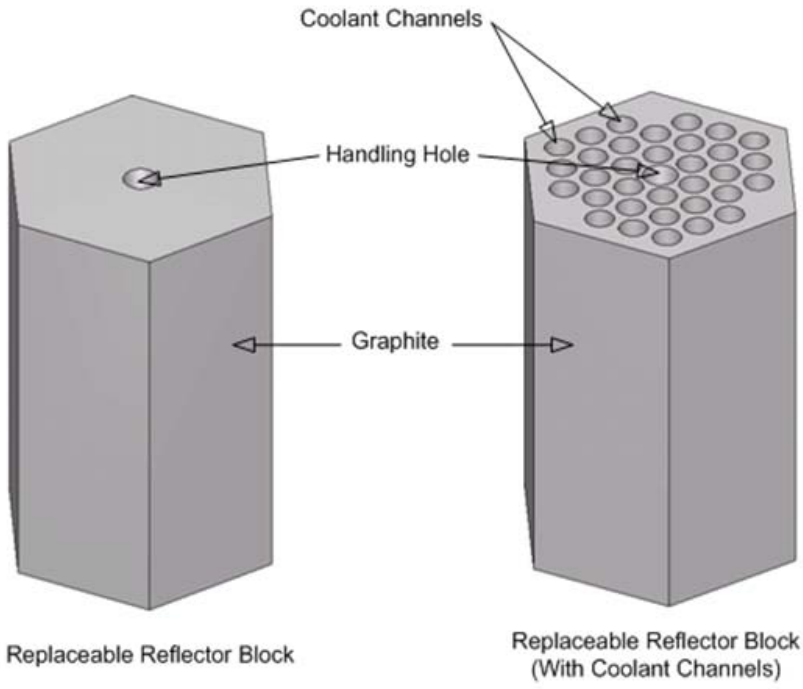

Figure 4.9. VHTR Replaceable Reflector Blocks.

The reflector blocks with the coolant channels are stacked directly above and below the fuel assembly blocks. This creates a fuel column, being composed of 2 replaceable reflector blocks on top, 13 fuel assembly blocks in the middle (active core), and 2 replaceable reflector blocks on the bottom. The replaceable reflector blocks with coolant channels have the same dimensions as the fuel graphite block within the same column, with the exception of not having the three burnable poison insertion holes. This allows the helium gas coolant to flow into the core, through the fuel assemble blocks and around the fuel elements, and then exit the core.

The final type of prismatic block is the control rod guide block. The block consists of a hexagonal graphite block with three large vertical borings. Like the fuel block, it is 58 cm in height and 36 cm in width across the flats. The holes created by the borings have a 12.3 cm diameter and extend through the entire length of the block. Two of the holes are used for the control rods to pass through, while the third is left empty to serve as the reserve shutdown system. In the center of each block is a fuel-handling hole. Figure 4.10 shows the arrangement and dimensions of the control rod guide block and Table 4.9 lists the properties of the block.

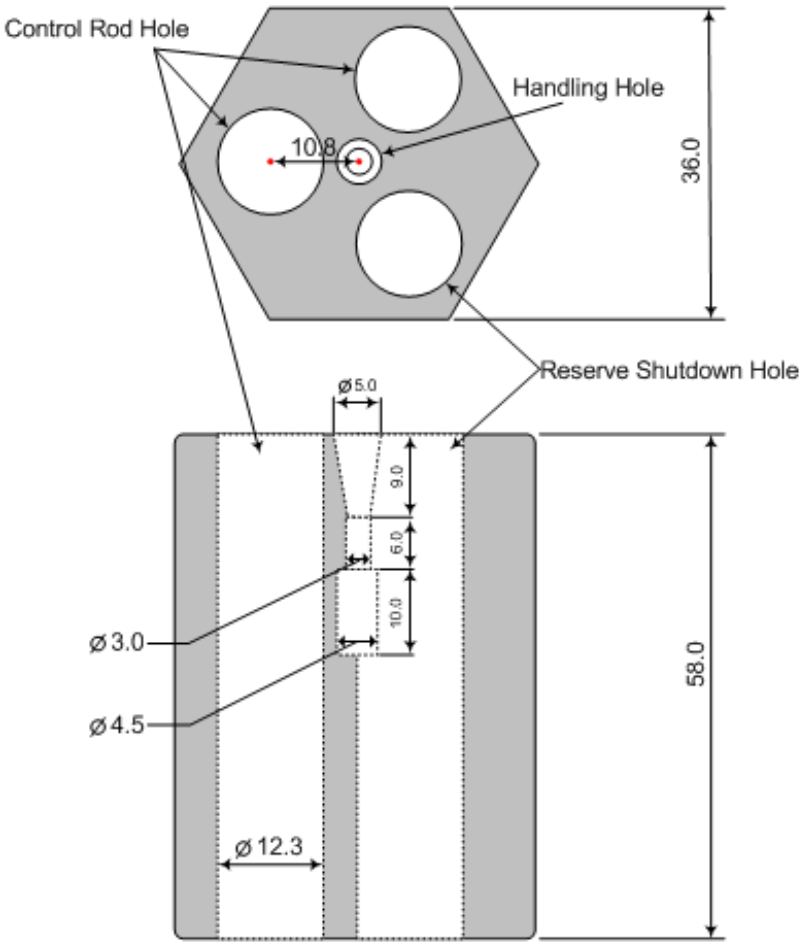

Figure 4.10. VHTR Control Rod Guide Block (measurements in cm).

Table 4.9. VHTR Control Rod Guide Block Properties.

Material	*IG-110 Graphite*
Density (g/cm³)	*1.77*
Height (cm)	*58*
Width across the flats (cm)	*36*
Number of control rod holes in block	*2*
Control rod hole diameter (cm)	*12.3*
Control rod hole height (cm)	*58*
Number of reserve shutdown holes in block	*1*
Reserve shutdown hole diameter (cm)	*12.3*
Reserve shutdown hole height (cm)	*58*

The model can now be described by fuel columns, control columns, the central reflector, and the outer reflector. The fuel and control columns are arranged in an annular configuration that is three blocks wide to create the fueled region of the core. The central graphite column and surrounding graphite reflector make up the remainder of the core. The active core is composed

of 66 fuel columns and 36 control columns that have 13 blocks per column. The bottom reflector is 160 cm thick and the top reflector is 116 cm thick. The active core is 754 cm in height and the overall core is 1030 cm in height. The radial distance from the center of the core to the closest fuel column is 144 cm and the fueled region is 108 cm thick (three fuel/control columns across). The outer reflector is 88 cm thick giving an outer cylindrical core radius of 340 cm. Figure 4.11 shows a 3D and 2D view of the VHTR model with geometry details.

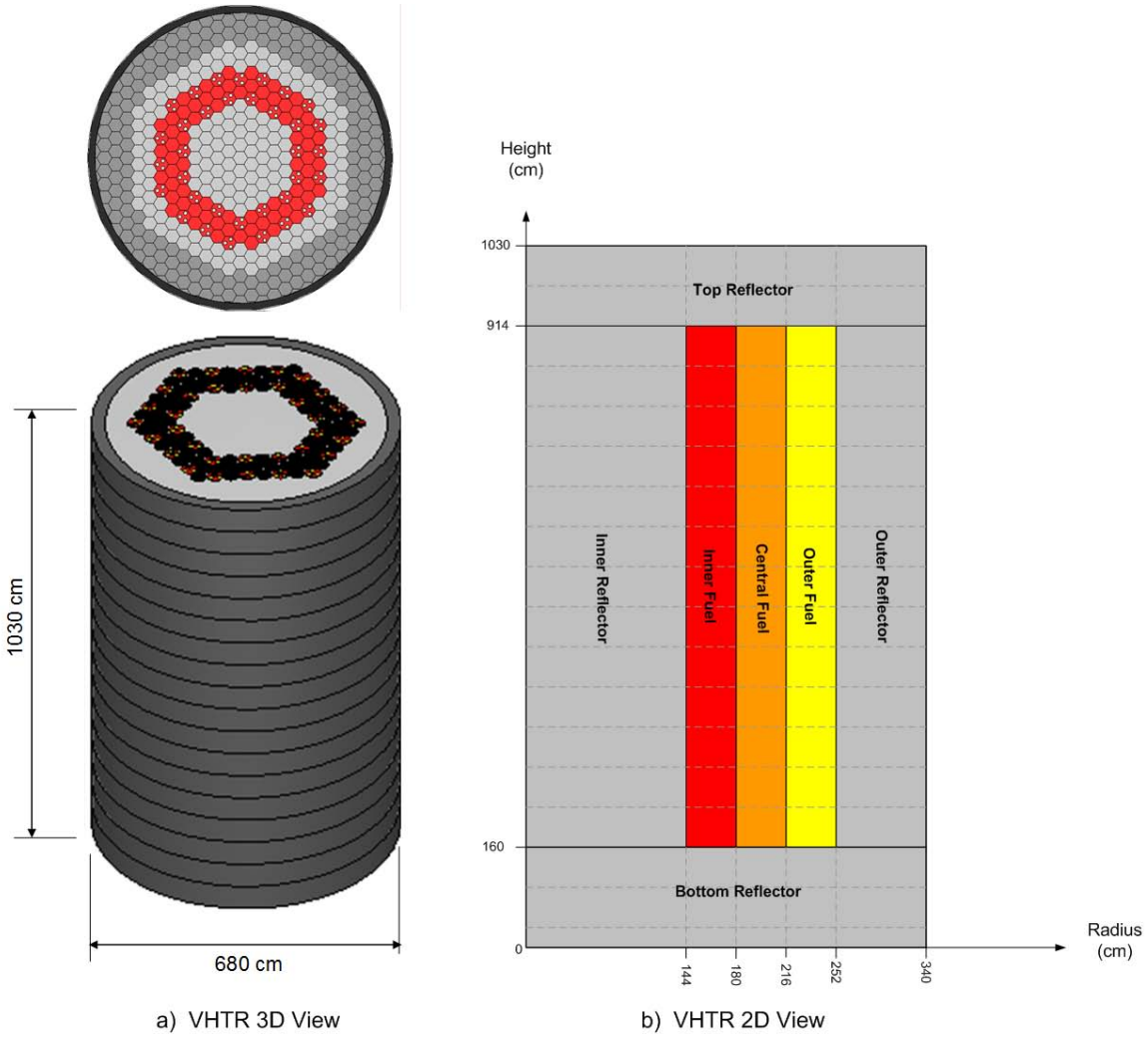

Figure 4.11. VHTR Whole-core 3D Model Geometry Details.

Benchmark Analysis

Many of the well-established computer code systems available for VHTR analysis were originally developed and validated for evaluating LWRs. Although VHTRs and LWRs are both thermal neutron spectrum reactors and share much in common, the VHTR presents unique phenomena that may not be accounted for correctly by the code system and, therefore, must be addressed. The main concern is the randomness in particle distribution and related multi-heterogeneity effects associated with VHTRs. Due to this concern, a detailed benchmark procedure was developed for the VHTR model.

Greater importance was placed on the ability to perform experiment-to-code benchmarking and to combine that with additional code-to-code comparisons. The availability of experimental results led to the HTTR of the JAERI, from which startup core physics results are provided by the IAEA in a Technical Document publication [38]. The major design specifications for the HTTR are given in Table 4.10.

Table 4.10. HTTR Design Specifications.

Thermal Power (MW)	*30*
Outlet Coolant Temperature (°C)	*950*
Inlet Coolant Temperature (°C)	*395*
Primary Coolant Pressure (MPa)	*4*
Core Structure	*Graphite*
Equivalent Core Diameter (cm)	*230*
Effective Core Height (cm)	*290*
Average Power Density (W/cm³)	*2.5*
Fuel	*UO_2*
Uranium Enrichment (wt. %)	*3 to 10*
Type of Fuel	*Pin-in-block*
Burnup Period (days)	*660*
Coolant Material	*Helium gas*
Flow Direction in Core	*Downward*
Top Reflector Thickness (cm)	*116*
Side Reflector Thickness (cm)	*99*
Bottom Reflector Thickness (cm)	*116*
Number of Fuel Assemblies	*150*
Number of Fuel Columns	*30*
Number of Pairs of Control Rods	*16*
In Core	*7*
In Reflector	*9*

In addition to the HTTR benchmark model description provided in this section, complete details of material compositions and geometry specifications are included in Appendix A. The SCALE code system was chosen as the computational tool for modeling the HTTR due to its flexibility in geometry representation, existing temperature treatment options, availability of techniques accounting for double heterogeneity effects, and computational run time for complex whole-core 3D models.

An assessment was performed to determine the best possible method to account for the double heterogeneity effects [39]. This was accomplished by creating two HTTR models, one using the provided DOUBLEHET unit cell treatment available in SCALE 5.1, while the other bypasses the feature. Instead the Dancoff correction factor is independently determined by the code system DANCOFF-MC [40] and manually entered into the model as an external parameter. Table 4.11 provides a comparison of the results for the two different treatments of the heterogeneity effects. As shown, a higher degree of accuracy was accomplished with the DOUBLEHET model; therefore, it was chosen to represent the HTTR model for further benchmark efforts.

Table 4.11. Results for Different Heterogeneity Treatments.

HTTR Model	k_{eff}	Error (%)
Experimental	*1.1363*	-
SCALE 5.0 (with DANCOFF-MC)	*1.1122*	*2.12%*
SCALE 5.1 (with DOUBLEHET)	*1.1368*	*0.04%*

The benchmark problems are related to start-up core physics tests and include the analysis of the effective multiplication factor for the fully loaded core with control rods fully withdrawn and fully inserted, control rod position at criticality, and the isothermal temperature coefficient of reactivity.

Following the established international benchmark program practices, in the present analysis 10% discrepancy between computed values and the available experimental values were considered as the model's acceptability threshold. As evident in Table 4.12, the results are well within acceptable range. Aside from the temperature coefficient, each of the benchmark cases is within 0.25% of the experimental values and fall within the experimental error value. The computed value of the isothermal temperature coefficient deviates by approximately 2% from the corresponding experimental value. However, the experimental value is within the standard deviation limits of the computational result. It is expected that increasing the sample size of the model would result in reducing the discrepancy to within the range of the other benchmark tests, but for the benchmark calculations a maximum computational run time was set and higher accuracy results were not obtained in the present analysis.

Table 4.12. HTTR Experiment-to-code Benchmark Results.

Benchmark		HTTR (experimental)	VHTR model (calculated)	Error (%)
Control Rods Fully Withdrawn	k_{eff}	1.1363 ± 0.041	1.1368 ± 0.0023	0.044
Control Rods Fully Inserted	k_{eff}	0.685 ± 0.010	0.6858 ± 0.0019	0.117
Critical Insertion Depth (300K)	cm	177.5 ± 0.5	177.1	0.225
Critical Insertion Depth (418K)	cm	190.3 ± 0.5	189.9	0.210
Temperature Coefficient	Δk/k/K	-1.42×10^{-4}	-1.45×10^{-4}	2.113

The HTTR configuration with the control rods fully withdrawn was chosen as the prototype VHTR configuration. The best agreement with experimental data was observed for that case.

Table 4.13 summarizes the basic reactor physics characteristics obtained for the prototype VHTR configuration.

Table 4.13. Basic Reactor Physics Results (Withdrawn Control Rods).

k_{eff}	Fission-Inducing Energy (eV)	System Mean Free Path (cm)	Fission Neutron Yield
1.1368 ± 0.0023	0.814041 ± 0.0002014	2.9445 ± 0.00121	2.43872 ± 0.00001

The HTTR is currently the only operating VHTR prismatic core design; making it a focal point for VHTR related research. The HTTR was designed according to established objectives, which categorize it as a small-scale VHTR. The future VHTR power reactors will most likely consist of annular core designs, whereas the HTTR is a cylindrical core design. An annular core is one of the promising core types for the future VHTRs because of its high inherent safety characteristics related to a loss of coolant accident. The decay heat removal is enhanced by the introduction of the annular core because the heat transfer path will be shortened due to the relatively thin active core region. As a result, the fuel temperature in a loss of coolant accident can be maintained at less than the fuel temperature limit of 1600 °C [41].

The prismatic whole-core 3D model was adjusted from the original cylindrical core of the HTTR to that of a larger annular power core (600 MW_{th}), which represents the VHTR model used in the nuclear energy system within this study, as described in Table 4.4 and Figure 4.11.

To maintain the consistency of the annular VHTR model an exact model was built in MCNP to perform a code-to-code benchmark for the new configuration. A comparison of the multiplication factor for the SCALE and MCNP models is provided in Table 4.14.

Table 4.14. VHTR Code-to-code Results.

Code System	k_{eff}	% difference
MCNP5	1.26737	0.124
SCALE (KENO-VI)	1.26580	

In addition to the multiplication factor, the average energy-dependent neutron flux within the fuel compacts was also evaluated for the models. As shown in Figure 4.12 the flux profile is typical for that of VHTRs, but what is of more interest is the direct comparison of the spectrums produced by the two code systems, which are almost indistinguishable.

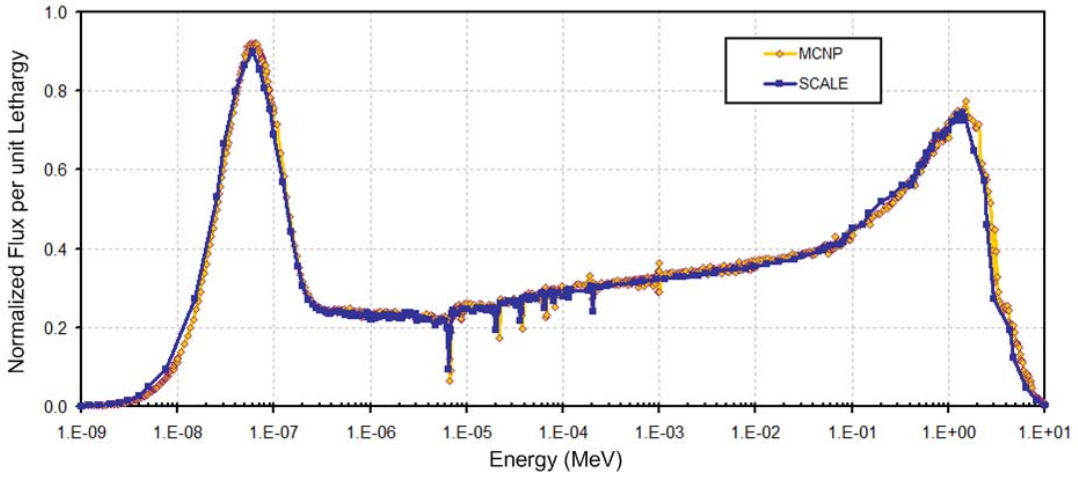

Figure 4.12. Neutron Flux Profiles in the VHTR Fuel Compacts (MCNP vs. SCALE).

4.1.3 High-energy External Source Transmuter (HEST)

Subcritical cores driven by an external neutron source (often referred to as hybrid nuclear reactor systems) have been the subject of many earlier research studies dating back to the early 1950s [42,43,44]. The foreseen advantages for fuel generation, energy production, and most recently, waste minimization have driven such efforts. Even so, hybrid nuclear systems have never advanced past the conceptual study phase, making them quite different from the AP1000 and VHTR reactor units. Both of these designs (especially the AP1000) rely on previous operating experience and on proven designs.

In recent years a great deal of interest, or a renewal of interest, has been displayed worldwide in hybrid reactors mainly due to the perceived advantages for transmuting the long-lived actinides of spent nuclear fuel into a much more manageable waste form [8-14, 45]. These advantages stem from the safety features that accompany subcritical systems, allowing for extremely high transmutation efficiencies as compared to other options.

External Neutron Source Survey

Potential neutron sources for hybrid systems must meet two important criteria: 1) be a high intensity source and 2) produce high-energy neutrons. In addition, the size of the neutron source can play an important role, with the ultimate goal being a small compact source.

Many possibilities for neutron sources have been identified and studied. In regard to hybrid systems, the most promising and consequently the most investigated neutron sources fall into two main categories: 1) accelerator driven system (ADS) spallation neutron sources, and 2) fusion neutron sources.

ADS neutron sources use proton accelerators, which deliver continuous wave neutron beams with an energy of 1GeV. The accelerator is either the linac or cyclotron type. The protons are

impinged upon a heavy element spallation target to produce source neutrons. The spectrum of spallation neutrons is similar to the fission neutron spectrum but shifted to a slightly higher energy. In addition, very high neutron yields are attainable. The production of extremely intense and high-energy neutrons makes ADS systems attractive for driving subcritical cores for waste elimination and energy generation. High cost and reliability issues are the main detractors for ADS systems.

A similar alternative to ADS is a photonuclear-based neutron source using an electron linear accelerator [46]. Comparatively, electron LINAC-based neutron sources are an attractive alternative to spallation neutron sources due to being inherently compact, economical, reliable, ease to handle, and less hazardous in nature. Of course a tradeoff comes in the intensity and energy spectrum of the neutrons produced, and it is debatable whether the tradeoffs make it a serious contender for hybrid systems. With that in mind, and looking to the future, promise has been shown towards improving neutron yields to a level that might make electron LINAC-based neutron sources advantageous to the more expensive and complicated ADS.

The most promising fusion neutron sources use the neutrons produced from the deuterium and tritium fusion reaction. The nuclei of two isotopes of hydrogen, deuterium (D), and tritium (T) react to produce a helium nucleus (α) and a neutron (n). In each reaction 17.6 MeV of energy is liberated:

$$D + T \rightarrow n\left(14.1\ MeV\right) + \alpha\left(3.5\ MeV\right)$$

There are a number of different options for creating the conditions necessary for the D-T fusion reaction, which are classified as follows:

- Strong magnetic field concepts: involves suspending a plasma in a magnetic field and increasing its temperature and pressure to immense levels.
  - Tokamaks: magnetic field is used to confine a plasma in the shape of a torus (pulsed operation)
  - Stellarators: like the Tokamak, has a toroidal magnetic field topology, but is not azimuthally symmetric (continuous operation)
  - Mirror machines: "open" system that uses mirrors to reflect ions and electrons back towards the plasma (continuous operation)
- Inertial confinement devices: process where nuclear fusion reactions are initiated by using intense energy beams for heating and compressing a fuel target.
  - Laser-driven inertial confinement: uses laser light to compress and heat target (pulsed).
  - Z-pinch: intermediate of magnetic and inertial confinement. A type of plasma confinement system that uses an electrical current in the plasma to generate a magnetic field that compresses it (pulsed).
  - Inertial electrostatic confinement (IEC): involves the creation of deep electrostatic potential wells within a plasma in order to accelerate ions up to energies sufficient for fusion reactions to occur (continuous or pulsed).
- Muon-catalyzed fusion (μCF): process allowing nuclear fusion to take place at temperatures significantly lower than the temperatures required for thermonuclear fusion. (cold fusion).

Model Description

The HEST analysis focuses more on the potential for TRU transmutation as opposed to the technological feasibility of specific concepts. A physics approach to transmutation [47,48] was utilized for a full understanding of the transmutation potential of different neutron fields.

The neutron consumption/fission (D_j) of isotope J is defined as the number of neutrons needed to transform the nucleus and its reaction products into fission products. The evaluation of D_j considers a core with an average neutron flux that is fed by actinides at a rate S (nuclides/s). Under irradiation the transmutation of the feed nuclides (J-vectors representing the in components) yields the out components of the J-vectors. The transmutation behavior of each the J-vectors can be considered separately and it is possible to calculate the number of neutrons produced/consumed by each during irradiation. The branching of the J-vectors, a result from the many nuclear reactions, leads to paths that will have one of three out comes: 1) consume neutrons, 2) produce more neutrons, or 3) have no influence on the total neutron balance. The total number of neutrons D_j is calculated by:

$$D_J = \sum_{J1_i} P_{J\to J1_i}\left\{R_{J\to J1_i} + \sum_{J2_i} P_{J1\to J2_i}\left[R_{J1\to J2_k} + \sum_{J3_n} P_{J2_k\to J3_n}(....)\right]\right\}, \qquad (20)$$

where $P_{JNr\to J(N+1)s}$ is the probability of transmutation of the nuclide JNr into the nuclide J(N+1)s. $R_{A\to B}$ is the neutron consumption factor representing the number of neutrons consumed during the transition A→B, with each reaction type defined as:

- Neutron capture (n,γ) with 1 neutron being captured
- Neutron capture and subsequent multiplication (n,mn) with $(1\text{-}m)$ neutrons being produced,
- Fission with $(1\text{-}\nu_f)$ neutrons being produced,
- Natural decay with 0 neutrons being captured,
- Discharge and nuclide loss with 0 neutrons being captured.

In accordance with the above definitions, Table 4.15 gives the values for the neutron consumption factor $R_{A\to B}$.

Table 4.15. Neutron Consumption Factor for Different Reaction Types.

Reaction Type	Capture (n,γ)	Fission (n,f)	$(n,2n)$	Radioactive Decay
$R_{A\to B}$ =	1	$(1\text{-}\nu_f)$	-1	0

If parasitic neutron consumption (fission products, structural material, etc.) and neutron leakage is neglected, then the total number of neutrons, D_j, consumed by the given J-vector is a measure of the capability of the core to achieve destruction of a given J-vector feed. Positive D_j indicates neutron consumption dominates over neutron production and the core requires a supplementary neutron source to support transmutation. Negative D_j indicates the core produces enough neutrons to support transmutation.

The linearity properties of the neutron concentration equation make it simple to determine D_{fuel} for a mixture of isotopes using the formula below:

$$D_{fuel} = \sum_J \varepsilon_J D_J \tag{21}$$

where ε_J is the fraction of the J-vector in the feed stream.

The D-factor concept helps to understand if transmutation is feasible in a particular type of reactor. However, to gain a complete understanding, the global neutron balance of a core needs to be considered. The general equation for the Neutron Surplus (NS_{core}) expressed in units of neutrons per fission then becomes:

$$NS_{core} = S_{ext} - D_{fuel} - C_{par} - C_{FP} - L_{core} \tag{22}$$

where S_{ext} is a potential external neutron source, C_{par} is parasitic capture in structural material, C_{FP} is capture in fission products, and L_{core} is neutrons lost to leakage.

By equations (20) and (21) the neutron balance, D_{mix}, can be determined for a composition consisting of *i*-components by:

$$D_{mix} = \sum_i \sum_r R_r^{(i)} P_r^{(i)} \bar{N}_i \tag{23}$$

where $\bar{N}_i$ is the asymptotic solution of the nuclide production/destruction equations, $R_r^{(i)}$ is the neutron consumption factor for reaction (r) and nuclide (i), $P_r^{(i)}$ is the reduced transition rate for reaction (r) and nuclide (i). Table 4.16 shows $R_r^{(i)}$ and $P_r^{(i)}$ for the main reactions.

Table 4.16. $R_r^{(i)}$ and $P_r^{(i)}$ for Reaction Type.

Reaction, *r*	P_r	R_r
Radiative Capture	$\sigma_c\phi$	1
Fission	$\sigma_f\phi$	$1-\nu_f$
Radioactive Decay	λ	0

Consider the nuclide production/destruction equation in the following form:

$$\frac{d}{dt}\bar{N} = \hat{M}\cdot\bar{N}\phi - \bar{F} \tag{24}$$

where $\bar{N}$ is a column vector of the atomic concentrations, $\hat{M}$ is a nxn matrix related to all nuclear interaction processes, ϕ is the flux, and $\bar{F}$ is the nuclei feed vector. A problem of this form has an exponential solution. As $t \to \infty$, the asymptotic solution corresponds to the equilibrium case, in which $d\bar{N}/dt = 0$. Thus the solution can be expressed in matrix form by:

$$\bar{N} = \hat{A}^{-1}\bar{F} \tag{25}$$

where $\hat{A} = \hat{M} \times \phi$ and $\bar{F} = [F_i : i = 0,1,...I]$; I = number of nuclides. The linear character of equation (6) allows evaluation of the concentrations of each vector nuclide independently, with a "unit" source for the corresponding feed, $F_i = 1$.

Equations (21), (23), and (25) can be used to calculate the neutron balance for the TRU fuel (D_{eq}^{TRU}) and the individual TRU nuclides (D_{eq}^{I}) as a function of the core flux, assuming the TRU

feed isotopic concentrations and all the nuclear interaction processes of the $\hat{M}$ matrix are known. The TRU composition is predetermined by the VHTR burnup calculations and the subsequent decay time before irradiation in the HEST. However, determining the one group microscopic cross-sections and average number of fission neutrons liberated for each of the isotopes of interest is no trivial feat, since they are spatially and energy dependent.

In order to produce the microscopic cross-sections (σ) and fission neutrons (ν) for the TRU isotopes, whole-core 3D models were created in MCNP. Two HEST core configurations were chosen for evaluation. The first utilizes the concept of an intense external fusion neutron source placed at the center of a subcritical core. The core design is the same as the VHTR, with the central graphite column removed and the surrounding graphite reflector replaced with a stainless steel type reflector and shield.

Figure 4.13 shows the core cross section for the HEST Concept I. The isotropic 14.1 MeV neutron source has an intensity ranging from 10^{17} – 10^{20} n/s. The fuel assemblies are hexagonal graphite blocks with fuel compacts containing used TRISO fuel from the VHTR. The presence of graphite will moderate a portion of the neutrons, but the spectrum is still expected to be skewed towards high energy levels.

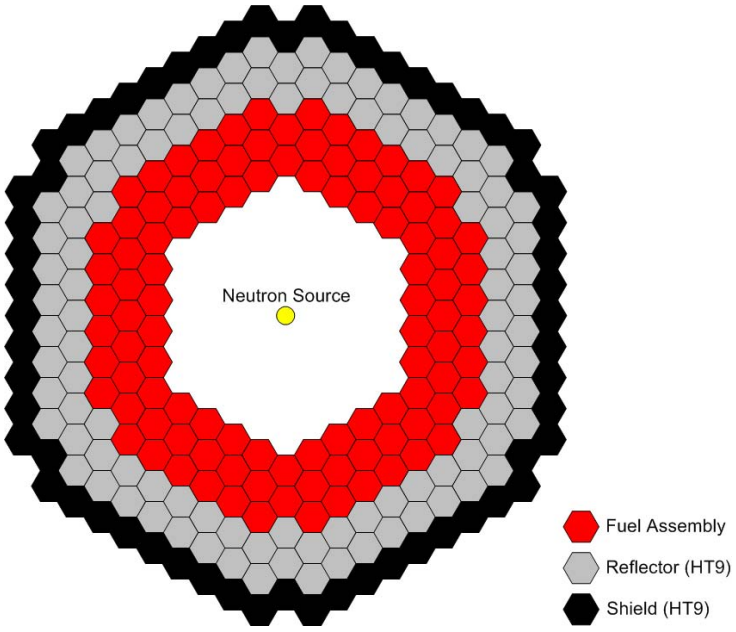

Figure 4.13. HEST Concept I.

The second concept utilizes the small compact IEC fusion neutron source. Compared to the first concept, the intensity of the IEC source is considerably lower, but its small size, portability, and low cost make it possible to implant the source very close to the fuel elements. In addition, a large number of sources can be used to provide a distribution of source neutrons, to provide flexibility in core design, and in flux profile control.

Figure 4.14 shows the HEST Concept II, which consist of a VHTR fuel assembly block with a cylindrical IEC neutron source placed in a boring running lengthwise through the center of the

block. The cylindrical IEC acts as a line source emitting 14.1 MeV neutrons at an intensity of $10^{10} – 10^{14}$ n/s.

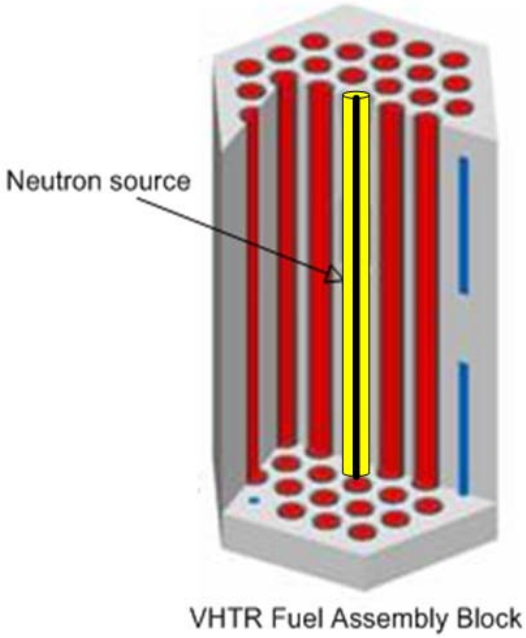

Figure 4.14. HEST Concept II.

Currently, IEC sources are commercially available from a number of companies. NSD-Fusion GmbH of Germany produces cylindrical type IEC devices that produce 10^{11} n/s at 14.1 MeV. IEC concepts carried out on the laboratory scale have reached over 10^{12} n/s and development plans target a 10^{14} n/s prototype in the intermediate term, followed by a full demo unit at 10^{18} n/s [49]. The IEC is driven electrically and is very compact in size. Compared to the other neutron sources it is particularly simple, much less expensive, and requires considerably less to implement.

The HEST Concept II model does not include a reflector, so neutron leakage is expected to be high. The model performance will be extrapolated to that expected for a core made up of multiple assembly blocks all embedded with IEC drivers.

The neutron balance calculations are performed by the MATLAB code system. An algorithm was developed to use the output generated by the MCNP5 models for HEST Concept I and II (core specific one group microscopic cross-sections and fission neutrons for the TRU nuclides) to solve for the equilibrium concentrations as defined by equation (6). The concentrations are then used to solve for the neutron balance for the TRU fuel, D_{eq}^{TRU}, by equation (4) and then the neutron balance for the individual TRU nuclides, D_{eq}^{I}, equation (2) are calculated. The model provides the neutron balance results as a function of average core flux, allowing for a range of neutron source intensities to be evaluated for TRU transmutation potential.

4.2 Fuel Cycle Components

4.2.1 Front-end Components

Accompanying the reactor units in NES are the fuel cycle components. Composing the front-end portion of the cycle are the mining, milling, conversion, enrichment, and fuel fabrication. As a result of front-end procedures, DU and mill tailings are accumulated and must be stored as LLW. The main concern for the front-end is material flow and its effect on mining and waste storage strategies.

The IAEA's simulation system NFCSS was used to model the portion of the NES that includes the front-end components and the AP1000, as shown in Figure 4.15. NFCSS is a scenario based computer model for the estimation of nuclear fuel cycle material and service requirements. It has been designed to quickly estimate long-term fuel cycle requirements and actinide production. Natural uranium, conversion, enrichment, and fuel fabrication quantities are predicted. Additionally, the quantities and qualities (isotopic composition) of unloaded fuels are evaluated.

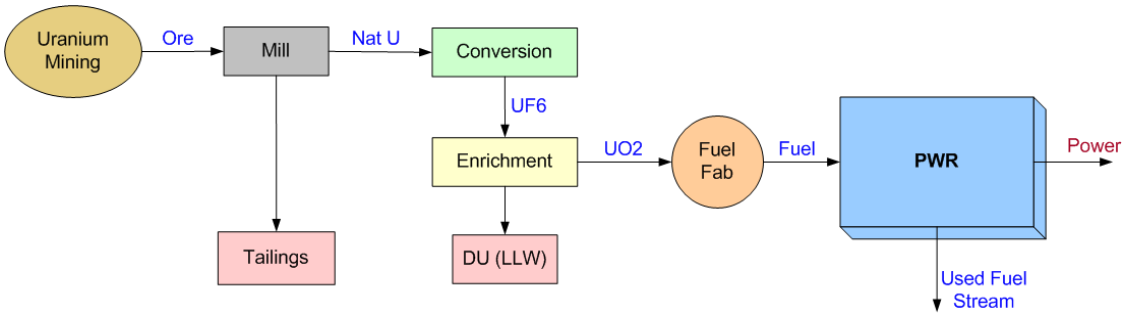

Figure 4.15. NFCSS Components.

The NFCSS model tracks the overall material flow in each of the processes described in the fuel cycle as presented in Figure 4.16. The model assumes zero losses in the conversion, enrichment, and fuel fabrication stages. The reactor model (fuel depletion model) is the most important part of the simulation since it calculates the inventory of used fuel after irradiation. The reactor model is required to be an optimum combination of simplicity, accuracy, and speed. Therefore, the IAEA developed CAlculation of INventory of spent fuel (CAIN) specifically for the needs of NFCSS. CAIN solves the Bateman's Equations for a point assembly using one group neutron cross-sections. In order to meet the accuracy, simplicity, and speed requirements, a set of assumptions were built into the code. CAIN currently has 28 reaction and decay chains during irradiation and 14 decay chains during cooling. The main assumptions built into CAIN are listed below [27].

- The selection of the nuclides has been performed for the importance of the nuclides in radiotoxicity of the spent fuel and their nuclear characteristics.
- Although natural uranium includes ^{234}U (<0.01%), this nuclide is ignored, because the transmutation from ^{234}U to ^{235}U is too small.

- Nuclides with short half-lives (half life < 8 days) are ignored. That is, ^{237}U (7 days), ^{238}Np (2 days), ^{238}Pu (5hrs), ^{242}Am (16 hrs), ^{244}Am (10 hrs), and ^{244m}Am (26 min) are assumed to decay and go to the next nuclide simultaneously.
- Long half-life nuclides (half-life > 400 years) are assumed as stable for the irradiation period. As example, ^{241}Am (432 yr) is treated as stable during irradiation. For decay (cooling) period after discharge, all nuclides are treated by their actual decay scheme.
- In the chain shown in Figure 4.16 transmutation is terminated for certain nuclides (shown as "x").
- The 28 reaction chains and 14 decay chains are selected to be suitable for fresh fuels containing any of the 14 nuclides of the CAIN library. Some reaction chains are neglected due to their contribution to the composition of the spent fuel. The nuclides included in the calculations are listed in Table 4.17.
- Among 14 nuclides, decays of ^{238}Pu (87.7 yr), ^{241}Pu (14.4 yr), ^{242}Cm (0.447 yr), and ^{244}Cm (18.1 yr) are considered during irradiation. Figure 4.16 shows the transmutation chain after specification for the CAIN code.

Table 4.17. Nuclides Included in CAIN Calculation.

Uranium	^{235}U	^{236}U	^{238}U		
Neptunium	^{237}Np				
Plutonium	^{238}Pu	^{239}Pu	^{240}Pu	^{241}Pu	^{242}Pu
Americium	^{241}Am	^{242m}Am	^{243}Am		
Curium	^{242}Cm	^{244}Cm			

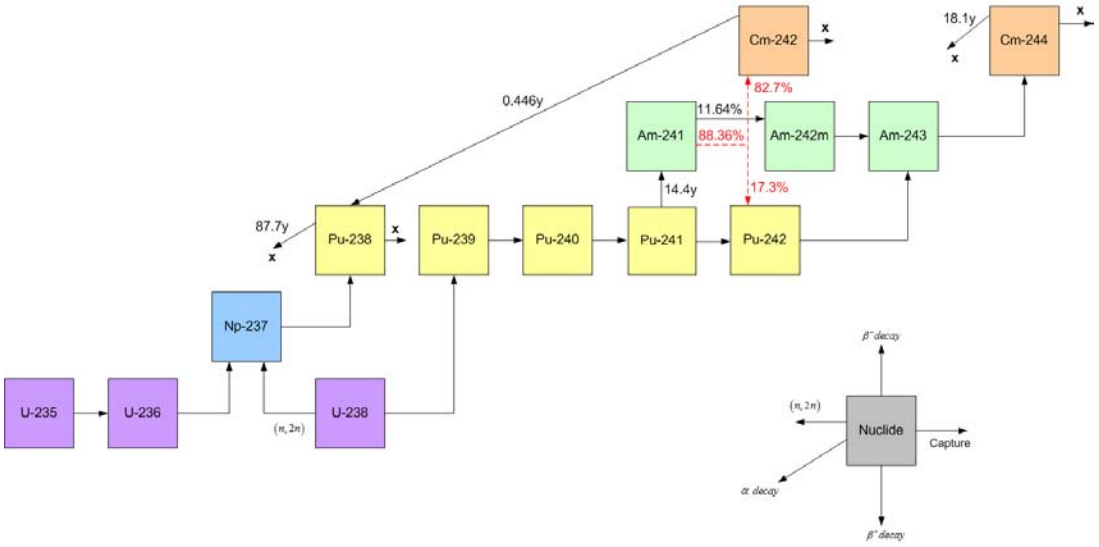

Figure 4.16. CAIN Transformation Chain.

The input parameters for the model are mostly dependent on the parameters for the AP1000 model, with the exception of the grade of the uranium ore and the enrichment tail assay, which are both adjusted to current typical values for each case. The mine grade is set at a value of 1% uranium containment within the ore, and the tail assay, which is defined as the percent of ^{235}U

remaining in the depleted stream of enrichment operations is 0.30%. The parameters consisting of reactor type, fuel type, power, and thermal efficiency are determined by the design parameters for the AP1000. The remaining input parameters of load factor, enrichment, and average discharge burnup are dependent on the optimum values determined for the NES. Table 4.18 lists the input parameters for the NFCSS.

The NFCSS model produces output indicating the required quantity of uranium ore, the natural uranium needed for the conversion process, the amount of UF_6 needed for enrichment, the final quantity of UO_2 for reactor operation, and the amount of DU produced. The Separative Work Unit (SWU) is also calculated for the system in addition to the isotopic composition of the used fuel.

Table 4.18. NFCSS Input Parameters.

Reactor Type	PWR
Fuel Type	UO_2
Nuclear Power (MW_e)	1115
Load Factor	Variable
Thermal Efficiency	32.8
Average Discharge Burnup (GWd/tIHM)	Variable
Initial ^{235}U Enrichment (wt. %)	Variable
Mine Grade (% U)	1.0
Tail Assay (% ^{235}U)	0.3

4.2.2 Reprocessing - Partitioning/Separation

The computational model representing the reprocessing process was designed to track the material streams while accounting for radioactive decay and material losses accrued during the procedure. The material tracks are modeled according to the URanium Extraction (UREX) process in which the Uranium and Technetium are separated from each other and the other FP and actinides. A suite of UREX+ processes offer the ability to produce different product lines with varying mixtures of actinides and FPS. The process used for the NES model is UREX+1a, which has five product lines made up of: 1) Uranium, 2) Technetium, 3) Cesium/Strontium, 4) TRU, and 5) remaining FP. In addition to tracking materials, the model creates a database for storing material compositions for varying AP1000 input parameters making them easily assessable for analysis. The numerical computational environment MATLAB is utilized for the simulation procedure and material database storage.

4.2.3 High Level Waste Storage Facility

The computational model for the waste storage facility applies the normalized heat factors and normalized radiotoxicity factors for the TRU and the related isotopic priority rankings developed in Chapter III to quantify repository performance, which in turn can be used for making comparisons to other fuel cycles. It will simulate a geological repository by tracking isotopic compositions over long periods of time and calculating resulting heat load and dose

measurements in order to analyze waste management strategies. The ORIGEN-S code package is utilized for predicting radionuclide inventories after many years of decay. MATLAB is used for data processing involving dose and heat load calculations for assorted isotopic compositions.

4.3 Integrated System Model

The Integrated System Model (ISM) was developed within the MATLAB/Simulink environment. Simulink works with MATLAB to offer modeling, simulation, and analysis of multidomain dynamic systems under a graphical user interface environment. Simulink includes a comprehensive set of customizable block libraries for both linear and nonlinear analyses. As Simulink is an integral part of MATLAB, it is easy to switch back and forth during analysis making it possible to take advantage of the features offered in each environment. The available options and flexibility of MATLAB/Simulink make it an ideal candidate for the ISM.

The main objective of the NES integrated model is to develop an approach to seamlessly couple the various models that compose the environmentally benign system. The goal being to devise a computational shell that effectively controls the set of reactor and fuel cycle component models with command over key user input parameters and the ability to effectively consolidating vital output results into readily usable form, and to do so in a manner that allows uncertainty/sensitivity analysis and optimization procedures to be performed in a realistic and time efficient manner.

In basic terms, the ISM is a MATLAB/Simulink based computational model that uses a specially prepared database to predict overall system performance and behavior based on a number of different input parameters that are allowed to vary over a specified range. The input parameters are introduced into a database and the appropriate data is retrieved and prepared to construct a function that describes the behavior of the data. An interpolation or extrapolation method is then called to calculate the corresponding data, which is then processed and manipulated into final output form, or fed back into the system and the procedure is repeated as many times as necessary to obtain a set of output results as related to the input parameters. Figure 4.17 shows the basic operational procedures for the ISM.

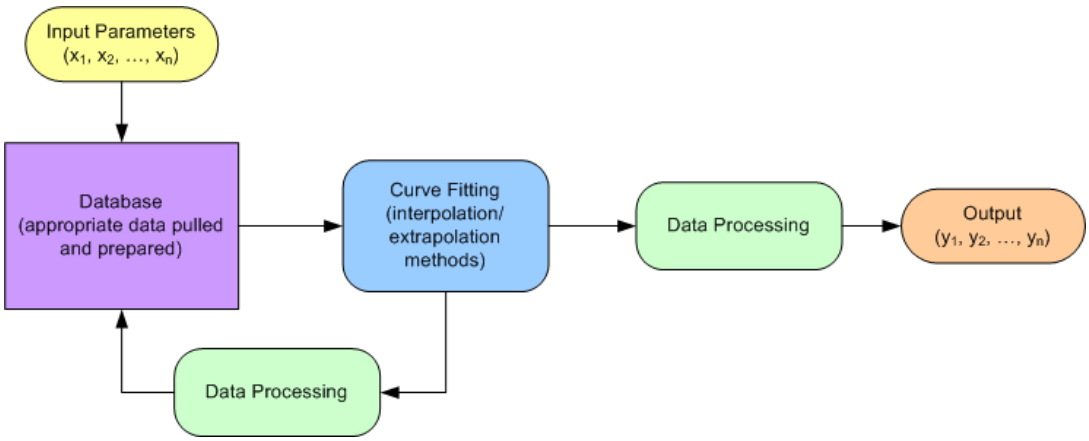

Figure 4.17. ISM Basics Flowchart.

To describe the ISM in further detail the overall system is broken down into its individual components, which can be thought of as a set of interacting or interdependent entities (subsystems) forming an integrated whole. Each of the subsystems can also contain input variables, which, may or may not, progressively rely on one another as additional subsystems are added to the system.

The reactors and fuel cycle components within the NES, as described earlier in this chapter, represent the individual subsystems. Before detailing the procedures of the ISM as it directly relates to the NES, the procedure will be described in general terms. The rational is that although the ISM was developed with the NES in mind, it can be modified to fit other systems that share common characteristics. For example, reactor components can be added or removed from the NES along with their related input variables, thus producing an entirely different advance nuclear fuel cycle. Even so, the new system's structure, behavior, and interconnectivity are very similar to the NES and, likewise, it can be modeled by the ISM with minor modifications. A good candidate for simulation by the ISM is any system that operates under similar characteristics and is composed of complicated subsystems that are extensively time consuming to model or study experimentally.

Changes made to system dependencies or to the dataflow in the system will be reflected in the database for the ISM. The database structure and indexing is directly related to the subsystems, input variables, and their interdependence within the system.

4.3.1 Generic System

The features of the ISM can best be described by a generic system, named SystemABC. The system is composed of three separate but interdependent subsystems, called subsystem-A, subsystem-B, and subsystem-C. Each subsystem contains input variables, such that subsystem-A has input variables a_1 and a_2; subsystem-B has input variables b_1, b_2, and b_3; and subsystem-C has input variables c_1 and c_2. Figure 4.18 shows the arrangement of SystemABC. In general, the number of subsystems and input variables that makeup the system are arbitrary, as each system will be different. The arrangement for SystemABC was chosen to illustrate the modeling procedure.

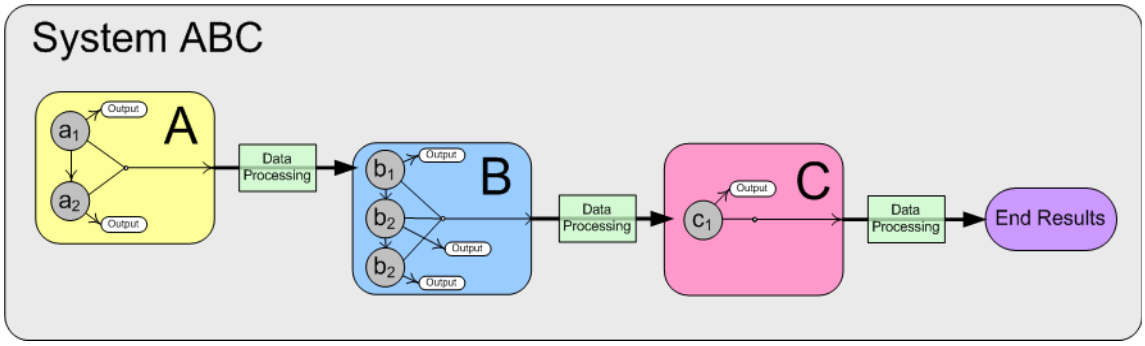

Figure 4.18. Arrangement of Generic SystemABC.

ISM Database

The backbone of the ISM is its extensive database. The database can be viewed as a set of multi-degree arrays that are arranged to allow quick computational access. The database is structured to match the number of subsystems and input variables within the system and the interdependence between them. With the database correctly populated and indexed, the system can efficiently map input to a set of output values by assembling a lookup table and then constructing the appropriate mathematical functions between selected data points and applying curve fitting techniques for interpolation or extrapolation methods.

The input variables determine the degree of the array needed for the database in order to support the ISM. As the number of input variables increases, so do the dimensions of the array. One variable needs a 1D data array, two variables require a 2D array, three input variables require a 3D array, and so forth. To support the SystemABC, a 6D array is required for the database.

Each of the input variables is allowed to vary within a specified range. For example, within subsystem-A variable a_1 has a range that is represented by:

$$a_1 = a_{1,1} \rightarrow a_{1,n},$$

where $a_{1,1}$ is the smallest value for the variation in a_1, and $a_{1,n}$ is the largest value. Each of the input variables in the overall system will have its own specified range according to the desired analysis related to each.

Breakpoints within the specified range for each of the input variables is assigned according to user knowledge related to the effect that the variable of interest has on the subsystem. This includes experience from prior analysis and/or the difficulty involved with producing the needed data. For instance, if the input variable has a highly randomized effect on the system relative to small variations in that parameter, then a higher number of breakpoints would be suggested. Whereas, if the input parameter has a minimal effect or it results in a change that is a smooth steady transition, then fewer breakpoints would be needed. Also of concern is the difficulty and time involved in producing results at each breakpoint, as it can limit the amount of achievable breakpoints. The breakpoints assigned to a_1 are as follows:

$$a_1 = a_{1,b1},\ a_{1,b2},\ ....,\ a_{1,bn},$$

where $a_{1,b1}$ is the first breakpoint for a_1, and each additional breakpoint increases monotonically until the final breakpoint $a_{1,bn}$ is achieved. The breakpoints are required to increase monotonically in order for the lookup table to operate correctly, which creates index values for the interpolation and extrapolation procedures. Similarly, the remaining breakpoints within the system are assigned for each input parameter.

Demonstratively, the number of breakpoints for SystemABC is arbitrarily set as follows: $a_1 = 5$, $a_2 = 3$, $b_1 = 4$, $b_2 = 3$, $b_3 = 4$, and $c_1 = 6$. Each set of breakpoints are spaced an equal distance apart in the example, but this is a choice of the user, as ideal spacing between each breakpoint will be dependent on the input variable and its effect on the subsystem. Additionally, the index search method for the ISM can be set to one of three methods for improved performance depending on the spacing of the breakpoints. If the breakpoint data is evenly spaced the greatest speed can be achieved by using the "evenly spaced points" index search method. For irregularly spaced breakpoint sets with input signals that do not vary much from one step to the next, the

"linear search" method offers the best performance. If the breakpoints are irregularly spaced with rapidly vary input signals that produce large variations in the subsystem, the "binary search" method produces the best performance. The binary search method is the default setting for the ISM.

The breakpoints determine the number of the elements required within each dimension of the multi-dimensional array that comprises the database. Each breakpoint will represent an element within the array and is indexed according to the input variable it is associated with. Therefore, the overall size of the database is set by the total system input variables (array dimension) and the breakpoints for each variable (elements within the multi-dimensional array). Thus, the database required to support SystemABC is a 6D array of size 5x3x4x3x4x6, indicating that 4320 elements are needed to populate the database.

The ISM is arranged so that output information can be gathered for each input variable signifying the affect that that particular variable has at its specified level in the system. To accomplish this the database must include an individual data array, or lookup table, for each of the input variables. The dimension of the array is incremental with the position of the variable in the overall system. Each array is a portion of the overall system's multi-dimensional array, just of a lesser dimension. In any case, this feature increases the size of the database, but the uniqueness of the elements making up the database remain the same.

With the database populated and indexed accordingly, the system model calls the appropriate data for curve fitting and uses interpolation or extrapolation algorithms for calculating output data. If the input value matches a specified breakpoint value then the corresponding elemental value in the multi-dimensional array is output. If the input does not match a specified breakpoint, the interpolator generates the appropriate output. If the input is beyond the range of the breakpoints, the extrapolator outputs appropriate values.

Interpolation Methods

The ISM offers the choice of three types of interpolation methods that present a trade-off between computational time and smoothness of the results. The first method uses rounding methods and is the quickest but least smooth. The second method is linear interpolation and is slower than rounding but generates smoother results, except at breakpoints where the slope changes. The third and final method is cubic spline interpolation that is the slowest but produces the smoothest results.

The rounding method simply checks if an input value falls between breakpoint values or outside the range of a breakpoint data set and then rounds the value to an adjacent breakpoint and returns the corresponding output value. Three choices are available for rounding. The first uses input nearest, which returns an output value corresponding to the nearest input value. The second uses input below, returning an output value corresponding to the breakpoint value that is immediately less than the input value. If no breakpoint value exists below the input value, it returns the breakpoint value nearest the input value. The third uses input above, which returns an output value corresponding to the breakpoint value that is immediately greater than the input value. If

no breakpoint value exists above the input value, it returns the breakpoint value nearest the input value.

The linear interpolation method fits a curve using linear polynomials between breakpoints. In effect, a straight line is produced between breakpoints and the output value corresponding to the input is produced. As example, for a value x in the interval $[x_0, x_1]$, the value y along the straight line is given by:

$$y = y_0 + (x - x_0)\frac{y_1 - y_0}{x_1 - x_0}. \tag{26}$$

The cubic spline interpolation method fits a cubic spline to the adjacent breakpoints, and returns the point on that spline corresponding to the input. The cubic spline technique is used to generate a function to fit the supplied data. The process uses a series of unique cubic polynomials that are fitted between each of the breakpoints, with the stipulation that the curve obtained be continuous and appear smooth. The cubic splines can then be used to determine rates of change and cumulative change over an interval. The governing idea behind the process is to fit a piecewise function of the form:

$$S(x) = \begin{cases} s_1(x) & for \quad x \in [x_1, x_2] \\ s_2(x) & for \quad x \in [x_2, x_3] \\ \quad \square & \\ \quad \square & \\ s_{n-1}(x) & for \quad x \in [x_{n-1}, x_n] \end{cases} \tag{27}$$

where s_i is a third degree polynomial defined by:

$$s_i(x) = a_i + b_i(x - x_i) + c_i(x - x_i)^2 + d_i(x - x_i)^3 \tag{28}$$

for $i = 1, 2, \ldots, n\text{-}1$. The function S($x$) has $4n$ - 4 unknowns, and in order to uniquely define the function, each unknown has to be accounted for, which can be achieved by imposing certain constraints on the system. In this case, it is accomplished by requiring the cubic spline to conform to the following stipulations:

1. The piecewise function S(x) will interpolate all data points,
2. S(x) will be continuous on the interval $[x_1, x_n]$,
3. dS(x)/dx will be continuous on the interval $[x_1, x_n]$, (29)
4. $d^2S(x)/dx^2$ will be continuous on the interval $[x_1, x_n]$,
5. "Not-A-Knot" spline: $d^3S(x)/d^3$ will be continuous at x_2 and x_{n-1}.

Applying stipulation 1, the piecewise function S(x) will interpolate all of the data points, and can be represented by:

$$s_i(x_i) = y_i = a_i, \text{ for } i = 1,2,\ldots,n\text{-}1. \tag{30}$$

Given stipulation 2, the curve S(x) must be continuous across the interval, therefore, it can be concluded that each sub-function must join at the interior points (breakpoints) such that:

$$s_i(x_{i+1}) = s_{i+1}(x_{i+1}) = y_{i+1}, \text{ for } i = 1,2,\ldots,n\text{-}2. \tag{31}$$

Additionally, at the far right value of x, the single constraint applies as follows:

$$s_{n-i}\left(x_n\right) = y_n \,. \tag{32}$$

To satisfy stipulation 3, the curve S(x) must be smooth across the interval, thus the derivatives must be equal at the breakpoints, giving:

$$\frac{d}{dx} s_i\left(x_i\right) = \frac{d}{dx} s_{i-1}\left(x_i\right), \text{ for } i = 1,2,\ldots,n\text{-}2. \tag{33}$$

Similarly, stipulation 4 instates a second smoothness condition by requiring the second derivatives of curve S(x) to be equal at the breakpoints, represented by:

$$\frac{d^2}{dx^2} s_i\left(x_i\right) = \frac{d^2}{dx^2} s_{i-1}\left(x_i\right), \text{ for } i = 1,2,\ldots,n\text{-}2. \tag{34}$$

The final stipulation is the implementation of the not-a-knot boundary conditions, which requires continuity of the third derivative of S(x) at the two interior breakpoints x_2 and x_{n-1}, such that:

$$\frac{d^3}{dx^3} s_1\left(x_2\right) = \frac{d^3}{dx^3} s_2\left(x_2\right), \text{ and} \tag{35}$$

$$\frac{d^3}{dx^3} s_{n-2}\left(x_{n-2}\right) = \frac{d^3}{dx^3} s_{n-1}\left(x_{n-2}\right). \tag{36}$$

Equations (30-36) impose 4_n - 4 constraints matching the 4_n - 4 unknowns for equation (27), thus the cubic spline is defined uniquely, and any point on the interval [x_1, x_n] can be solved for explicitly.

The interpolation method utilized for each input variable is not required to be the same. The three methods can be used interchangeably within any system and depends on the most suitable choice for that particular input variable.

Extrapolation Methods

When input falls outside the breakpoint data set's range, extrapolation methods can be used to determine output values. Caution must be practiced for ISM analysis of input values that are not contained within the breakpoints for that particular input variable. Large errors can be associated with input values that are well outside of the set of breakpoint's range, as the curve fit between the outermost pair of breakpoints cannot be expected to predict actual data indefinitely. Accordingly, the ISM will generate a warning when an input value is outside the range of its breakpoint data sets. It is recommended that input values for each input parameter do not precede/exceed breakpoint endpoints by a measure greater than the distance between the first/last two breakpoints associated with that input parameter. The user must use caution when evaluating data outside breakpoints and to make note when it occurs outside the breakpoints.

The extrapolation methods are very similar to the interpolation methods. In both cases a curve fitting technique is employed to match a function between breakpoints, but with extrapolation the curve is extended beyond the end breakpoints for deriving output data corresponding to input

values outside the breakpoint data range. As with interpolation, three options are available, including both linear and cubic spline extrapolation. The first option is to disable extrapolation and in the event that the input value is outside the breakpoints, an output value corresponding to the end of the breakpoint data set range is returned. The second option is linear extrapolation, which operates the same as linear interpolation except that the linear polynomial is fit between the first or last pair of breakpoints, depending if the input is less than the first or greater than the last breakpoint. It then extends the line and returns the point on it that corresponds to the input. The third option is cubic spline extrapolation, which operates the same as cubic spline interpolation except that the spline is fit between the first or last pair of breakpoints, depending if the input is less than the first or greater than the last breakpoint. It then extends the curve and returns the point that corresponds to the input. The cubic spline extrapolation method is only an option if the cubic spline interpolation method is also utilized.

Optimally, the choice of breakpoints used to populate the database should minimize the need for extrapolation methods to be called for within the ISM and interpolation will be utilized to a much greater extent during analysis.

Data Processing

At all levels within the system the data can be processed and manipulated to fit the desired output form. In SystemABC, data processing is performed between each subsystem in order to maintain system compatibility. The output from subsystem-A must be formatted properly for input into subsystem-B, and so forth. Also, output results from the ISM can be processed and presented in many different forms giving the user latitude of selecting from many options. For example the data can be plotted, normalized, arranged in table or matrix format, compared to previous results, formatted for immediate use by other software analysis tools, stored for future use, etc. The available tools for processing data include, but are not limited to, the mathematical operations existing in the MATLAB/Simulink environment.

4.3.2 Integrated System Model for the Nuclear Energy System

The first step to effectively simulate the NES is to define the overall system. This includes assigning and characterizing the subsystems and components that compose the system and then identifying and showing the interdependence of each. Figure 4.19 illustrates the NES as it functions in the ISM environment. The components or subsystems of the NES are the AP1000, the reprocessing and fuel fabrication facility, the VHTR, the HEST, and the HLW repository.

The AP1000 includes fuel enrichment and lag time as input variables. The fuel enrichment can range between 3% and 6%. The lag time is defined as the span of time from which the fuel is removed from irradiation in the AP1000 reactor core until it is sent to the reprocessing facility. The lag time is required to allow the used fuel to decay to an acceptable level in order to perform reprocessing. During this time period the used fuel is stored onsite at the AP1000 facility in designated cooling pools. The input variable representing lag time can vary from 0 and 20 years. The burnup level of the fuel in relation to enrichment is provided as output and is used in the external code system NFCSS for front-end fuel cycle analysis. The energy generated by the

AP1000 core according to fuel enrichment is supplied as output as well. The composition of the used fuel, as related to enrichment and lag time, is also presented as output.

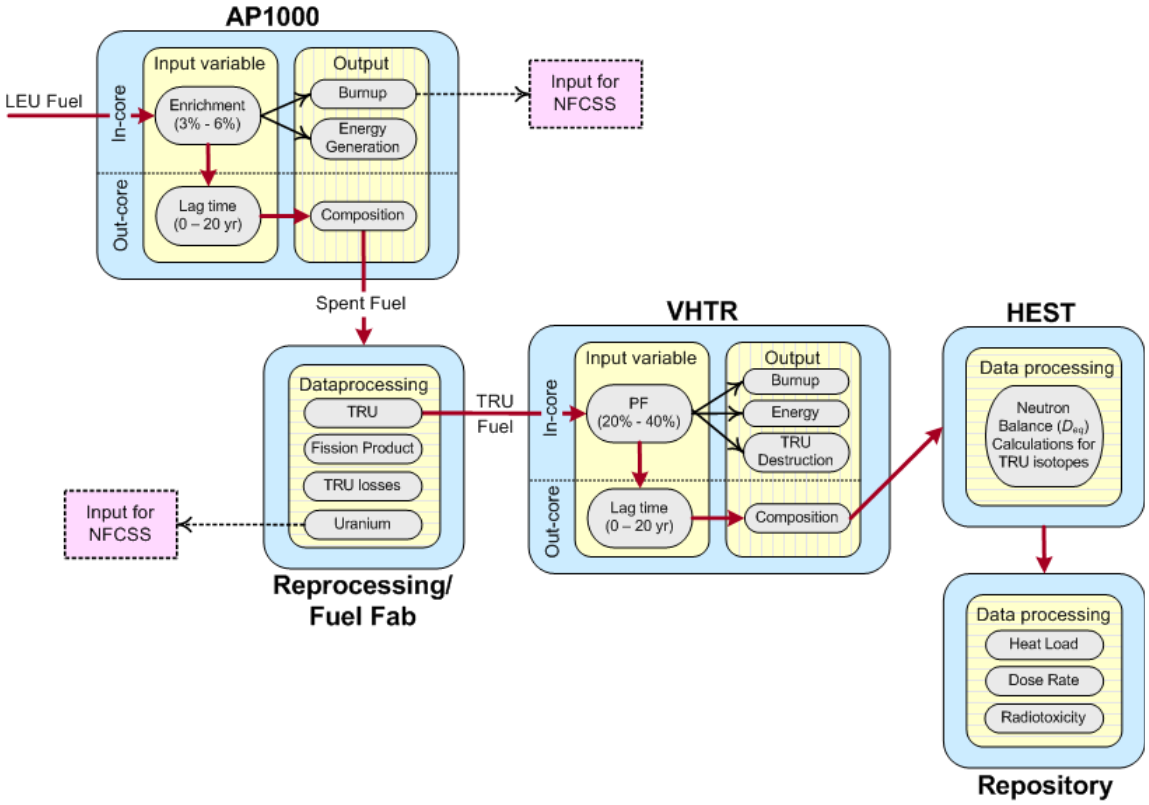

Figure 4.19. NES Interdependence Flowchart for ISM Simulation.

The composition of the used fuel from the AP1000 is then provided to the reprocessing/fuel fabrication subsystem. The data is processed by segregating the used fuel material into streams consisting of uranium, TRU, or FP. The mass of the uranium is calculated and used as an input parameter for the NFCSS code for front-end fuel cycle analysis. The mass of the FP are calculated for waste management analysis. The FP are grouped as a whole in each case, but the uranium and TRU are broken into individual nuclide constituents, with the TRU output being in terms of composition by nuclide weight percentage related to the total amount of TRU. Reprocessing losses associated with TRU separation process for a range of 0.1% to 0.0% are also calculated and stored as mass values.

The calculated TRU composition is then passed to the VHTR subsystem as the fuel component. The input variables for the VHTR are the packing fraction of the TRISO fuel particles within the fuel compact and the lag time. The packing fraction can vary from 20% to 40%, and the lag time can fall within the time range of 0 to 20 years. The output results for the VHTR will be dependent of the input parameters for the AP1000, along with the corresponding VHTR input variable. The core burnup level, energy generation, and TRU production/destruction rate output results are dependent on the TRISO packing fraction in addition to the AP1000 fuel enrichment

and lag time. Likewise, the TRU composition will be dependent on the same input variables, but will also include the lag time associated with the VHTR subsystem.

The used fuel from the VHTR is then passed to the HEST subsystem model and the physics approach method for calculating the neutron economy balance (D_{eq}^{TRU} and D_{eq}^{I}) for the TRU nuclides under irradiation conditions in the HEST is applied. The output results allow a measure of the feasibility and degree of transmutation by fission achievable in the HEST as a function of the system's input variables.

The data is then evaluated in the repository subsystem model by applying the methods developed for determining normalized heat factors and normalized radiotoxicity factors for the TRU and the related isotopic priority rankings. By doing so provides a means for the final results produced by the ISM to be used to quantify repository performance, which in turn can be used for making comparisons to other fuel cycles.

As explained previously, the size and structure of the multi degree arrays that form the ISM database are the key to successfully simulating systems within the ISM. The NES includes 4 input variables translating to a database composed of 4 arrays, which progressively increases from a 1D array to a 4D array. The data entries within each of the arrays are determined by the breakpoint sets for each input variable. The input variable for the AP1000 fuel enrichment has 7 breakpoints set at: [3.0, 3.5, 4.0, 4.5, 5.0, 5.5, 6.0] weight percent. The lag time variable for the AP1000 includes 4 breakpoints at: [5, 10, 15, 20] years. The packing fraction for TRISO particles in the VHTR represents the third input variable and its corresponding breakpoint set is: [20, 30, 40] percent. The final input variable is the lag time associated with the VHTR, which has the breakpoint set of: [5, 10, 15, 20] years.

With the input variables and breakpoint sets assigned, the database size and structure is fixed. The 1D array is simply composed of 7 elements. The 2D array is a 7x4 matrix, the 3D array is 4x3x7, and the 4D array is 3x4x4x7. The resulting database will require 455 data entries. The system model for the NES must produce results for a number of individual isotopes and element groups for each input variable. Therefore, the database must be expanded accordingly. The tracking of the TRU elements include 15 individual isotopes, uranium includes 4 different isotopes, and the FP are grouped together as one, plus the burnup values for both the AP1000 and VHTR must be accounted for. Taking this into consideration, the data entries for the ISM database is expanded from 455 to 9,121.

The data entries are produced by the high fidelity whole-core 3D exact geometry models for the AP1000 and VHTR, as detailed in sections 4.1.1 and 4.1.2. Whole-core depletion calculations for each reactor are performed using MCNPX. In the case of the AP1000, the core (for each of the breakpoint values for enrichment) is depleted until it can no longer support criticality, after which it is decayed in ORIGEN for the specified breakpoints for lag time. Thus, producing the data entries (fuel isotopic concentrations) needed for the database as related to the AP1000 subsystem. Similarly, the VHTR core is depleted and decayed to produce database entries for the specified breakpoints, providing the remaining entries needed to complete the ISM database. To fully populate the database, the minimum number of depletion calculations to be performed is set at 64. However, being that the cores are required to be depleted exactly to critical ($k_{eff} = 1$),

the number of calculations is doubled to 128. Considering that the average MCNPX depletion runtimes for the available computer platform (2 - Xeon E5530 2.4GHz quad core CPU, 12.0 GB memory), the total computational cost for generating input data for the ISM database is approximately 7000 hours of continual runtime. The cost can be reduced by a factor of about 7 if the depletion cases are configured to execute in parallel, or if multiple cases are run simultaneously.

The completed database is entered into the framework of the ISM. With the database in place, the ISM is set to interpolate and extrapolate data using the cubic spline method. The input parameters are entered into the ISM and then the simulation is executed. Upon completion the output results are provided in the MATLAB environment for further processing and analysis if desired. Figure 4.20 shows the data path and setup for the NES simulation. The grey blocks contain the subsystems so they can be easily identified. The green path (uranium) and the red path (TRU) both represent multiple isotopes, indicating that each has been collapsed to contain information that is applied similarly to the each of the isotopes they contain. The uranium path controls 4 isotopes, while the TRU path controls 15 isotopes.

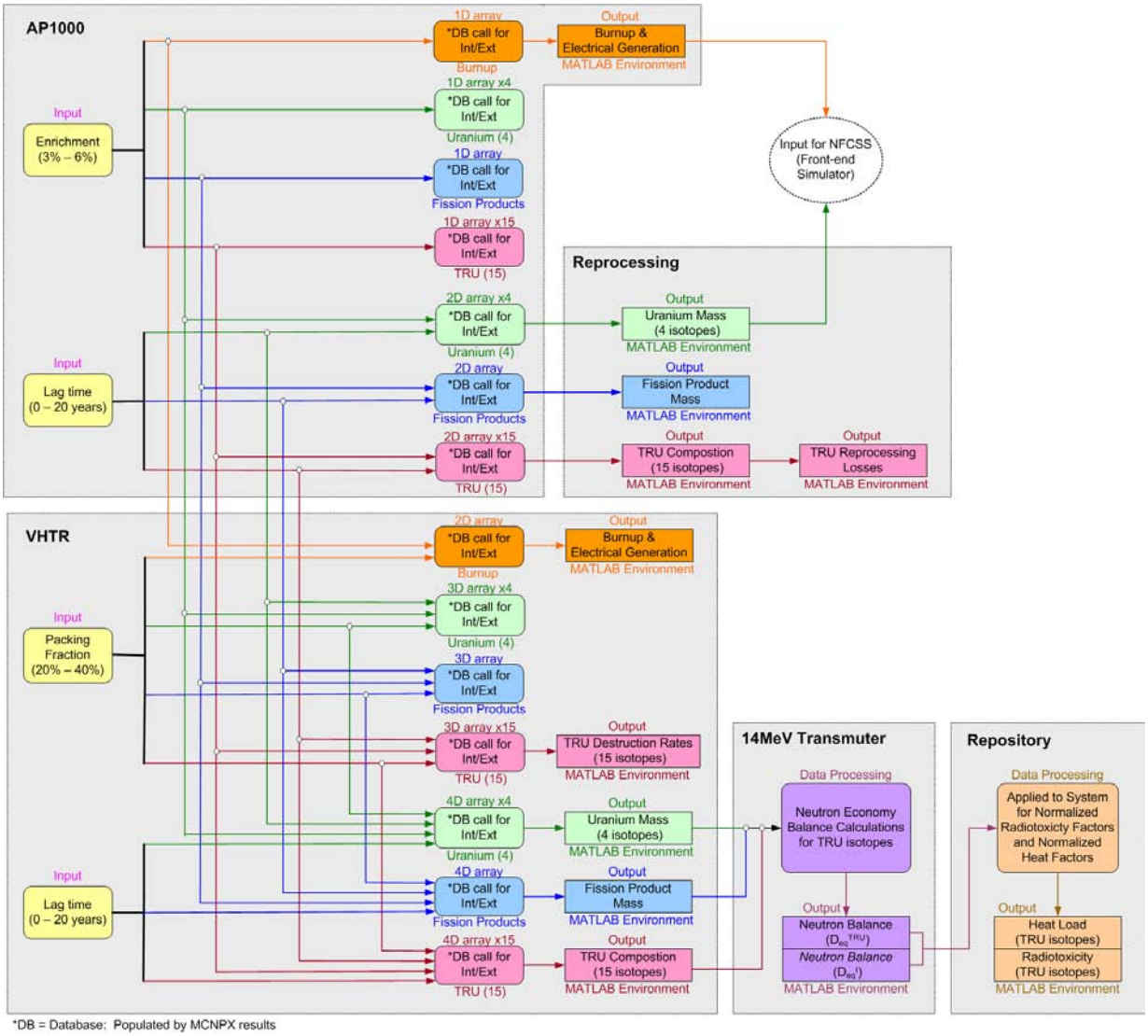

Figure 4.20. Detailed Mapping of the ISM Dataflow as Related to the NES.

The integrated model for the NES offers control and manipulation of the input parameters and the output can be modified countless different ways, since it is produced within the MATLAB environment. In addition, the computational cost of the simulation is minimal, especially when compared to MCNPX depletion calculations for the AP1000 and VHTR. On average the ISM computational cost is approximately five orders of magnitude less than that for a single MCNPX depletion calculation.

5 ENERGY SYSTEM NEUTRONIC AND FUEL COMPOSTION ANALYSIS

5.1 AP1000

The reference core has an average fuel enrichment of 4.5 wt.% and uses a single batch fuel management scheme. The ENDF/B-VII cross-section library was used for fuel temperatures at 900K and moderator temperatures at 600K. Depletion calculations were performed by MCNPX using 50 day intervals and 700,000 neutron histories per interval.

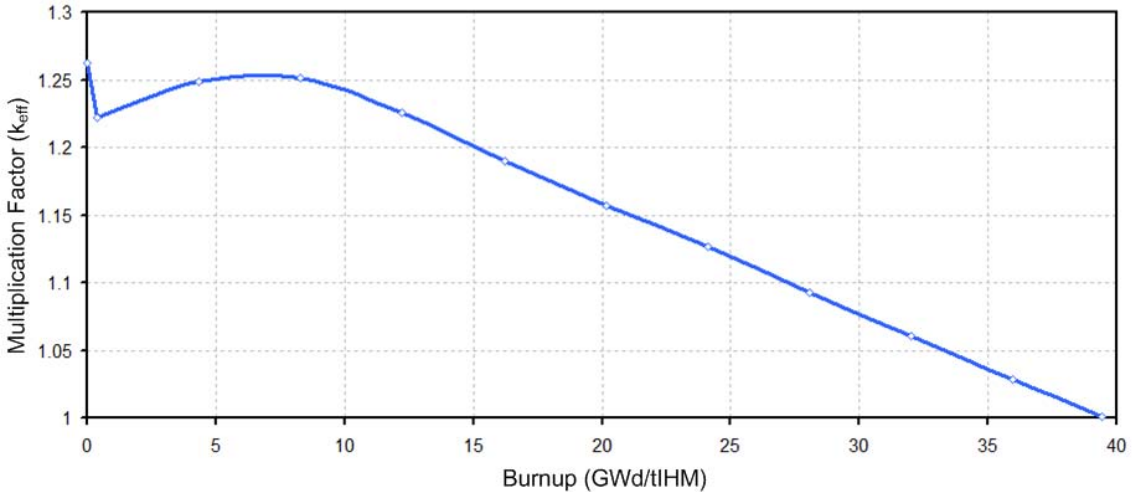

Figure 5.1. AP1000 Whole Core Depletion.

Figure 5.1 shows the time evolution of the AP1000 core k_{eff} determined by MCNPX. The core has an initial k_{eff} value of 1.26. A short time step was incorporated in the burnup scheme to show the neutron poison effect accompanying the introduction of FPs into the core at reactor startup. The reactivity level of the core then gradually increases for a short time period before decreasing again. The PYREX rods and IFBA rods that are present in the core cause the initial increase in k_{eff}. At Beginning of Cycle (BOC) the boron in the PYREX and IFBA rods acts as a strong neutron poison and significantly depresses the reactivity of the core, but as time progresses the boron is depleted, which is evident by the increase in k_{eff}. The core reaches a subcritical level at approximately 39.4 GWd/tIHM, which is equivalent to 997 Effective Full Power Days (EFPD).

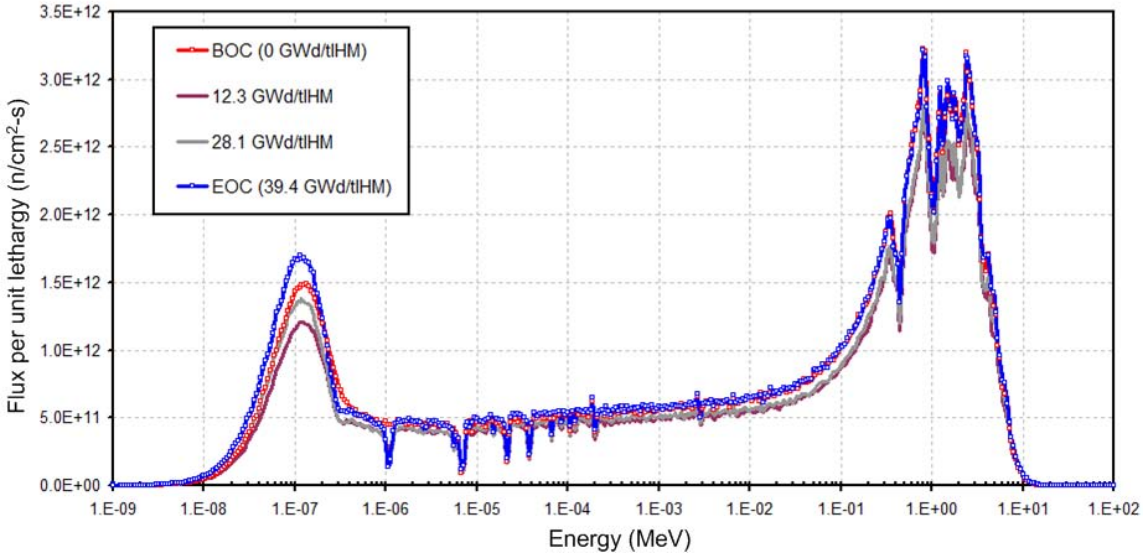

Figure 5.2. AP1000 Spectra at Different Burnup Levels.

The profile of the average neutron flux in the fuel elements at different burnup levels are provided in Figure 5.2. To maintain a constant power throughout the core lifetime, the flux must constantly change to compensate for the isotopic transformations caused by neutron irradiation. The main competing factors in the process are the consumption/production of fissile nuclides, the depletion of the burnable poisons, and the accumulation of fission products in the core. The spectrum profile in each case is similar with the most notable difference being the thermal energy peak. At BOC, the burnable poisons are at full strength, but as time evolves the powerful thermal energy neutron absorber ^{10}B is depleted and consequently less thermal energy neutrons are removed from the system. The depletion of Burnable Poison (BP) happens early in the core's lifetime and only a small fraction of the ^{10}B remains at a fuel burnup level of 15 GWd/tIHM. The effect is evident by the decrease in the flux between BOC and 12.3 GWd/tIHM. Additionally, as the burnup level increases the amount of total FP in the core continues to grow. The FP are neutron absorbers and over time have a strong negative effect on the core's neutron economy. Also, the fissionable material in the core is gradually decreased as ^{235}U is diminished throughout core lifetime and the production of ^{239}Pu and ^{241}Pu levels off towards the End of cycle (EOC). The cumulative effect translates to an increase in neutron flux, as shown by the flux plots for burnup levels between 12.3 GWd/tIHM and EOC.

The core is initially loaded with 86 Metric tons of Uranium (MTU), with approximately 3.9 tones being ^{235}U. From the time of reactor startup until EOC, the fissile component ^{235}U is depleted but other fissile components are produced when ^{238}U is transmuted to higher actinides, particularly ^{239}Pu and ^{241}Pu. Figure 5.3 shows the time evolution of important isotopes within the core, from which a comparison can be made between the consumption of the fuel and the production of TRU isotopes.

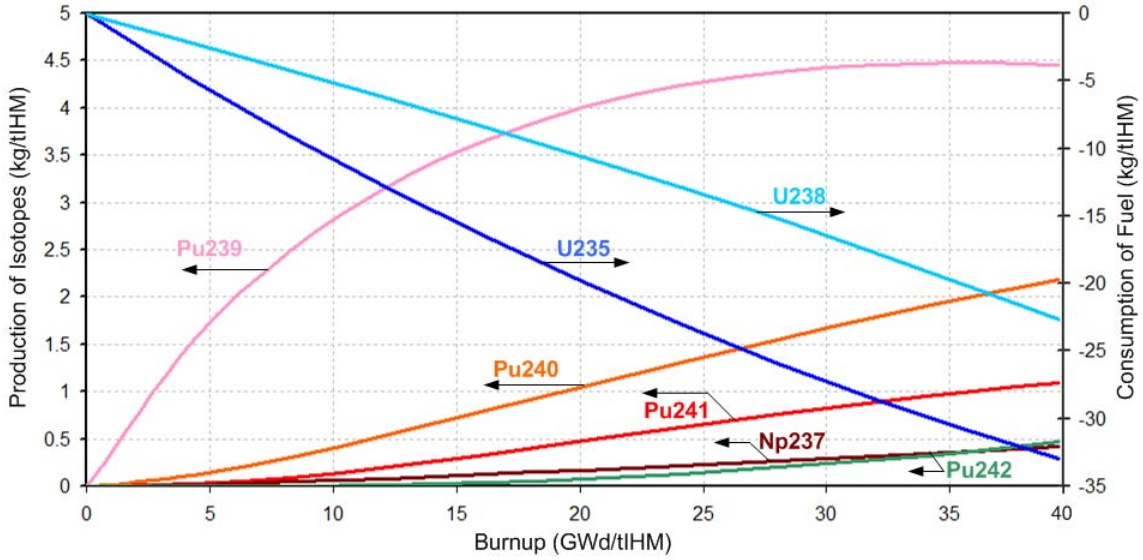

Figure 5.3. AP1000 Production and Consumption of Higher Isotopes.

The TRU produced during the lifetime of the AP1000 core is dominated by Pu, which accounts for more than 93% of the TRU. Even so, the production of higher actinides is crucial because of the impact they can have on waste management. Figure 5.4 shows the production rate of the higher actinides that buildup quickest in the core. As indicated by the trend lines for TRU nuclide production, higher fuel burnup results in greater concentrations of TRU in the core. The lone exception being ^{239}Pu, in which the production rate plateaus, and with high enough burnup will begin to be consumed. Generally, higher burnup core configurations are targeted for economic reasons, but the increased buildup of higher actinides and how it effects the overall fuel cycle must also be taken into consideration when designing for high burnup PWR cores.

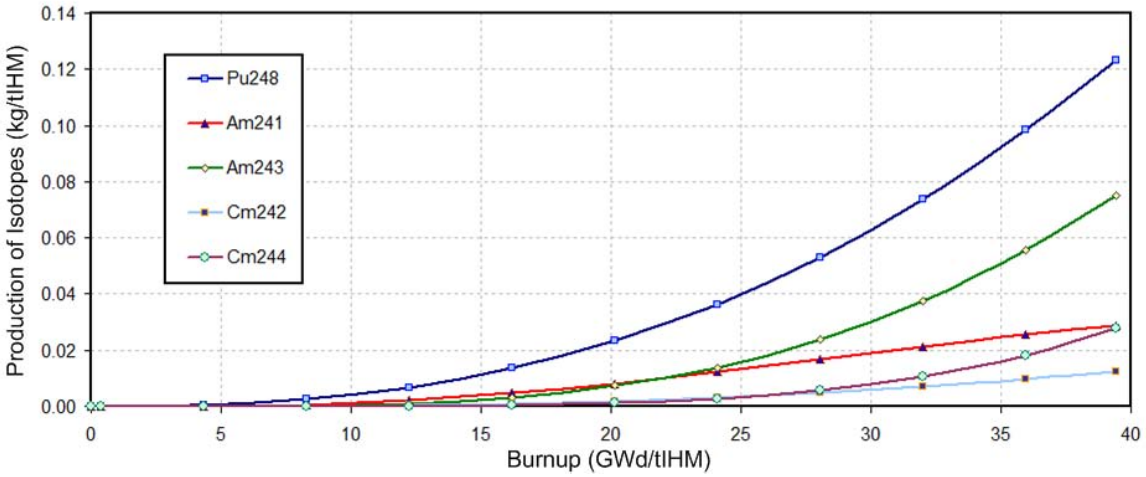

Figure 5.4. AP1000 Production of Higher Isotopes.

A more complete tabulation of the actinide and FP transformations within the core is provided in Table 5.1. The mass is given for the actinides produced and consumed at various burnup levels, along with the FPs as a group. At EOC (39.4 GWd/tIHM), the used fuel is almost entirely composed of Uranium, which is 96.5% of the total by weight. The FP make up about 2.5%, with the TRU only accounting for 1% of the fuel at EOC.

Of greater importance is the isotopic composition of the TRU produced during the core lifetime as it will become the fuel component for the VHTR. The used fuel is very "hot" immediately after removal and must be stored in the onsite reactor cooling pool before being transported to other facilities for reprocessing and fuel fabrication. The reprocessing and fuel fabrication procedures will also involve a substantial amount of time, which translates to a decay/cool-down time period between fuel removal from the AP1000 up to the time the recycled fuel is ready to be loading into the VHTR.

Table 5.1. Nuclide Masses in the AP100 at Different Burnup Levels.

Nuclide		Average Fuel Burnup (GWd/tIHM)					
		0	**8**	**16**	**24**	**32**	**39.4**
Mass (kg/core)	^{234}U	0.0	0.056	0.099	0.135	0.168	0.202
	^{235}U	3867	3081	2445	1887	1408	1029
	^{236}U	0.0	141.5	251.8	343.1	417.9	472.9
	^{238}U	82190	81820	81460	81080	80660	80240
	^{237}Np	0.0	3.883	10.39	18.44	27.52	36.15
	^{238}Pu	0.0	0.225	1.174	3.12	6.35	10.59
	^{239}Pu	0.0	215.3	315.0	365.1	382.9	383.8
	^{240}Pu	0.0	26.34	68.51	112.4	153.8	188.2
	^{241}Pu	0.0	7.768	28.93	53.63	76.62	93.45
	^{242}Pu	0.0	0.471	3.822	11.38	23.98	40.39
	^{244}Pu	0.0	0.0	0.00003	0.00015	0.00050	0.00121
	^{241}Am	0.0	0.056	0.400	1.058	1.831	2.462
	^{242}Am	0.0	0.0	0.002	0.006	0.010	0.013
	^{243}Am	0.0	0.014	0.269	1.182	3.216	6.448
	^{242}Cm	0.0	0.004	0.068	0.259	0.613	1.062
	^{243}Cm	0.0	0.0	0.0	0.003	0.009	0.020
	^{244}Cm	0.0	0.001	0.032	0.229	0.898	2.392
	^{245}Cm	0.0	0.0	0.001	0.007	0.036	0.113
	^{246}Cm	0.0	0.0	0.0	0.0	0.003	0.012
	FP	0.0	760	1470	2180	2890	3550

Table 5.2 provides the isotopic composition of the TRU produced at a burnup level of 40 GWd/tIHM for a range of decay times. For thermal neutron spectrum systems ^{239}Pu and ^{241}Pu are important because they are fissile isotopes. The decay chain and long half life for ^{239}Pu (2.41 x10^4 yrs) cause it to remain at a stable rate for the time range of concern, but ^{241}Pu has a shorter half life (14.4 yrs) and decreases noticeably. ^{241}Am and ^{237}Np demonstrate neutronic properties that classify them as burnable poisons in thermal neutron spectrum systems. The very long half-life of ^{237}Np (2.14x10^6 yrs) makes it stable during the decay time, but the long half-life and

decay chain (beta-decay of ^{241}Pu) for ^{241}Am (433 yrs) cause it to increase significantly over the 20 year period. The remaining TRU isotopes are considered neutron absorbers with very low fission probability in thermal neutron spectrums, and none of them change much over the given time period. The combination of the decrease in ^{241}Pu and increase in ^{241}Am is important because extended periods of decay time can have a negative impact on the neutronic properties (e.g. difficulty achieving and/or maintaining criticality) of the recycled TRU when considered as a fuel component for thermal neutron spectrum systems such as the VHTR.

Table 5.2. AP1000 TRU Vectors at 40 GWd/tIHM.

Nuclide		Decay/Cool-Down Time (years)				
		0	5	10	15	20
Weight %	^{237}Np	4.72	4.79	4.82	4.87	4.93
	^{238}Pu	1.38	1.46	1.40	1.35	1.30
	^{239}Pu	50.16	50.62	50.65	50.68	50.72
	^{240}Pu	24.60	24.35	24.39	24.44	24.47
	^{241}Pu	12.21	9.54	7.50	5.90	4.63
	^{242}Pu	5.28	5.22	5.23	5.23	5.23
	^{244}Pu	1.57×10^{-4}	1.56×10^{-4}	1.56×10^{-4}	1.57×10^{-4}	1.57×10^{-4}
	^{241}Am	0.32	2.91	4.93	6.50	7.71
	^{242}Am	1.75×10^{-3}	1.70×10^{-3}	1.66×10^{-3}	1.62×10^{-3}	1.58×10^{-3}
	^{243}Am	0.843	0.843	0.843	0.844	0.844
	^{242}Cm	0.1388	6.27×10^{-5}	4.36×10^{-6}	4.23×10^{-6}	4.130^{-6}
	^{243}Cm	2.60×10^{-3}	2.28×10^{-3}	2.03×10^{-3}	1.80×10^{-3}	1.59×10^{-3}
	^{244}Cm	0.313	0.257	0.212	0.175	0.145
	^{245}Cm	0.015	0.015	0.015	0.015	0.015
	^{246}Cm	1.54×10^{-3}	1.53×10^{-3}	1.53×10^{-3}	1.52×10^{-3}	1.52×10^{-3}

5.2 VHTR

The results for the VHTR prismatic core were produced by the MCNP code package. Depletion calculations were performed by MCNPX, with core criticality evaluations by MCNP5. The MAKXSF code was used to create temperature dependent neutron cross-section libraries necessary for temperature coefficients of reactivity calculations performed by MCNP5.

5.2.1 LEU Fuel

The reference VHTR core has a ^{235}U fuel enrichment of 8.0 wt.% and uses a single batch fuel management scheme. The Evaluated Nuclear Data Files – Basic VII (ENDF/B-VII) cross-section library was used for fuel temperatures at 1200K and moderator temperatures at 900K. Depletion calculations were performed by MCNPX using 50 day intervals and 600,000 neutron histories per interval.

Figure 5.5 shows the change of the core k_{eff} as a function of fuel burnup. The core has an initial k_{eff} value of 1.20. A short time step was incorporated in the burnup scheme to show the neutron poison effect accompanying the introduction of FPs into the core at reactor startup. The

reactivity level of the core then increases until a burnup level of approximately 13.5 GWd/tIHM is achieved at which time the core reactivity reaches a maximum value of about 1.22. The burnable absorber rods present in the fuel assembly blocks cause the initial increase in k_{eff}. The core reaches a subcritical level at approximately 56.5 GWd/tIHM, which is equivalent to 473 EFPD.

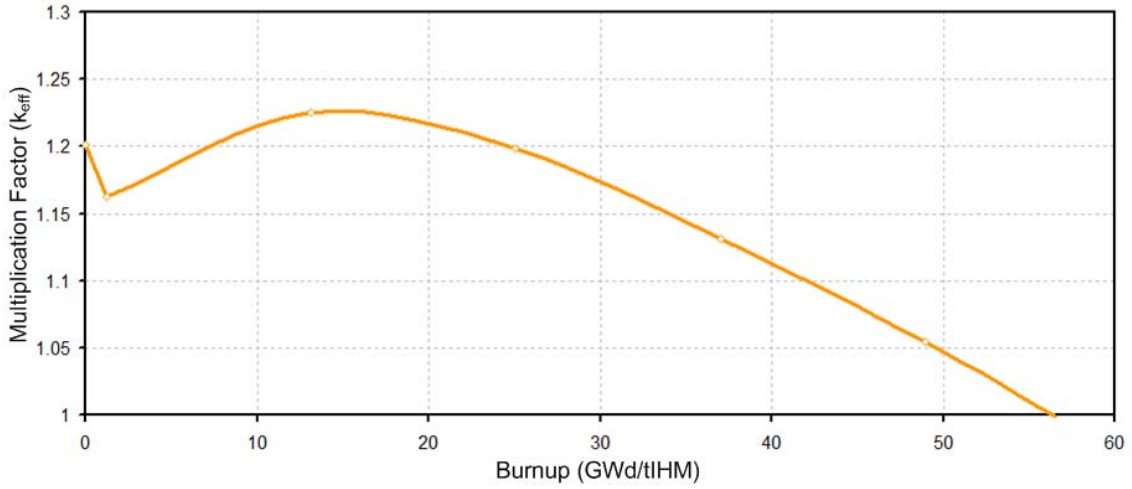

Figure 5.5. LEU-fueled VHTR Whole Core Depletion.

The neutron flux for different core levels is provided in Figure 5.6. The fuel particle and fuel compact produce similar profiles. The somewhat larger thermal energy peak and smaller fast peak in the fuel block spectrum signify the additional neutron moderation due to the graphite prismatic fuel block. The same effect is even more pronounced as the average flux for the core is taken into consideration.

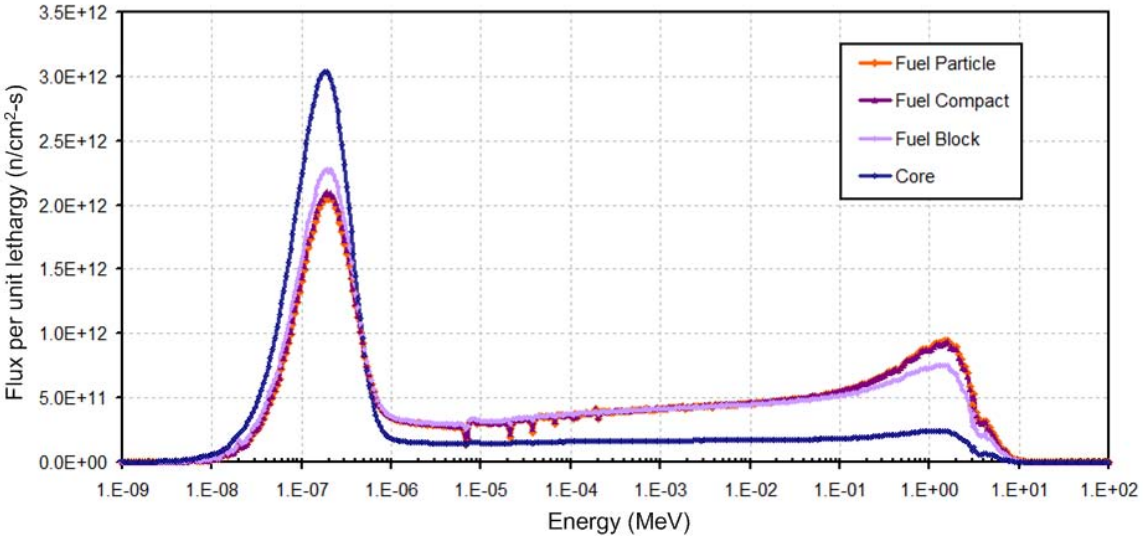

Figure 5.6. LEU-fueled VHTR Spectra for Core Regions.

Figure 5.7 shows the time evolution of important isotopes within the core. A quick comparison between the normalized production and consumption rates for the major isotopes in the AP1000 and VHTR indicate similar trends. The two main differences being: 1) the faster rate of consumption of ^{235}U in the VHTR due to its higher enrichment content, and 2) the increased production of ^{239}Pu in the AP1000. Otherwise, during the lifetime of each core the isotopic compositions are very similar.

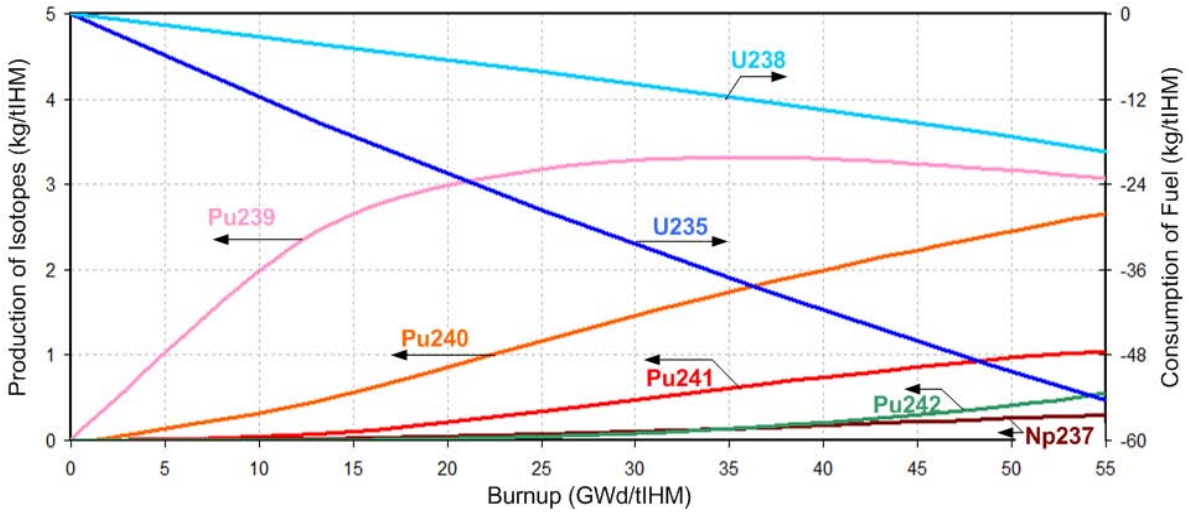

Figure 5.7. Production and Consumption of Higher Isotopes in LEU-fueled VHTR.

The AP1000 and VHTR share many similarities, most significantly they are both thermal neutron spectrum systems and operate on LEU fuel. The similarities make it useful to compare the performance of both in order to gain further understanding of each. Figure 5.8 shows the average flux in the fuel component for each reactor. The VHTR has a larger thermal neutron spectrum peak and somewhat higher epithermal neutron spectral component, due to the difference in moderator material, when compared to the AP1000. The graphite moderator of the VHTR has a much smaller thermal energy neutron absorption cross-section than the water moderator of the AP1000, thus the larger thermal energy neutron peak. However, the hydrogen in water is a very effective moderator and slows high-energy neutrons to lower energies more efficiently than graphite. Therefore, the VHTR has a much higher moderator-to-fuel ratio, which results in much lower power density and much higher specific power. The higher operating temperature of the VHTR shifts the thermal neutron spectrum peak to a higher energy compared to the AP1000, giving the VHTR a harder spectrum and effecting the initial enrichment requirements and transmutation capabilities of each.

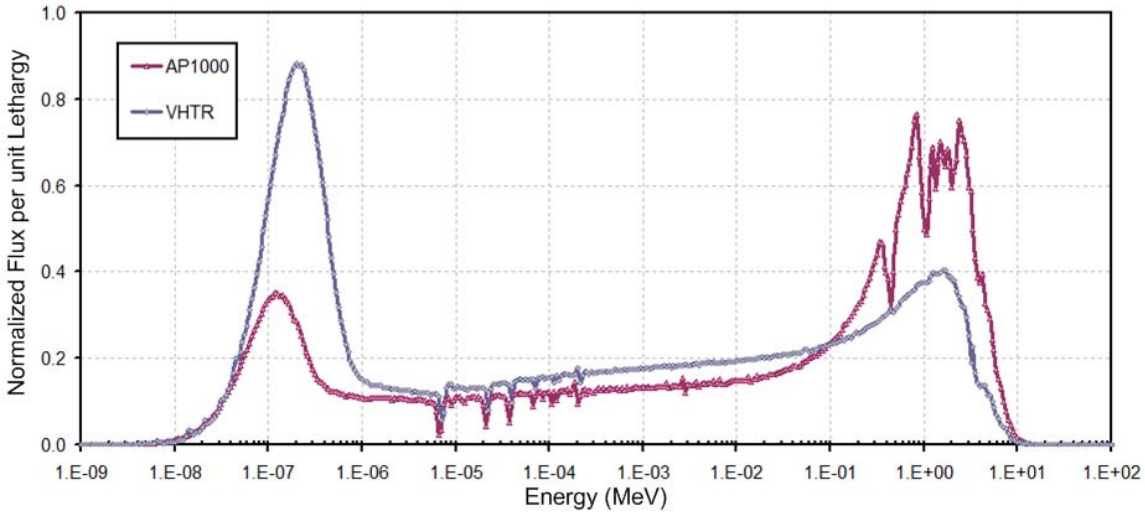

Figure 5.8. Average Neutron Flux in the Fuel Components for the AP1000 & VHTR.

A comparison of important results between the AP1000 and the VHTR is provided in Table 5.3. The VHTR has close to twice the initial enrichment as the AP1000 and produces a higher fuel burnup, but at about half the duration (EFPD) of the AP1000. The VHTR also produces less Pu and TRU than the AP1000, which is even more apparent when the TRU production is normalized to electricity generation.

Although the results are useful, one must take into consideration that neither reactor has been optimized for performance and the comparison is for a generalized once through fuel cycle. As expected, optimized fuel shuffling schemes and higher burnup cores (particularly for the VHTR) would affect the results, but general trends can be established from the results.

Table 5.3. LEU-fueled VHTR vs. AP1000.

Parameter	AP1000	VHTR
Burnup (GWd/tIHM)	39.4	56.5
EFPD	997	473
Enrichment (wt.%)	4.5	8.0
Enrichment at EOC (wt.%)	1.26	2.62
Pu content (kg/tIHM)	8.32	7.48
TRU content (kg/tIHM)	8.89	7.87
TRU production ($g/GW_t d$)	226	139
Thermal Efficiency (%)	34	48
TRU production ($g/GW_e d$)	663	290

5.2.2 TRU Fuel

The results presented in this section focus on the performance of the VHTR fueled with the recycled TRU arising from the AP1000 used fuel. Countless possibilities exist for the isotopic

composition of the TRU, as they are dependent on control parameters for the AP1000. The TRU-fueled VHTR reference case stems from the used AP1000 fuel, which had an initial fuel enrichment of 4.5 wt.%, reached a burnup level of 40 GWd/tIHM, and had a decay/cool-down time of 10 years. The resulting fuel composition for the TRU-fueled VHTR is listed in Table 5.4.

The reference TRU-fueled VHTR core uses a single batch fuel management scheme. The ENDF/B-VII cross section library was used for fuel temperatures at 1200K and moderator temperatures at 900 K. Depletion calculations were performed by MCNPX using 91 day intervals and 600,000 neutron histories per interval.

Table 5.4. Fuel Composition for the TRU-fueled VHTR.

Nuclide	Mass (kg)	Weight %
^{237}Np	243.31	4.8301
^{238}Pu	70.86	1.4067
^{239}Pu	2550.57	50.6321
^{240}Pu	1231.89	24.4547
^{241}Pu	376.29	7.4698
^{242}Pu	263.54	5.2316
^{241}Am	247.23	4.9078
^{242m}Am	0.08	0.0017
^{243}Am	42.09	0.8356
^{243}Cm	0.10	0.0020
^{244}Cm	10.67	0.2119
^{245}Cm	0.73	0.0146
^{246}Cm	0.08	0.0015
Total	5037.44	100.0000

Figure 5.9 shows the reactivity as a function of burnup for the TRU-loaded VHTR. The k_{eff} at BOC is 1.17 and criticality is maintained up to a burnup level of 264 GWd/tIHM, which equates to a cycle length of 2,220 EFPD. It is clear that the core reactivity decreases much slower and a much higher burnup is achieved as compared to the LEU-fueled VHTR. The small reactivity swing and high fuel burnup is the result of many contributing factors, which can be reduced to just a few dominating phenomena. Throughout the core lifetime ^{240}Pu is being converted into the fissile isotope ^{241}Pu at a greater rate than ^{241}Pu is being depleted. In addition, the fissile isotope ^{239}Pu is also being produced by neutron capture in ^{238}Pu, albeit at a slower rate, than it is being destroyed, but the combination of the two (^{241}Pu and ^{239}Pu generation) counteract the depletion of the main fissile component ^{239}Pu, allowing the core to stay above critical for long periods of time. Furthermore, ^{240}Pu comprises a large percentage of the TRU fuel and is also produced by neutron capture in ^{239}Pu throughout core life, which along with the large absorption cross section of ^{240}Pu make it a very effective burnable absorber; effectively limiting the reactivity swing from BOC to EOC.

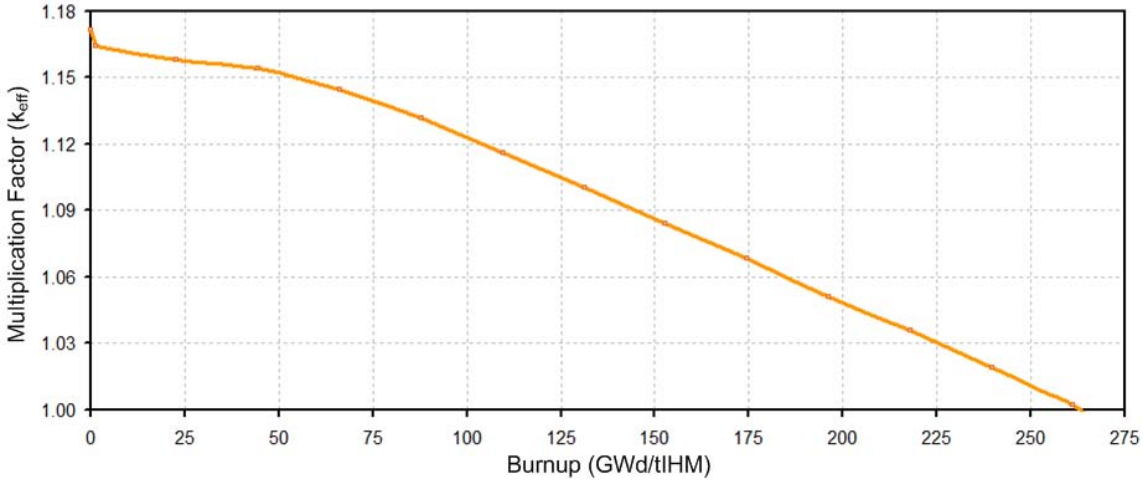

Figure 5.9. TRU-fueled VHTR Whole Core Depletion.

As the case in the previous section, the flux profile for different core levels is provided in Figure 5.10. Compared to the LEU-fueled VHTR, there is a very noticeable difference in the thermal energy region of the flux profiles. The thermal energy peak is almost completely depressed in the fuel particle and compact, but more distinguishable in the fuel block. The large thermal energy absorption cross-sections for ^{231}Am and ^{240}Pu in particular, and also ^{237}Np and ^{242}Pu work together to remove a large portion (as compared to LEU fuel) of the thermal spectrum neutrons causing the depressed peak. This effect can have safety implications as the fuel Doppler reactivity coefficient is reliant on the broadening of low energy resonances cross-sections in order to provide core stability (negative reactivity feedback for increases in fuel temperature). To assure the stability of the TRU-fueled VHTR, a complete analysis of the temperature coefficients of reactivity (fuel Doppler, moderator, and isothermal) throughout core lifetime was performed and presented in the next section.

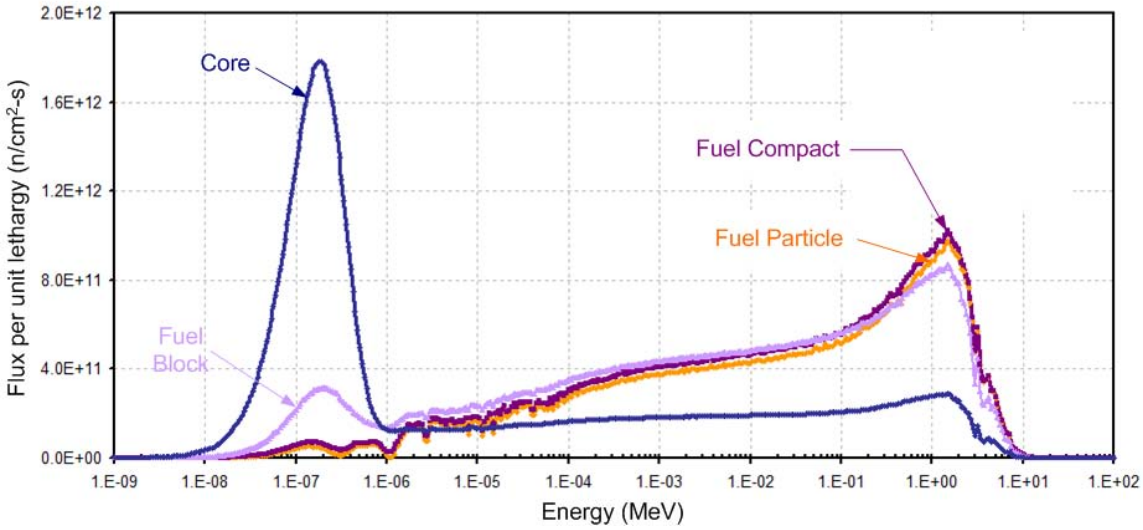

Figure 5.10. TRU-fueled VHTR Spectra for Core Regions.

Figure 5.11 shows the time evolution of TRU consumption within the core. Plotted on the right axis is the consumption of ^{239}Pu which, by far, has the greatest consumption rate, registering an EOC consumption of more than -300 kg/tIHM. The three other nuclides (^{237}Np, ^{240}Pu, and ^{241}Am) are plotted on the right axis, showing EOC consumption of ^{237}Np and ^{241}Am at about -20 kg/tIHM and -16 kg/tIHM. Although ^{240}Pu is produced during the first half of the core lifetime at EOC, its consumption rate is such that there is a lesser amount present than at BOC, with a slight overall consumption of -2.5 kg/tIHM.

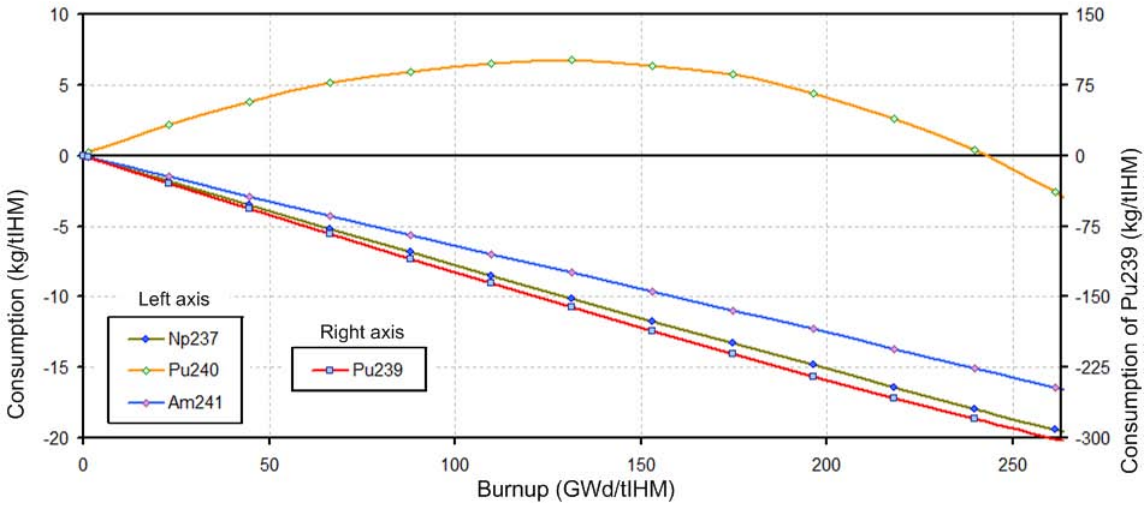

Figure 5.11. TRU-fueled VHTR Actinide Consumption.

The production of TRU isotopes is presented in Figure 5.12. The greatest production rate is that of ^{238}Pu, plotted on the right axis, reaching 33 kg/tIHM at EOC. The remaining nuclides are all plotted on the left axis and all remain under 10 kg/tIHM. ^{244}Cm has the highest production over the core lifetime and at EOC it is at about 9.5 kg/tIHM. The production of ^{241}Pu is the next greatest at EOC being about 9 kg/tIHM, which is important because it is one of the two major fissile nuclides, and as described earlier, is instrumental in allowing high burnup levels. It is important to consider the buildup and production/consumption rate trends of the higher actinides due to their effect on core performance and future waste management.

The core is initially loaded with 5,037 kg of TRU, where as the amount of TRU generated by the AP1000 is approximately 770 kg. Therefore, the ratio for AP1000-to-VHTR is roughly 6.5. At EOC the amount of TRU discharged from the VHTR is about 3,674 kg, giving an overall TRU destruction of 27%. The consumption of plutonium is over 28% including a 60% consumption of ^{239}Pu.

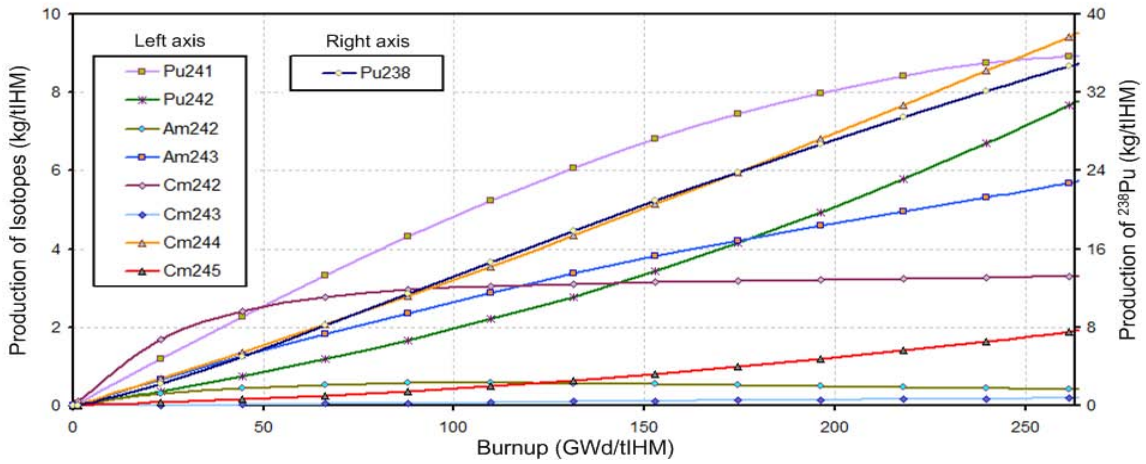

Figure 5.12. TRU-fueled VHTR Actinide Production.

Table 5.5 includes details for TRU consumption/production during the core lifetime. A negative value in the Percent Change (BOC → EOC) column represents consumption, with a positive value indicating production. Some of the higher actinides have very large percent increases, but their TRU composition fractions remain very small (fractional in most cases). Of main concern is the buildup of ^{244}Cm and ^{243}Am, having EOC concentrations of 58.7 kg and 70.9 kg, with each contributing to over 1.5% each of the TRU composition. Increases in the inventory of these highly radiotoxic long-lived isotopes need to be limited, if possible. ^{242}Cm is also exceptionally radiotoxic and experiences a large buildup going from 0 to 16.7 kg at EOC, but the short half-life (163 days) renders it to be of little concern in the long term. However, the very high heat load associated with the decay of ^{242}Cm makes it potentially problematic in the short term, as preparation for irradiation in the HEST is considered.

Table 5.5. BOC and EOC Fuel Composition for the TRU-fueled VHTR.

Nuclide	BOC Initial Loading (kg)	EOC Discharge (kg)	Percent Change BOC → EOC (%)
^{237}Np	243.31	144.70	-40.53
^{238}Pu	70.86	246.90	248.43
^{239}Pu	2550.57	1019.00	-60.05
^{240}Pu	1231.89	1217.00	-1.21
^{241}Pu	376.29	421.30	11.96
^{242}Pu	263.54	302.80	14.90
^{241}Am	247.23	163.50	-33.87
^{242m}Am	0.08	2.12	2452.73
^{243}Am	42.09	70.93	68.51
^{242}Cm	0.00	16.65	na
^{243}Cm	0.10	0.97	852.12
^{244}Cm	10.67	58.69	449.81
^{245}Cm	0.73	9.62	1211.57
^{246}Cm	0.08	0.53	586.88
Pu	4493.14	3207.00	-28.62
TRU	5037.44	3674.71	-27.05

Temperature Coefficients of Reactivity

The reactivity effects due to core temperature excursions were analyzed and the temperature dependent reactivity coefficients for: 1) fuel Doppler, 2) moderator, and 3) isothermal were calculated. The fuel and moderator temperature distributions were assumed to remain uniform throughout the core. The fuel is TRU oxide discharged from the AP1000 with particle packing fraction of 30%, and the moderator includes the graphite material (graphite in the fuel, fuel blocks, reflector blocks, and permanent reflector) within the core. In each case the ENDF/B-VII cross-section libraries were utilized for depletion and criticality calculations. The temperature coefficients were evaluated using the effective multiplication factors according the following relationship:

$$\alpha\left(T_{n,n+1}\right)=\frac{dk}{dT}=\frac{k_{n+1}-k_n}{k_{n+1}\cdot k_n}\cdot\frac{1}{T_{n+1}-T_n} \tag{37}$$

$$T_{n,n+1}=\frac{T_n+T_{n+1}}{2} \tag{38}$$

where α is the temperature coefficient between T_n and T_{n+1}, T_n is the core temperature at n^{th} measurement, and k_n is the effective multiplication factor at T_n.

To accurately predict the coefficients at different burnup levels during the core lifetime, whole-core depletion calculations at reference core temperature (fuel 1200K, moderator 900K) were performed by MCNPX with 3 million neutron histories per burnup step. The fuel and burnable poison material compositions were then retrieved at the burnup levels of interest (0, 66, 130, 200, 260, and 326 GWd/tIHM) to be used for additional standalone MCNP5 criticality calculations, which were performed at a series of varying fuel and/or moderator temperature levels in order to provide the required data for calculating the temperature coefficients corresponding to each selected burnup level. Figure 5.13 shows a graphical representative of the procedure for calculating the reactivity temperature coefficients.

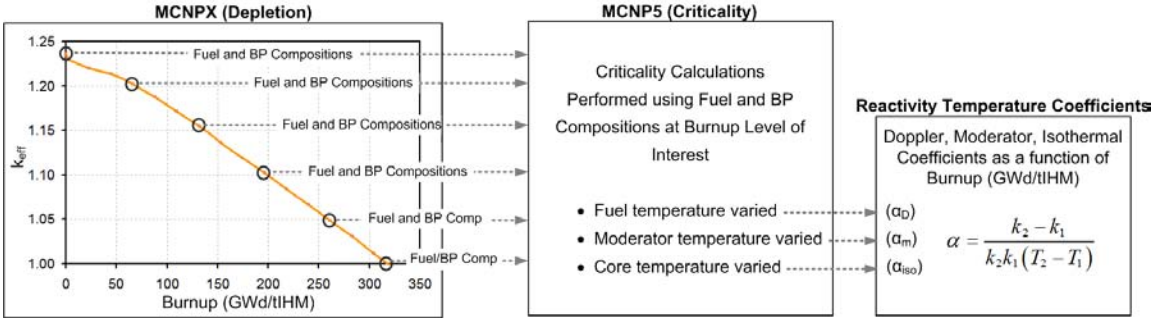

Figure 5.13. Procedure for Calculating Reactivity Temperature Coefficients.

Temperature dependent neutron cross-section libraries were created by the MAKXSF code [23], which is a utility program for manipulating cross-section library files for MCNP5. Capabilities of MAKXSF utilized for the temperature coefficient study include: Doppler broadening of resolved data to any higher temperature, interpolation of unresolved resonance data between

datasets at two different temperatures, and interpolation of thermal scattering kernels (S(α,β) data) between datasets at two different temperatures.

Due to the high sensitivity of the temperature coefficients to core reactivity changes, the k_{eff} value computed by MCNP5 was limited to a standard deviation of 0.00020 or less. This high accuracy is needed because the error propagation introduced by the uncertainty in k_{eff} can produce a substantial error in the temperature coefficient calculated by Equation (1). With the criticality limit set, the coefficients are assured to have minimal associated errors in all cases. To accomplish this, the MCNP5 criticality calculations required 15 million neutron histories to be used for k_{eff} estimates.

Fuel Doppler

The fuel Doppler coefficient (α_D) of reactivity was estimated for six burnup conditions: BOC or 0, 66, 130, 200, 260, and 326 (EOC) GWd/tIHM. The calculated core k_{eff} assumes that the graphite moderator temperature is fixed at 900 K and the fuel temperature varies from 293.6 - 2500 K. Six fuel temperature steps: 1) 293.6 – 600 K, 2) 600 – 900 K, 3) 900 – 1200 K, 4) 1200 – 1500 K, 5) 1500 K – 1800 K, and 6) 1800 K – 2500 K, were used to produce α_D estimates representing each of the burnup steps. Figure 5.14 shows the calculated α_D values for the six fuel temperature ranges, along with an overall averaged value, as a function of fuel burnup. All coefficients are negative and range from -2.36×10^{-6} to -1.53×10^{-5} Δk/k/K. The general trend indicates that as the temperature increases, the magnitude of α_D decreases, and as burnup increases, the magnitude of α_D increases. This trend is easily identified by the fuel Doppler coefficient averaged over the entire temperature range (293.6 K – 2500 K) shown in bold black.

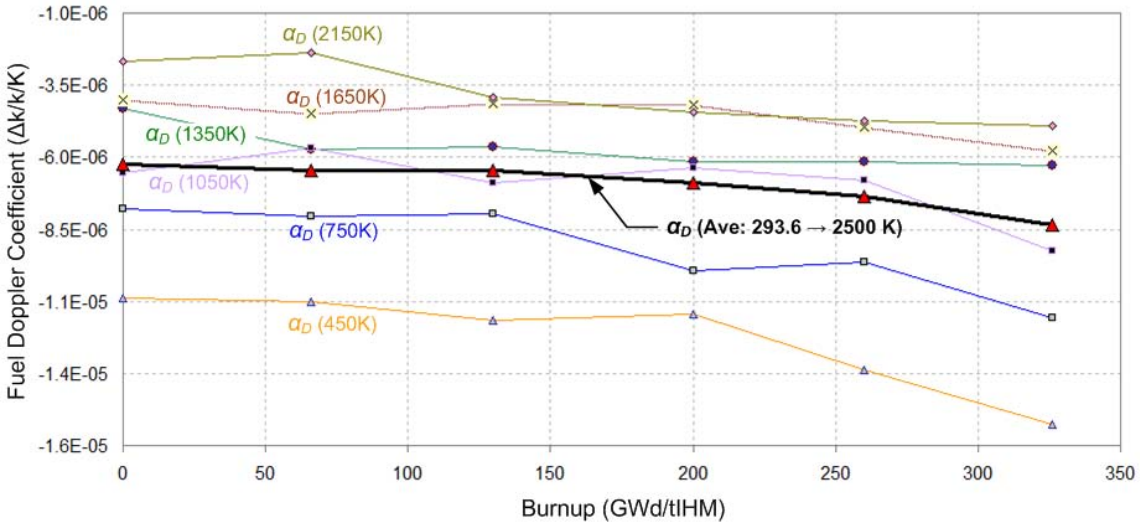

Figure 5.14. Fuel Doppler Coefficient at Specified Temperatures as Function of Burnup.

Changes in α_D are attributed to enhanced neutron absorption as cross-section peaks in the resonance region are broadened due to fuel temperature increases. The large resonance integral of ^{240}Pu is the main contributor to negative α_D values. The large resonance of ^{242}Pu also

contributes to the negative feedback but to a lesser extent due the smaller fraction present in the TRU fuel. As the TRU fuel composition is continually changing with burnup, so does α_D. In general, the increase in ^{240}Pu and ^{242}Pu throughout the lifetime of the core outweighs the positive fuel temperature feedback mechanisms of the other nuclides and α_D remains fairly constant or becomes more negative as burnup increases from BOC to EOC. The effect of fuel temperature variations on reactivity is more strongly felt at lower temperatures.

Moderator Temperature Coefficient

The moderator temperature coefficient (α_{mod}) of reactivity was estimated for six burnup conditions: BOC or 0, 66, 130, 200, 260, and 326 (EOC) GWd/tIHM. The calculated core k_{eff} assumes that the fuel temperature is fixed at 1200 K and the graphite moderator temperature varies from 293.6 - 2000 K. Five moderator temperature steps: 1) 293.6 – 600 K, 2) 600 – 900 K, 3) 900 – 1200 K, 4) 1200 – 1600 K, and 5) 1600 – 2000 K, were used to produce α_{mod} estimates as a function of burnup.

Figure 5.15 shows the calculated α_{mod} values for the five moderator temperature specifications as related to fuel burnup. For the lowest temperature range (293.6 – 600 K) the coefficients are positive and increase with fuel burnup. The coefficients calculated for the next lowest temperature range (600 – 900 K) are negative, except at EOC where it becomes slightly positive. The remaining coefficients are all negative. The overall range for α_{mod} is from 7.59×10^{-5} to -1.18×10^{-4} Δk/k/K.

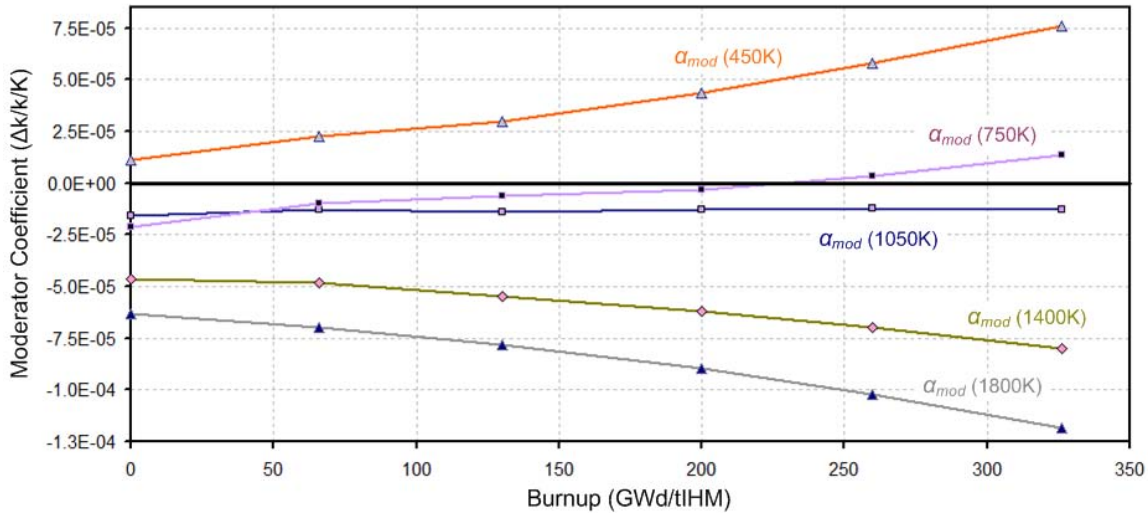

Figure 5.15. Moderator Coefficient at Specified Temperatures as Function of Burnup.

Temperature changes in the moderator will affect reactivity feedback differently than temperature changes in the fuel. Instead of Doppler broadening the resonance cross-sections, fluctuations in moderator temperature will cause a shift in the thermal neutron flux peak. Figure 5.16 shows the average neutron flux in a VHTR fuel block for moderator temperatures of 300 K, 1000 K, and 2000 K. The flux is overlaid on capture-to-cross ratio plots for the four most

abundant nuclides in the TRU fuel (^{239}Pu, ^{240}Pu, ^{241}Pu, and ^{242}Pu). The ^{240}Pu and ^{242}Pu ratios have been decreased by a factor of 4000 in order to fit them on the plot and keep the necessary resolution for relevant analysis of α_{mod} variations. The actual values for the ^{240}Pu and ^{242}Pu ratios are not as important as the trends they exhibit and the fact that they are orders of magnitude above unity. As shown, the thermal energy neutron peak shifts from 0.075 eV to 0.5 eV as the moderator temperature increases from 300 K to 2000 K. This shift significantly affects the moderator temperature coefficient as the alignment of the thermal energy neutron peak aligns with the peaks and valleys of the capture-to-fission ratio of the fissionable isotopes ^{239}Pu and ^{241}Pu. Consequently, when the thermal energy neutron flux peak shifts along an energy region in which the capture-to-fission ratio for ^{241}Pu is decreasing, the corresponding temperature increase causes reactivity to be added to the system, evident by the positive α_{mod} values at very low temperatures. As the moderator temperature continues to increase, the thermal energy neutron peak is then pushed to higher energies where within both the ^{241}Pu and ^{239}Pu capture-to-fission ratio are increasing, thus reducing the reactivity of the system and producing negative α_{mod} values. In addition, at higher temperatures (900 – 2000 K) neutron absorption by ^{240}Pu and ^{242}Pu is increased as the thermal energy neutron peak shifts to higher energies and captures this phenomenon. Of the four nuclides, only ^{239}Pu continually decreases with core lifetime, while the others buildup over time. This explains the increase in α_{mod} with burnup at lower temperatures, caused mainly by the production of ^{241}Pu. In contrast, at higher temperatures the effect is the exact opposite. The increase in ^{241}Pu translates to a strong negative reactivity insertion, with ^{240}Pu and ^{242}Pu also contributing to additional neutron absorption as burnup increases.

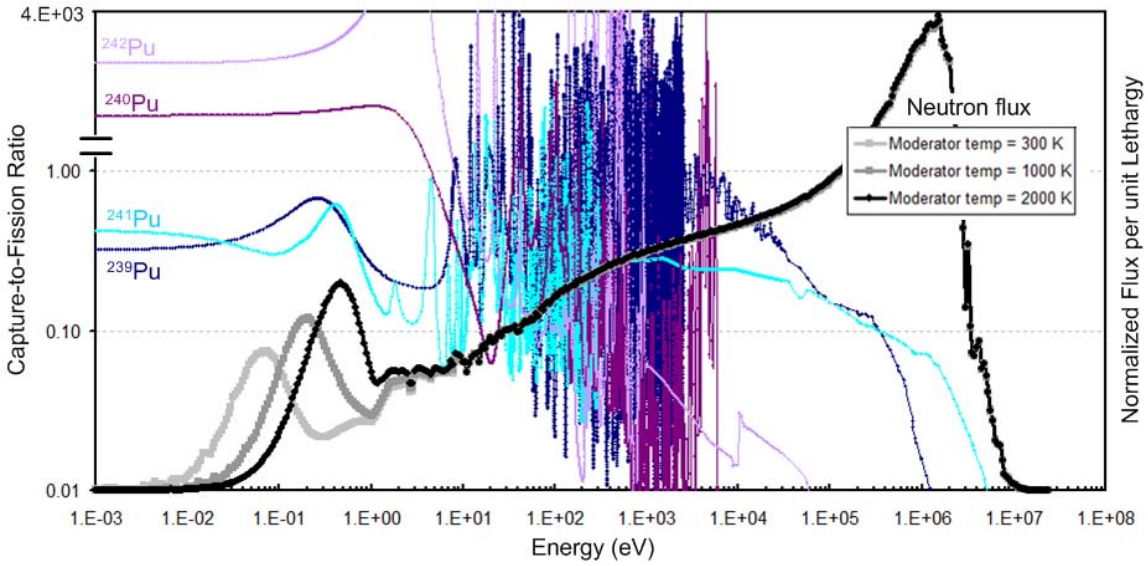

Figure 5.16. Neutron Flux and Capture-to-cross Section Ratios.

Isothermal Temperature Coefficient

The isothermal temperature coefficient (α_{iso}) of reactivity was estimated for six burnup conditions: BOC or 0, 66, 130, 200, 260, and EOC or 326 GWd/tIHM. The calculated k_{eff} assumes that the temperature across the core is constant; fuel and graphite moderator

temperatures are identical. Five core temperature steps: 1) 293.6 – 600 K, 2) 600 – 900 K, 3) 900 – 1200 K, 4) 1200 – 1600 K, and 5) 1600 – 2000 K were used to produce α_{iso} estimates for each of the burnup steps.

Figure 5.17 shows the calculated α_{iso} values for the five core temperature ranges as a function of fuel burnup. At BOC α_{iso} values are all negative, but positive values appear as burnup increases for the lower temperature (293.6 K – 600 K) cases. The overall range for α_{iso} is from 5.89×10^{-5} to -1.32×10^{-4} Δk/k/K. The value of the isothermal coefficient depends on both Doppler broadening from increased fuel temperatures and spectrum shifting due to changes in the moderator temperature, which is evident by values and trends shown in Figure 5.17.

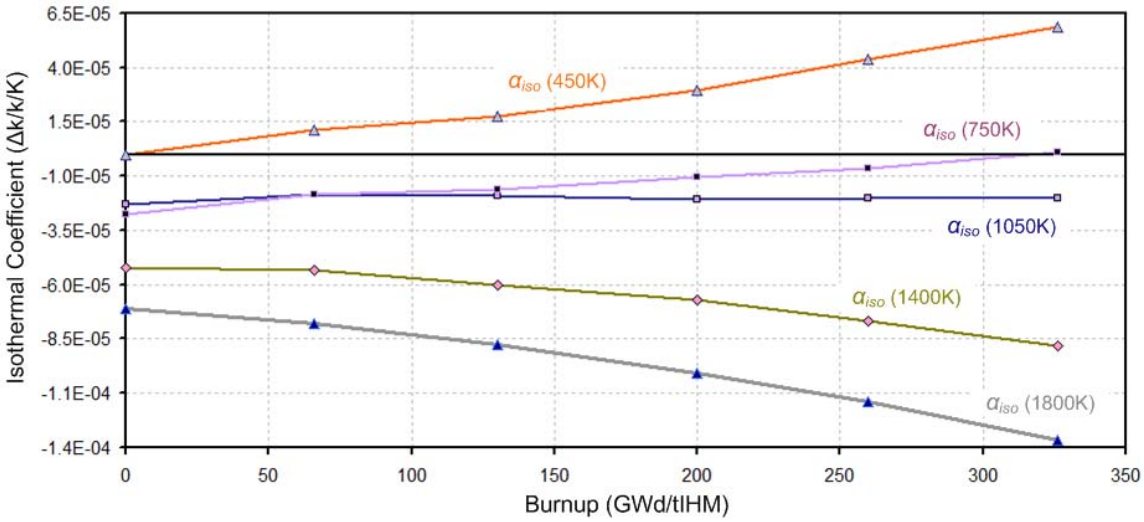

Figure 5.17. Isothermal Coefficient at Specified Temperatures as Function of Burnup.

The temperature coefficients of reactivity for fuel Doppler, moderator, and isothermal at different burnup levels and averaged over the entire temperature range are given in Table 5.6. As indicated, all coefficients are strongly negative and range from -6.29×10^{-6} to -2.97×10^{-5} Δk/k/K.

Table 5.6. Temperature Coefficients Averaged Over Entire Temperature Range.

Temperature Coefficient of Reactivity (Δk/k/K)						
Average for T (296.3 - 2000 K)	Burnup (GWd/tIHM)					
	0	66	130	200	260	326
Fuel Doppler	-6.29×10^{-6}	-6.53×10^{-6}	-6.56×10^{-6}	-7.09×10^{-6}	-7.61×10^{-6}	-8.84×10^{-5}
Moderator	-2.13×10^{-5}	-1.68×10^{-5}	-1.67×10^{-5}	-1.47×10^{-5}	-1.26×10^{-5}	-9.64×10^{-6}
Isothermal	-2.97×10^{-5}	-2.51×10^{-5}	-2.57×10^{-5}	-2.44×10^{-5}	-2.33×10^{-5}	-2.23×10^{-5}

Although the averaged coefficients are all negative values, analysis of smaller temperature step increases in the moderator, that fall within the lower temperature range (particularly 296.3 K – 600 K), produce positive reactivity insertion over the core lifetime. The expected operating

temperatures of the VHTR are considerably higher, but startup core conditions could be of concern. The current analysis did not take into account graphite expansion with temperature, which reduces neutron thermalization to provide an additional negative moderator feedback and when factored in could flip the positive coefficients. Adding a burnable poison that has an absorption resonance in the energy range of concern (0.03 – 0.1 eV) can also provide desired coefficients, e.g., ^{154}Eu.

5.3 High-energy External Source Transmuter (HEST)

The main purpose of the HEST model is to assess the TRU transmutation potential of two externally driven subcritical core configurations (Concept I and Concept II). In each case a MATLAB algorithm is used to produce the neutron consumption per fission (D_{eq}^{TRU}, D_{eq}^{I}) values. The system dependent nuclear interaction processes (microscopic cross sections and fission neutrons) are provided by whole-core 3D MCNP calculations.

5.3.1 HEST Concept I

The average neutron flux within the fuel particle for the TRU-fueled VHTR and the HEST Concept I is shown in Figure 5.18. The VHTR flux is included to provide a reference point and comparison case for the HEST Concept I. Overall, the HEST Concept I core produces a harder spectrum. This is evident by the nearly nonexistent thermal energy neutron peak, greater epithermal region component, and the increased portion of neutrons in the fast energy region of HEST Concept I. At 14.1 MeV there is a large spike representing the external neutron source within the HEST, which provides a considerable amount of neutrons beyond energies of the neutron fission spectrum (above 3 MeV). Another distinguishing attribute that is shared by each system is a significant downward spike in the flux at an energy of 1 eV, caused by the very large absorption resonance cross-section of ^{240}Pu.

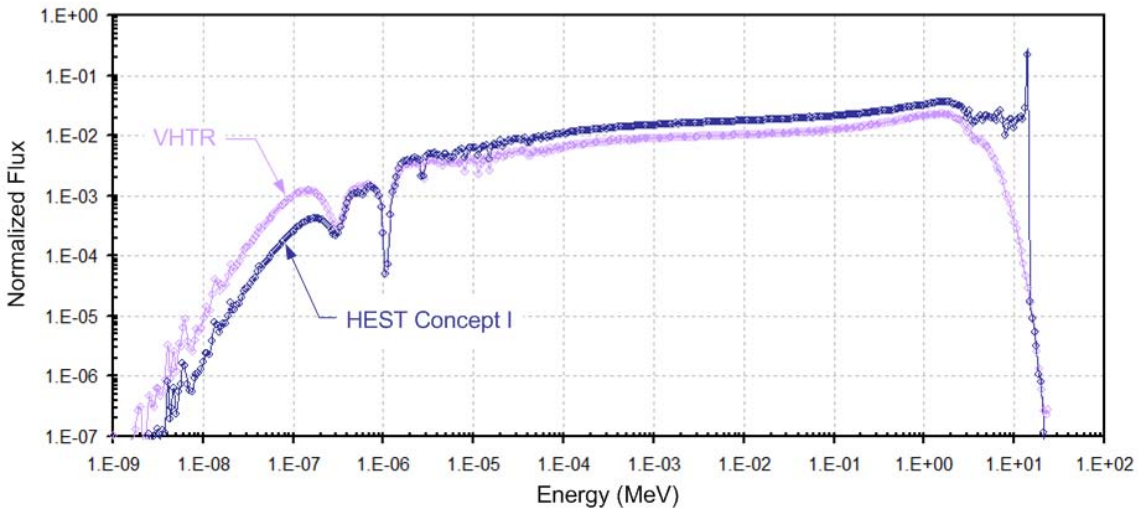

Figure 5.18. Neutron Flux Spectrum in the Fuel Particle for HEST Concept I and VHTR.

The transmutation potential of a system can be assessed by calculating the neutron balance (D_{fuel}) following the physics approach described in Chapter 5.1.3. The D_{fuel} value represents the neutron consumption per fission of the fuel component, and is defined as 'production' when values are negative ($-D_{fuel}$). Therefore, large $-D_{fuel}$ values indicate greater transmutation feasibility for that particular system.

The equilibrium case (asymptotic solution) for the atomic concentrations was employed to calculate the D_{eq}^{TRU} values for the HEST Concept I and VHTR systems. Figure 5.19 shows the D_{eq}^{TRU} values as a function of neutron flux for the VHTR and HEST Concept I. Both systems produce positive values at low fluxes but crossover to negative values at about 7.0×10^{13} n/cm^2-s for the HEST Concept I, and about 1.3×10^{14} n/cm^2-s for the VHTR. The HEST Concept I system has smaller D_{eq}^{TRU} values for the entire flux range, with the average value being approximately a factor of 2 lower. Thus, it is expected to provide superior transmutation potential.

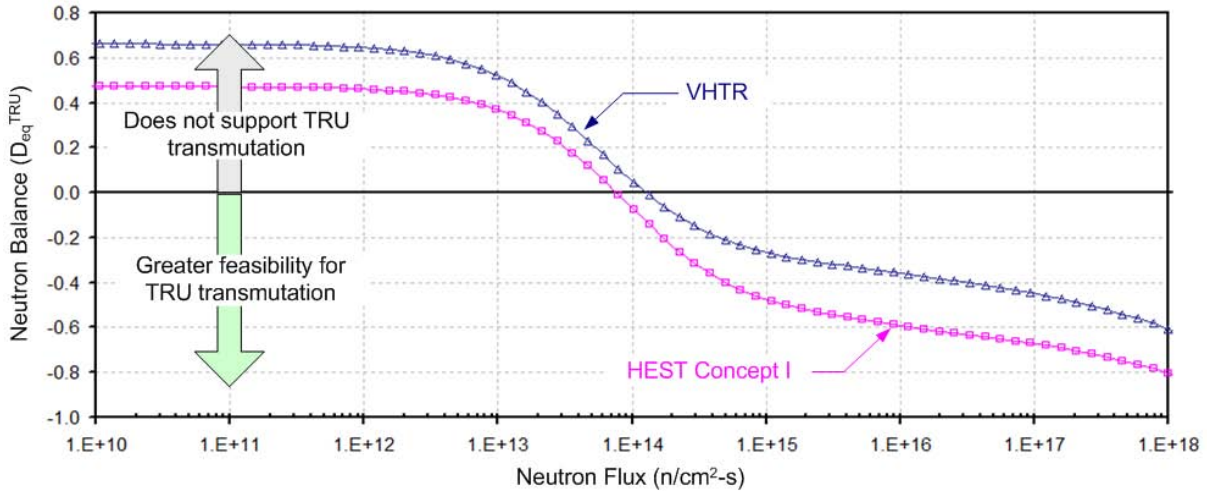

Figure 5.19. D_{eq}^{TRU} (neutron consumption/fission) for VHTR and HEST Concept I.

To gain further understanding of the system, the neutron balance values for the individual TRU nuclides (D_{eq}^{I}) at different flux levels are provided in Table 5.7. Also included in the table are the TRU compositions used for the D_{eq}^{TRU} calculations. Compositions match those for the reference TRU-fueled VHTR at a burnup level of 264 GWd/tIHM with a 7 year decay period. Appendix B contains individual TRU nuclide plots of the D_{eq}^{I} values as a function of neutron flux for the HEST Concept I system.

The transmutation capabilities of the HEST Concept I system are sensitive to the neutron flux levels. At a flux of 10^{12} n/cm^2-s, more than half of the TRU isotopes are neutron consumers per fission, whereas at 10^{16} n/cm^2-s only ^{237}Np and ^{242}Pu are neutron consumers, and at 10^{18} n/cm^2-s only ^{242}Pu is a consumer and very close to unity. However, neutron flux levels of the HEST Concept I system are a function of the source strength and constrained by design limitations such as the multiplication factor and heat generation. As previously stated, a physics approach to

transmutation feasibility is targeted; therefore the evaluation takes into consideration the possible flux levels attainable for the HEST Concept I as it relates to the external source strength. At the upper achievable limits for a 14.1 MeV neutron source is a generation rate of about 10^{20} n/s, [14,50], which, when combined with the HEST Concept I subcritical core produces an average core flux of approximately 10^{16} n/cm^2-s.

Table 5.7. D_{eq}^{I} Values for VHTR and HEST Concept I.

TRU (I)	TRU (%)	VHTR				HEST Concept I			
		Neutron Flux, φ (n/cm^2-s)							
		10^{12}	10^{14}	10^{16}	10^{18}	10^{12}	10^{14}	10^{16}	10^{18}
^{237}Np	4.071	1.069	0.791	0.533	-0.492	0.623	0.409	0.175	-0.618
^{238}Pu	6.670	0.137	-0.147	-0.313	-0.349	-0.263	-0.486	-0.686	-0.711
^{239}Pu	27.900	-0.372	-0.722	-0.926	-0.971	-0.517	-0.829	-1.107	-1.143
^{240}Pu	33.786	1.356	0.405	-0.150	-0.273	1.150	0.319	-0.421	-0.516
^{241}Pu	7.119	0.450	-0.529	-1.100	-1.226	0.366	-0.520	-1.310	-1.412
^{242}Pu	8.293	1.850	1.217	0.687	0.189	1.680	1.305	0.439	0.039
^{241}Am	8.786	0.478	0.469	-0.049	-1.780	0.385	0.373	-0.175	-1.265
^{242m}Am	0.055	-2.351	-2.351	-2.351	-2.351	-2.500	-2.500	-2.500	-2.500
^{243}Am	1.940	0.948	0.298	-0.238	-0.248	0.912	0.219	-0.407	-0.419
^{243}Cm	0.021	-2.031	-2.120	-2.193	-2.195	-2.145	-2.241	-2.329	-2.331
^{244}Cm	1.096	-0.015	-0.672	-1.215	-1.225	-0.015	-0.714	-1.356	-1.368
^{245}Cm	0.263	-2.170	-2.170	-2.170	-2.170	-2.285	-2.285	-2.285	-2.285

Considering neutron flux levels greater than 10^{14} n/cm^2-s, especially in the vicinity of 10^{16} n/cm^2-s, the HEST Concept I possesses the capability of transmuting most of the TRU nuclides as a neutron production process. In the case of the Pu isotopes, only the ^{242}Pu transmutation is a neutron consuming process for all flux levels considered. Whereas, the transmutation of ^{240}Pu becomes a neutron production process at $\varphi = 2.3 \times 10^{14}$ n/cm^2-s. The transmutation of ^{241}Am and ^{243}Am become neutron production processes at $\varphi = 5.3 \times 10^{15}$ n/cm^2-s and 2.0×10^{14} n/cm^2-s. The remaining TRU nuclides are all neutron producers for flux levels between 10^{14} and 10^{16} n/cm^2-s.

The HEST Concept I spectrum is not a true fast neutron spectrum as there is still a considerable epithermal and thermal energy component due to the graphite in the core. A shift to higher energies would result in more favorable $-D_{fuel}$ values for transmutation, but there are some transmutation advantages that accompany the HEST Concept I spectrum. The main advantage being the greater reaction rates due to the much higher cross section values at thermal energies. Thus, the destruction rate of the TRU nuclides is more rapid than it would be for a harder spectrum system.

5.3.2 HEST Concept II

The average neutron flux within the fuel particle for the HEST Concept I and the HEST Concept II is shown in Figure 5.20. Overall, the HEST Concept II core produces a significantly harder

spectrum. The difference between the flux level in the thermal energy range and the fast region for Concept II is more than 4 orders of magnitude, whereas it is only about 2 orders of magnitude for Concept I. Also noticeable for Concept II is the flux spike at 14.1 MeV representing the external neutron source. Another distinguishing attribute shared by each are significant downward spikes in the fluxes at an energy of 1.0 and 0.3 eV, caused by the very large absorption resonance cross sections of ^{240}Pu and ^{239}Pu respectively.

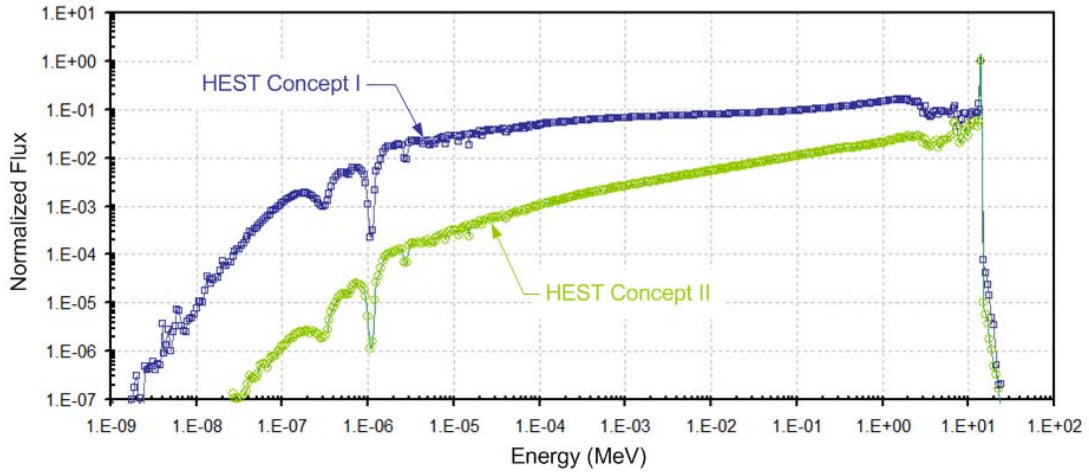

Figure 5.20. Neutron Flux Spectrum in the Fuel Particle for HEST Concept I and II.

The calculated D_{eq}^{TRU} values as a function of neutron flux for the VHTR, HEST Concept I, and HEST Concept II are shown in Figure 5.21. The D_{eq}^{TRU} values are not as sensitive to flux level changes as they are for the VHTR and Concept I. At flux measurements below 10^{13} n/cm^2-s the D_{eq}^{TRU} values are essentially non-changing as they are no longer dependent on flux. At flux measurements greater than 10^{17} n/cm^2-s, the same is true as the D_{eq}^{TRU} values remain fairly constant. Therefore, the D_{eq}^{TRU} values for Concept I are only flux dependent between 10^{13} n/cm^2-s and 10^{17} n/cm^2-s, and within this range do not change a great deal. Additionally, no matter what the flux level, the D_{eq}^{TRU} value is strongly negative.

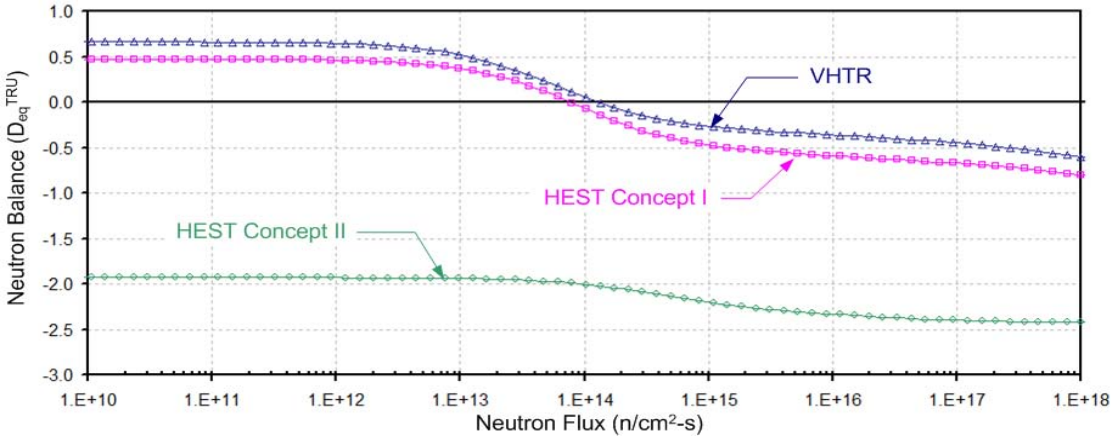

Figure 5.21. D_{eq}^{TRU} (neutron consumption/fission) for HEST Concept II.

To gain further understanding of the system, the neutron balance values for the individual TRU nuclides (D_{eq}^{I}) at different flux levels are provided in Table 5.8. Also included in the table are the TRU compositions used for the D_{eq}^{TRU} calculations. TRU Compositions match those for the reference TRU-fueled VHTR at a burnup level of 264 GWd/tIHM with a 7 year decay period. Appendix B contains individual TRU nuclide plots of the D_{eq}^{I} values as a function of neutron flux for the HEST Concept II system.

Table 5.8. D_{eq}^{I} (neutron consumption/fission) for VHTR, HEST Concept I and II.

TRU (I)	TRU (%)	VHTR		HEST Concept I		HEST Concept II	
		Neutron Flux, φ (n/cm^2-s)					
		10^{12}	10^{14}	10^{14}	10^{16}	≤ 10^{13}	10^{14}
^{237}Np	4.071	1.069	0.791	0.409	0.175	-1.965	-1.967
^{238}Pu	6.670	0.137	-0.147	-0.486	-0.686	-2.464	-2.468
^{239}Pu	27.900	-0.372	-0.722	-0.829	-1.107	-2.420	-2.437
^{240}Pu	33.786	1.356	0.405	0.319	-0.421	-1.902	-1.990
^{241}Pu	7.119	0.450	-0.529	-0.520	-1.310	-1.312	-1.567
^{242}Pu	8.293	1.850	1.217	1.305	0.439	-1.662	-1.777
^{241}Am	8.786	0.478	0.469	0.373	-0.175	-1.312	-1.317
^{242m}Am	0.055	-2.351	-2.351	-2.500	-2.500	-2.990	-2.990
^{243}Am	1.940	0.948	0.298	0.219	-0.407	-0.650	-0.975
^{243}Cm	0.021	-2.031	-2.120	-2.241	-2.329	-2.745	-2.804
^{244}Cm	1.096	-0.015	-0.672	-0.714	-1.356	-0.012	-0.544
^{245}Cm	0.263	-2.170	-2.170	-2.285	-2.285	-2.886	-2.886

The flux levels attainable for the HEST Concept II are considerably lower than for Concept I. Mainly because the model does not include a reflector and the source intensity is much smaller. Estimates for the flux are in the range of 10^9 n/cm^2-s when considering an external source strength of 10^{13} n/s. Although the design of the HEST Concept II is not the focus, a variant of the model that includes multiple fuel blocks, each with its own IEC external neutron source configured in a cylindrical core shape surrounded by a reflector is envisioned. Such a design could be optimized to produce a significantly higher neutron flux, create conditions necessary for manageable criticality levels, effectively destroy TRU, and enable energy generation.

Considering that the D_{eq}^{I} values are unaffected by neutron flux levels less than 10^{13} n/cm^2-s, the lower flux for Concept II is not of concern, at least when considering the transmutation feasibility as related to D_{eq}^{I} values. All TRU nuclides show strongly negative D_{eq}^{I} values except for ^{244}Cm, which is only slightly negative.

The HEST Concept II spectrum provides favorable conditions for transmuting the TRU nuclides. The strongly -D_{fuel} values make it an ideal candidate for incinerating the TRU component remaining after irradiation in the VHTR. Coupled with the AP1000 and VHTR, a NES that greatly limits actinide waste and efficiently utilizes fuel resources is complete.

5.4 Integrated System Model

The purpose of the ISM is for analysis of systems that are composed of a set of interacting subsystems. In the case of the NES, the ISM couples the individual reactor models and fuel cycle component models together for an effective and time efficient system analysis tool that is capable of accounting for different subsystem input parameters that vary over a range of interest. The computational timesaving of the ISM are directly related to the treatment of the whole-core 3D depletion models representing the AP100 and VHTR systems.

The output of the ISM includes the following NES features:

1) TRU mass and composition at AP1000 EOC
2) TRU mass and composition after reprocessing and at VHTR BOC
3) TRU mass and composition at VHTR EOC
4) TRU composition for D_{eq}^{TRU} (neutron consumption/fission) calculations specific to HEST Concepts I and II.
5) EFPD for AP1000
6) EFPD for VHTR
7) Fuel burnup levels (GWd/tIHM) for AP1000
8) Fuel burnup levels (GWd/tIHM) for VHTR
9) Electricity generation for AP1000 (GWd)
10) Electricity generation for VHTR (GWd)
11) Total FP mass separated during reprocessing
12) Total FP mass generated during VHTR operation
13) Uranium mass and composition at AP1000 EOC
14) Uranium mass and composition at VHTR EOC
15) TRU production rates for AP1000
16) TRU production/destruction rates for VHTR
17) Uranium ore requirements
18) Quantity of UO_2 for NES operation
19) DU generated during frontend enrichment procedures

To illustrate the capabilities of the ISM, a reference case was created for NES simulation. The reference case includes the following input parameters:

- mine grade 1% U,
- tail assay 0.3% ^{235}U,
- AP1000 LEU fuel enriched to 3.8%,
- AP1000 thermal efficiency of 32.8%,
- 12 years decay time between AP1000 EOC and VHTR BOC,
- 100% separation procedures during reprocessing,
- Reprocessed TRU becomes fuel component for VHTR,
- TRISO packing fraction of 27%,
- VHTR thermal efficiency of 48%,
- 7 year lag time before HEST *D*-factor calculations.

A set of selected results for the reference ISM case are listed in Table 5.9 (a-d).

Table 5.9. ISM Reference Case Results.
(a) Front-End.

Uranium Ore (mine grade 1% U)	73,343 MT
Natural Uranium	735.3 MT
DU stock from enrichment process (0.3% ^{235}U)	647.3 MT
DU recovered from reprocessing (1.5% ^{235}U)	82.42 MT
AP1000-to-VHTR support ratio	4.6

(b) AP1000 and VHTR.

	AP1000 EOC		**VHTR EOC**	
	Mass (kg)	TRU (w/o)	Mass (kg)	TRU (w/o)
FP	1760		818.1	
^{234}U	0.14		4.78	
^{235}U	950		1.23	
^{236}U	383.3		0.68	
^{238}U	81090		0.0023	
^{237}Np	28.02	4.000	108.88	3.375
^{238}Pu	7.25	1.035	210.69	6.530
^{239}Pu	368.43	52.59	893.28	27.69
^{240}Pu	172.97	24.69	1094.90	33.94
^{241}Pu	82.67	11.80	387.12	12.00
^{242}Pu	32.42	4.628	250.56	7.766
^{244}Pu	0.001	0.00012	0.009	0.00027
^{241}Am	1.898	0.271	143.04	4.434
^{242m}Am	0.010	0.0014	1.795	0.056
^{243}Am	4.610	0.658	60.81	1.885
^{242}Cm	0.774	0.110	16.60	0.515
^{243}Cm	0.013	0.0018	0.981	0.030
^{244}Cm	1.436	0.205	49.29	1.528
^{245}Cm	0.060	0.0085	7.894	0.245
^{246}Cm	0.006	0.00080	0.443	0.014
TRU	700.58	100	3226.3	100
Burnup	32.63 GWd/iTHM		284.9 GWd/iTHM	
EFPD	826		2160	
Elec. Gen.	921.1 GWd		441.2 GWd	

(c) TRU Production/Destruction in VHTR.

Nuclide	BOC (kg)	EOC (kg)	TRU Production/Destruction (%) (- values indicate destruction)
^{237}Np	188.61	108.88	-42.27
^{238}Pu	47.71	210.69	341.58
^{239}Pu	2431.45	893.28	-63.26
^{240}Pu	1120.48	1094.90	-2.28
^{241}Pu	301.34	387.12	28.46
^{242}Pu	209.81	250.56	19.42
^{244}Pu	0.0054	0.0086	59.77
^{241}Am	245.25	143.04	-41.68
^{242m}Am	0.06	1.80	2839.02
^{243}Am	29.85	60.81	103.75
^{242}Cm	0	16.60	na
^{243}Cm	0.07	0.98	1370.98
^{244}Cm	5.92	49.29	733.21
^{245}Cm	0.39	7.89	1946.49
^{246}Cm	0.04	0.44	1126.57
TRU	4580.97	3226.30	-29.57
Pu	4110.80	2836.57	-31.00

(d) D_{eq}^{TRU} (neutron consumption/fission) Results for HEST.

HEST	φ =10^{10} (n/cm^2-s)	φ =10^{12} (n/cm^2-s)	φ =10^{14} (n/cm^2-s)	φ =10^{16} (n/cm^2-s)	φ =10^{18} (n/cm^2-s)
Concept I	0.46	0.45	-0.12	-0.65	-0.82
Concept II	-1.91	-1.91	-1.99	-2.37	-2.41

The ISM is very useful because it can quickly produce results for the NES while also allowing user control over input parameters. To exemplify this point the ISM is compared to results obtained by executing each of the models individually and manually linking them together to produce the same system as with the ISM.

The path of execution for the individual models starts with AP1000 whole-core 3D depletion/decay calculations in MCNPX followed by output data processing in order to manipulate the data into the form required as input for the VHTR model. As with the AP1000, the VHTR model utilizes MCNPX for depletion/decay calculations followed by output processing for extracting the data needed for calculating D_{eq}^{TRU} values for the HEST Concept I and II systems. In addition, the MCNP5 models representing the HEST Concept I and II have to be integrated with post processing for producing the remaining data needed for completing the D_{eq}^{TRU} value calculations in MATLAB. By far the most time intensive procedure for the individual models is the MCNPX depletion calculations for the AP1000 and VHTR, and that is why the ISM uses predictive methods for simulating depletion in order to greatly reduce computational run time.

Since the AP1000 and VHTR must meet the depletion criteria of the EOC being coincidence with k_{eff} = 1.00, it requires the MCNPX depletion calculation to be run twice for each reactor. Once to determine the burnup level at which k_{eff} = 1.00 and then again to stop the depletion sequence at that pre-determined burnup level and follow it with decay time calculations. Since a single depletion sequence for the AP1000 has a computational time of 30 hours and the VHTR a time of 42 hours, the total computational time is 144 hours. This does not include the time necessary for pre and post data processing and additional calculations, which can be significant, but in comparison to the MCNPX depletion sequences, are minimal.

The main capability of the ISM is to quickly predict fuel cycle parameters related to material depletion within the AP1000 and VHTR, and then use the information to determine key fuel cycle characteristics. Table 5.10 list the differences of the ISM results with the results obtained by performing the calculations with MCNPX. The input parameters for each were set to:

- AP1000 enrichment = 3.8%
- Lag time between AP1000 EOC and VHTR BOC = 12 years
- VHTR TRISO packing fraction = 27%
- Decay period after VHTR irradiation = 7 years

The savings in computational time for the ISM is over -5 orders of magnitude when compared to MCNPX and the difference between the results are minimal. For the AP1000, the TRU nuclides with very small masses produce larger differences, particularly the Cm isotopes. The same is true for the VHTR, most notably ^{242}Cm at 7 years decay, which due to its short half-life only remains at very small quantities. Overall, the differences between the ISM and MCNPX calculations are minimal, and the computational time efficiency of the ISM provides much more flexibility for NES evaluation.

Table 5.10. Percent Difference MCNPX to ISM.

	AP1000		VHTR	
Parameter	EOC (%)	Lag, 12 yr (%)	EOC (%)	Decay, 7 yr (%)
^{234}U	0.82	1.65	-1.29	-1.29
^{235}U	-0.80	-0.80	-2.50	-2.18
^{236}U	0.23	0.23	-1.60	-0.82
^{238}U	-0.02	-0.02	0.18	0.18
^{237}Np	0.31	0.28	0.02	-0.01
^{238}Pu	1.35	1.41	0.01	-0.10
^{239}Pu	-0.53	-0.53	0.46	0.79
^{240}Pu	0.07	0.13	-0.45	-0.57
^{241}Pu	0.77	0.23	-0.47	-1.60
^{242}Pu	2.25	2.24	0.45	0.47
^{244}Pu	2.34	2.39	-0.42	-1.21
^{241}Am	0.53	0.57	0.73	0.58
^{242m}Am	0.58	0.51	2.37	1.93
^{243}Am	2.83	2.83	0.03	0.05
^{242}Cm	1.82	-4.91	-0.59	-5.60
^{243}Cm	4.39	4.56	-0.36	0.10
^{244}Cm	4.51	4.02	0.26	-0.14
^{245}Cm	6.00	6.25	0.43	0.45
^{246}Cm	6.99	7.15	-1.37	-1.11
FP	1.24	na	0.15	na
Burnup	0.85	na	-1.21	na
Computational Time				
MCNPX	144+ hours			
ISM	< 1 second			

The options for NES analysis are expanded significantly by the ISM, as the input variables can take on any value between the defined ranges specified for each. Additionally, when considering the cross-matching between each of the variables, the possible combinations are limitless. As one example, the ISM is adjusted so that a ramp function produces input for the AP1000 fuel enrichment. Thus, ISM results for the NES as a function of AP1000 fuel enrichment alone are produced. Figure 5.22 shows how the quantities of ^{239}Pu and ^{240}Pu at the EOC for the VHTR are affected by fuel enrichment changes in the AP1000.

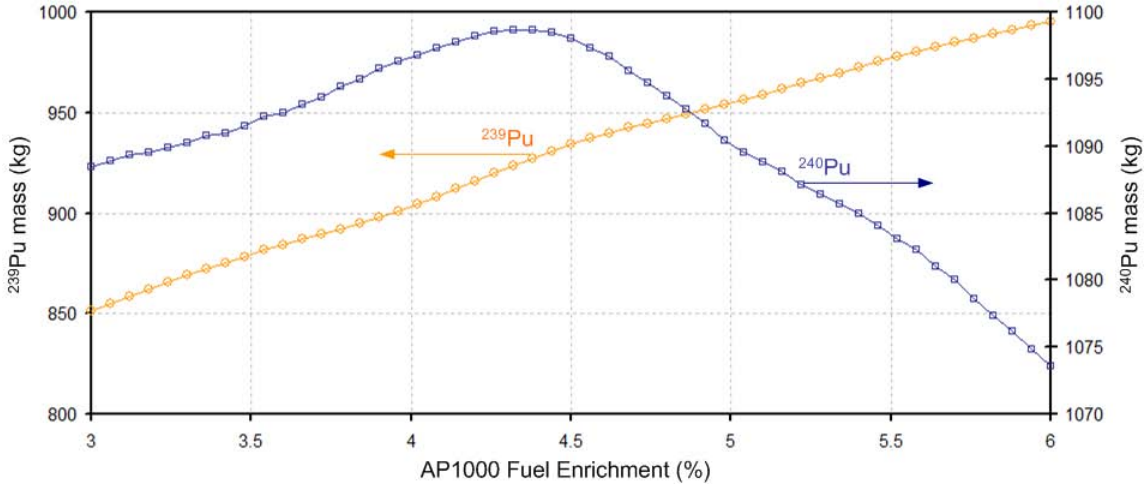

Figure 5.22. VHTR EOC Mass as a Function of AP1000 Fuel Enrichment.

Figure 5.23 shows the effect that the fuel enrichment of the AP1000 has on the electricity generated by both the AP1000 and VHTR. As expected, an increase in enrichment leads to greater electricity production for the AP1000 over the core lifetime, but at the same time the opposite effect is true for the electricity generated by the VHTR, which produces less electricity as enrichment increases. However, it is evident that the total electricity generation (AP1000 + VHTR) increases as enrichment increases.

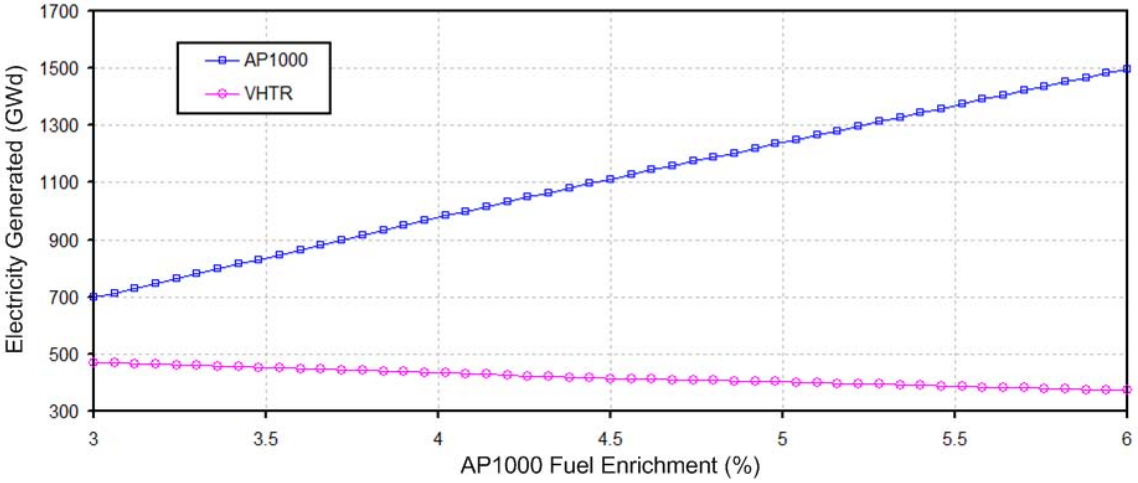

Figure 5.23. Electricity Generation as a Function of AP1000 Fuel Enrichment.

Figure 5.24 shows the overall percentage of TRU destruction in the VHTR as it relates to the fuel enrichment of the AP1000, which clearly indicates a lower destruction rate for higher enrichments. By evaluating the change in enrichment alone, it appears that reducing TRU waste and fuel utilization are competing factors, indicating that additional analysis is required, which is addressed in the next chapter (Chapter VI: Sensitivity/Uncertainty Analysis).

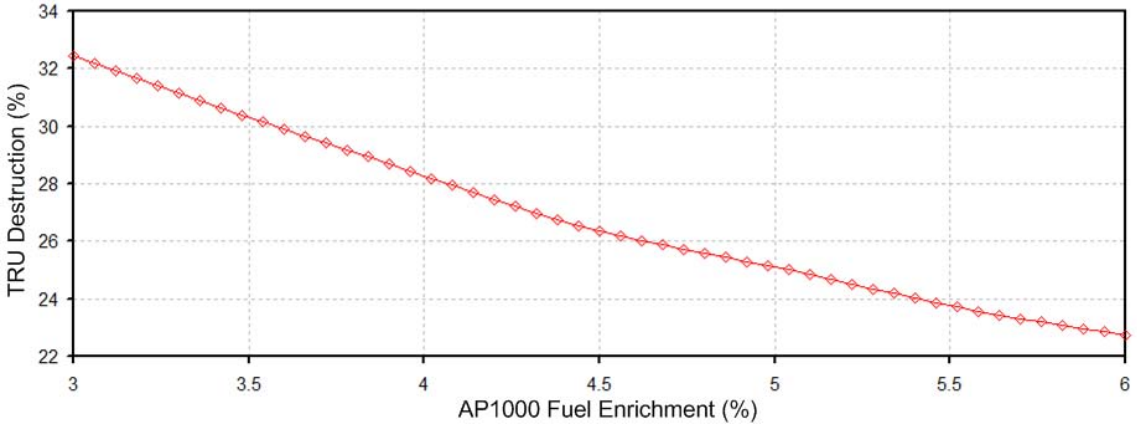

Figure 5.24. TRU Destruction in VHTR as a Function of AP1000 Fuel Enrichment.

The ISM presents many options for evaluating the NES, especially in regard to the research objectives outlined in Chapter 1. The next chapter discusses ISM approaches for simulating scenarios that minimize the problematic TRU nuclides generated by the NES while at the same time aiming to fully utilizing fuel resources. By doing so, it not only reduces the burden on nuclear waste management and ensures a sustainable energy source, but also diminishes the environmental impact of front-end fuel cycle procedures, such as uranium mining and tailings disposal.

6 SENSITIVITY/UNCERTAINTY ANALYSIS

The capabilities of the ISM make it possible to assess how variations in input will affect the NES on multiple levels. For instance, a change in AP1000 fuel enrichment not only generates enrichment dependent results for the AP1000 system, but it will also affect the results related to other NES components such as: decay calculations during lag time, irradiation related results for the VHTR, neutron balance calculations for the HEST, long-term TRU radiotoxicity calculations for waste management, and fuel resource needs for front-end procedures. Being able to perform such applications and effectively track the results in a time efficient manner allows many possibilities for sensitivity/uncertainty analysis.

6.1 Sensitivity/Uncertainty Analysis

Systematic changes were made to parameters in the NES to determine the effects of the changes on the system. The ISM was adjusted to accomplish the study by setting input parameters to linearly increase by using a ramp function, which allowed for the generation of system wide results as a function of increasing input. Separate cases were performed for each input variable, with the parameter of interest allowed to change while the remaining variables were held constant. The ramp function performed system calculations at equally spaced intervals for each input variable of interest according to:

$$f(t) = \left(\frac{v_u - v_l}{n} \right) t + v_l, \qquad for \quad t = [0,1,....,n] \tag{39}$$

where v_l is the lower bound for input variable v, v_u is the upper bound for the input variable v, n is the total number of intervals, and the input variables evaluated for the system include:

1) AP1000 enrichment (3% → 6%)
2) Lag time between AP1000 and VHTR (5yr → 20yr)
3) TRISO packing fraction in VHTR fuel compact (20% → 40%)
4) Lag time between VHTR and HEST (0yr → 20yr)

System wide results were collected and processed for conducting the sensitivity analysis. Figure 6.1 provides a diagram of how the sensitivity calculations were performed by the ISM. The diagram indicates the inclusion of a ramp function for generating input values for the AP1000 enrichment, with the remaining input ramp functions turned off. The generated output is, therefore, a function of a linear increasing enrichment value. Additional calculations were performed as the ramp function for each input variable was alternated between on and off.

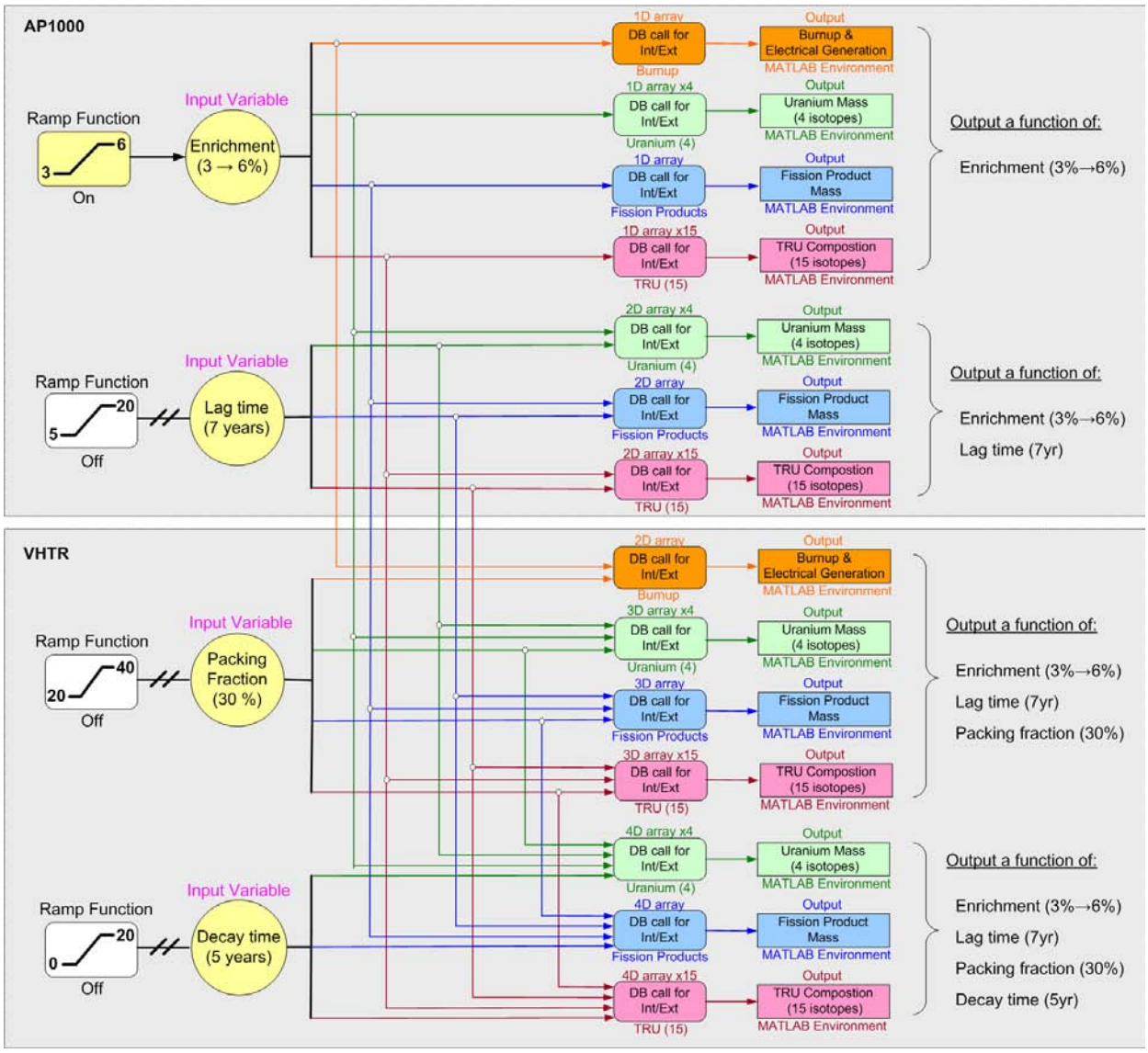

Figure 6.1. Example of Sensitivity Calculations Performed within the ISM Structure.

Considering that the input variables have different dimensions and different ranges of values, a non-dimensional sensitivity coefficient was introduced to characterize sensitivity as follows:

$$S_{V_i,X_j} \cong \frac{\partial X_j}{\partial V_i} \cdot \frac{V_i}{X_j} \cong \frac{\delta X_j}{\delta V_i} \cdot \frac{V_i}{X_j} \qquad (40)$$

where $S_{Vi,Xj}$ is the non-dimensional sensitivity coefficient, V_i is the ith variable, and X_j is the jth output variable. A positive/negative sensitivity coefficient $S_{Vi,Xj}$ indicates that output X_j will increase/decrease as the variable V_i increases. The larger the sensitivity coefficient, the larger effect the variable has on the output. The closer the value is to zero, the less impact the variable has on the output.

Table 6.1 lists sensitivity coefficients representing the affect different input variables have on selected output values. A large number of coefficients were determined, taking into

consideration small increments over the range of interest for each input variable, but the reported sensitivity coefficients in the table signify the change associated with the full span of the input variable under investigation.

Table 6.1. Non-dimensional Sensitivity Coefficients for Overall System.

Input variation		1. AP1000 Enr(3→6%)	2. AP1000 Enr(3→6%)	3. AP1000 Enr(3→6%)	4. Lag Time (5→20yr)	5. VHTR PF (20→40%)	6. VHTR PF (20→40%)
NES component		AP EOC	VHTR EOC	VHTR EOC	VHTR BOC	VHTR EOC	VHTR EOC
Output		mass	mass	P/D rate	mass	mass	P/D rate
Non-Dimensional Sensitivity Coefficient (S)	^{234}U	2.928	0.149				
	^{235}U	0.408	-0.103				
	^{236}U	1.367	-0.309				
	^{238}U	-0.044	0.057				
	^{237}Np	1.873	1.299	-0.225(1)	0.010	0.851	0.082(1)
	^{238}Pu	2.599	0.348	-0.671	-0.036	1.052	0.072
	^{239}Pu	0.247	0.169	-0.177(1)	0.001	1.189	-0.070(1)
	^{240}Pu	0.422	-0.014	-0.942(1)	0.002	1.056	-1.256(3)
	^{241}Pu	0.713	-0.037	-0.777	-0.169	0.574	-0.978
	^{242}Pu	1.429	0.370	-0.675	0.001	0.880	-0.243
	^{244}Pu	3.079	0.013	-1.072(2)	0	0.694	-0.569
	^{241}Am	2.025	0.302	-0.071(1)	0.542	1.458	-0.350(1)
	^{242m}Am	2.560	0.360	-0.463	-0.020	1.898	0.509
	^{243}Am	2.779	0.324	-0.769	0	0.734	-0.252
	^{242}Cm	2.533	0.198	-1.375	-0.312	0.246	-0.362
	^{243}Cm	5.082	0.001	-0.699	-0.100	0.557	-0.223
	^{244}Cm	6.361	0.271	-0.794	-0.142	0.768	-0.123
	^{245}Cm	11.774	0.157	-0.879	-0.002	0.995	0.013
	^{246}Cm	17.789	-0.035	-0.949	-0.003	1.115	0.081
	TRU	0.483	0.144	-0.299(1)	0	1.003	-0.063(1)
	FP	1.208	-0.304	-	-	0.827	-
	Elec.(GWd)	1.150	-0.206	-0.206	-0.055	0.866	0.866

(1) indicates destruction for given variable range
(2) indicates switchover from production to destruction as variable increases
(3) indicates switchover from destruction to production as variable increases

The Table's first three columns of sensitivity measurements are representative of changes made to the AP1000 fuel enrichment starting at 3% and increasing to 6%. Columns 1 and 2 signify how increased enrichment affects output masses for the TRU isotopes, total FP, U isotopes, total TRU, and the electricity generated by the AP1000. Column 1 considers the mass results tabulated for the AP1000 at EOC, with column 2 for the VHTR at EOC. Column 3 considers the TRU production/destruction (P/D) rates during irradiation in the VHTR.

The forth column of coefficients takes into account the amount of lag time between the AP1000 EOC and VHTR BOC and how it affects the amount of TRU by nuclide during that period. Additionally, the bottom row of column 4 represents the sensitivity of lag time to the electricity generated by the VHTR.

The last two columns (5 and 6) list sensitivity coefficients that account for changes in the input variable representing the TRISO particle packing fraction (PF) within the fuel element of the VHTR. Column 5 contains coefficients for the output parameter of mass for TRU, U, and total FP. Coefficients for the output variables representing TRU production/destruction rates and the electricity generation for the core lifetime of the VHTR are listed in column 6.

Sensitivity coefficients listed in column 1 indicate that as enrichment increases all output masses for the nuclides calculated at AP1000 EOC also increase, except for ^{238}U. The reason being, higher enrichment leads to an increase in fuel burnup, which translates to a greater accumulation of actinides. The results most sensitive to changes in enrichment are the masses for the higher actinides, especially ^{245}Cm and ^{246}Cm. The TRU nuclide that shows the least sensitivity is ^{239}Pu.

The sensitivity coefficients listed in column 2 indicates similar trends, as most of the TRU nuclides at EOC for the VHTR also increase in mass as the fuel enrichment for the AP1000 increases. The exception being ^{240}Pu ^{241}Pu, and ^{246}Cm, which all show a slightly negative sensitivity coefficient. Of the TRU nuclides, ^{237}Np shows the highest sensitivity to enrichment changes. Also of notice is the negative coefficient for electricity generation, which is the opposite of the affect for the AP1000.

The third column of sensitivity coefficients shows that as AP1000 enrichment increases, the production and destruction rates for all the TRU nuclides decreases. ^{239}Pu, which constitutes the majority of the TRU composition, shows weak sensitivity to enrichment, while ^{240}Pu, the second largest constituent, shows much stronger sensitivity. Taken as a whole, as the AP1000 enrichment increases the overall TRU destruction rate in the VHTR is slightly reduced.

The sensitivity coefficients listed in column 4 are associated with TRU compositions and the nuclide decay constants. Most of the nuclides are long-lived and only small composition changes are experienced during the lag time between AP1000 and the VHTR. Of note, is the relatively strong sensitivity for the fissile isotope ^{241}Pu indicating a decrease in mass and the even stronger sensitivity for ^{241}Am indicating an increase in mass. Also, VHTR electricity generation is weakly affected by lag time, as increased lag time causes a slight decrease in generated energy.

Sensitivity coefficients listed in column 5 indicate that as the TRISO particle packing fraction is increased, the TRU masses, total FP mass, and electricity generated also increase. The response is as expected, considering that the amount of TRU in the system is being increased as the packing fraction increases, resulting in higher fuel burnup and, thus, greater Packing Fraction (FP) buildup and higher electricity output. Although all the output variables increase with packing fraction, the rate at which they increase is not as easily discernable and the coefficients provide information in this regard.

The sensitivity coefficients in column 6 indicate that as the packing fraction increases the production and destruction rates for most of the TRU nuclides decreases. The exceptions being: ^{237}Np, ^{239}Pu, ^{242m}Am, ^{245}Cm, and ^{246}Cm. As a group, the TRU nuclides show low sensitivity to the packing fraction, with ^{240}Pu and ^{241}Pu showing the highest sensitivity levels.

The sensitivity coefficients are a useful tool for quickly assessing system behavior, but additional information may be needed to give a complete picture of how the input variables affect the output for the system. The coefficients listed in Table 6.1 give information relevant to the end points of the input variables. Therefore, interior behavior might be overlooked, especially if sensitivity is strongly non-linear within the variable range. To account for this possibility a set of plots showing normalized output results as a function of the corresponding input variable were generated. The slope of the curve indicates the degree of sensitivity, such that the steeper the slope, the greater the sensitivity. A positive slope signifies an increase in the corresponding output variable and a negative slope signifies a decreasing value.

Figure 6.2 shows the normalized isotopic production/destruction rates in the VHTR for the Pu isotopes as they relate to TRISO packing fraction in the VHTR fuel element. The plot provides a useful means of easily comparing the sensitivity of many parameters at once. Also, it provides the ability to pinpoint import information such as the change from destruction to production rates as seen with ^{240}Pu at a packing fraction greater than 35.2%.

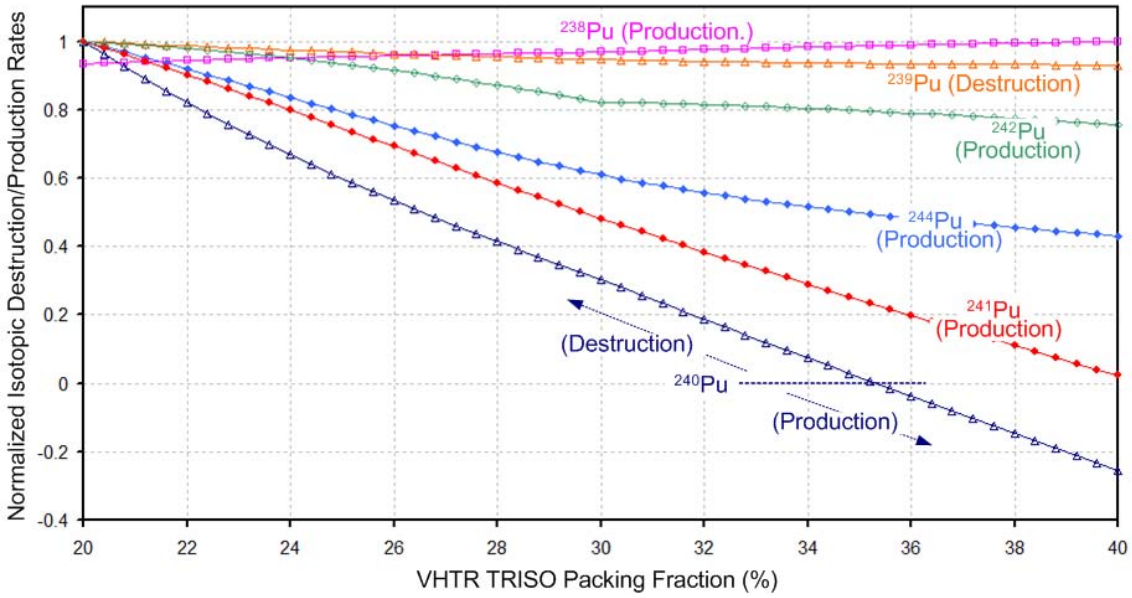

Figure 6.2. Pu Production /Destruction Rates in the VHTR vs. TRISO Packing Fraction.

The normalized production/destruction rates in the VHTR for relevant Am isotopes and ^{237}Np, as a function of the TRISO packing fraction, are shown in Figure 6.3. The plot indicates that ^{241}Am is most sensitive to changes in packing fraction and experiences a reduction in destruction rate as the packing fraction increases. ^{237}Np also undergoes destruction, but shows less sensitivity. ^{242m}Am and ^{243}Am are produced during irradiation in the VHTR, but the former increases in production rate, while the later decreases in production rate as the packing fraction increases.

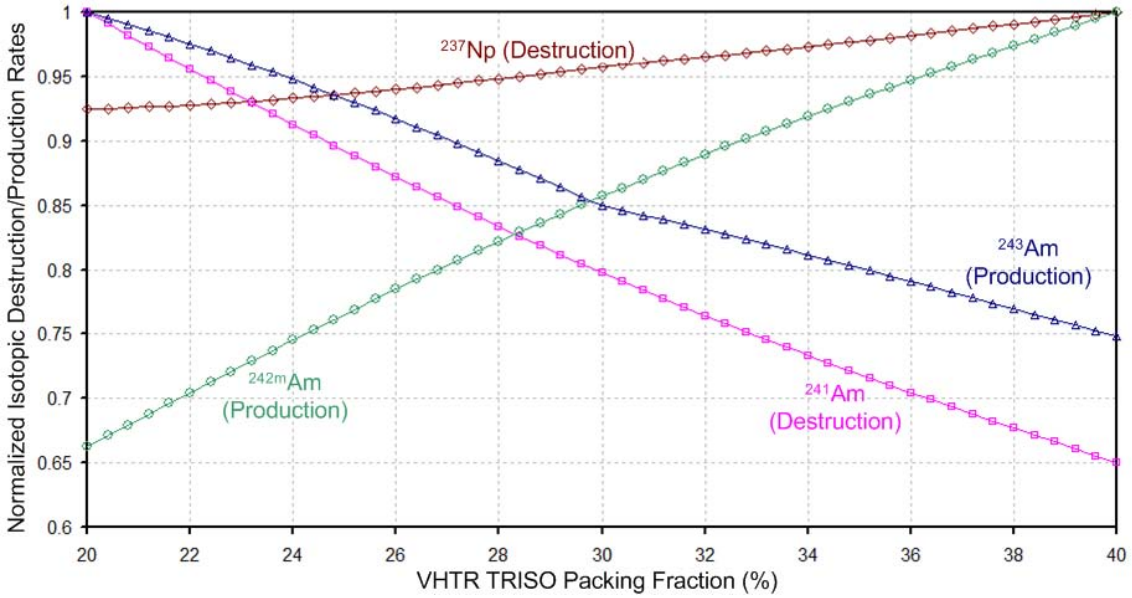

Figure 6.3. Am and ^{237}Np Production/Destruction Rates in the VHTR vs. TRISO PF.

Figure 6.4 is an example of two results that are not linear over the input variable range. Shown are the normalized production rates for ^{240}Pu and ^{242}Cm during irradiation in the VHTR as a function of the fuel enrichment in the AP1000. The ^{242}Cm does not even register a production rate until enrichment levels above 3.54% are achieved, due to its short half-life, causing it to decay away during the lag time for lower enrichment levels. Then when it is present, its production rate drops rapidly at first, and then levels off for enrichment levels above 4%. ^{240}Pu also show erratic behavior over the enrichment range. In both cases the behavior would not be discernable by the sensitivity coefficient alone.

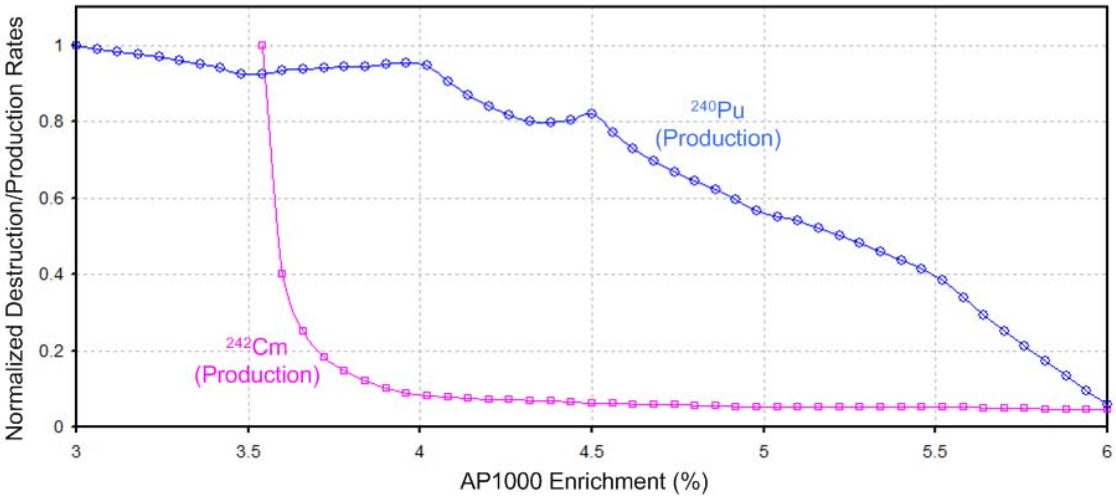

Figure 6.4. ^{240}Pu and ^{242}Cm Production Rates in the VHTR vs. AP1000 Enrichment.

7 DOMAIN IDENTIFICATION VIA MIN/MAX SEARCH FOR OPTIMIZATION STUDIES

The capabilities of the ISM make it possible to assess how variations in input will affect the NES on multiple levels. For instance, a change in AP1000 fuel enrichment not only generates enrichment dependent results for the AP1000 system, but it will also affect the results related to other NES components such as: decay calculations during lag time, irradiation related results for the VHTR, neutron balance calculations for the HEST, long-term TRU radiotoxicity calculations for waste management, and fuel resource needs for front-end procedures. Being able to perform such applications and effectively track the results in a time efficient manner allows many possibilities for implementing optimization techniques.

7.1 Domain Identification

In this report, the conceptual approach for optimization procedures is broken down into the following steps: 1) create a population of random solutions, 2) search for a set of optimum solutions, and 3) select best solution based on criteria preferences.

The population size of random solutions must be large enough to assure that the sampling space accounts for the infinite combinations possible for the input variables. To accomplish this, random number generators are applied to the ISM to produce input values within the specified range of each input variable. The random number generator assigned to each input variable is unique in its specified interval and starting seed. One million input values are randomly generated for each variable, thus assuring that the sampling space provides enough random solutions for complete analysis.

The randomly selected input values (10^6 for each input) and subsequently generated solutions (10^6 for each output parameter) are stored within the MATLAB environment, where a subroutine is called to search and retrieve minimum and maximum output values along with their matching input values. Table 7.1 list the minimum and maximum output results for a selection of output parameters along with the input values used to produce the results for each case.

The P/D parameter listed in Table 7.1 signifies whether a nuclide is produced or destroyed during irradiation in the VHTR. The output units for P/D are in fractional form and determined by the following relation:

$$\left(P/D\right)_i = \left(\frac{m_{out} - m_{in}}{m_{in}}\right)_i \tag{41}$$

where m_{out} is the mass measurement at VHTR EOC, m_{in} is the mass measurement at VHTR BOC, i is the TRU isotope of interest, and P/D is either the production or destruction rate for the i^{th} nuclide. As defined, P/D represents the production rate (P) if the outcome is a positive value and the destruction rate (D) if the value is negative. In some cases the nuclide is listed as P/D, meaning that the minimum output value is production and the maximum is destruction.

Table 7.1. NES Minimum and Maximum Output Data.

Output Parameter	Minimum				Maximum			
		Input				Input		
	Output	Enrich (%)	Lag time (yr)	PF (%)	Output	Enrich (%)	Lag time (yr)	PF (%)
^{237}Np (D)	-0.295	6.0	19.8	29.3	-0.492	3	5	30
^{238}Pu (P)	1.723	5	5	20	4.233	3.4	11	40
^{239}Pu (D)	-0.458	6	20	30	-0.735	3	5	20
^{240}Pu (P/D)	0.032	6	20	40	-0.068	3	5	20
^{241}Pu (P/D)	0.692	3.8	17	20	-0.096	5.2	8	40
^{242}Pu (P)	0.051	6	20	40	0.442	3	5	20
^{244}Pu (P/D)	1.664	3	5	20	-0.446	6	20	40
^{241}Am (D)	-0.040	3	5	30	-0.497	3.8	17	20
^{242m}Am (P)	12.37	5	5	20	43.75	4	20	40
^{243}Am (P)	0.335	6	20	40	1.965	3	5	20
^{242}Cm (P)	3958	5	5	30	na	na	na	na
^{243}Cm (P)	4.541	5	5	30	22.25	3.8	17	20
^{244}Cm (P)	2.890	5.4	11	40	11.83	3	5	20
^{245}Cm (P)	3.401	6	20	30	45.67	3	5	30
^{246}Cm (P)	0.413	6	20	30	40.05	3	5	30
TRU (P/D)	0.183	6	20	30	-0.373	3	5	20
VHTR: EFPD (d)	1136	5.8	17	20	3478	3.2	8	40
BU (GWd/tIHM)	200.0	5.8	17	20	313.7	3.2	8	40
Elec. (GWd)	257.8	5.8	17	20	679.6	3.2	8	40
AP1000: EFPD (d)	624.9	3	-	-	1343	6	-	-
BU (GWd/tIHM)	24.69	3	-	-	53.07	6	-	-
Elec. (GWd)	696.9	3	-	-	1498.0	6	-	-

The data set provided by Table 7.1 offers the ability to select single output parameters for optimization, but to select a best solution among all the options, further analysis is required. To complete the procedure requires utilizing the NES base of knowledge obtained thus far. In particular, the information collected in Chapter 3 (TRU Characterization), the neutron balance (D_{eq}^{TRU}) values calculated for the HEST system, the information gather for the sensitivity analysis, and the data in Table 7.1, are all used collectively to set up a criteria preference for reducing long-term HLW waste management concerns, while best utilizing fuel resources for energy generation.

7.2 Criteria Preference Method

The criteria preference method considers many NES parameters for identifying a single best solution set. The procedure uses a system to weight parameters according to importance relative to final overall NES performance goals.

Given that the AP1000 is considered primarily as a means to supply clean, abundant, economic, and safe base load electricity; the enrichment is weighted heavily for this means. The VHTR is an energy provider, but not on the same scale as the AP1000. The AP1000 generates more than twice the electricity output of the VHTR. Additionally, the support ratio of AP1000 to VHTR is anywhere from 4:1 to 11:1, depending on the input variables used. Therefore, the total electricity generation by the AP1000 is between 8.8 and 24.2 times greater than that for the VHTR.

Increasing the enrichment variable for the AP1000 causes an increase in TRU inventory and a decrease in isotopic production/destruction rates in the VHTR. Considering the goal of TRU destruction, lower enrichment cases are ideal, but the sensitivity to enrichment is quite low nonetheless. Also, P/D rates for the individual isotopes can be evaluated separately and adjusted accordingly.

The lag time between AP1000 and VHTR has low sensitivity on the P/D rates. Overall, the shorter the lag time, the better, for both VHTR electricity generation and TRU destruction.

An increase in TRISO packing fraction results in greater quantities of TRU at the EOC for the VHTR with the sensitivity of the individual isotopes varying differently for each. In addition, increases in packing fraction will result in higher fuel burnup, which in turn, translates to more electrical energy being generated by the VHTR core.

The fast fluence levels for the TRISO particles act as a constraint on the optimizations parameters. The guideline for fast fluence limitations is approximately 10^{26} n/m^2 [51,52,53]. The calculated fast fluence levels for the VHTR (neutron energies greater than 0.1 MeV) are between 5.2×10^{21} and 1.6×10^{22} n/cm^2. Therefore, the input parameters that produce maximum EFPD measurements in the VHTR approach the traditional TRISO fast fluences limitations. Considering that the used VHTR fuel is not reprocessed before irradiation in the HEST system, it is recommended that fast fluence levels in the VHTR be minimized.

The HEST Concept II was selected for the criteria preference method. Primarily because it is foreseen to operate at much lower flux levels than the HEST Concept I, providing greater flexibility for fast fluence limitations. Additionally, HEST Concept II produces a harder energy spectrum, which translates to a more favorable environment for TRU transmutation.

The neutron balance (D_{eq}^{TRU}) values calculated for the HEST Concept II system provide additional guidance for the optimal TRU compositions entering the HEST and ultimately the final TRU composition and quantity to be stored as HLW.

Table 7.2. NES Optimum Input Values by Criteria Preference Method.

	Optimum Input Variable		
Parameter	Enrichment (%)	Lag Time (yr)	PF (%)
Electricity Gen. AP1000	6	-	-
TRU Inventory AP1000	3	-	-
(P/D) rate VHTR	3	5	20
TRU Inventory VHTR	3	5	20
Electricity Gen. VHTR	3.2	8	40
EFPD VHTR	5.8	17	20

Table 7.2 provides the optimum input values according to the criteria preference method. The preferences consist of maximizing electricity generation for the AP1000 and VHTR systems, minimizing the TRU inventory, maximizing TRU destruction rates, and minimizing EFPD for the VHTR.

Considering preferential destruction rates for the TRU and minimization of the TRU inventory the input values of 3% enrichment, 5 years lag time, and 20% PF are used for the ISM, with results listed in Table 7.3. As shown, over 73% of ^{239}Pu and 37% of the total TRU is destroyed in the VHTR. The fast fluence at EOC for the VHTR is 8×10^{21} n/cm^2. Considering additional irradiation in the HEST Concept II, the residence time will be limited by the fast fluence. A neutron flux level of 10^{12} n/cm^2-s for the HEST Concept II restricts the irradiation time to 30,000 days. Even so, the expected final transmutation rate for the TRU within the NES is expected to approach 95% destruction, based on the "physics approach to transmutation" as described in Chapter 5.

Table 7.3. Criteria Preference Method Results.
(a) NES.

AP1000 Electricity (kW·hr)	2.31×10^{10}
AP1000 BU (GWd/tIHM)	25.12
AP1000 EFPD	696.9
VHTR Electricity (kW·hr)	8.12×10^{9}
VHTR BU (GWd/tIHM)	365.7
VHTR EFPD	2077
VHTR fast fluence (n/cm^2)	8×10^{21}
AP1000:VHTR ratio	5
Total Electricity (kW·hr)	1.24×10^{11}
Uranium recycled (MT)	411.5

(b) Isotopic Results.

Nuclide	VHTR EOC Mass (kg)	VHTR P/D rate (%)
^{237}Np	56.77	-47.81
^{238}Pu	116.6	380.7
^{239}Pu	510.3	-73.48
^{240}Pu	773.1	-6.808
^{241}Pu	331.1	13.86
^{242}Pu	180.3	44.20
^{244}Pu	0.007	166.4
^{241}Am	66.71	-22.30
^{242m}Am	0.731	2044
^{243}Am	44.34	196.5
^{242}Cm	10.81	na
^{243}Cm	0.555	1711
^{244}Cm	38.04	1183
^{245}Cm	6.194	4445
^{246}Cm	0.408	729.6
TRU	2617.8	-37.3

8 ENVIRONMENTAL IMPACT ANALYSIS

Federal and state laws strictly regulate nuclear power plants to insure the protection of human health and the environment. Even so, there is a wide variation of environmental affects associated with nuclear power generation. In order to assess the environmental impacts of nuclear energy the various operations involved in the nuclear power industry must be considered. These operations are the mining and milling of uranium, enrichment, fuel fabrication, reactor operation, reprocessing (only in the case of the recycle option), transport of radioactive materials, management of radioactive waste, and decommissioning of nuclear facilities.

Considering these operations, the environmental impact of nuclear energy is categorized as follows:

1. Air emissions: Energy generated by nuclear power plants does not produce greenhouse gases; however, fossil fuel emissions are associated with the mining, enrichment, and transportation of the fuel.
2. Water resource use: The amount of water usage is a concern as populations increase and possible droughts are considered.
3. Waste heat: Discharge of waste heat to rivers, lakes, seawater and its affect on water quality and aquatic life.
4. Radioactive waste: The protection of the biosphere from all radioactive waste produced during the nuclear fuel cycle.
5. Radioactive emissions: Emissions occurring during normal operation as well as the possibility of the release of radioactive material due to abnormal operation or accident scenarios.
6. Reserves: Usage of natural resources and the sustainability of the energy source.
7. Land resource use: The area of land needed to support energy production, including: mining, enrichment, power plant, and waste storage.

The effect that nuclear power and other energy producing systems have on the environment has been studied in great detail in the past. The NES will share many of the environmental aspects associated with current nuclear power plants and the once-through fuel cycle. The purpose of the NES environmental impact analysis is to identify and evaluate the similarities and differences that occur between the NES and other energy sources, with focus placed on current nuclear power plants utilizing the once-through fuel cycle.

8.1 Air Emissions

Since energy generated by nuclear fission produces no greenhouse gases, the advanced reactors of the NES and the reactors currently used in the once-through fuel cycle do not emit any greenhouse gases to the atmosphere. However, when front-end procedures are included, there will be some subtle variations. The NES utilizes recycling, which provides an additional source of uranium feed. The uranium separated during the reprocessing stage is available for reuse in the AP1000, which is not the case for the once-through LEU fuel cycle. The additional uranium feed effectively reduces the amount uranium ore needed, therefore, reducing the mining related greenhouse gas emissions.

When evaluating the sources of electricity generation in the United States, fossil fuels are by far the largest source, accounting for more than 68% of the total [48]. Considering that the electricity generated by the NES would most likely replace fossil fuel sources, a useful evaluation is the greenhouse gas emissions, particularly CO_2, savings provided by the NES when compared to fossil fuels.

Table 8.1 shows the average amount of CO_2 emissions that would be eliminated if the NES were to replace fossil fuel sources, using 2009 emissions data [54]. To put the emission reductions into perspective, it would be equivalent to taking roughly 10.5 million cars of the road.

Table 8.1. CO_2 Emissions Reductions per Year.

Source (% of total fossil fuel generation in U.S.)	NES CO_2 Reductions (MT/year)
Coal (65%)	4.78E+07
Natural Gas (33%)	1.91E+07
Petroleum (2%)	4.02E+07

8.2 Water Resource Use

Water requirements for nuclear power plants are higher than for other major energy generation sources [55]. The NES includes the VHTR and HEST systems, which operate without the need for large amounts of cooling water, thus water needs compared to the LEU once-through fuel cycle are lessened. However, since multiple AP1000 reactors are required to support the TRU fuel needs for a single VHTR, and the fact that each AP1000 outputs much greater energy ($3400MW_{th}$ vs. $600MW_{th}$), indicates that the water savings for the NES are not very large, but nonetheless water needs are reduced.

Other strategies can be implemented to significantly reduce the amount of water taken from the water table. Such would be the case for dry cooling systems, but advancements would be needed to improve the economic aspects related to dry cooling. One possibility is to use sewage cooling as is done at the Palo Verde Nuclear Generating Station. Using seawater is another option, but it constricts the location of the energy system.

8.3 Waste Heat

The waste heat from energy generation is often dissipated into the surrounding environment. In some cases this involves cooling with natural bodies of water, which can affect the aquatic ecosystem. Comparing the NES to the once-through cycle, consider that both systems reject waste heat to bodies of water containing aquatic life. The impact for each is evaluated the same way as it is for water resource use. The NES will have a slightly smaller environmental impact due to the VHTR and HEST systems not requiring cooling by large water sources.

The best course for reducing the environmental impact due to waste heat is to use other sources for cooling, such as: dry cooling, dedicated cooling ponds, cooling towers, sewage water, etc.

8.4 Radioactive Waste

Radioactive waste comes from a number of sources and is classified according to the physical, chemical, and radiological properties. The most widely used classification system separates waste into three classes: Low Level Waste (LLW), Intermediate Level Waste (ILW), and high level waste (HLW). These classes address activity content, radiotoxicity, and thermal power.

As stated in the research objectives, one of the main goals for the NES is to alleviate HLW management issues by targeting the transmutation of TRU. Significant reductions to the TRU remaining after irradiation can have an important impact on the timescale involved with isolating HLW from the environment and greatly reducing the burden on long-term HLW management.

Therefore, a useful measure is the difference in timescale necessary for isolating the HLW from the biosphere for the NES and the LEU once-through fuel cycle. Since long-term (greater than 1,000 years) effects are targeted, only the radiotoxicity behavior of the TRU is evaluated, as the fission products decay away to insignificant levels after about 300 years.

Figure 8.1 show radiotoxicity levels resulting from the irradiated fuel that is removed from the reactor systems in the NES for a time period extending out to 1 million years. The ORIGEN-S code system was used to compute time-dependent concentrations and radiation source terms of the isotopes of interest, while undergoing radioactive decay. The isotopic activity levels and effective dose coefficients for ingestion $e_{ing}(50)$ [34] are used to produce radiotoxicity measurements. The results in the plot are normalized to the amount of natural uranium from which the HLW originated. The radiotoxicity for the AP1000 is representative of that for a typical PWR and is used as the reference case for the LEU once-through fuel cycle.

The results in Figure 8.1 show that the TRU produced by the LEU-fueled AP1000 will remain above the radiotoxicity level of the original uranium ore for at least 100,000 years. The VHTR, which is fueled by the TRU resulting from the AP1000, is effective in destroying a decent fraction of the TRU (particularly the Pu). As a result, the TRU removed from the VHTR reaches uranium ore radiotoxicity levels at 50,000 years. Considering another 95% reduction takes place in the HEST system and the TRU radiotoxicity now drops below uranium ore levels in less than 2,000 years.

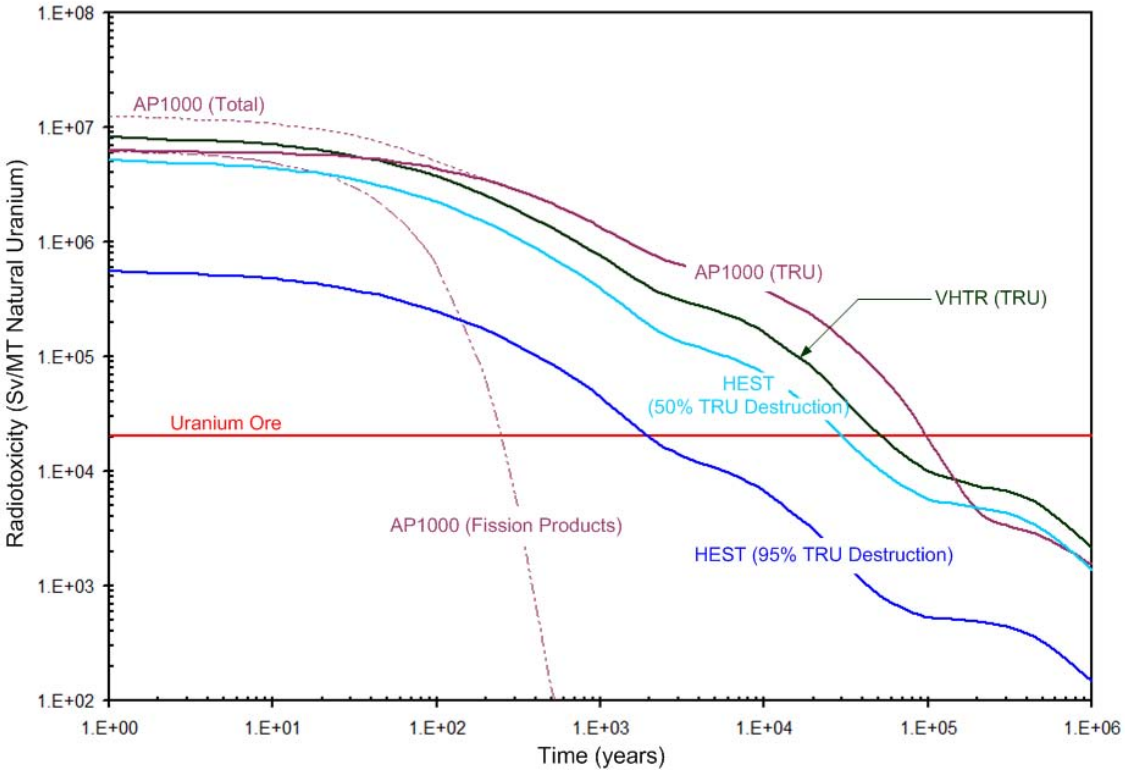

Figure 8.1. TRU Radiotoxicity Measure as a Function of Time.

For even greater time reductions, individual radionuclides can be targeted for destruction in the HEST. Figure 8.2 shows how the major TRU isotopes contribute to the overall radiotoxicity of the TRU produced in the AP1000. Concentrating on strategies to preferentially destroy ^{239}Pu, ^{240}Pu, ^{241}Am, and ^{241}Pu (^{241}Pu because it beta-decays to ^{241}Am) in the HEST can produce even better results, eventually approaching the 300 year limit imposed by the fission products.

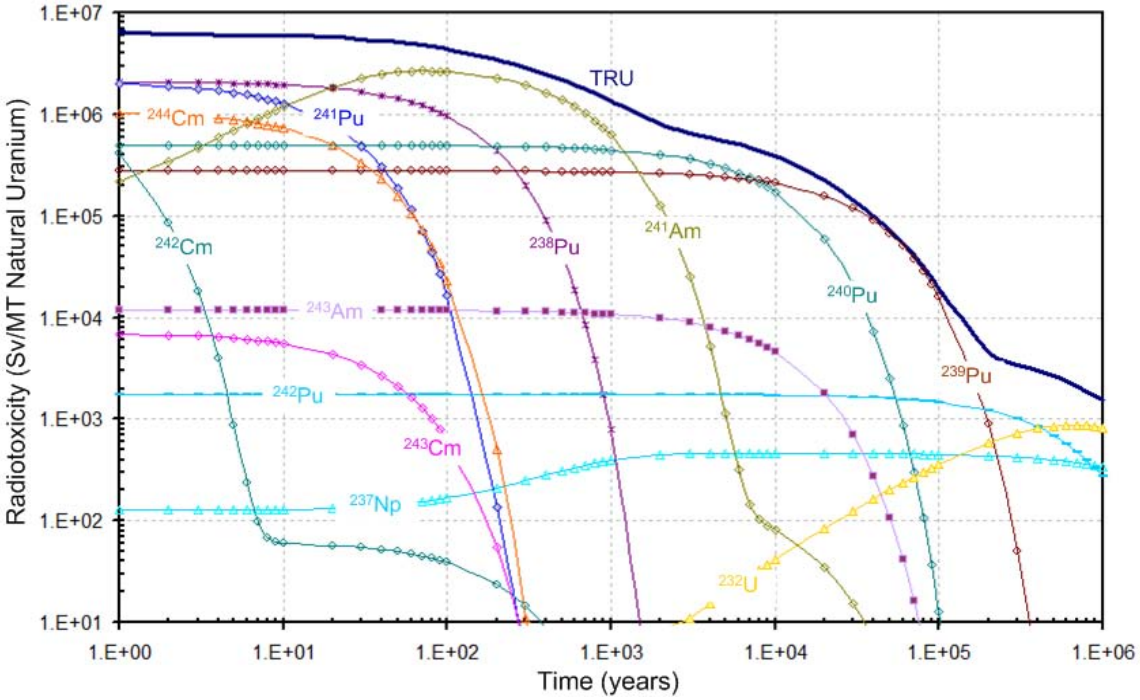

Figure 8.2. Isotopic Radiotoxicity Measure as a Function of Time.

All energy sources produce waste materials that are hazardous and have adverse affects on the environment. The NES is no exception, as radioactive waste must be properly treated to protect humans and the environment. Radioactive waste differs from waste produced by other energy sources in two respects. First, the risk associated with radioactive waste decreases with time, as shown in Figure 8.2. Second, the volume of waste (per unit energy) is much smaller than most other sources. Table 8.2 provides a comparison of HLW nuclear waste produced by the NES and the waste product associated with a typical coal fired power plant [56]. The results in the table are normalized to quantities of waste products produced annually from the generation of 1000 MW_e. The values for HLW correspond to the NES with 90% TRU destruction in the HEST system.

Table 8.2. Annual Waste Production from 1000MW_e.

Coal	Mass (MT)	NES	Mass (MT)
Fuel Consumption / year	2,300,000	Fuel Consumption / year	2.5
Waste Produced / year		Waste (HLW) Produced / year	
Bottom Ash	50,000	TRU	0.06
Fly Ash Retained	248,000	Fission Products	2.5
Sulphur Retained	46,000		
Total	344,000	Total	2.56
Direct Air Emissions / Year		Direct Air Emissions / year	
CO_2	6,000,000	CO_2	0
NO_x	27,000	NO_x	0
SO_2	24,000	SO_2	0
Fly Ash	1,000	Fly Ash	0
CO	1,000	CO	0
Mercury	5	Mercury	0
Arsenic	5	Arsenic	0
Nickel	5	Nickel	0

8.5 Radioactive Emissions

Radioactive emissions occur during normal operation of nuclear power plants. Strict limits on the amount of radioactive emissions allowed to be released to the environment have been established by the U.S. NRC. The U.S. Environmental Protection Agency and the NRC monitor radioactive effluents from nuclear facilities to insure appliance. An example of the emission levels are provided by the American Nuclear Society, stating that individuals living within 50 miles of a nuclear power plant typically receive about 0.01 mrem dose per year. For comparison, a person living within 50 miles from a coal power plant receives about 0.03 mrem per year. The average dose per person from all sources is about 360 mrem per year and International Standards allow exposure to as much as 5,000 mrem per year for nuclear industry workers. Thus, emissions for both the NES and once-through fuel cycle are negligible, but the NES would most likely produce more radioactive effluents under normal operating conditions because of the addition of reprocessing facilities. The reprocessing facilities would be under the same emissions monitoring as power plants.

Another environmental concern is the potential radiation exposure during an accident that may result in the release of radionuclides to the environment. The evaluation of the risk associated with such occurrences is performed by probabilistic risk assessment techniques. The risk associated with the current fleet of LWR reactors is determined to be extremely low and accidents resulting in significant radiation release to the environment are extraordinarily unlikely. The reactor systems within the NES are passively safe systems, thus the NES will have even lower associated risk levels for such unlikely events.

8.6 Reserves

The amount of effort and expenditure that has been put into uranium exploration and development pales in comparison to that for gas and oil. It is widely believed that with greater uranium exploration and development, the conventional resources would increase significantly. Credence is given to this prediction by the occurrence of continually increasing reserves as demand grows and more effort is put into exploration. Additionally, the history of oil and gas shows, as investments are made into exploration, technology development, and extraction, more and more reserves are found.

Nevertheless, uranium resources are sufficient to sustain projected nuclear energy requirements long into the future [6]. Table 8.3 indicates this trend. The duration time assumes unchanged usage rates and unchanged technology (LEU once-through cycle). The identified resources are those that are already "in hand." The prognosticated resources are based on geological investigation utilizing detailed exploration methods, which are normally performed at current mining sites. Considering the identified and prognosticated resources, current nuclear energy demands can be met for about 260 years. In addition, uranium can be extracted from phosphates and seawater if demand required. These resources add significantly to the amount of available uranium and extend the sustainability of nuclear energy for many more hundreds of years into the future.

Table 8.3. Uranium Resources.

Reported Resources	Mass (MT)	Duration (yr)
Indentified	5.5	90
Prognosticated	10.5	170
Phosphate deposits	22	356
Seawater	4000	65,000

Considering the strong possibility of an increase in worldwide nuclear capacity the duration time results in Table 8.3 can be somewhat misleading. As the work in this research project has clearly pointed out there are many advantages and great potential for utilizing nuclear as a future energy source. Therefore, it is strongly recommended that nuclear energy play a leading role in the world's future energy portfolio, which would result in worldwide usage rates increasing greatly. This would considerably shorten the duration time for the identified uranium resources and it is unclear if cost increases for extracting uranium from phosphate deposits and/or seawater are reasonable assumptions for future resources. However, other possibilities exist within advanced fuel cycles for making nuclear power a truly sustainable energy source no matter what increases in usage are experienced in the future. This primarily involves including breeder reactor technology, which would improve the utilization of uranium by 50-fold or more. Additionally, thorium can be utilized as a nuclear fuel source and extend fuel reserves greatly. In both cases the ISM can be modified for analysis of advanced fuel cycles that include breeder reactors or thorium fuels.

In the NES, the uranium is recovered and reused, extending uranium resources even more by recycling the used fuel. The TRU is also recovered and used to generate additional energy that would otherwise be lost. However, the largest boost to nuclear sustainability comes from the

recycling of the uranium present in legacy HLW waste that would now be considered as a large stockpile of uranium reserves, rather than waste that requires isolation from the environment.

8.7 Land Resource Use

Nuclear energy takes up a very small amount of land area per electricity unit generated relative to other energy sources. This is especially the case when compared to the land resources required for renewable sources such as wind, solar, and hydro.

As mentioned in the previous section, the NES recycles the uranium and TRU contained by the used fuel, thus effectively reducing the need for uranium resources produced by the mining and processing of uranium ore. Therefore, in this way the NES reduces the overall footprint associated with the LEU once-through fuel cycle.

However, recycling of the uranium means that reprocessing facilities are required, which is not the case for the once-through fuel cycle. Still it is expected that the land savings from reduced mining will outweigh the gain required by the addition of reprocessing.

9 CONCLUSIONS

New high-fidelity integrated system method (ISM) and analysis approach have been developed and implemented for consistent and comprehensive evaluations of advanced fuel cycles leading to minimized TRU inventories. The method has been implemented in a developed code system integrating capabilities of MCNPX for high-fidelity fuel cycle component simulations.

Using the developed computational tool, a nuclear energy system (NES) configuration was developed to take advantage of used fuel recycling and transmutation capabilities in waste management scenarios leading to minimized TRU inventories. The analysis takes into account fuel cycle performance characteristics as well as potential impact of used fuel handling on the environment and resource utilization.

The reactor systems and fuel cycle components that make up the NES were selected for their ability to perform in tandem to produce clean, safe, and dependable energy in an environmentally conscious manner. The reactor systems include the AP1000, VHTR, and HEST. The diversity in performance and spectral characteristics for each was used to enhance TRU waste elimination while efficiently utilizing uranium resources and providing an abundant energy source.

The HLW stream produced by typical nuclear systems was characterized according to the radionuclides that are key contributors to long-term waste management issues. It was determined that the TRU component becomes the main radiological concern for time periods greater than 300 years. A TRU isotopic assessment was performed to produce a priority ranking system for the TRU nuclides as related to long-term waste management and their expected characteristics under irradiation in the different reactor systems. Highest priority isotopes for destruction are: ^{239}Pu, ^{240}Pu, ^{241}Pu, and ^{241}Am. The medium high priority isotopes include: ^{238}Pu, ^{242}Pu, ^{243}Am, and ^{244}Cm. The medium low priority isotopes are: ^{242m}Am, ^{242}Cm, ^{243}Cm, and ^{245}Cm. The low priority isotopes are: ^{237}Np, ^{244}Pu, and ^{246}Cm.

Detailed 3D whole-core models were developed for analysis of the individual reactor systems of the NES. As an inherent part of the process, the models were validated and verified by performing experiment-to-code and/or code-to-code benchmarking procedures, which provided substantiation for obtained data and results. Reactor core physics and material depletion calculations were performed and analyzed. Although the reactor models are independent, in the NES they are coupled by the fuel cycle components and material flows between them.

The material flow in the NES starts with the front-end procedures of uranium mining, enrichment, and fuel fabrication. Next the LEU fuel is loaded in the AP1000, which is the primary energy producing reactor system in the NES. The TRU are generated via neutron capture by ^{238}U and subsequent decay. Upon removal from the AP1000 the used fuel decays for an allotted amount of time before it is reprocessed. During reprocessing the uranium, fission products, and TRU are separated. The fission products are prepared for waste storage, the uranium is available for reuse in the AP1000, and the TRU is fabricated into fuel for use in the VHTR. The VHTR operates on the TRU fuel produced by the AP1000, generating electricity while also effectively destroying a fraction of the overall TRU by fission. When the VHTR can

no longer maintain criticality the fuel blocks are prepared for further transmutation in the HEST. The last process is the removal of the fuel blocks from the HEST for long-term waste storage.

A computational modeling approach (ISM) was developed for integrating the individual models of the NES. A general approach was utilized allowing for the ISM to be modified in order to provide simulation for other systems with similar attributes. By utilizing this approach, the ISM is capable of performing system evaluations under many different design parameter options. Envisioned possible future analysis includes: applying AP1000 fuel shuffling schemes, including VHTR deepburn strategies, analysis of moderator-to-fuel ratio affects, providing HEST full-core depletion calculations, and implementing multiple recycles. The robustness of the ISM makes it possible to use the same procedure for evaluating advanced fuel cycles that include completely different reactor systems as well.

The ISM performance was assessed by comparing it to stand alone results acquired by manually linking the individual 3D whole-core models. The predictive capabilities of the ISM proved to be more than adequate with computational savings greater than -5 orders of magnitude. Given the same NES evaluation, when performed using the 3D whole-core models, the total computational time was 144 hours, while the ISM produced nearly identical results with a computational time of less than 1 second.

A method for assessing how variations in key system parameters affect the NES on multiple levels was implemented. The results provided valuable information pertaining to system performance that is imperative to gain insight on how subsystem changes can produce unforeseen affects on the overall system. Provided information can be used to assist in implementing design changes for producing system performance aimed at obtaining predetermined global system goals. Moreover, the results can be used for preparing future evaluations, as mentioned previously (shuffling schemes, deepburn strategies, etc.), making their implementation into the ISM more efficient and effective.

The potential for implementing multi-objective optimization techniques within the ISM structure have also been demonstrated. Parameter minimum/maximum searches were performed and a method for weighting system variables was applied. Overall, TRU destruction rates approach 40% in the VHTR, including upwards of 70% destruction of ^{239}Pu. TRU Destruction rates in the HEST are estimated to be greater than 90%. Overall system electricity generation is over 10^{11} kW·hr, with approximately 550 tons of uranium available for reuse in the next cycle.

The NES has demonstrated great potential for providing safe, clean, and secure energy and doing so with foreseen advantages over the LEU once-through fuel cycle option. The main advantages exist due to better utilization of natural resources by recycling the used nuclear fuel, and by reducing the final amount and time span for which the resulting HLW must be isolated from the public and the environment due to radiological hazard. Calculations for NES scenarios estimate that the HLW waste will decay to radiotoxicity levels matching the originating uranium ore in about 2,000 years. This is opposed to the 100,000 years estimated for the once-through fuel cycle, a reduction of 98,000 years, or 98%. In addition, strategies have been identified for optimizing the NES to achieve even greater reductions that approach the limitations imposed by

the radiotoxicity of the fission products, which would require the HLW waste to be isolated for only 300 – 500 years.

Considering if the ubiquitous fossil fuel energy sources of today were replaced by the NES, the reduction in CO_2 emissions would be immense, which would have a very positive affect on the environment. The yearly savings in emissions for the replacement of coal would be 47.8 million metric tons of CO_2. For natural gas it would be 19.1 million metric tons of CO_2 and for petroleum it would register at 40.2 million metric tons of CO_2. In more relative terms, the NES CO_2 emissions savings would be equivalent to taking 10.5 million cars of the road.

The completion of this project has provided the basis for future research that aims to aid in solving the energy crisis that faces future generations, with additional emphasis on addressing environmental concerns. The main advantages of the developed NES are the ability to recover and reuse material that is otherwise considered difficult to manage waste, substantial reduction of the radiotoxic term of spent fuel per unit of produced energy, and generation of safe, reliant, and clean energy that is sustainable for many generations into the future. If deployed, the NES can substantially reduce the long-term radiological hazard posed by current HLW, extend uranium resources, and approach the characteristics of an environmentally benign energy system.

10 REFERENCES

1. F.M. VANEK, L.D. ALBRIGHT, *Energy Systems Engineering: Evaluation and Implementation*, McGraw-Hill Professional, New York (2008).

2. "Human Development Report 2009: Overcoming Barriers: Human Mobility and Development" Palgrave Macmillan, United Nations Development Program, New York (2009).

3. A.D. PASTERNAK, "Global Energy Futures and Human Development: A Framework for Analysis," Lawrence Livermore National Laboratory, UCRL-ID-140773 (October 2000).

4. "Kyoto Protocol to the United Nations Framework Convention on Climate Change," Adopted Kyoto, 11 December 1997, Crown Copyright, United Kingdom, Treaty Series No. 6 (2005).

5. P.P. PORTNEY, R.N. STAVINS, *Public Policy for Environmental Protection*, 2nd Edition, RFF Press, Washington DC (2000).

6. NEA/IAEA, "Uranium 2007: Resources, Production and Demand," OECD, Paris, France (2008).

7. J.R. LAMARSH, A.J. BARRATTA, *Introduction to Nuclear Engineering*, 3rd Edition, Prentice Hall, Upper Saddle River, New Jersey (2001).

8. K. NOACK, A. ROGOV, A.A. IVANOV, E.P. KRUGLYAKOV, Yu.A. TSIDULKO, "The GDT-Based Fusion Neutron Source as Driver of a Minor Actinides Burner," *Annals of Nuclear Energy* **35**, pp. 1216-1222 (2008).

9. A. TAYLOR, M. DUNNE, S. BENNINGTON, S. ANSELL, et al., "A Route to the Brightest Possible Neutron Source?" *Science* **315**, pp1092 (2007).

10. T.A. MEHLHORN, B.B. CIPITI, C.L. OLSON, G.E. ROCHAU, "Fusion-Fission Hybrids for Nuclear Waste Transmutation: A Synergistic Step Between Gen-IV Fission and Fusion Reactors," *Fusion Engineering and Design* **83**, pp 948-953 (2008).

11. A.H. MARTINEZ, Y. KADI, G. PARKS, M. DAHLFORS, "Transmutation of Nuclear Waste in Accelerator-Driven Systems: Fast Spectrum," *Annals of Nuclear Energy* **34**, pp. 564-578 (2007).

12. Y. GOHAR, T.A. TAIWO, J.E. CAHALAN, P.J. FINCK, "Assessment of the General Atomics Accelerator Transmutation of Waste Concept Based on the Gas-Turbine Modular Helium Reactor Technology," Technology Development Division, Argonne National Laboratory (2001).

13. W.M. STACEY, V.L. BEAVERS, W.A. CASINO, J.R. CHEATHAM, Z.W. FRIIS, et al., "A Subcritical, Gas-Cooled Fast Transmutation Reactor with a Fusion Neutron Source," *Nuclear Technology* **150**, pp. 162-188 (May 2005).

14. M. KOTSCHENREUTHER, P.M. VALANJU, S.M. MAHAJAN, and E.A. SCHNEIDER, "Fusion-Fission Transmutation Scheme-Efficient Destruction of Nuclear Waste," *Fusion Engineering and Design* **84**, pp. 83-82 (2009).

15. R. B ROGLI, R . K RAKOWSKI, "Degree of Sustainability of Various Nuclear Fuel Cycles," LAUR-01-6939, ISSN 1019 -0643, Nuclear Energy and Safety Research Department, Paul Scherrer Institute (2002).

16. P. FINCK, N . E DELSTIEN, Y . A LLEN, C . B URNS, et al., " The Path to Sustainable Nuclear Energy: Basic and Applied Research Opportunities for Advanced Fuel Cycles," Technical Report, Office of Science, U.S. Department of Energy (2005).

17. E.E. BENDE, A.H. HOGENBIRK, J.L. KLOOSTERMAN and H. VAN DAM, "Analytical Calculation of the Average Dancoff Factor for a Fuel Kernel in a Pebble-Bed High-Temperature Reactor," *Nuc. Sci. Eng*. **133**, 147-162 (1999).

18. J. WRIGHT, I. PAZSIT, " Neutron Kinetics in Subcritical Cores with Application to the Source Modulation Method," *Annals of Nuclear Energy*, **33**, pp. 149–158 (2006).

19. P. COLELLA, T.H. DUNNING, W.D. GROPP, and D.E. KEYES, "A Science-Based Case for Large-Scale Simulation, Vol. 2," Technical Report, Office of Science, U.S. Department of Energy (September 2004).

20. *MCNP User Manual*, Version 5, LA-UR-03-1987, Vol. I, Los Alamos National Laboratory, Revised (2008).

21. *MCNP User Manual*, Version 5, LA-UR-03-1987, Vol. II, Los Alamos National Laboratory, Revised (2008).

22. D.B. PELOWITZ, Ed., *MCNPX User's Manual*, LA-CP-07-1473, Version 2.6.0, Los Alamos National Laboratory (April 2008).

23. F.B. BROWN, "The MAKXSF Code with Doppler Broadening," Los Alamos National Laboratory Report LA-UR-06-7002, Los Alamos, New Mexico, USA (2006).

24. "SCALE: *A Modular Code System for Performing Standardized Computer Analyses for Licensing Evaluation*, *Version 6*," ORNL/TM-2005/39, 3 Volumes (January 2009).

25. D.F. HOLLENBACH, L.M. PETRIE, S. GOLUOGLU, N.F. LANDERS, M.E. DUNN, "KENO-VI: A General Quadratic Version of the KENO Program," Vol. II, Sect. F17 of *SCALE*: *A Modular Code System for Performing Standardized Computer Analysis for Licensing Evaluation*, *Version 6*, ORNL/TM-2005/39, 3 Volumes (January 2009).

26. I.C. GAULD, O.W. HERMANN and R.M. WESTFALL, "ORIGEN-S: SCALE System Module to Calculate Fuel Depletion, Actinide Transmutation, Fission Product Buildup and Decay, and Associated Radiation Source Terms," Vol. II, Sect. F7 of *SCALE: A Modular Code System for Performing Standardized Computer Analyses for Licensing Evaluation, Version 6*, ORNL/TM-2005/39, 3 Volumes (January 2009).

27. "Nuclear Fuel Cycle Simulation System (VISTA)," IAEA-TECDOC-1535, International Atomic Energy Agency, Vienna, Austria (February 2007).

28. MATLAB version 7.9 (R2009b), The MathWorks Inc., Natick, Massachusetts, USA (2009).

29. G.F. VANDEGRIFT, M.C. REGALBUTO, S. AASE, A. BAKEL, T.J. BATTISTI, et al., "Design and Demonstration of the UREX+ Process Using Spent Nuclear Fuel," ATALANTE 2004: Advances for Future Nuclear Fuel Cycles International Conference, Nimes, France, (June 2004).

30. T. KIM, T. TAIWO, R. HILL, W. YANG, F. VENNERI, "A Feasibility Study of Reactor-Based Deep-Burn Concepts," ANL-AFCI-155, Argonne National Laboratory (2005).

31. D. WESTLEN, "Why Faster is Better – On Minor Actinide Transmutation in Hard Neutron Spectra," Ph.D. Thesis, January 2007, School of Engineering Sciences, KTH Engineering Sciences, Stockhom, Sweden (2007).

32. J. ALONSO, P. DE PRETER, A. HOOPER, H. UMEKI, et al., "Post-closure Safety Case for Geological Repositories: Nature and Purpose," NEA Report, OECD, Paris, France (2004).

33. R.A. WIGELAND, E.E. MORRIS, and T.H. BAUER, "Criteria Derived for Geological Disposal Concepts", OECD/NEA 9th Information Exchange Meeting on Actinide and Fission Product Partitioning and Transmutation, Nimes, France (September 2006).

34. "Dose Coefficients for Intakes of Radionuclides by Workers," ICRP Publication 68 in: Annals of the ICRP, Vol. 24, #4, Elsevier Science Inc., Tarrytown, New York (1995).

35. C.R. HAMMOND, "The Elements," in D. R. LIDE, Ed., *CRC Handbook of Chemistry and Physics, 90th Ed.*, CRC Press, Boca Raton, Florida (2009).

36. "Westinghouse AP1000 Design Control Documentation Rev. 16," Tier 2, Chapter 4, Reactor Section 4.3, Nuclear Design. ML071580897 (2007).

37. "Generation IV Nuclear Energy Systems Ten Year Program Plan Volume I," Office of Advanced Nuclear Research, DOE Office of Nuclear Energy, Science, and Technology, USDOE (March 2005).

38. "Evaluation of High Temperature Gas-cooled Reactor Performance: Benchmark Analysis Related to Initial Testing of the HTTR and HTR-10", IAEA-TECDOC-1382, International Atomic Energy Agency, Vienna, Austria (2003).

39. D.E. AMES II, P.V. TSVETKOV, "Benchmark Efforts to Support Studies of Advanced VHTRs", *Proc. 4th Intern. Conf. on HTR Technology (HTR2008)*, Sept. 28 – Oct. 1, 2008, Washington D.C., USA, paper HTR2008-58206, pp. 1 – 8, ASME (2008).

40. S. FEHER and P.F.A. DE LEEGE, "DANCOFF-MC: A Computer Program for Monte Carlo Calculation of Dancoff Factors in Irregular Geometries," Delft University of Technology, IRI-131-95-003, Delft, Netherlands (June 1997).

41. T.A. TAIWO, T.K. KIM, W. S. YANG, and H.S. KHALIL, "Evaluation of High Temperature Gas-Cooled Reactor Physics Experiments as VHTR Benchmark Problems", ANL-GenIV-059, Argonne National Laboratory, USA (September 2005).

42. "AEC Research and Development Report, Facilities for Electronuclear (MTA) Program," Report LWS-24736, Livermore, California, USA (1953).

43. W.B. LEWIS, "Accelerators for Intense Neutron Sources," Atomic Energy of Canada Ltd., report DL-90, Canada (1968).

44. G.A. BARTHOLOMEW and P.R. TUNNICLIFFE, "The AECL Study for an Intense Neutron-Generator: Technical Details," Atomic Energy of Canada Limited Report AECL 2600, Canada (1966).

45. C.D. BOWMAN, E.D. ARTHUR, P.W. LISOWSKI, G.P. LAWRENCE, et al., "Nuclear Energy Generation and Waste Transmutation Using an Accelerator-Driven Intense Thermal Neutron Source," *Nucl. Istrum. Meth. Res.* **A320**, p. 366; (1992).

46. M.A. REDA, J.F. HARMON, and S.B. SADINENI, "A Photo-Neutron Source for a Sub-Critical Nuclear Reactor Program," *AIP Conf. Proc.*, Volume **680**, pp. 800 -803, (August 2003).

47. M. SALVATORES, I. SLESSAREV, and M. UEMATSU, "A Global Physics Approach to Transmutation of Radioactive Nuclei," *Nuclear Science and Engineering* **116**, pp. 1 -18 (1994).

48. M. SALVATORES, R. HILL, I SLESSAREV, G. YOUINOU, "The Physics of TRU Transmutation – A Systematic Approach to the Intercomparison of Systems," Proceedings of PHYSOR 2004, The Physics of Fuel Cycles and Advanced Nuclear Systems: Global Developments, Chicago, IL, USA (April 2004).

49. G. H. MILEY, R. THOMAS, Y. TAKEYAMA, et al., "Driven Subcritical Fission Systems Using A Cylindrical Inertial Electrostatic Confinement (IEC) Neutron Source," DOE Office

of Fusion Energy Sciences, ReNeW, Gaithersburg, Maryland, USA (Sept. 30 – Oct. 2, 2009).

50. W.M. STACEY, "Tokamak D-T Fusion Neutron Source Requirements for Closing the Nuclear Fuel Cycle," Institute of Physics Publishing, *Nucl. Fusion* **47**, pp 217-221 (2007).

51. C. RODRIGUEZ, A. BAXTER, D. MCEACHERN, M. FIKANI, and F. VENNERI, 2003, "Deep-Burn: Making Nuclear Waste Transmutation Practical," *Nucl. Eng. Des.*, **2805**, pp. 1–19.

52. "Critical Experiments and Reactor Physics Calculations for Low-Enriched HTGRs," IAEA-TECDOC-1249, International Atomic Energy Agency, Vienna, Austria (2001).

53. K. MINATO, K. SAWA, T. KOYA, T. TOMITA, and A. ISHIKAWA, 2000, "Fission Product Release Behavior of Individual Coated Fuel Particles for High Temperature Gas-Cooled Reactors," *Nucl. Technol.*, **131**, pp. 36–46.

54. "CO_2 Emissions From Fuel Combustion," International Energy Agency, OECD/IEA, Paris, France (2009).

55. "Thirsty Energy: Water and Energy in the 21st Century," World Economic Forum, Cambridge Energy Research Associates, US DOE et al., (2009).

56. R.G. COCHRAN and N. TSOULFANIDIS, "The Nuclear fuel Cycle: Analysis and Management 2nd ed.," American Nuclear Society, La Grange Park, Illinois, USA (1999).

11 APPENDIX A

HTTR code-to-experiment benchmark supplemental data.

Fuel particle level:

TRISO particle

	material	density (g/cm³)	radius (cm)
Fuel kernel	UO_2	10.41	0.02985
1st coating	PyC	1.14	0.03588
2nd coating	PyC	1.89	0.03895
3rd coating	SiC	3.20	0.04184
4th coating	PyC	1.87	0.04645

Graphite matrix

Material	Density	Impurity
graphite	1.69 g/cm³	0.82 ppm B_{nat}

Unit cell measurements

Volume fraction of grains	Array Pitch	Number of particles per fuel element
0.3	0.1377 cm	176,515

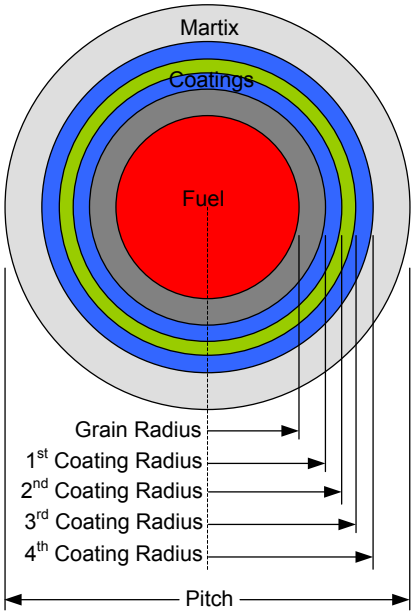

TRISO particle

Fuel element level:

Fuel element properties

Fuel Compact	
Number of fuel particles	176,515
Graphite matrix density	1.690 g/cm³
Graphite matrix Impurity	0.82 ppm B_{nat}
Diameter-inner	1.0 cm
Diameter-outer	2.6 cm
Effective height of fuel rod	54.6 cm

Graphite Sleeve	
Material	Graphite
Density	1.770 g/cm³
Impurity	0.37 ppm B_{nat}
Diameter-inner	2.6 cm
Diameter-outer	3.4 cm
Height	57.7 cm

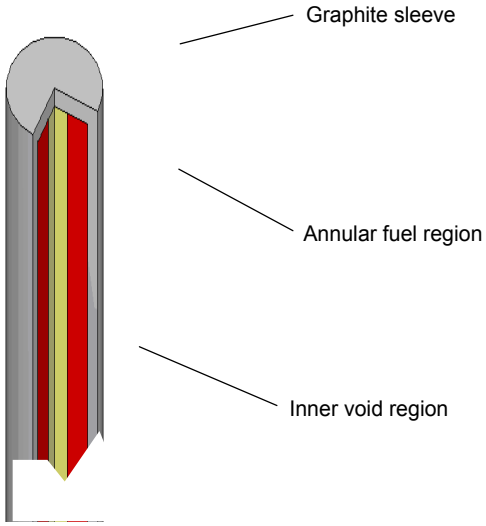

Annular fuel rod

Burnable Poison Rod Properties

Type	H-I	H-II
Absorber section material (2 per rod)	B_4C-C	B_4C-C
Density	1.79 g/cm³	1.82 g/cm³
Natural boron concentration	2.22 wt.%	2.74 wt.%
Diameter	1.39 cm	1.39 cm
Height	20 cm	20 cm
B-10 abundance ratio	18.7 wt.%	18.7 wt.%
Graphite section density	1.77 g/cc	1.77 g/cc
Diameter	1.40 cm	1.40 cm
Height	10 cm	10 cm

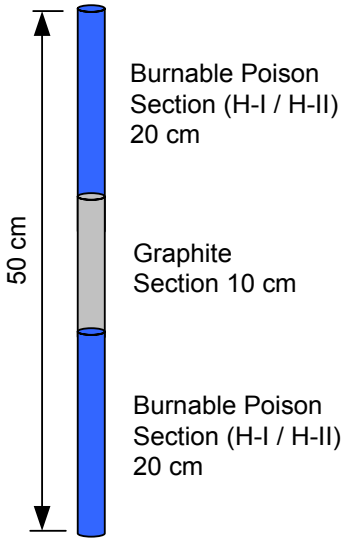

Fuel Assembly Block

Type	Pin-in-block
Configuration	Hexagonal
Material	IG-110 Graphite
Density	1.770 g/cm³
Impurity	0.40 ppm B_{nat}
Height	58.0 cm
Width across the flats	36.0 cm
Number of fuel holes in block	33 or 31
Fuel hole diameter	4.1 cm
Fuel hole height	58.0 cm
Burnable poison holes	3
Burnable poison hole diameter	1.5 cm
Burnable poison hole height	50.0 cm

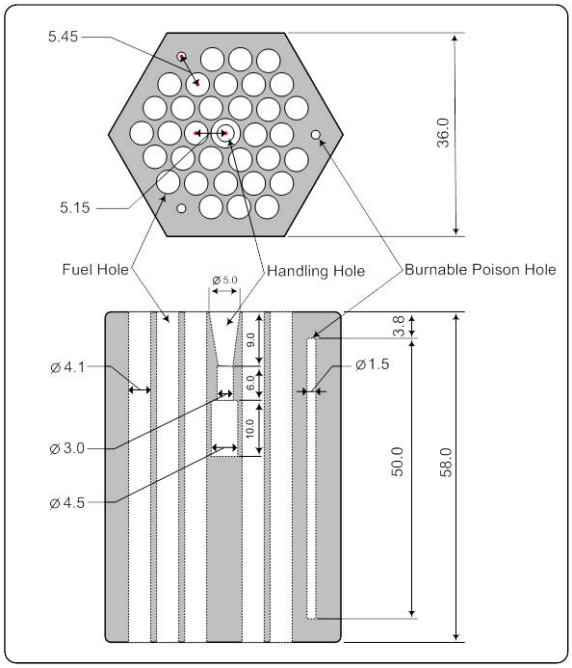

Unit cell measurements

Lattice type	Array Pitch (cm)	Fuel inner radius (cm)	Fuel outer radius (cm)	Sleeve inner radius (cm)	Sleeve outer radius (cm)	Fuel element height (cm)
Triangular	5.15	0.5	1.3	1.3	1.7	54.6

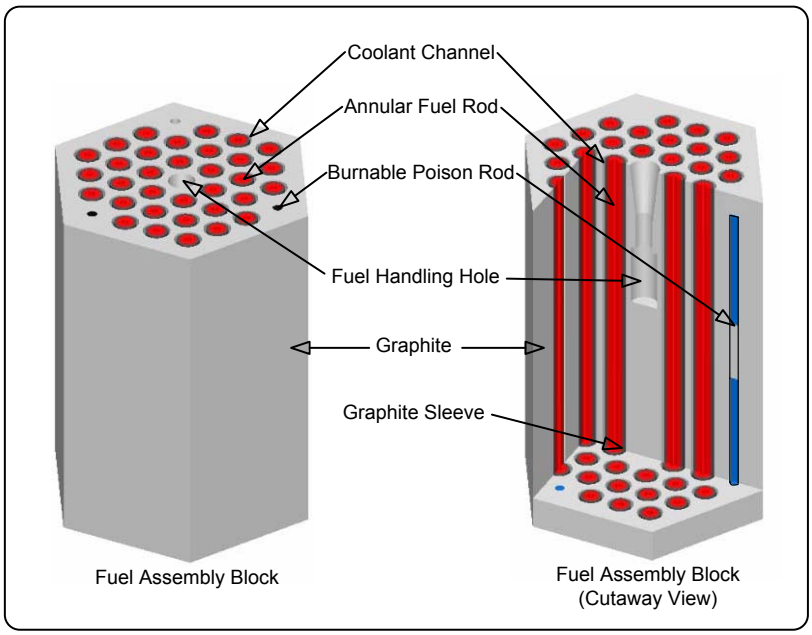

Fuel assembly block with top and quarter section removed to show fuel rods and BP rods.

Control Rod Block and Irradiation Block (irradiation block is identical to control rod block except the holes are used for nuclear instrumentation instead of control rods)

Material	IG-110 Graphite
Density	1.770 g/cm³
Impurity	0.40 ppm B_{nat}
Height	58.0 cm
Width across the flats	36.0 cm
Number control rod holes in block	2
Control rod hole diameter	12.3 cm
Control rod hole height	58.0 cm
Reserve shutdown holes in block	1
Reserve shutdown hole diameter	12.3 cm
Reserve shutdown hole height	58.0 cm

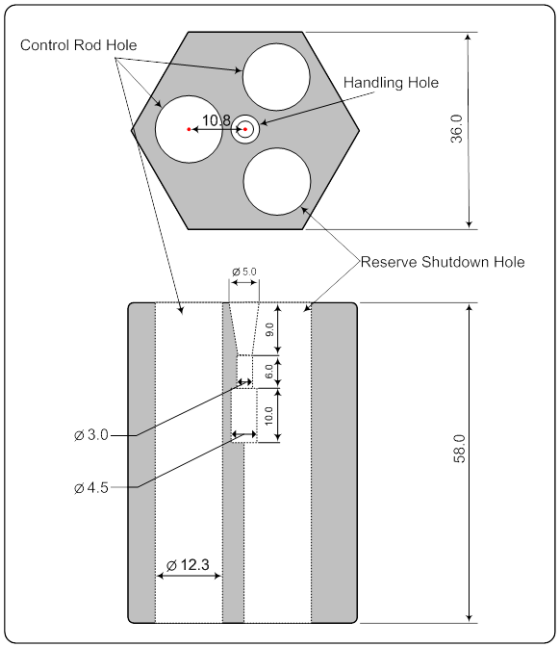

Control Rod Properties

Neutron Absorber Sections (annular)	
Number of neutron absorber sections in each control rod	10
Material	B_4C and C
Density	1.9 g/cm³
Diameter-inner	7.5 cm
Diameter-outer	10.5 cm
Height	29.0 cm
Effective height	290 cm (10 neutron absorber sections)
Spacing between neutron absorber sections	2.2 cm
Control Rod Sleeve	
Material	Alloy 800H
Thickness	0.35 cm
Control Rod	
Number of control rods	32 (16 pairs)
Number of control rods in active core	14 (7 pairs)
Number of control rods in replaceable reflector region	18 (9 pairs)
Diameter-inner	6.5 cm
Diameter-outer	11.3 cm
Height	310 cm

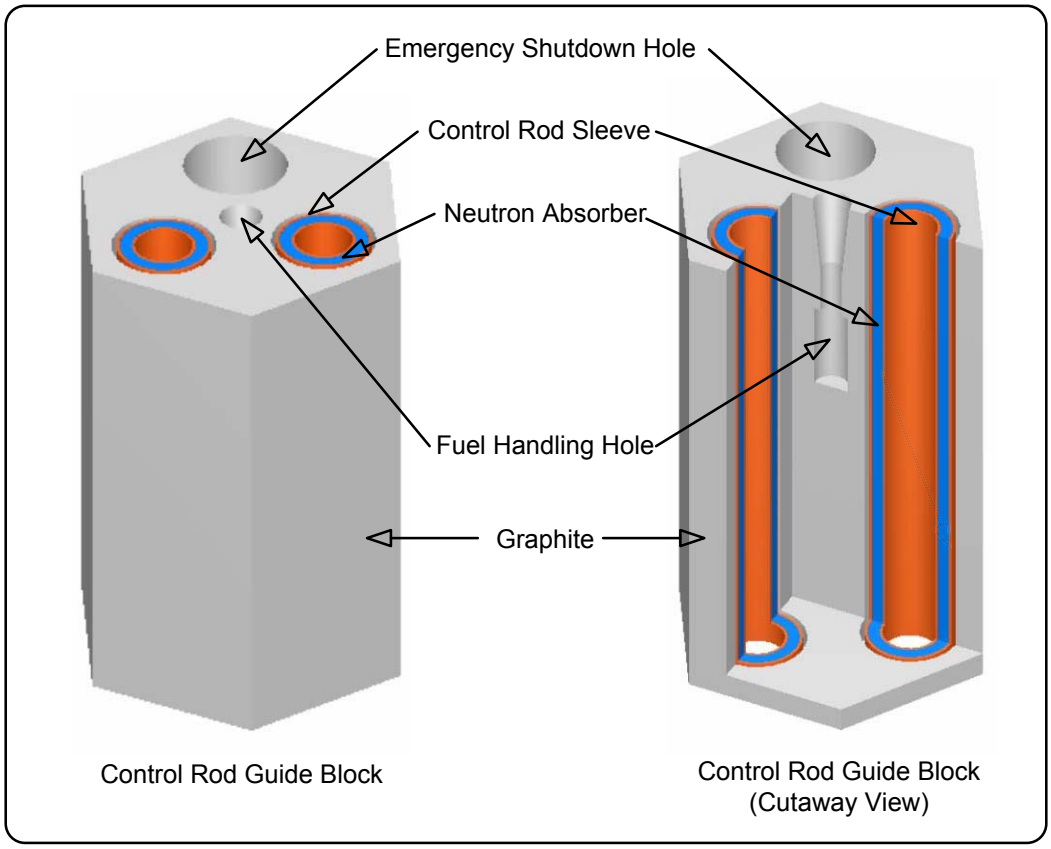

Control rod block with cutaway view

Replaceable Reflector Block (can be solid graphite block or have coolant channels to match the fuel assembly block that it would be associated with)

Configuration	Hexagonal
Material	IG-110 Graphite
Density	1.760 g/cm³
Impurity	0.37 ppm B_{nat}
Height	58.0 cm
Width across the flats	36.0 cm
Coolant channels (if applicable)	33/31
Coolant hole diameter	4.1 cm
Coolant hole height	58.0 cm

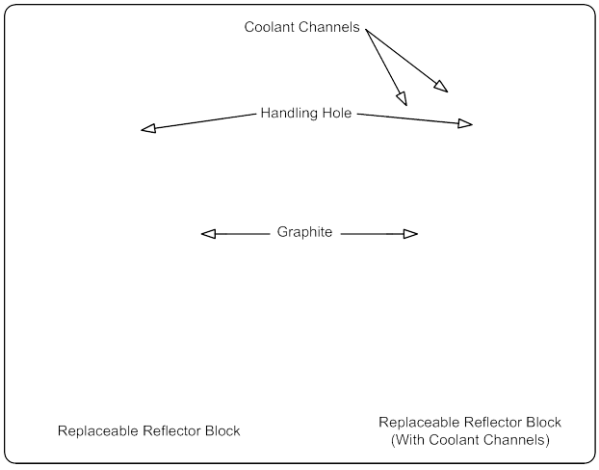

Core Level:

Core Columns

Column	Blocks
Fuel assembly	5 Fuel assembly blocks 4 Reflector blocks (channels)
Reflector	9 Reflector Blocks
Control Rod / Irradiation	9 Control rod blocks

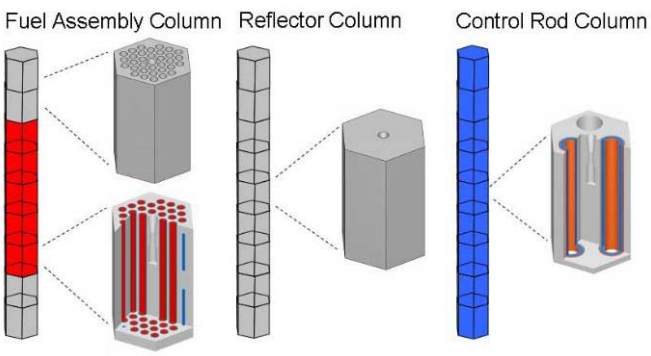

Permanent Reflector Properties

Material	IG-110 Graphite
Density	1.732 g/cm³
Impurity	2 ppm B_{nat}
Height	522 cm
Radius	215 cm

Overall Core Geometry

	Active core	Whole core
Height	290 cm	522 cm
Radius	115 cm (effective)	215 cm

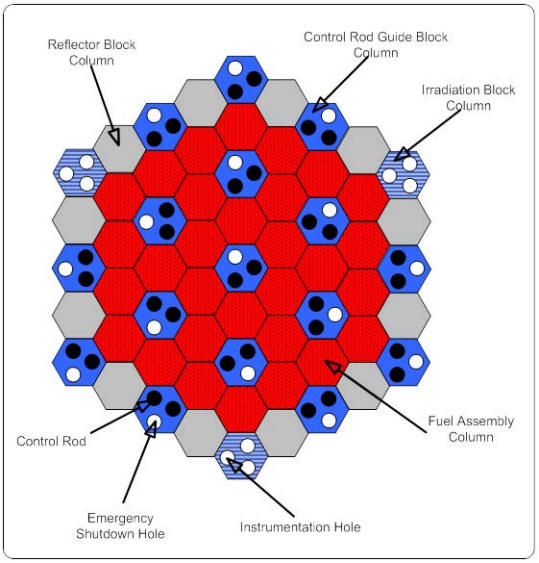

Cross-section core view

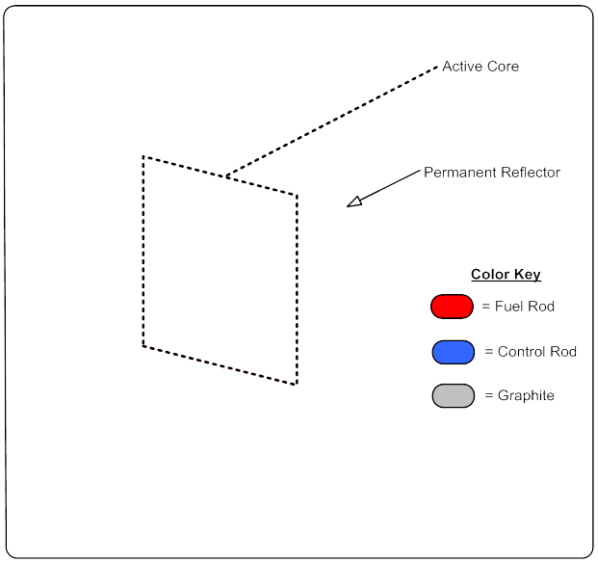

Whole core 3D view

Uranium Enrichments

number	1	2	3	4	5	6	7	8	9	10	11	12
wt. %	3.301	3.864	4.290	4.794	5.162	5.914	6.254	6.681	7.189	7.820	9.358	9.810

Core Arrangement

Layer number from top fuel block	Items	Fuel zone number			
		1	2	3	4
1	Uranium enrichment (wt. %) Number of fuel rods in graphite block Type of burnable poisons	6.681 33 H-I	7.820 33 H-I	9.358 31 H-I	9.810 31 H-I
2	Uranium enrichment (wt. %) Number of fuel rods in graphite block Type of burnable poisons	5.162 33 H-II	6.254 33 H-II	7.189 31 H-II	7.820 31 H-II
3	Uranium enrichment (wt. %) Number of fuel rods in graphite block Type of burnable poisons	4.290 33 H-II	5.162 33 H-II	5.914 31 H-II	6.254 31 H-II
4	Uranium enrichment (wt. %) Number of fuel rods in graphite block Type of burnable poisons	3.301 33 H-I	3.864 33 H-I	4.290 31 H-I	4.794 31 H-I
5	Uranium enrichment (wt. %) Number of fuel rods in graphite block Type of burnable poisons	3.301 33 H-I	3.864 33 H-I	4.290 31 H-I	4.794 31 H-I

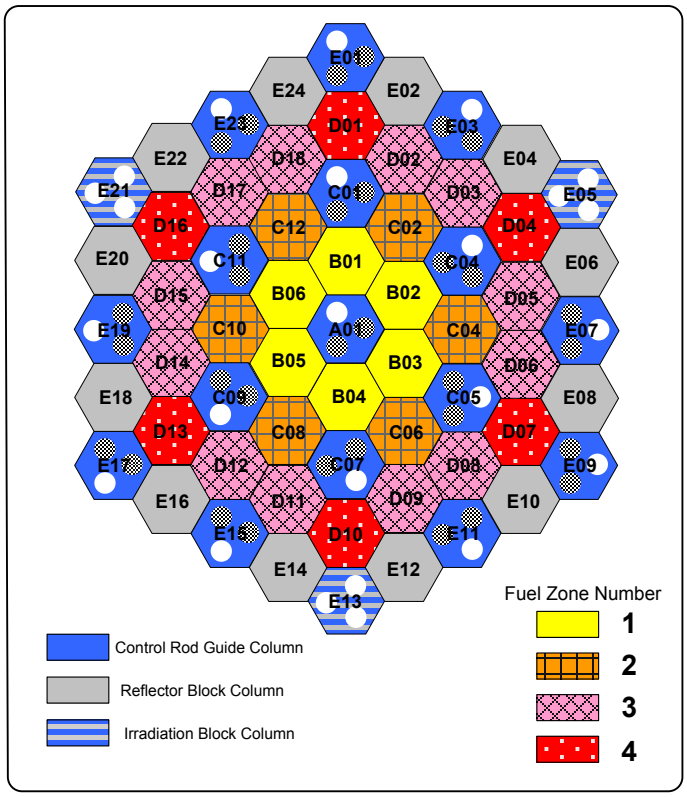

Core Map

Benchmark Results:

Benchmark		VHTR model (calculated)	HTTR (experimental)	Error (%)
Control Rods Fully Withdrawn	k-eff	1.1368 ± 0.0023	1.1363 ± 0.041	0.044
Control Rods Fully Inserted	k-eff	0.6858 ± 0.0019	0.685 ± 0.010	0.117
Critical Insertion Depth (core temperature 300K)	cm	177.1	177.5 ± 0.5	0.225
Critical Insertion Depth (core temperature 418K)	cm	189.9	190.3 ± 0.5	0.210
Temperature Coefficient	dk/k/K	-1.45E-04	-1.42E-04	2.113

12 APPENDIX B

HEST Concept I: Individual TRU Nuclides Neutron Balance (D_{eq}^{TRU}) as a Function of Flux.

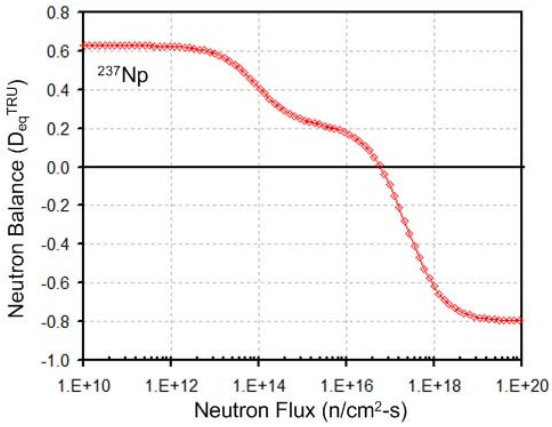

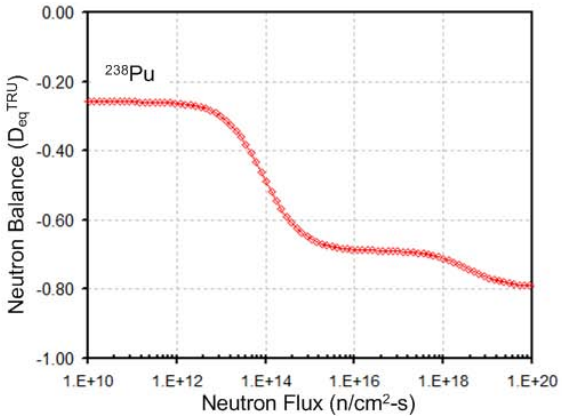

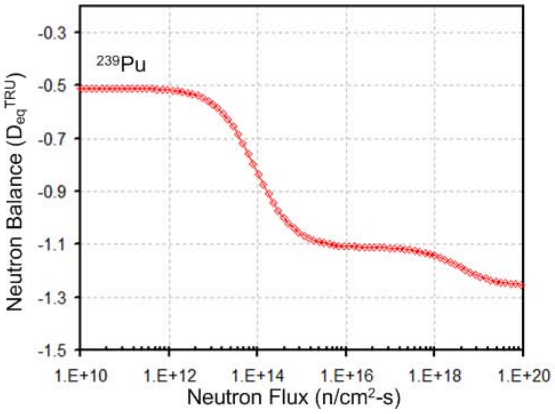

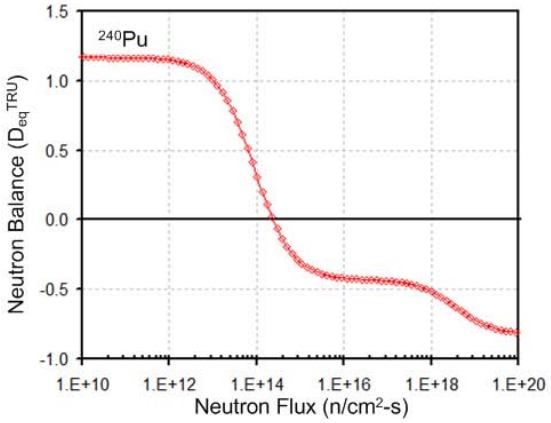

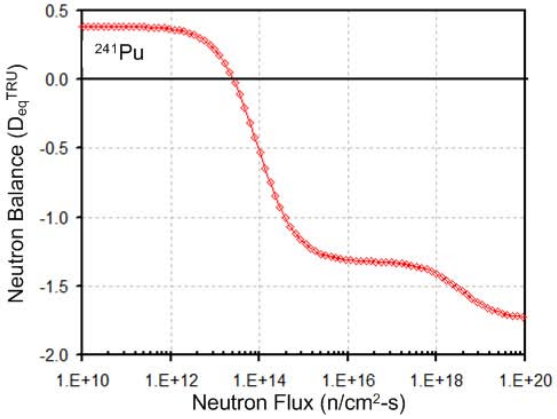

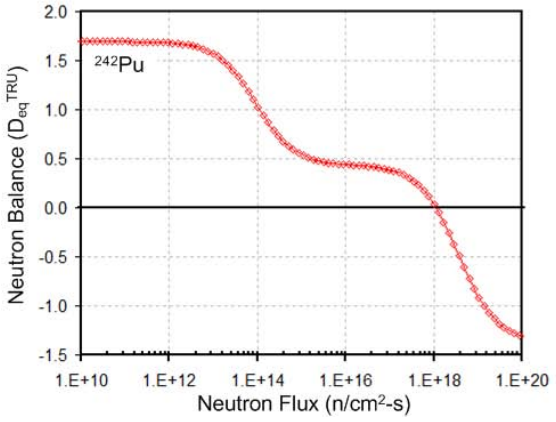
242Pu
Neutron Balance (Deq TRU)
Neutron Flux (n/cm2-s)
2.0
1.5
1.0
0.5
0.0
-0.5
-1.0
-1.5
1.E+10
1.E+12
1.E+14
1.E+16
1.E+18
1.E+20

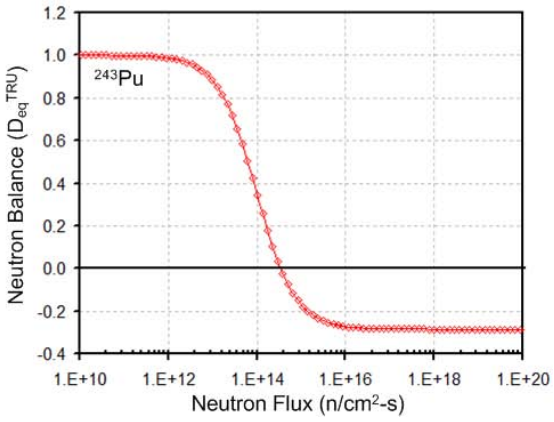
243Pu
Neutron Balance (Deq TRU)
Neutron Flux (n/cm2-s)
1.2
1.0
0.8
0.6
0.4
0.2
0.0
-0.2
-0.4
1.E+10
1.E+12
1.E+14
1.E+16
1.E+18
1.E+20

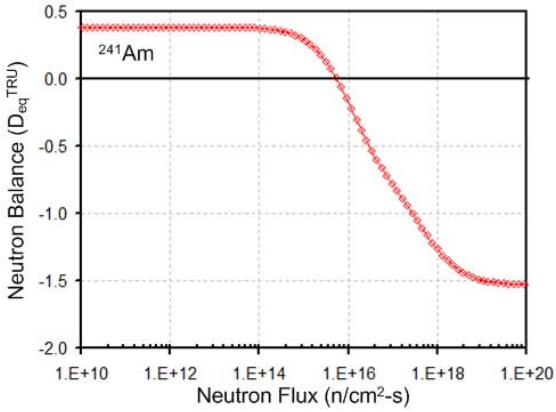
241Am
Neutron Balance (Deq TRU)
Neutron Flux (n/cm2-s)
0.5
0.0
-0.5
-1.0
-1.5
-2.0
1.E+10
1.E+12
1.E+14
1.E+16
1.E+18
1.E+20

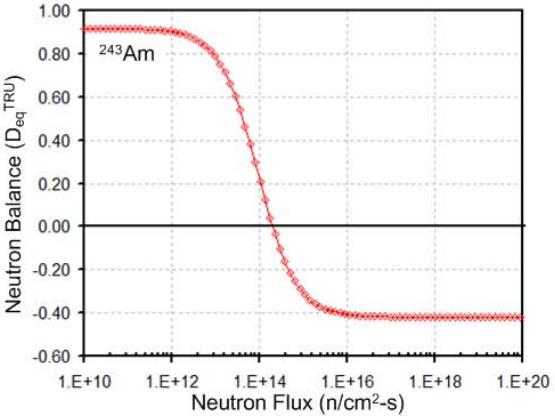
243Am
Neutron Balance (Deq TRU)
Neutron Flux (n/cm2-s)
1.00
0.80
0.60
0.40
0.20
0.00
-0.20
-0.40
-0.60
1.E+10
1.E+12
1.E+14
1.E+16
1.E+18
1.E+20

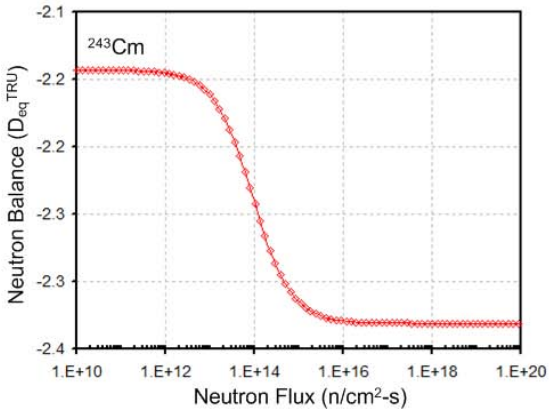
243Cm
Neutron Balance (Deq TRU)
Neutron Flux (n/cm2-s)
-2.1
-2.2
-2.2
-2.3
-2.3
-2.4
1.E+10
1.E+12
1.E+14
1.E+16
1.E+18
1.E+20

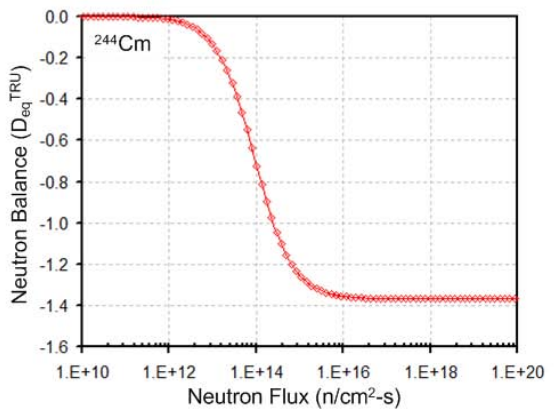
244Cm
Neutron Balance (Deq TRU)
Neutron Flux (n/cm2-s)
0.0
-0.2
-0.4
-0.6
-0.8
-1.0
-1.2
-1.4
-1.6
1.E+10
1.E+12
1.E+14
1.E+16
1.E+18
1.E+20

HEST Concept II: Individual TRU Nuclides Neutron Balance (D_{eq}^{TRU}) as a Function of Flux.

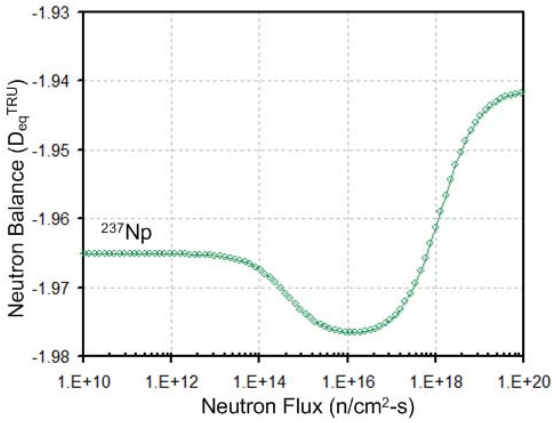

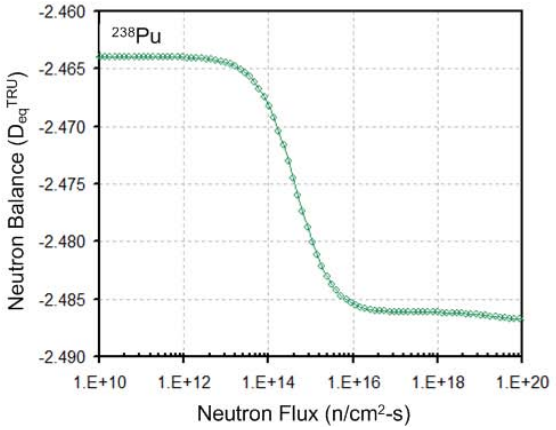

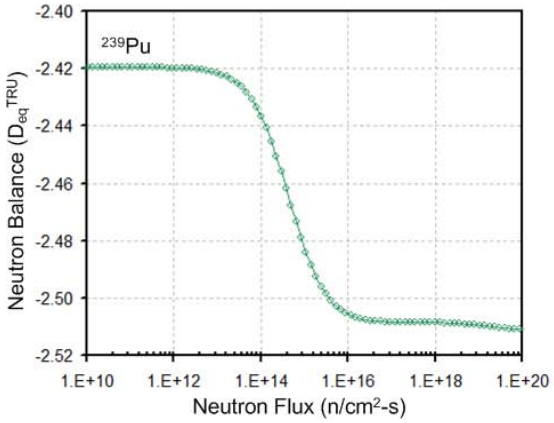

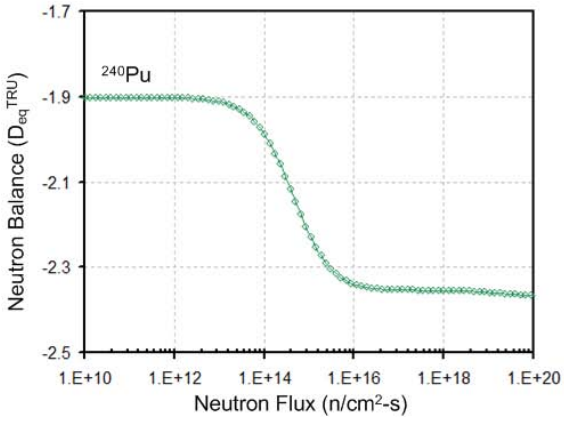

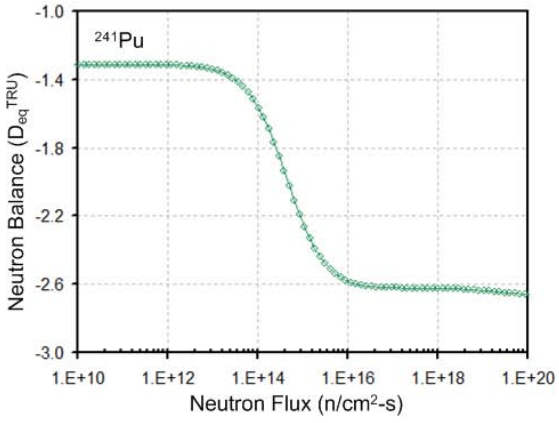

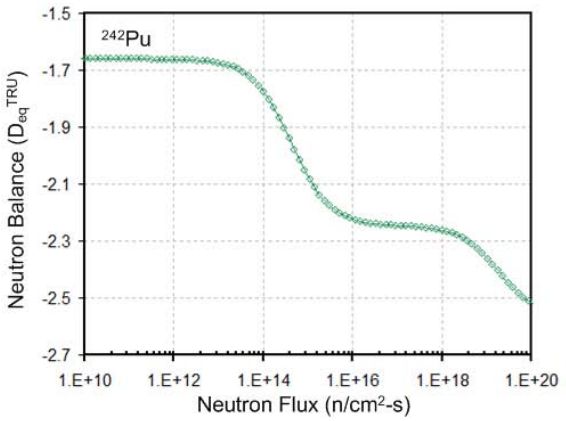
242Pu
Neutron Balance (Deq TRU)
-1.5
-1.7
-1.9
-2.1
-2.3
-2.5
-2.7
1.E+10
1.E+12
1.E+14
1.E+16
1.E+18
1.E+20
Neutron Flux (n/cm2-s)

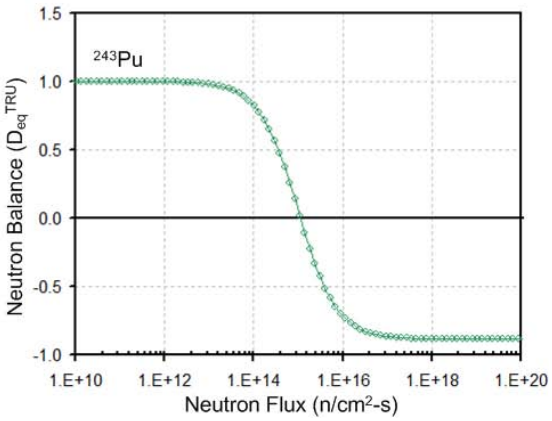
243Pu
Neutron Balance (Deq TRU)
1.5
1.0
0.5
0.0
-0.5
-1.0
1.E+10
1.E+12
1.E+14
1.E+16
1.E+18
1.E+20
Neutron Flux (n/cm2-s)

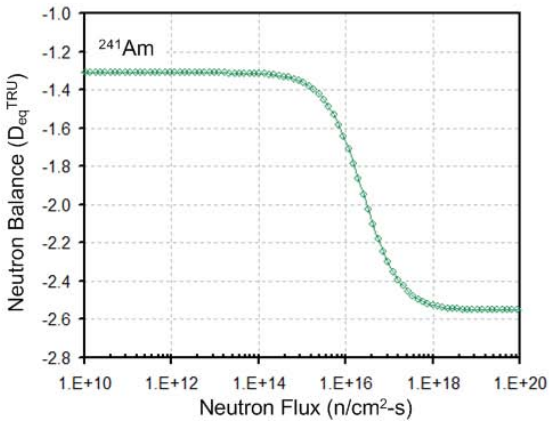
241Am
Neutron Balance (Deq TRU)
-1.0
-1.2
-1.4
-1.6
-1.8
-2.0
-2.2
-2.4
-2.6
-2.8
1.E+10
1.E+12
1.E+14
1.E+16
1.E+18
1.E+20
Neutron Flux (n/cm2-s)

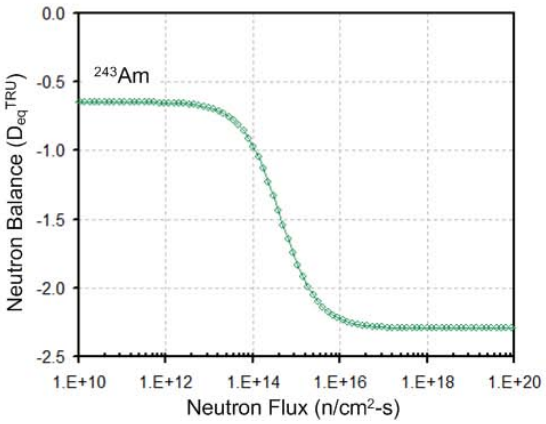
243Am
Neutron Balance (Deq TRU)
0.0
-0.5
-1.0
-1.5
-2.0
-2.5
1.E+10
1.E+12
1.E+14
1.E+16
1.E+18
1.E+20
Neutron Flux (n/cm2-s)

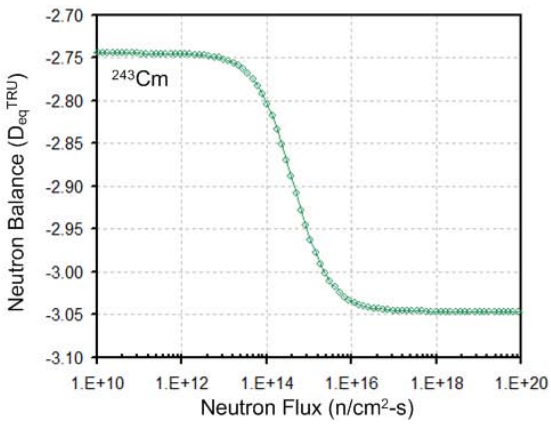
243Cm
Neutron Balance (Deq TRU)
-2.70
-2.75
-2.80
-2.85
-2.90
-2.95
-3.00
-3.05
-3.10
1.E+10
1.E+12
1.E+14
1.E+16
1.E+18
1.E+20
Neutron Flux (n/cm2-s)

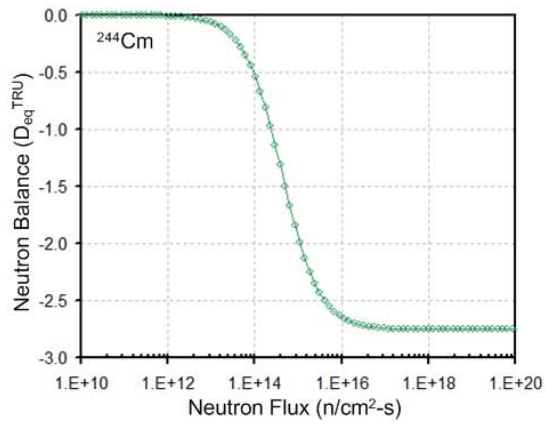
244Cm
Neutron Balance (Deq TRU)
0.0
-0.5
-1.0
-1.5
-2.0
-2.5
-3.0
1.E+10
1.E+12
1.E+14
1.E+16
1.E+18
1.E+20
Neutron Flux (n/cm2-s)

13 PUBLICATIONS LIST

1. D. E. Ames II, P. V. Tsvetkov, G. E. Rochau, S. Rodriguez, "High Fidelity Nuclear Energy System Optimization towards an Environmentally Benign, Sustainable, and Secure Energy Source", Sandia National Laboratory, October 2009, SAND2009-6831 (2009).

2. D. E. Ames II, P. V. Tsvetkov, G. E. Rochau, S. Rodriguez, "Nuclear Energy System Providing an Environmentally Benign, Sustainable, and Secure Energy Source", *Trans. Amer. Nucl. Soc.*, **101**, pp. 177 - 178, USA (2009).

3. D. E. Ames II, "High Fidelity Nuclear Energy System Optimization towards an Environmentally Benign, Sustainable, and Secure Energy Source", Ph.D. Dissertation, August 2010, Texas A&M University, Chair – P. V. Tsvetkov (2010).

4. D. E. Ames II, P. V. Tsvetkov, "High-Fidelity System Modeling of Advanced Nuclear Energy Systems Approaching a Zero-Nuclear-Waste Limit", *Progress in Nuclear Energy*, Invited, Under Review, PNUCENE-S-10-00169, American Nuclear Society (2010).

5. D. E. Ames II, P. V. Tsvetkov, G. E. Rochau, S. Rodriguez, "High-Fidelity Integrated System Modeling for Sustainability Analysis of Nuclear Energy Systems", ANS Winter Meeting, 2010, accepted, USA (2010).

14 DISTRIBUTION LIST

Texas A&M University

David Ames II, deames_99@yahoo.com
Ayodeji Alajo, dejialajo@neo.tamu.edu
Raymond Juzaitis, rjuzaitis@tamu.edu
Tom Lewis III, tglewis3@gmail.com
Pavel Tsvetkov, Tsvetkov@tamu.edu

Argonne National Laboratory

Mohamed Gohar, gohar@anl.gov
Robert Hill, bobhill@anl.gov
Temitope Taiwo Taiwo@anl.gov

U.S. Department of Energy

Madeline Feltus, MADELINE.FELTUS@nuclear.energy.gov
Alex Larzelere, alex.larzelere@nuclear.energy.gov
Rob Versluis, ROB.VERSLUIS@nuclear.energy.gov

General Atomics

Timothy Bertch, Timothy.Bertch@ga.com
Donald McEachern, Donald.McEachern@ga.com
Arkal Shenoy, Arkal.Shenoy@ga.com

General Electric

Eric Loewen, eric.loewen@ge.com
Russell Stachowski, Russell.Stachowski@gnf.com

Electric Power Research Institute

John H. Kessler, JKESSLER@epri.com

Idaho National Laboratory

Samuel E Bays, Samuel.Bays@inl.gov
Mark DeHart, Mark.DeHart@inl.gov
Hans Gougar, Hans.Gougar@inl.gov
D Scott Lucas, D.Lucas@inl.gov
Kathryn McCarthy, Kathryn.Mccarthy@inl.gov
David Nigg, David.Nigg@inl.gov
Abderrafi Ougouag, Abderrafi.Ougouag@inl.gov
Michael A Pope, Michael.Pope@inl.gov
Hongbin Zhang, Hongbin.Zhang@inl.gov

Laurence Livermore National Laboratory

Jeff Latkowski, latkowski@llnl.gov
Ralph Moir, RMoir@Pacbell.net

Logos Technologies

Francesco Venneri, fvenneri@mac.com

Oak Ridge National Laboratory

Ian C. Gauld, gauldi@ornl.gov
Jess Gehin, gehinjc@ornl.gov
Matthew A. Jessee, jesseema@ornl.gov
Bernadette L. Kirk, kirkbl@ornl.gov

Sandia National Laboratories

Benjamin Cipiti, MS0747 (Org 6774) bbcipit@sandia.gov
Evaristo J. Bonano, MS1370 (Org 6770) ejbonan@sandia.gov
Yolanda V. Moreno, MS0359 (Org 1912) ymoreno@sandia.gov
Gary E. Rochau, MS1136 (Org 6772) gerocha@sandia.gov
Salvador B. Rodriguez, MS0821 (Org 1532) sbrodri@sandia.gov
Stephen J. Rottler, MS0351 (Org 1000) jsrottl@sandia.gov
Donna L. Chavez, MS0359 (Org 1911) dchavez@sandia.gov
Technical Library, MS0899 (Org 9536) libref@sandia.gov


Sandia National Laboratories